



PhD-FSTM-2021-053
The Faculty of Science, Technology and Medicine

DISSERTATION

Defence held on 23/07/2021 in Esch-sur-Alzette

to obtain the degree of

DOCTEUR DE L'UNIVERSITÉ DU LUXEMBOURG

EN CHIMIE

by

Acerina TREJO MACHÍN

Born on 29 December 1992 in Arrecife (Spain)

DESIGN AND SYNTHESIS OF NOVEL BENZOXAZINES TO REPLACE TRADITIONAL REINFORCING RESINS IN RUBBER COMPOUNDS

Dissertation defence committee

Dr Pierre Verge, dissertation supervisor
Luxembourg Institute of Science and Technology, Luxembourg

Dr Alex Redinger, Chairman
Professor, Université du Luxembourg

Dr Marc Weydert, Vice Chairman
The Goodyear Tire and Rubber Company, Luxembourg

Dr Cédric Vancaeyzeele
CY Cergy Paris University, France

Dr Daniel Schmidt
Luxembourg Institute of Science and Technology, Luxembourg

Abstract

The mechanical performance of tires is controlled by many of the ingredients used in their production. Among them, novolac-type phenolic resins (PR) are petroleum-based materials commonly employed to reinforce rubber compounds. Even though overall performance is efficient, there is a growing societal need to develop alternatives to these resins as they are challenged by REACH regulations. Benzoxazine resins (Bz) are a new generation of materials that can be suitable for this purpose; they hold potential for improvement of both the mechanical properties and the sustainability of the rubber compounds. However, while PR have been extensively used and their interactions with tire compounds are well known, the use of benzoxazines in rubber compounds requires extensive studies and in-detail investigations.

This thesis aims at filling this gap and designing benzoxazine resins that could be relevant alternatives to PR. For this purpose, novel sulfur-containing dibenzoxazines were successfully synthesized and their interactions with rubber compounds were methodically investigated. Diphenolic compounds with either disulfide bonds (S–S), or monosulfide bonds (–S–) were reacted with monoamines such as furfurylamine, a bio-based amine produced from agricultural byproducts. These partially bio-based original precursors, which were never reported before, exhibited polymerization behaviors that greatly fit the required conditions for rubber vulcanization. Indeed, the curing of these novel benzoxazine monomers occurred during rubber vulcanization, allowing the elaboration of reinforced materials at the molecular scale without detrimental side-reactions with the curing package. A fine investigation of the mechanical and thermal properties of the resulting rubber compounds indicated the reinforcing effect of these new resins at the macroscale. Therefore, the potential of each benzoxazine to act as a reinforcing resin was tested in real tire parts confirming the potential of Bz to be used as alternatives to PR resins in carbon-black filled compounds.

In conclusion, the outcome of this thesis emphasizes that structural features of benzoxazines are a major parameter to be considered for their use in rubber reinforcement. Thanks to the knowledge generated, it was possible to develop novel benzoxazine resins capable of reinforcing rubber compounds in place of traditional phenolic resins. This study also paves the way to replace petroleum-based resins by partially bio-based precursors, improving the sustainability of tire compounds.

Contents

Abstract.....	i
List of Figures.....	ix
List of Schemes	xvii
List of Tables	xix
List of Abbreviations	xxi
List of Symbols and Units	xxv
General introduction	1
I Literature review	5
1 Introduction	5
2 Introduction to tire compounds and technologies	5
2.1 History of Tires	5
2.2 Basic tire design	6
2.3 Compound processing	7
2.4 Tire manufacturing	8
2.5 Rubber compounding	9
2.5.1 Polymers	10
2.5.2 Curing systems.....	10
2.5.3 Carbon black	14
2.5.4 Special compounding ingredients	18
3 Phenolic resins as additives in the rubber industry.....	19
3.1 Introduction	19
3.2 Phenolic resins used in rubber formulation.....	20
3.3 Novolac phenolic resins used for rubber reinforcement	21
4 Benzoxazine resins	23
4.1 Synthesis of benzoxazine monomers	23
4.2 Benzoxazine polymerization	25
4.3 Structure-to-property relationship	27
4.3.1 Class A	27
4.3.2 Class B	32
5 State of the art of benzoxazine resins and rubber	38

5.1	Blends of benzoxazine resins and rubber	38
5.2	Functionalization of rubbers with benzoxazines	40
5.3	Interactions between benzoxazines and rubber ingredients.....	41
6	Interactions between benzoxazine resins and sulfur	42
6.1	Inverse vulcanization	43
6.2	Elemental sulfur and benzoxazines	44
6.2.1	Elemental sulfur as a catalyst	44
6.2.2	Elemental sulfur as a co-reagent	45
6.3	COLBERT reaction	46
7	Application of benzoxazine resins in the tire industry.....	48
8	Conclusion	51
II	Synthesis, molecular and thermal characterization of benzoxazine resins.....	55
1	Introduction.....	55
2	Synthesis and characterization of the structural features of benzoxazines	55
2.1	4,4'-substituted benzoxazines	56
2.1.1	Synthesis pathway	56
2.1.2	Characterization by NMR	57
2.1.3	Characterization by FTIR.....	61
2.1.4	Characterization by Raman	62
2.1.5	Synthesis and structural features of additional benzoxazines	63
2.2	3,3'-substituted benzoxazines	65
2.2.1	Synthesis pathway	65
2.2.2	Characterization by NMR	66
2.2.3	Characterization by FTIR.....	68
2.2.4	Characterization by Raman	68
2.3	Discussion.....	70
3	Thermal and thermomechanical characterizations.....	71
3.1	Thermal behavior by DSC	71
3.1.1	General comments about the characterization of benzoxazines by DSC.....	71
3.1.2	DSC of benzoxazine monomers prepared from furfurylamine.....	72
3.1.3	DSC of benzoxazine monomers prepared from aniline	74
3.1.4	DSC of benzoxazine monomers prepared from stearylamine.....	75

3.2	Thermal stability by TGA	76
3.3	Polymerization behavior by rheology	78
3.4	Viscoelastic properties of polybenzoxazine	80
3.5	Discussion	81
4	Conclusion	82
III	Application of benzoxazine resins in unfilled compounds.....	87
1	Introduction	87
2	Investigation of benzoxazine curing in the presence of curing system	87
2.1	Effect of sulfur on the thermal behavior of the benzoxazine precursors.	88
2.2	Effect of sulfur on the polymerization of benzoxazine precursors	89
2.3	Solubility of polybenzoxazines in the presence of sulfur	90
2.4	Discussion	91
3	Application of dibenzoxazines precursors in unfilled compounds.....	92
3.1	Curing of unfilled green compounds containing benzoxazine precursors	93
3.2	Morphological characterization and nanomechanical properties of unfilled compounds by AFM.....	96
3.3	Mechanical properties of unfilled compounds by tensile test.....	98
3.4	Discussion	99
4	Comparison of 3DPDS-fa to other resin-reinforced unfilled compounds.....	99
4.1	Comparison to model dibenzoxazine monomers	100
4.2	Comparison to traditional phenolic compounds.....	100
4.3	Discussion	101
5	Conclusion.....	101
IV	Application of benzoxazine resins in filled compounds.....	105
1	Introduction	105
2	Application of 3DPDS-fa in filled compounds	105
2.1	Understanding the reinforcing mechanism of 3DPDS-fa in filled compounds ...	106
2.1.1	Preparation of green compounds with 3DPDS-fa.....	106
2.1.2	Effect of 3DPDS-fa on the curing of the green compounds	107
2.1.3	Reinforcing effect of 3DPDS-fa in filled compounds	109
2.1.4	Study of the performance of filled compounds with 3DPDS-fa by cyclic tensile test	115

2.2	Investigation of the effect of 3DPDS-fa on the dynamic mechanical properties of filled compounds	117
2.2.1	DMA strain sweep.....	117
2.2.2	DMA temperature sweep.....	120
2.3	Morphological characterization and nanomechanical properties of filled compounds with 3DPDS-fa.....	121
2.3.1	Morphological characterizations	121
2.3.2	Nanomechanical properties	123
2.4	Discussion.....	125
3	Comparison of 3DPDS-fa with other resins	126
3.1	Comparison with additional dibenzoxazine precursors	126
3.2	Comparison with traditional phenolic resins	128
3.2.1	Curing behavior by MDR.....	128
3.2.2	Tensile test.....	129
3.2.3	Dynamic mechanical analysis	130
3.2.4	Cyclic tensile test.....	132
3.3	Discussion.....	133
4	Conclusion	134
	General conclusion.....	137
	Outlook for future research	139
	References.....	143
	Acknowledgement	155
	Publication list.....	157
Annex A.	Materials and methods	159
A.1	Synthesis, molecular and thermal characterization of benzoxazine resins	159
A.1.1	Materials.....	159
A.1.2	Nuclear magnetic resonance (NMR).....	159
A.1.3	Fourier transform infrared spectroscopy (FTIR)	159
A.1.4	Elemental analysis (EA).....	159
A.1.5	Raman spectroscopy	160
A.1.6	Differential scanning calorimetry (DSC).....	160
A.1.7	Thermo-gravimetric analysis (TGA)	160
A.1.8	Rheological measurements	160

A.1.9	Preparation of polybenzoxazines.....	160
A.2	Application of benzoxazine resins in unfilled compounds.....	160
A.2.1	Materials	160
A.2.2	Rubber compounding	161
A.2.3	Moving die rheometer (MDR).....	161
A.2.4	Curing of rubber compounds.....	162
A.2.5	Crosslinking density	162
A.2.6	Atomic force microscopy (AFM).....	163
A.2.7	Tensile test.....	163
A.2.8	Solubility of polybenzoxazines in the presence of sulfur.....	163
A.3	Application of benzoxazine resins in tire compounds.....	163
A.3.1	Materials	163
A.3.2	Rubber compounding	164
A.3.3	Moving die rheometer (MDR).....	165
A.3.4	Curing of rubber compounds.....	165
A.3.5	Crosslinking density	165
A.3.6	Tensile test.....	166
A.3.7	Dynamic mechanical analyses (DMA).....	166
A.3.8	Atomic force microscopy (AFM).....	167
Annex B.	Synthesis and molecular characterization of the structural features.....	168
B.1	Synthesis and characterization of 4DPDS-fa.....	168
B.2	Synthesis and characterization of 4DPDS-a	168
B.3	Synthesis and characterization of 4DPDS-ste.....	169
B.4	Synthesis and characterization of 4DTP-fa.....	170
B.5	Synthesis and characterization of 4DTP-a.....	172
B.6	Synthesis and characterization of BA-fa.....	174
B.7	Synthesis and characterization of BA-a.....	176
B.8	Synthesis and characterization of 3DPDS-fa.....	177
B.9	Synthesis and characterization of 3DPDS-a	178
B.10	Synthesis and characterization of 3DPDS-ste.....	180
Annex C.	Thermal and thermomechanical characterization of benzoxazine resins	183
C.1	Thermal behavior by DSC	183

C.2	Thermal stability by TGA	186
Annex D.	Investigation of benzoxazine curing in the presence of curing system.....	187
D.1	Effect of sulfur on the thermal behavior of benzoxazine precursors	187
D.2	Effect of sulfur on the polymerization of benzoxazine precursors	189
D.3	Solubility of polybenzoxazines in the presence of sulfur.....	189
Annex E.	Application of benzoxazine resins in unfilled compounds	191
E.1	Additional images by AFM.....	191
E.2	Additional figures from tensile test	191
E.3	Additional figures for unfilled compounds with BA-fa	192
E.4	Additional figures for unfilled compounds with PR	193
Annex F.	Application of benzoxazine resins in tire compounds	195
F.1	Additional figures by tensile test of compounds with 3DPDS-fa	195
F.2	Additional images from AFM	196
F.3	Additional figures of compounds with additional diBz	197
F.4	Additional figures of compounds with PR	197

List of Figures

Figure I.1. Tire constructions: a) Bias ply tire and b) radial tire. ¹	6
Figure I.2. Cross-section of a passenger tire. ²	7
Figure I.3. Schematic representation of the most common mixers for rubber compounding: a) internal mixer, and b) two-roll mill. ⁴²	8
Figure I.4. The tire manufacturing process. ⁴⁵	9
Figure I.5. Basic compound components.	9
Figure I.6. Crosslinking network formation during vulcanization. ³²	11
Figure I.7. Generic rheometer cure curve. ⁶⁰	12
Figure I.8. Carbon black: a) particles; b) aggregate; c) agglomerate. ⁷⁰	14
Figure I.9. Surface chemistry of carbon black. ⁷¹	15
Figure I.10. Schematic representation of G' and G'' for a carbon black compound. ⁶⁸	17
Figure I.11. Different contributions to the storage modulus as a function of the strain. ⁷⁵	17
Figure I.12. Schematic illustration of cyclic stress softening behavior of elastomers. ⁸⁰	18
Figure I.13. DSC thermograms of Bz containing 0, 0.5, 1, 2.5 and 5 wt%. ³⁰	45
Figure II.1. ¹ H NMR spectrum in CHCl ₃ of 4DPDS-fa.	57
Figure II.2. ¹³ C NMR spectrum in CHCl ₃ of 4DPDS-fa.	58
Figure II.3. 2D NMR spectra in CHCl ₃ of 4DPDS-fa a) HSQC, b) HMBC.	59
Figure II.4. ¹ H NMR spectrum in DMSO of 4DPDS-a.	59
Figure II.5. ¹³ C NMR spectrum in DMSO of 4DPDS-a.	60
Figure II.6. ¹ H NMR spectrum in CHCl ₃ of 4DPDS-ste.	60
Figure II.7. ¹³ C NMR spectrum in CHCl ₃ of 4DPDS-ste.	61
Figure II.8. FTIR transmission spectrum of 4DPDS-fa.	62
Figure II.9. Raman spectrum of 4DPDS-fa.	63
Figure II.10. Raman spectra of a) 4DPDS-ste, and b) 4DPDS-a.	63
Figure II.11. ¹ H NMR spectrum in CHCl ₃ of 3DPDS-fa.	66
Figure II.12. ¹³ C NMR spectrum in CHCl ₃ of 3DPDS-fa.	67
Figure II.13. FTIR transmission spectrum of 3DPDS-fa.	68
Figure II.14. Raman spectrum of 3DPDS-fa.	69
Figure II.15. Raman spectra of a) 3DPDS-a, and b) 3DPDS-ste.	69

Figure II.16. DSC thermograms at 10 K·min ⁻¹ of diBz: a) BA-fa, b) 4DTP-fa, c) 4DPDS-fa, and d) 3DPDS-fa.....	72
Figure II.17. FTIR transmission spectra of diBz a) 4DPDS-fa, b) 3DPDS-fa, c) 4DTP-fa, and d) BA-fa before and after curing at 170 °C for 1hour.....	73
Figure II.18. DSC thermograms at 10 K·min ⁻¹ of diBz: a) BA-a, b) 4DTP-a, c) 4DPDS-a, and d) 3DPDS-a.	75
Figure II.19. DSC thermograms at 10 K·min ⁻¹ of diBz: a) 4DPDS-ste, and b) 3DPDS-ste....	76
Figure II.20. TGA thermograms of dibenzoxazines from furfurylamine: a) 3DPDS-fa, b) 4DPDS-fa, c) 4DTP-fa, and d) BA-fa.....	77
Figure II.21. Polymerization of furfurylamine-containing diBz followed by rheology over time at 150 °C: a) complex viscosity; b) G' (full line) and G'' (dash line).	78
Figure II.22. Polymerization of aniline-containing diBz followed by rheology over time at 150 °C: a) complex viscosity; b) G' (full line) and G'' (dash line).	79
Figure II.23. Polymerization of stearylamine-containing diBz followed by rheology over time at 150 °C: a) complex viscosity; b) G' (full line) and G'' (dash line).	79
Figure II.24. Rheology curves in temperature sweep mode of a) poly(3DPDS-fa), b) poly(4DPDS-fa), c) poly(4DTP-fa), and d) poly(BA-fa).	80
Figure II.25. Rheology curves in temperature sweep mode of a) poly(4DTP-a), and b) poly(BA-a).....	81
Figure III.1. a) DSC thermogram of 3DPDS-fa with DCBS, ZnO, stearic acid, and sulfur; b) Evolution of T _{poly} with the presence of curing system.....	87
Figure III.2. a) DSC thermogram of 3DPDS-fa, 4DPDS-fa, and 4DTP-fa with and without 30 wt% of sulfur; b) Evolution of T _{poly} of 3DPDS-fa, 4DPDS-fa, and 4DTP-fa as a function of sulfur content. Dash lines serve to guide the eye.	89
Figure III.3. a) Curing behavior of 3DPDS-fa, 4DPDS-fa, and 4DTP-fa with and without 5 wt% of sulfur by rheo-kinetics measurement at 150 °C followed by complex viscosity over time; b) Gelation times of 3DPDS-fa, 4DPDS-fa, and 4DTP-fa as a function of sulfur content. Dash lines are drawn to guide the eye.	90
Figure III.4. MDR cure curves of unfilled compounds without diBz and with a) 5 phr of diBz, b) 15 phr of diBz, and c) 30 phr of diBz.	93
Figure III.5. a) Evolution of t ₉₀ and b) evolution of S' _{max} as a function of the amount of the diBz for unfilled compounds.	94
Figure III.6. Evolution of v _c as a function of the amount of the diBz for unfilled compounds.	94
Figure III.7. a) AFM-AM-FM images of the modulus of unfilled compounds with and without 15 phr of polyBz, b) Measurements of the moduli in each of the phases in the materials.	96
Figure III.8. AFM-AM-FM modulus images and respective histograms of a) poly(3DPDS-fa), b) poly(4DPDS-fa), and c) poly(4DTP-fa). Images depict an area of 5x5µm ²	97

Figure III.9. a) Young modulus as a function of the amount of benzoxazine; b) Stress at 200% of strain as a function of the amount of benzoxazine.	98
Figure III.10. a) Stress-strain curves and b) Stress (MPa) (\pm SD): Young modulus, $\sigma_{200\%$ of strain, $\sigma_{600\%$ of strain, and σ_{break} (from left to right), of reference compound (PI) and compounds containing 3DPDS-fa, and phenolic resin.	101
Figure IV.1. MDR cure curves of compounds with a) 20 phr of CB, b) 50 phr of CB, and c) 80 phr of CB; d) evolution of S'_{max} as the function of 3DPDS-fa.	108
Figure IV.2. a) Evolution of S'_{min} and b) evolution of t_{s1} and t_{90} as a function of the amount of 3DPDS-fa for compounds with 50 phr CB.	108
Figure IV.3. Stress-strain curve of filled compounds with and without 15 phr of 3DPDS-fa.	110
Figure IV.4. a) E and b) $\sigma_{50\%}$ as a function of CB loading for the compounds with and without 15 phr of 3DPDS-fa.	111
Figure IV.5. a) Full stress-strain curve and b) stress-strain curve up to 100% of strain of rubber compound with 20 phr of CB and with 0, 15, and 30 phr of 3DPDS-fa.	111
Figure IV.6. a) Stress-strain curve of rubber compound with 50 phr of CB and with 0, 5, 10, 15, 20, and 30 phr of 3DPDS-fa (on the left); Evolution of $\sigma_{25\%}$ and $\sigma_{150\%}$ as a function of the amount of 3DPDS-fa (on the right); b) Stress-strain curve of rubber compound with 80 phr of CB and with 0, 10, 15, and 30 phr of 3DPDS-fa (on the left); Evolution of E, $\sigma_{15\%}$ and $\sigma_{75\%}$ as a function of the amount of 3DPDS-fa (on the right).	112
Figure IV.7. Crosslinking density of filled compound as a function of the amount of 3DPDS-fa.	113
Figure IV.8. a) Stress-strain curve of rubber compounds with 15 phr of 3DPDS-fa and 80 phr of CB with varying sulfur content (2.8, 5.5 and 6.9 phr); b) Evolution of E, $\sigma_{15\%}$ and $\sigma_{75\%}$ as a function of the sulfur content.	113
Figure IV.9. The first and last cyclic loop for different content of 3DPDS-fa in compounds with a) 20 phr CB; b) 50 phr CB; and c) 80 phr CB.	115
Figure IV.10. Example of the procedure followed to determined ΔE by transforming stress-strain curve into “local” modulus: a) First and last cycling curve; b) Derivative of the curves.	116
Figure IV.11. Normalized softening effect ($\Delta E/\Delta E_{Ref}$) of compounds with different content of 3DPDS-fa and loadings of CB a) as a function of the strain; b) as a function of the ratio 3DPDS-fa/CB.	116
Figure IV.12. DMA strain sweep at 25 °C (on the left) and at 70 °C (on the right) of compounds with 80 phr of CB and with and without 15 phr of 3DPDS-fa; a) b) G' and fitting curve by Kraus model; c) d) G'' , and e) f) $\tan\delta$ (in G'' and $\tan\delta$ the line is to guide the eye).	119
Figure IV.13. DMA temperature sweep of compounds with 80 phr of CB and with and without 15 phr of 3DPDS-fa (E' dashed line; E'' dotted line; $\tan\delta$ full line).	120

Figure IV.14. AFM-AM-FM phase images of rubber compounds with and without 15 and 30 phr of 3DPDS-fa with 80 phr of CB.	122
Figure IV.15. a) AFM-AM-FM phase images of compounds with 20 phr of CB and with and without 15 and 30 phr of 3DPDS-fa, b) average particles' diameter and distance between particles, and c) AFM-AM-FM topography image of PI(CB) ₂₀ (3DPDS-fa) ₃₀	122
Figure IV.16. AFM-AM-FM phase images of rubber compounds with 50 phr of CB and with and without 15 and 30 phr of 3DPDS-fa.....	123
Figure IV.17. a) AFM-AM-FM images of the modulus of rubber compounds with and without 15 and 30 phr of 3DPDS-fa with 80 phr of CB; b) measurements of the moduli in each of the phases in the compounds.....	124
Figure IV.18. a) AFM-AM-FM images of the modulus of rubber compounds with and without 15 and 30 phr of 3DPDS-fa with 20 phr of CB; b) measurements of the moduli in each of the phases in the compounds.....	125
Figure IV.19. a) Stress-strain curve of rubber compounds with 15 phr of diBz and 80 phr of CB; b) Evolution of E and $\sigma_{100\%}$ for the compounds.	127
Figure IV.20. a) Stress-strain curves of rubber compound with 80 phr of CB with and without reinforcing resins; b) Evolution of E, $\sigma_{15\%}$ and $\sigma_{50\%}$ for the compounds.....	129
Figure IV.21. a) Stress-strain curves of rubber compound with 80 phr of CB with and without PR, and with 3DPDS-fa with 6.9 phr of sulfur; b) Stress responses at 15, 25, 50, and 100% of strain.....	130
Figure IV.22. Strain sweeps at 25 °C (on the left) and at 70 °C (on the right) of compounds with 80 phr of CB and with and without 15 phr of 3DPDS-fa or PR; a) b) G' and fitting curve by Kraus model; c) d) G'', and e) f) tan δ (in G'' and tan δ the line is to guide the eye).	131
Figure IV.23. DMA temperature sweep of compounds with 80 phr of CB and with and without 15 phr of 3DPDS-fa or PR (E' dashed line; E'' dotted line; tan δ full line).....	132
Figure IV.24. Stress-strain hysteresis loops of cyclic test of a) PI(CB) ₈₀ (3DPDS-fa) ₁₅ , and b) PI(CB) ₈₀ (PR) ₁₅ ; Stabilized stress-strain hysteresis loop after 10 th cycles of c) PI(CB) ₈₀ (3DPDS-fa) ₁₅ , and d) PI(CB) ₈₀ (PR) ₁₅	133
Figure A.1. The cyclic tensile test program to evaluate cyclic stress softening behavior.	166
Figure B.1. 2D NMR spectra in DMSO of 4DPDS-a HSQC on the left and HMBC on the right.	169
Figure B.2. FTIR transmission spectrum of 4DPDS-a.	169
Figure B.3. FTIR transmission spectrum of 4DPDS-ste.....	170
Figure B.4. ¹ H NMR spectrum in CHCl ₃ of 4DTP-fa.	171
Figure B.5. ¹³ C NMR spectrum in CHCl ₃ of 4DTP-fa.	171
Figure B.6. 2D NMR spectra in CHCl ₃ of 4DTP-fa HSQC on the left and HMBC on the right.	172
Figure B.7. FTIR transmission spectrum of 4DTP-fa.....	172

Figure B.8. ^1H NMR spectrum in DMSO of 4DTP-a.	173
Figure B.9. ^{13}C NMR spectrum in DMSO of 4DTP-a.	173
Figure B.10. 2D NMR spectra in DMSO of 4DTP-a HSQC on the left and HMBC on the right.	174
Figure B.11. FTIR transmission spectrum of 4DTP-a.....	174
Figure B.12. ^1H NMR spectrum in CHCl_3 of BA-fa.	175
Figure B.13. ^{13}C NMR spectrum in CHCl_3 of BA-fa.....	175
Figure B.14. FTIR transmission spectrum of BA-fa.	175
Figure B.15. ^1H NMR spectrum in DMSO of BA-a.	176
Figure B.16. ^{13}C NMR spectrum in DMSO of BA-a.	177
Figure B.17. FTIR transmission spectrum of BA-a.....	177
Figure B.18. 2D NMR spectra in CHCl_3 of 3DPDS-fa HSQC on the left and HMBC on the right.....	178
Figure B.19. ^1H NMR spectrum in CHCl_3 of 3DPDS-a.....	179
Figure B.20. ^{13}C NMR spectrum in CHCl_3 of 3DPDS-a	179
Figure B.21. 2D NMR spectra in CHCl_3 of 3DPDS-a HSQC on the left and HMBC on the right.	179
Figure B.22. FTIR transmission spectrum of 3DPDS-a.....	180
Figure B.23. ^1H NMR spectrum in CHCl_3 of 3DPDS-ste.	180
Figure B.24. ^{13}C NMR spectrum in CHCl_3 of 3DPDS-ste.....	181
Figure B.25. FTIR transmission spectrum of 3DPDS-ste.	181
Figure C.1. DSC thermograms at 5, 10 and 20 $\text{K}\cdot\text{min}^{-1}$ of 3DPDS-fa, and 4DPDS-fa.	183
Figure C.2. DSC thermograms at 5, 10 and 20 $\text{K}\cdot\text{min}^{-1}$ of 4DTP-fa, and BA-fa.....	183
Figure C.3. Kissinger and Ozawa plots for 3DPDS-fa, and 4DPDS-fa.	183
Figure C.4. Kissinger and Ozawa plots for 4DTP-fa, and BA-fa.....	184
Figure C.5. DSC thermograms at 5, 10 and 20 $\text{K}\cdot\text{min}^{-1}$ of 3DPDS-a, and 4DPDS-a.	184
Figure C.6. DSC thermograms at 5, 10 and 20 $\text{K}\cdot\text{min}^{-1}$ of 4DTP-a, and BA-a.	184
Figure C.7. Kissinger and Ozawa plots for 3DPDS-a, and 4DPDS-a.	185
Figure C.8. Kissinger and Ozawa plots for 4DTP-a, and BA-a.	185
Figure C.9. DSC thermograms at 5, 10 and 20 $\text{K}\cdot\text{min}^{-1}$ of 3DPDS-ste, and 4DPDS-ste.....	185
Figure C.10. Kissinger and Ozawa plots for 3DPDS-ste, and 4DPDS-ste.....	186
Figure C.11. TGA thermograms of dibenzoxazines from aniline: a) 3DPDS-a, b) 4DPDS-a, c) 4DTP-a, and d) BA-a.....	186

Figure C.12. TGA thermograms of dibenzoxazines from stearylamine: a) 3DPDS-ste, and b) 4DPDS-ste.....	186
Figure D.1. DSC thermograms at 10 K·min ⁻¹ of 3DPDS-fa, and 4DPDS-fa with and without 1, 5, 10, 20 and 30 wt% of sulfur.....	187
Figure D.2. DSC thermograms at 10 K·min ⁻¹ of 4DTP-fa with and without 1, 5, 10, 20 and 30 wt% of sulfur.....	187
Figure D.3. DSC thermograms at 5, 10 and 20 K·min ⁻¹ of 3DPDS-fa, and 4DPDS-fa with 30 wt% of sulfur.....	187
Figure D.4. DSC thermograms at 5, 10 and 20 K·min ⁻¹ of 4DTP-fa with 30 wt% of sulfur.	188
Figure D.5. Kissinger and Ozawa plots for 3DPDS-fa, and 4DPDS-fa, with 30 wt% of sulfur.	188
Figure D.6. Kissinger and Ozawa plots for 4DTP-fa, with 30 wt% of sulfur.....	188
Figure D.7. Curing behavior of 3DPDS-fa, and 4DPDS-fa with and without 1, and 5 wt% of sulfur by rheo-kinetics measurement at 150 °C followed by complex viscosity over time...	189
Figure D.8. Curing behavior of 4DTP-fa with and without 1, and 5 wt% of sulfur by rheo-kinetics measurement at 150 °C followed by complex viscosity over time.	189
Figure E.1. AFM-AM-FM loss tangent images and measurements of the property in each of the phases in the material. Images depict an area of 20x20 μm ²	191
Figure E.2. Stress-strain curves of unfilled compounds with and without 5, 15 and 30 phr of 3DPDS-fa, 4DPDS-fa, and 4DTP-fa.....	192
Figure E.3. MDR cure curves of unfilled compounds with and without 5, 15, and 30 phr of BA-fa.....	192
Figure E.4. Stress-strain curves of unfilled compounds with and without 5, 15, and 30 phr of BA-fa.....	192
Figure E.5. Stress-strain curves of unfilled compounds with and without 15 phr of PR.....	193
Figure F.1. All stress-strain curves of rubber compound with 20 and 50 phr of CB and various amount of 3DPDS-fa.....	195
Figure F.2. All stress-strain curves of rubber compound with 80 phr of CB and various amount of 3DPDS-fa and different sulfur content.	195
Figure F.3. Average particles' diameter and distance between particles from AFM-AM-FM phase images of rubber compounds with 50 phr of CB and with and without 15 and 30 phr of 3DPDS-fa.	196
Figure F.4. AFM-AM-FM images of the modulus of rubber compounds with and without 15 and 30 phr of 3DPDS-fa with 50 phr of CB. Measurements of the moduli in each of the phases in the compounds (at the bottom).	196
Figure F.5. MDR cure curves and stress-strain curves of filled compounds with and without 15 phr of diBz.	197

Figure F.6. MDR cure curves and stress-strain curves of filled compounds with 7 and 15 phr of PR. 197

List of Schemes

Scheme I.1. Chemical structure of main elastomers used in rubber compounding: a) Natural rubber or polyisoprene, b) polybutadiene, and c) styrene-butadiene rubber.	10
Scheme I.2. Reaction scheme for accelerated-sulfur vulcanization with benzothiazole-sulfenamide accelerators. ³²	14
Scheme I.3. Schematic structure of phenol-formaldehyde resins a) novolac resin b) resole resin.	19
Scheme I.4. Chemical structures of commonly used curing agent for novolac resin a) HMT b) HMMM.....	20
Scheme I.5. Crosslinking of novolac phenolic resin with hexamethylenetetramine (HMT), a) novolac resin, b) crosslinked novolac with HMT.....	20
Scheme I.6. Modification of phenolic resins with tall oil (TO) or cashew nut shell liquid (CNSL).	22
Scheme I.7. Synthesis of benzoxazine resin.....	23
Scheme I.8. Two-step mechanism for the synthesis of monobenzoxazine monomers. ¹⁰⁵	24
Scheme I.9. Schematic representation of benzoxazine monomers.....	24
Scheme I.10. Ring-opening polymerization of benzoxazines.	25
Scheme I.11. Proposed polymerization temperature and catalyst effect on benzoxazine polymerization mechanism and inner structure of polybenzoxazines. ³³	26
Scheme I.12. Polymerization routes of furan-containing benzoxazines.	28
Scheme I.13. Synthesis of functionalized polybutadiene with side-chain Bz. ²¹	40
Scheme I.14. Thiol functionalized benzoxazine.....	41
Scheme I.15. The reversible ring-opening reaction of sulfur.....	42
Scheme I.16. Pictorial depiction of the structure of random copolymer of sulfur and cardanol based benzoxazine. ¹⁷⁹	43
Scheme I.17. Synthesis of polyBz copolymers with bisphenol A and allylamine benzoxazine and sulfur.	43
Scheme I.18. Synthesis of self-healing polyBz by using PPOB, B-al, and S ₈ with various mixing ratios.	44
Scheme I.19. Reaction mechanism between S ₈ and benzoxazines through the SRTC reaction and thiol-benzoxazine addition reaction. ³¹	45
Scheme I.20. The reaction of benzoxazine derived from aliphatic amines with aromatic and aliphatic thiols.	46

Scheme I.21. The reaction of benzoxazine derived from aromatic amines with aromatic thiol.	47
Scheme I.22. Proposed mechanism for the ring-opening of benzoxazines by thiols.....	47
Scheme I.23. Reversible polymerization-depolymerization of BA-a and 1,6-hexanedithiol. .	47
Scheme I.24. Synthesis of polybenzoxazine precursor and its modification with thiols. ¹⁸⁵	48
Scheme I.25. Dibenzoxazine monomer from bisphenol F and aniline (BF-a).	48
Scheme I.26. Dibenzoxazine from phenol and 4,4'-diaminodiphenylmethane (P-ddm).	48
Scheme I.27. DiBz from bisphenol and silicon-containing amine.	49
Scheme I.28. Polybenzoxazines for adhesion between metallic cord and rubber.	49
Scheme I.29. Sulfurized polybenzoxazines for coating metallic cord and bonding to rubber.	50
Scheme I.30. Main chain benzoxazines from bisphenol A and 4,4'-diaminodiphenylmethane (BA-ddm) where n is a number from 0 to 10 a) BA-ddm end-capped with ethanolamine, b) BA-ddm end-capped with allylamine.	50
Scheme II.1. Chemical structures of the diphenols.....	55
Scheme II.2. Synthesis of 4,4'-substituted benzoxazine monomers containing disulfide bond.	56
Scheme II.3. Synthesis of 4,4'-substituted benzoxazine monomers from bisphenol A and 4,4'-thiodiphenol.	63
Scheme II.4. Synthesis of 3,3'-substituted benzoxazine monomers containing disulfide bond.	65
Scheme III.1. Schematic representation of the effect of sulfur on benzoxazine monomers previously reported: a) Triggering effect of sulfur on the ROP of benzoxazines ³⁰ ; b) Reaction between sulfur and benzoxazines to form copolymers ³¹	88
Scheme III.2. Schematic representation of possible reactions between elemental sulfur and benzoxazines a) through the oxazine ring SRTC reaction ^{14,31} , and b) through the disulfide bond forming a polysulfide (in the case of 4DPDS-fa).	91

List of Tables

Table I.1. The most widely used accelerators for sulfur vulcanization.	13
Table I.2. Summary of the chemical features of the diphenols and monoamines used for the synthesis of Class A diBz and their thermal properties.	29
Table I.3. Summary of the chemical features of the diamines and monophenols used for the synthesis of Class B diBz and their thermal properties.	34
Table I.4. Type of benzoxazine and rubber used for the elaboration of blends and their properties.	39
Table I.5. Summary of the content of the patent literature related to tires and benzoxazines..	50
Table II.1. Abbreviations, chemical structure of the diphenols and the monoamines used for the synthesis of 4,4'-substituted Bz containing disulfide, reaction conditions, and yields.....	57
Table II.2. Structural characteristics by NMR of 4,4'-substituted Bz containing disulfide bond.	61
Table II.3. Characteristic IR absorption bands from 4,4'-substituted Bz containing disulfide bond.	62
Table II.4. Abbreviations, chemical structure of the diphenols and the monoamines used for the synthesis of 4,4'-substituted Bz, reaction conditions, and yields.	64
Table II.5. Structural features of 4,4'-substituted Bz by NMR and FTIR.	64
Table II.6. Abbreviations, chemical structure of the diphenols and the monoamines used for the synthesis of 3,3'-substituted Bz containing disulfide, reaction conditions, and yields.....	65
Table II.7. Structural characteristics by NMR of 3,3'-substituted Bz containing disulfide bond.	67
Table II.8. Characteristic IR absorption bands from 3,3'-substituted Bz containing disulfide bond.	68
Table II.9. Summary of the structural features, and purity of the synthesized dibenzoxazines monomers.	70
Table II.10. Thermal behavior and polymerization kinetic parameters of furfurylamine-containing diBz.....	74
Table II.11. Thermal behavior and polymerization kinetic parameters of aniline-containing diBz.....	75
Table II.12. Thermal behavior and polymerization kinetic parameters of stearylamine-containing diBz.....	76
Table II.13. Thermal stability of diBz by TGA.....	77
Table II.14. Gelation time of diBz by rheological measurements at 150 °C.....	80
Table II.15. The α -relaxation temperatures of polyBz by rheological measurements.	81

Table II.16. Summary of thermal and curing properties of the synthesized diBz monomers and their polyBz.....	82
Table III.1. Thermal behavior and polymerization kinetic parameters of 3DPDS-fa, 4DPDS-fa, and 4DTP-fa with 30 wt% of sulfur.....	89
Table III.2. Gelation time of 3DPDS-fa, 4DPDS-fa, and 4DTP-fa with 1 and 5 wt% of sulfur by rheological measurements at 150 °C.....	90
Table III.3. Formulation of unfilled polyisoprene compounds with 3DPDS-fa, 4DPDS-fa, and 4DTP-fa system and carbon black	92
Table III.4. Summary of the curing properties and crosslinking densities of unfilled compounds with and without dibenzoxazines.....	95
Table III.5. Summary of the mechanical properties of unfilled compounds with and without dibenzoxazines.....	98
Table III.6. Summary of the mechanical properties of unfilled compounds with BA-fa.	100
Table III.7. Summary of the mechanical properties of unfilled compounds with PR.	100
Table IV.1. Recipe of a model formulation for apex compounds.....	106
Table IV.2. Summary of the formulations of compounds with 3DPDS-fa and carbon black.....	107
Table IV.3. MDR data for compounds with carbon black and 3DPDS-fa.	109
Table IV.4. Summary of the tensile test data and crosslinking density for compounds with CB and 3DPDS-fa.	114
Table IV.5. Viscoelastic results from DMA test in strain sweep mode for compounds with CB and 3DPDS-fa.	119
Table IV.6. Viscoelastic results by DMA tests in temperature sweep mode for compounds with CB and 3DPDS-fa.....	120
Table IV.7. MDR data for compounds with carbon black and diBz.	126
Table IV.8. Summary of the tensile test data and crosslinking density for compounds with CB and diBz.	127
Table IV.9. Formulation of compounds with PR system and carbon black.	128
Table IV.10. MDR data for compounds with carbon black, 3DPDS-fa and PR.	128
Table IV.11. Summary of the tensile test data and crosslinking density for compounds with CB and PR.....	130
Table IV.12. Viscoelastic results from DMA test in strain sweep mode for compounds with CB and PR.....	131
Table A.1. Procedure carried out for the rubber compounding for unfilled compounds.....	161
Table A.2. Procedure carried out for the rubber compounding for filled compounds.....	164
Table E.1. Formulation containing polyisoprene and phenolic system.	193

List of Abbreviations

1,10BOP	4,4'-(Butane-1,10-diyibis(oxy)diphenol)
1,12da	1,12-Diaminododecane
1,3da	1,3-Diaminopropane
1,4BOP	4,4'-(Butane-1,4-diyibis(oxy)diphenol)
1,4da	1,4-Diaminobutane
1,5DHN	1,5-Dihydroxynaphtalene
1,6BOP	4,4'-(Butane-1,6-diyibis(oxy)diphenol)
1,6da	1,6-Hexanediamine
1,8BOP	4,4'-(Butane-1,8-diyibis(oxy)diphenol)
1,8da	1,8-Diaminooctane
3,BO	3-Buthoxyphenol
3,MO	3-Methoxyphenol
34appe	Bis-(3-(4-aminophenoxy)phenyl)ether
3DPDS	3,3'-Dihydrohydiphenyldisulfide
44appe	(4-(4-Aminophenoxy)phenyl)ether
4DPDS	4,4'-Dihydrohydiphenyldisulfide
4DTP	4,4'-Thiodiphenol
a	Aniline
Abbr.	Abbreviation
abn	4-Aminobenzonitrile
AFM	Atomic force microscopy
ala	Allylamine
apa	Aminophenyl acetylene
appe	Propargyl ether aniline
appp	2,2-Bis(4-(4-aminophenoxy)phenyl)propane
ASTM	American Society for Testing and Materials
ATBN	Amine terminated butadiene/acrylonitrile rubber
BA	Bisphenol A
ba	Butylamine
BC	Before Christ
BF	Bisphenol F

BN	β -Naphthol
BO	Bisphenol O
BP	Bisphenol P
BPBA	Benzaldehyde-based bisphenol
BR	Butadiene rubber
BS	Bisphenol S
BZ	Bisphenol Z
Bz	Benzoxazine
ca	Cyclohexylamine
CAR	Cardanol
CB	Carbon black
CBS	N-Cyclohexyl benzothiazole-2-sulfenamide
CHCl₃	Chloroform
CNSL	Cashew nut shell liquid
COLBERT	Catalytic opening of the lateral benzoxazine rings by thiols
CT	Catechol
CTBN	Carboxyl terminated butadiene/acrylonitrile rubber
CY	Char yield
da	Ethylenediamine
DABA	2,2'-Diallylbisphenol A
DCBS	N,N'-Dicyclohexylbenzothiazole-2-sulfenamide
dde	(4-Aminophenyl)ether
ddm	4,4'-Diaminodiphenylmethane
ddpo	4,4'-(p-Biphenylenedioxy) dianiline
ddps	1,4[Bis(4'-aminophenoxy) phenyl sulfone]
dds	4,4'-Diamino diphenyl sulfone
diBz	Dibenzoxazine monomer
DMA	Dynamic mechanical analysis
DMF	Dimethylformamide
DMSO	Dimethyl sulfoxide
DPA	4,4-Bis(4-hydroxyphenyl)valeric acid
DSC	Differential scanning calorimetry
DZ	Daidzein
E	Eugenol

EA	Elemental analysis
ETBN	Epoxy-terminated liquid nitrile rubber
fa	Furfurylamine
FTIR	Fourier transform infrared spectroscopy
G	Guaiacol
HEBD	High epoxy content butadiene rubber
HMBC	Heteronuclear multiple bond correlation
HMMM	Hexamethoxymethylmelamine
HMT	Hexamethylenetetramine
HPPDIO	1-(4-Hydroxyphenyl)-1h-pyrrole-2,5-dione
HSQC	Heteronuclear single quantum coherence
HTBD	Hydroxyl-terminated butadiene rubber
ima	Isomannide diamine
LEBD	Low epoxy content butadiene rubber
M	Magnolol
MBT	2-Mercaptobenzothiazole
MBTS	2,2'-Dithiobisbenzothiazole
mBz	Monobenzoxazine monomer
MDR	Moving die rheometer
NaOH	Sodium hydroxide
NBR	Nitrile-butadiene rubber
NMR	Nuclear magnetic resonance spectroscopy
npda	2,7-Bis(4-aminophenoxy)naphtalene
NR	Natural Rubber
oAP	o-Allylphenol
P	Phenol
pd	1,4-Phenylenediamine
ph	Phthalonitrile
phr	Parts per hundred rubber
PI	Polyisoprene / isoprene rubber
polyBz	Polybenzoxazine
PPOB	Poly(propylene oxide)benzoxazine
PR	Phenolic resin
R	Resorcinol

REACH	Registration, evaluation, authorization and restriction of chemicals
Ref.	Reference
RES	Resveratrol
ROP	Ring-opening polymerization
RR	Rolling resistance
S₈	Elemental sulfur
SBR	Styrene-butadiene rubber
SiO₂	Silica
SRTC	Sulfur radical transfer and coupling reaction
ste	stearylamine
TYM	Thymol
TBBS	N-t-Butyl benzothiazole-2-sulfenamide
TBzTD	Tetrabenzylthiuram disulfide
TEM	Transmission electron microscope
TGA	Thermo-gravimetric analysis
TMTD	Tetramethylthiuram disulfide
TMTM	Tetramethylthiuram monosulfide
TO	Tall Oil
tu	Thiourea
U	Urushiol
V	Vanillin
ZDEC	Zinc diethyldithiocarbamate
ZDMC	Zinc dimethyldithiocarbamate
ZnO	Zinc oxide

List of Symbols and Units

°C	Degree Celsius
E	Young modulus
E' / G'	Elastic or storage modulus
E'' / G''	Loss or viscous modulus
E_{1st}	Derivative ($\delta\sigma/\delta\varepsilon$) of the first cycle
E_{5th}	Derivative ($\delta\sigma/\delta\varepsilon$) of the fifth cycle
E_a	Activation energy
g	Gram
h	hour
Hz	Hertz
J	Joule
K	Kelvin
m	Meter
min	Minute
N	Newton
Pa	Pascal
s	Second
S'	Torque
S'_{max}	Maximum torque
S'_{min}	Minimum torque
T_{5%}	5 wt% Loss temperature
t₉₀	Optimum cure time
tanδ	Loss factor
T_g	Glass transition temperature
t_{gel}	Gelation time
T_m	Melting temperature
T_{onset}	Onset temperature
T_{poly}	Ring-opening polymerization temperature
t_{s1}	Scorch time
wt%	Weight percentage

β	Heating rate
γ	Shear amplitude
γ_c	Critical amplitude
ΔE	Rate of cyclic stress softening
$\Delta G'$	Payne effect
ΔH	Enthalpy of ring-opening polymerization
ε	Strain / elongation
η^*	Complex viscosity
ν_c	Crosslinking density
σ	Stress

General introduction

Tires are essential elements in our daily lives as they are key components of most of the means of transportation such as automobiles, trucks, and aircraft.¹ Tires are complex composites composed of several parts assembled together, each of which has specific features.² The combination of different materials such as rubber, fillers, chemical additives, cord and steel is present in modern pneumatic tires, which enables to reach the required performance.³ Among the different component of a tire, the apex is a triangular extruded profile that is attached on the beads, which are non-extensible steel wires.² Their main responsibility is to lock the tire on the wheel. Particularly, the apex compound provides a cushion between the rigid bead and the flexible inner structure of the tire. The compound used to produce the apex is usually formulated to have good dynamic stiffness, strength, and durability thanks to the combination of fillers and additives such as conventional reinforcing polymeric resins.

Among the polymeric resins, novolac-type phenolic resins (PR) are the most employed.⁴⁻⁵ These thermoplastic type PR are formaldehyde pre-condensates from phenol or resorcinol and are commonly cured to get a crosslinked structure.⁶⁻⁷ Phenolic resins are usually mixed with the rubber in the presence of an *in-situ* crosslinker, which allows the crosslinking of the PR simultaneously with the rubber vulcanization.⁸⁻⁹ During the compounding, PR generally melt reducing the viscosity of the compounds and therefore improving their processability. However, after the vulcanization the formed crosslinking network enables the resin to improve the stiffness and strength of the tire part. Even though a good performance is observed, several shortcomings are arising from the use of PR being more and more challenged by European regulations such as REACH (registration, evaluation, authorization and restriction of chemicals).¹⁰⁻¹¹ Moreover, phenolic resins are mainly produced from petroleum-based reagents being also challenged by society. The development of suitable and more sustainable alternatives has become desirable.

In this context, benzoxazine resins (Bz) have emerged as a promising substitute for phenolic resins with the possibility to overcome the shortcomings mentioned above. Benzoxazines are monocomponent resins, readily synthesized in a one-step reaction through a Mannich-like condensation of phenolic compounds, formaldehyde, and primary amines.¹² Then, they are polymerized through a thermally triggered, auto-catalyzed ring-opening polymerization (ROP) to form polybenzoxazines (polyBz).¹³ Interestingly, the release of byproducts during their polymerization is substantially lower than those released during the polymerization process of traditional resins.^{12, 14} In comparison to phenolic resins, polyBz show better thermal properties, modulus, strength, and elongation at break allowing the investigation of polybenzoxazines as reinforcing resins for tire applications.^{12,15} Moreover, polyBz exhibit an extremely rich molecular design flexibility making possible to tailor the mechanical and physical properties for the target application. This molecular versatility also allows the partial or total replacement of petroleum-based reagents by bio-based resources for their synthesis allowing the improvement of sustainability.

Heretofore the combination of rubber and benzoxazines has been mainly focused either on the improvement of the toughness of polybenzoxazine matrixes¹⁶⁻²⁰ or the employment of

benzoxazines to functionalize rubbers²¹⁻²³. The prior art of polybenzoxazines to reinforce rubber compounds is very limited and do not clearly lead to a substitution of phenolic resins.²⁴⁻²⁹ Surprisingly, the literature concerning this topic is not rich, despite the potential scope of this field due to the versatility of polybenzoxazines. Two main reasons could impede the development of polyBz to reinforce rubber: (1) the potential interactions and/or reactions between the rubber curing additives and benzoxazines previously reported³⁰⁻³¹, and (2) disparities on the curing kinetic of rubber and benzoxazine resins³²⁻³³. In conclusion, the application of polybenzoxazines to reinforce rubber compounds, and more precisely, to replace phenolic resins, remains uncertain.

The main objective of this work is to study the feasibility of benzoxazine resins to be used as potential alternatives to phenolic resins to reinforce rubber compounds. Ideally, the develop of polybenzoxazines more sustainable and not covered by prior art is desirable. In this context, the design of traditional and novel benzoxazine monomers was performed. Along the manuscript, the different problematics to be considered for the employment of these resins in tire compounds are addressed. To that aim, the investigation of the impact of the curing package on the polymerization of the benzoxazine precursors was carried out. This deep understanding was expected to elucidate potential structural features of benzoxazines to reinforce carbon black filled compounds. In order to address these topics, this thesis is divided in four chapters.

In the first chapter, a literature review is reported covering an introduction to tire compounds emphasizing the use of phenolic resins for rubber applications. The recent state of the art of benzoxazine resins is thus introduced, outlining the relevant prior art to the topic investigated in this study. The potential interactions between benzoxazine resins and rubber curing additives are also reported, highlighting the potential challenges to employ polyBz to reinforce rubber.

Chapter II describes the design, synthesis, molecular and thermal characterization of novel benzoxazine precursors. Traditional and new benzoxazine molecules were designed. The incorporation of bio-based reagents enabled the production of more sustainable monomers. Moreover, the impact of the benzoxazine functional groups on the reactivity and properties of the materials was assessed. Finally, the precursors with the most promising thermomechanical and processing properties were selected to be used as potential reinforcing resins in rubber compounds.

The application of the selected benzoxazines in unfilled rubber compounds is reported in Chapter III. The chapter addresses first the polymerization behavior of the monomers in the presence of the curing package, specially sulfur. A second part of the chapter concerns the investigation of the curing and reinforcing effect of the benzoxazine precursors in a simplified tire recipe, i.e. exempted of fillers. This study helps to highlight the most important parameter to be considered when benzoxazines are considered for the reinforcement of a vulcanized rubber compounds.

Finally, in Chapter IV, the experimental results generated from the characterization of carbon black filled compounds prepared with the novel benzoxazines are presented and discussed. In this chapter is described the effect of the filler loading and benzoxazine amounts, allowing the mapping of the formulation-to-properties relationship. The reinforcing effects are finally compared to traditional compounds prepared with phenolic resins.

Chapter I:

Literature review

I Literature review

1 Introduction

This chapter is divided in six sections. The first part reports a literature review related to tire compounds and technology covering from basic tire design to rubber compounding. The literature review of the use of phenolic resins to reinforce rubber compounds is described in the second part. The third section covers an introduction to benzoxazine resins, their chemistry and synthesis, and the structure-to-properties relationship. After that, a state of the art of the use of polybenzoxazines for rubber applications and the potential interactions between benzoxazine resins and rubber curing additives is reported. These studies highlight the potential challenges to employ polyBz to reinforce rubber compounds. Finally, a summary of the prior art of polybenzoxazine in tire applications is gathered allowing to find the gap to be able to develop new alternatives to reinforce rubber compounds based on polybenzoxazines.

2 Introduction to tire compounds and technologies

2.1 History of Tires

The wheel was invented around 3500 BC, becoming one of humanity's greatest inventions.³⁴ In its earliest form, the wheel was a curved piece of wood, eventually coated with leather or reinforced with copper or iron to prevent damages to the wooden wheel frame. Over time, rubber replaced the leather. The original rubber tire was a solid rubber, without air, used for low-speed vehicles.³⁵

Afterward, one of the most important discoveries in the field of wheels was the vulcanization of rubber in 1839 by Goodyear, making possible the conversion of rubber from a sticky soft material to a firm pliable material, particularly suitable to the shape and specifications of tires.³⁶ Additionally, in 1847, the first vulcanized pneumatic tire consisting of a rubber air tube fixed onto a wheel was patented.³⁷ This invention aimed at reducing both the power required for the vehicle to move and the noise produced by the contacts of the wheels with the ground.³⁷ However, it was not until the 1880s when the first practical pneumatic tire was developed for bicycles.³⁸ All these inventions together with the industrial revolution enabled the tire to evolve from a rubberized canvas covering a rubber tube to a complex fabric, steel, and elastomeric composite.³⁵ Tires are key elements for most of the means of transportation such as automobiles, trucks, and aircraft. The pneumatic tire is the most complex composite produced in large scale and also one of the most complex part of a vehicle.¹

In the 1950s, most of the tires were built following a bias ply construction. Bias ply tires are constructed with ply cords laid diagonally across the tire at a degree angle ranging from 30 to 45° of the tread centerlines, from bead to bead. They required the use of an inner tube for air retention (Figure I.1).¹

In the 1960s, the radial tire emerged with significant improvements in mileage, fuel economy, and safety. Radial tires are built with ply cords laid at a 90° angle to the direction of the travel extended from bead to bead (Figure I.1). Reinforcing belts are added between the radial plies and the tread to stabilize the casing. They are usually made of steel or fabric oriented at a

relatively low angle (12-25°). This development was followed by the introduction of the tubeless tire constructed with halogenated butyl rubber liners.¹

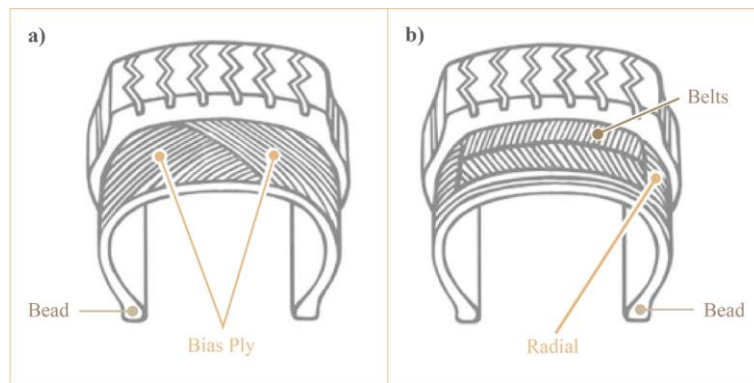


Figure I.1. Tire constructions: a) Bias ply tire and b) radial tire.¹

Overall, pneumatic tires must meet a fundamental set of performance features. They must be durable and safe throughout their expected service life.³⁵ Tires have to provide load-carrying capacity and damping at the same time that they generate minimum noise and vibrations. Additionally, they are required to transmit driving cornering, steering, and braking torque.¹ Finally, tires must resist abrasion and have low rolling resistance. Generally speaking, the rolling resistance (RR) of a tire on a surface accounts for the amount of energy wasted by the automobile vehicle to move forward. The mechanical energy is converted into heat.³⁹ Among all the internal and external factors affecting RR, it is estimated that hysteretic losses represent around 80-95% of the total rolling resistance.³⁹ The hysteresis is the dissipation of energy that occurs as a result of the viscoelastic behavior of the tire compounds when they are cyclically deformed during rolling.³⁹ Improvements in rolling resistance are crucial as the automotive industry strives for a better fuel economy. Because of this, it is essential that a careful selection of the materials to produce tires.⁴⁰ This topic will be addressed later on in the text.

2.2 Basic tire design

A tire is a complex cord-rubber composite composed of different parts, each of which has specific functions in the service and performance of the product. An example of a cross-section of a tire is displayed in Figure I.2.²

The primary components governing the performances of a tire are the inner liner, plies, belts, beads, sidewalls, and tread.²

- The inner liner, also known as halobutyl liner, consists of compounded elastomers with low air permeability. Bromobutyl rubber or chlorobutyl rubber are commonly employed allowing the air retention inside the tire.
- Plies are textile or steel cords coated with rubber extending transversely from bead to bead and serve as the main reinforcement of the tire casing.
- Belts are rubber-coated layers of textile, steel, and other materials which serve to stiffen the casing. They are located between the tread and the plies. Belts protect the plies and improve wear performance, vehicle stability, and damage resistance.

- Beads are non-extensible steel wires, which anchor the plies and lock the tire onto the wheel. Bead area includes the apex or bead filler which is a triangular piece of stiff rubber that provides a cushion between the rigid bead and the flexible body plies in the sidewall and the inner liner.
- Sidewalls are located on each side of the tire between the edge of the tread and the beads. The sidewall protects the tire casing from damage and assists in tread support.
- The tread is the part of the tire that is in contact with the road and provides traction, wet skid, and fuel economy, and service-related damage. A tread base is commonly placed under the tread to dissipate heat from the tread and to ensure good adhesion between the tread and the tire casing. Tread components are mainly rubber, fillers and additives.

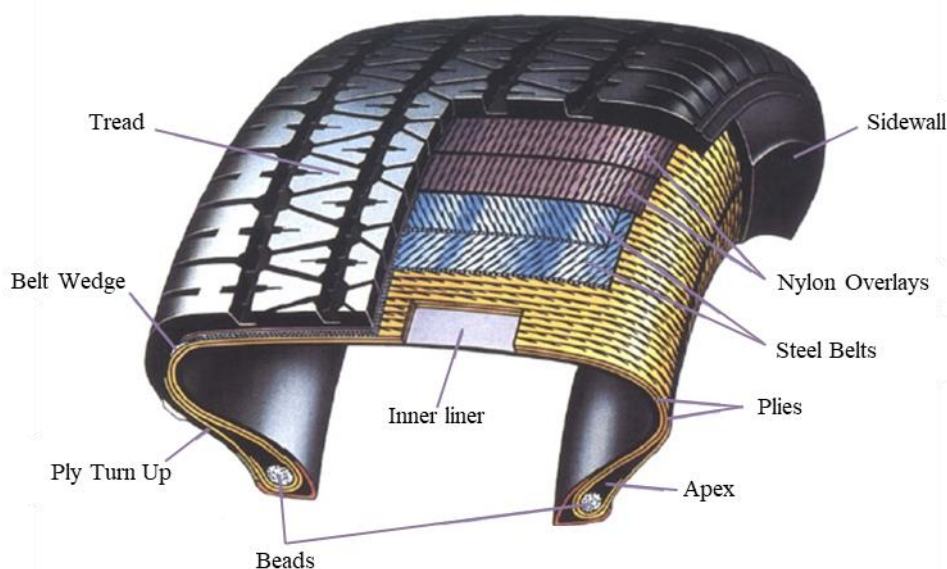


Figure I.2. Cross-section of a passenger tire.²

2.3 Compound processing

The rubber compounds are commonly prepared using internal mixers.⁴¹ A schematic representation of an internal mixer is depicted in Figure I.3a.⁴² They consist of two rotors counter-rotating in an enclosed metal cavity so-called mixing chamber. The rubber ingredients are introduced into the chamber through a loading chute, the hopper. The generation of mixing shear forces allows the incorporation of the fillers, sulfur, and other raw materials into the rubber resulting in the production of homogenous compounds.³ The ram is a floating weight assembled on the top of the chamber and serves to confine the batch in the mixing space and apply pressure on it.⁴³ Once the mixing time is reached, the compound is dropped onto a two-roll mill to finish the mixing and convert it into a sheet for further processing (Figure I.3b). The mixing operation is carefully designed to enable a uniform dispersion of all the ingredients. Mixing speed, mixing time and temperature are defined for each compound.⁴⁴ The mixing process can be divided in different steps depending on the complexity of the formulation, and application for which the compound is intended. In the first stages, typically, the rubber, fillers, oils, antioxidants, zinc oxide and stearic acid are mixed, in one or several steps. Finally, in the last stage, the curing system is added to the compound and mixed up to a temperature not exceeding 110-115 °C to avoid early vulcanization.³

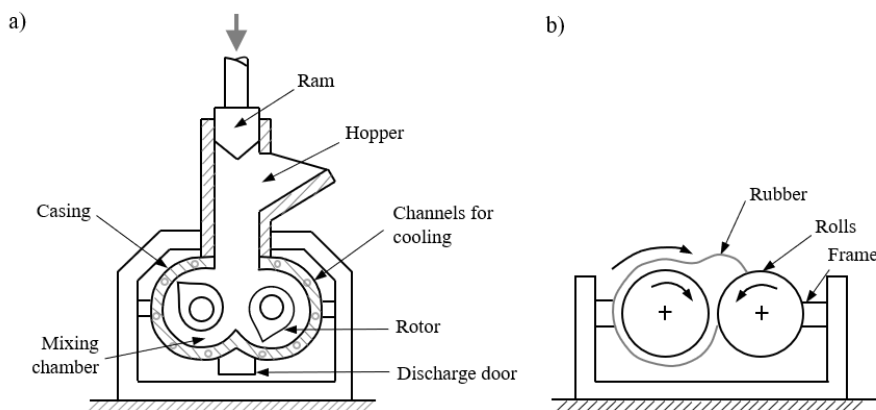


Figure I.3. Schematic representation of the most common mixers for rubber compounding: a) internal mixer, and b) two-roll mill.⁴²

Additionally, the presence of sensors and controllers in modern internal mixers enables computer monitor and control of the mixing variables such as mixing speed, mixing times, drop temperatures, and temperature gradients through the mixing chamber.³ This allows to produce high-quality compounds in large volumes. The uncured mixed compound so-called green compound is then transported to either extruders or calenders.³ These processes are described in the following section.

2.4 Tire manufacturing

The manufacture of tires consists of several processes that are listed below and illustrated in Figure I.4.⁴⁵ The first process is the compound processing reviewed earlier in section 2.3. In essence, in this step the basic components, polymer, filler, vulcanization system, and additional additives are mixed.³ This step is followed by the calendaring of fabrics and steel cord with rubber and the extrusion of rubber components. In the calendaring stage, the rubber compound is sheeted or spread onto fabric and steel wires.³ The calender is equipped with three or more heated rolls through which fabric or wire is passed, and the rubber compound is applied above and below to fully cover the material.³ Belts and plies are usually produced by calendaring.⁴⁶ Key compound requirements are minimum shrinkage, optimum tack, and enough scorch safety. On the other side, the green compound can be also fed into conventional screw-type extruders where many of the parts of a tire, such as treads, sidewalls, and apex, are formed.³

After that, the different components are assembled on the tire building machine.⁴⁵ The initial stage entails the application of the inner liner on the cylindrical drum, followed by the ply and any other additional barrier components. Then, the beads are positioned, and the ply is turned up over them. Finally, the sidewalls, belts, and tread are applied, and the green tire is transferred to the curing mold.³ During this process, the green tire is molded and heated under pressure. Thanks to this step, the tire is converted into a high-quality engineered product. In the curing press, the compound flows into the mold shape to give a design to the tread and the desired thickness to the sidewalls.³ A good flow must be ensured and completed before the cure begins. Finally, the tire inspection takes place and the quality and performance criteria are evaluated.

The selection of the appropriate materials for each part of the tire is critical to the performance of the ensuing rubber compounds.⁴⁷⁻⁴⁸ The following part is dedicated to the different

ingredients used in tire rubber compounding, highlighting their role in achieving tire performance criteria.

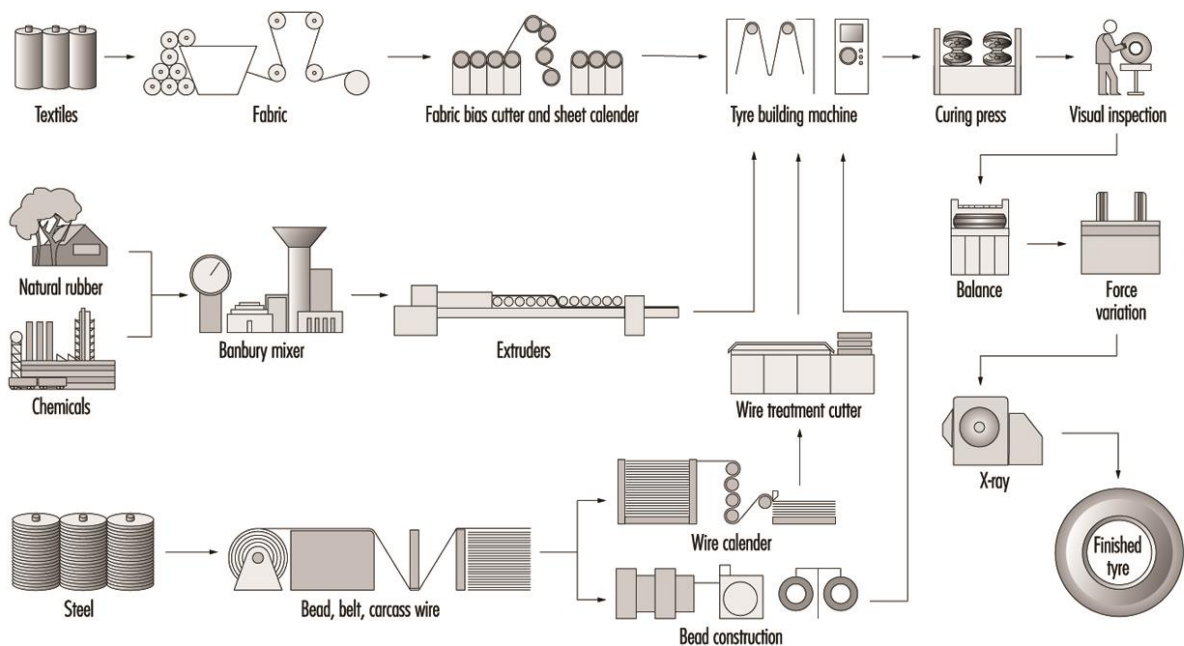


Figure I.4. The tire manufacturing process.⁴⁵

2.5 Rubber compounding

Rubber compounding is a complex multidisciplinary field that describes the science of elastomer chemistry and the modification and blends of elastomers by the addition of other materials to optimize properties or to meet a set of requirements.¹ Rubber compounds are found in several applications such as tires, conveyor belts, large dock fenders, building foundations, automotive engine components, and a wide range of domestic appliances.³ For all of these applications, as well as for each of the considered rubbers, formulations and conception of the material are different. For this reason, it is not conceivable in the frame of this manuscript to cover all these applications and compositions. This project aims to develop new materials for the reinforcement of tires. Henceforth this state of the art will focus on rubber compounding for this specific application. However, additional information about the general formulations of rubbers is detailed in the literature.^{1, 49}

The main ingredients employed for the formulation of rubber compounds can be divided into five categories: polymers, fillers, curing system, and additives (Figure I.5).³

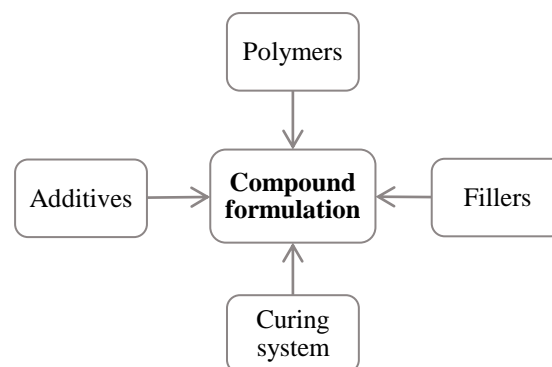
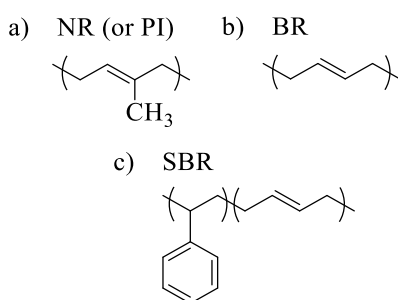


Figure I.5. Basic compound components.

2.5.1 Polymers

In 2019, the worldwide rubber production was around 28.8 million metric tons.⁵⁰ It is divided into natural rubber (NR), which constitutes about 47% of global production, and the remaining 53% correspond to synthetic rubber.⁵⁰ The balance of synthetic rubbers consists of styrene-butadiene rubber (SBR), polybutadiene rubber (BR), polyisoprene rubber (PI), and a range of specialty polymers. It is common to blend more than one type of rubber to meet the tire performance parameters.³

Natural rubber is the most produced elastomer available nowadays (Scheme I.1a).⁵¹ NR is a polymer of isoprene obtained from renewable resources.⁵² It is capable of rapid deformation and recovery and shows good abrasion resistance, good hysteretic properties, and high tensile strength. However, it may also display poor fatigue resistance and poor tire performance in areas such as wet skid and traction compared to selected synthetic elastomers.⁵¹



Scheme I.1. Chemical structure of main elastomers used in rubber compounding: a) Natural rubber or polyisoprene, b) polybutadiene, and c) styrene-butadiene rubber.

Regarding synthetic rubbers, the tire industry consumes approximately 60% of the global production.⁵³⁻⁵⁴ Styrene-butadiene rubber is the largest-volume polymer followed by BR (Scheme I.1b and c). SBR is extensively used in tire treads because it exhibits good tire performance such as traction and wet skid while keeping good abrasion resistance. Polybutadiene is usually employed in treads and sidewalls due to its good abrasion resistance, wear performance, and enhancement of fatigue resistance.⁵³ Halobutyl rubbers are used primarily in the inner liner owing to low air permeability. This elastomer exhibits also good aging and fatigue resistance.³

2.5.2 Curing systems

The curing of rubber is a key process in rubber technology. It is a process that converts physically soft rubber compounds into high-quality engineering products.⁵⁵ The curing involves the formation of chemical crosslinks between long rubber molecules, forming a three-dimensional elastic network.⁵⁶ Therefore, curing increases elasticity while decreasing plasticity. The most popular method for rubber curing employs sulfur better known as vulcanization (Figure I.6).³²

The vulcanization of a rubber leads to an improvement of its elasticity, resilience, tensile strength, viscosity, and hardness. Additionally, crosslinking greatly reduces hysteresis being considered as the ratio between the viscous component and the elastic component.³²

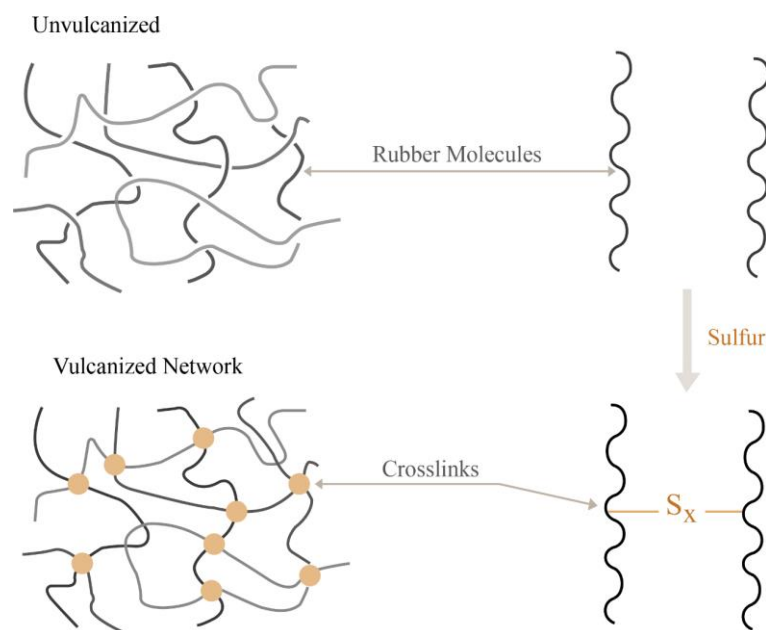
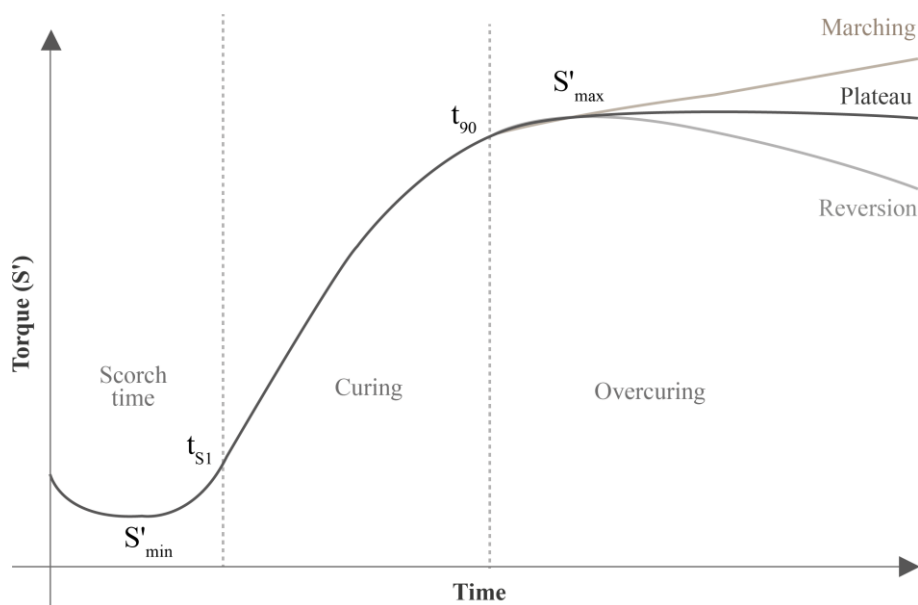


Figure I.6. Crosslinking network formation during vulcanization.³²

The curing process is characterized by several factors such as the time elapsed before the vulcanization, the rate of crosslinking formation, and the extent of crosslinking at the end of the process. The scorch time can be defined as the time available at a given temperature before the compound starts to cure and it is affected by the vulcanization system.³² This allows the compound to be mixed, shaped, formed, and to flow in the mold before the curing. Scorch resistance or induction time is usually measured by the time required for the onset of crosslinking formation. After that, the vulcanization should be fast and controlled.³²

The vulcanization process can be followed by a cure meter. Nowadays, the most commonly used one is the moving die rheometer, better known as MDR.⁵⁷ The green compound is placed inside the device previously heated to the curing temperature of the compound. During the curing, the shear modulus increases due to the formation of a three-dimensional network of rubber chains as the material is crosslinking. The torque (S') required to shear the compound is commonly plotted as a function of time to get a so-called cure curve (e.g. Figure I.7). The cure curve gives complete information on the overall kinetics of crosslinking formation and it is typically divided in three main steps.⁵⁷ The first region, which limits processing safety, is an induction period or a scorch delay. The scorch time (t_{s1}) is usually defined as the time required for the torque to rise one unit ($\text{dN}\cdot\text{m}$) above the minimum torque.⁵⁸ The minimum torque (S'_{\min}) is lowest point in the cure curve and is related to the viscosity of the compound.⁵⁸ The second part is the cure period where the network is formed due to the crosslinking of the compound. The optimum cure time (t_{90}) is determined as the time required to reach 90% of the change from minimum torque toward maximum achieved torque.⁵⁹⁻⁶⁰ The maximum torque (S'_{\max}) is the highest point where the curve plateaus and represent the highest crosslinking level.⁵⁸ The third region gives information about reversion or marching, both signs of overcuring, for a given rubber compound. Therefore, it is also used as a control for quality and uniformity of rubber stocks.

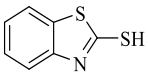
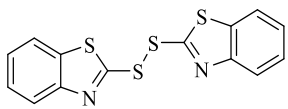
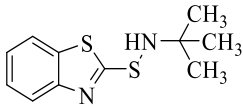
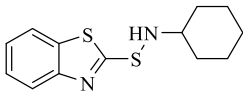
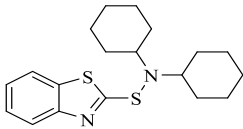
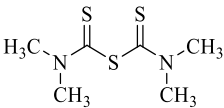
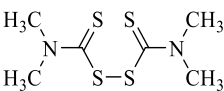
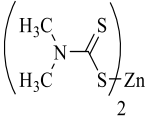
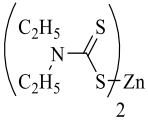
Figure I.7. Generic rheometer cure curve.⁶⁰

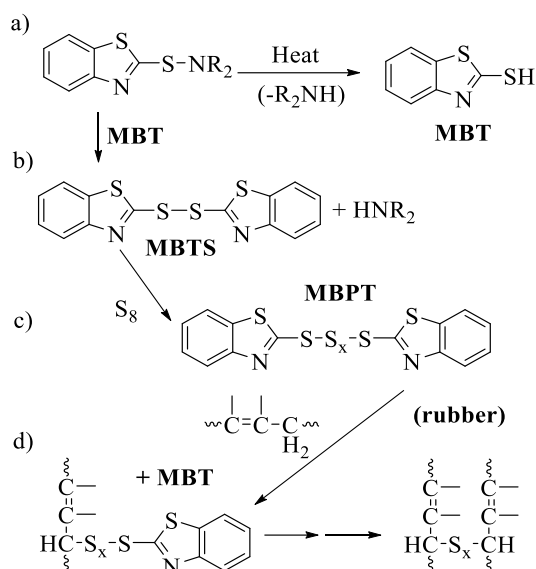
A typical curing system consists of three main components: curing agents, accelerators, and activators.³ The combination of zinc oxide (ZnO) and stearic acid is the most common activator system.⁶¹ Their combination produces zinc stearate, which forms metal complexes with accelerators and reaction products. Their purpose is to enhance the rate and efficiency of accelerated sulfur vulcanization. The use of accelerator, even in low concentrations, reduces the curing time from hours to a few minutes.³² As a consequence, accelerated-sulfur⁶² The system crosslinks quickly, but requires some time to be triggered, allowing the mixing, processing, reshaping, and forming before the curing.⁴⁹ There is a wide variety of accelerators and they can be readily classified in regards to their role toward the rate of vulcanization.³ In Table I.1 are gathered the most common accelerators employed in rubber vulcanization, their effect on vulcanization rate and their chemical structures.

A binary curing system is frequently employed to obtain a synergic effect.⁶³ A mixture of accelerators can avoid pre-vulcanization and allows the curing to proceed faster.⁶⁴ Among all the types, sulfenamide accelerators, e.g., TBBS, CBS, and DCBS, represent the largest class and widely used.⁶⁵ They can be employed alone or in binary systems, especially with thiuram accelerators such as tetrabenzylthiuram disulfide (TBzTD).⁶⁶⁻⁶⁷

The general reaction scheme of sulfenamide accelerated-sulfur vulcanization is depicted in Scheme I.2.³² Firstly, in the presence of sulfur, the sulfenamide accelerator decomposes due to heat into MBT and the respective amine (Scheme I.2a). Then, MBT reacts with remaining sulfenamide molecules to form MBTS and release amine molecules (Scheme I.2b). These two reactions offer the scorch time characteristic of the sulfenamide accelerators. This step is followed by the reaction between elemental sulfur and the formed MBTS giving a polysulfide (MBPT) which is an active sulfurating agent (Scheme I.2c). Afterward, MBPT attacks the allylic position of the rubber molecule. Finally, a second rubber molecule is attacked to the crosslinking precursor by the MBT addition to form a crosslinking containing mono-, di- or polysulfide bonds (Scheme I.2d).

Table I.1. The most widely used accelerators for sulfur vulcanization.

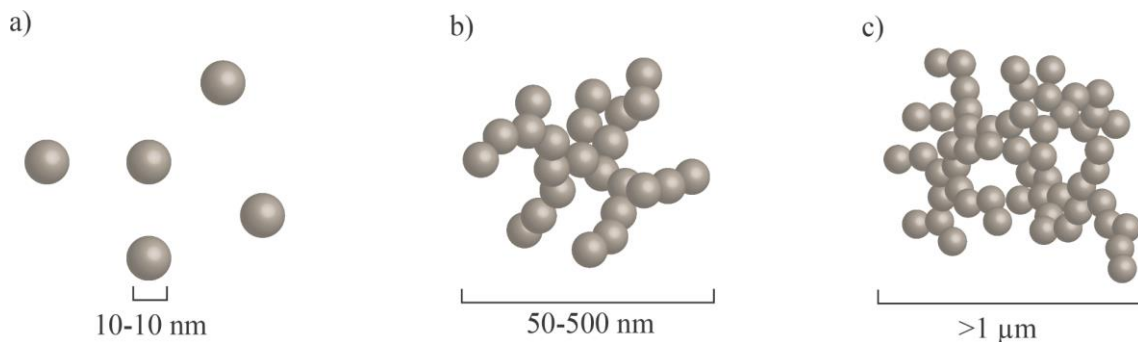
Compound	Rate of vulcanization	Abbr.	Chemical structure
Thiazoles			
2-Mercaptobenzothiazole	Fast	MBT	
2,2'-Dithiobisbenzothiazole		MBTS	
Sulfenamides			
N-t-Butylbenzothiazole-2-sulfenamide	Fast with delay action	TBBS	
N-Cyclohexylbenzothiazole-2-sulfenamide		CBS	
N-Dicyclohexylbenzothiazole-2-sulfenamide		DCBS	
Thiuram			
Tetramethylthiuram monosulfide	Very fast	TMTM	
Tetramethylthiuram disulfide		TMTD	
Dithiocarbamates			
Zinc dimethyldithiocarbamate	Ultra-fast	ZDMC	
Zinc diethyldithiocarbamate		ZDEC	

Scheme I.2. Reaction scheme for accelerated-sulfur vulcanization with benzothiazole-sulfenamide accelerators.³²

2.5.3 Carbon black

The reinforcement of rubbers by particulate fillers has been and is still extensively studied. The main reason is the need for an improvement in their mechanical properties enlarging the screen of their applications. Particularly, the use of reinforcing fillers in elastomers induces an increase in modulus and deformation at the break.⁶⁸ The enhancement of these two features provides unique properties to reinforced rubbers. Carbon black (CB) is one of the most widely used fillers for rubber reinforcement in tire applications.⁶⁹ On average, a typical tire contains 30-35% of CB.

Carbon black is usually obtained from the partial combustion of organic substances and contains carbon as the main element.¹ Nowadays, the most dominant process to obtain carbon black for rubber grade is the furnace process. Carbon black is composed of primary particles fused together in the form of aggregates. The aggregate size can range from about 50 to 500 nm (Figure I.8).⁷⁰ Several aggregates assembled together are called agglomerates. These agglomerates are clusters of physically bound and entangled aggregates thanks to the van der Waals forces and are larger than a micrometer being able to reach a few millimeters. The reinforcing effect of carbon black is directly related to both the size of the particle and the structure of aggregates.⁷¹ Moreover, the quality control of carbon black is crucial as it is directly related to the carbon black's performance in rubber compounds.⁶⁸

Figure I.8. Carbon black: a) particles; b) aggregate; c) agglomerate.⁷⁰

One of the most important parameters is the specific surface area of carbon black because it represents the extension of the interface between the rubber and the filler surface.⁶⁸ The specific surface area is the available area in square meters per grams of carbon black.¹ This parameter is typically determined using absorption measurements. The adsorption of molecules such as iodine or nitrogen is measured and then either the amount adsorbed per unit mass is reported or a specific surface area is calculated based on current adsorption theories.¹ Apart from the specific surface area, the carbon black interactions with rubber and other components are affected by the surface activity of the particles. Carbon blacks employed for rubber reinforcement contain small quantities of chemically combined hydrogen (0.2-1.0%), oxygen (0.1-4.0%), and sulfur (up to 1.0%) depending on the raw materials and production process. Several oxygen-containing functional groups can be found in trace amounts such as carboxyl and hydroxyl groups, lactones, quinones, ketones, aldehydes, and hydroperoxides (Figure I.9).⁷¹

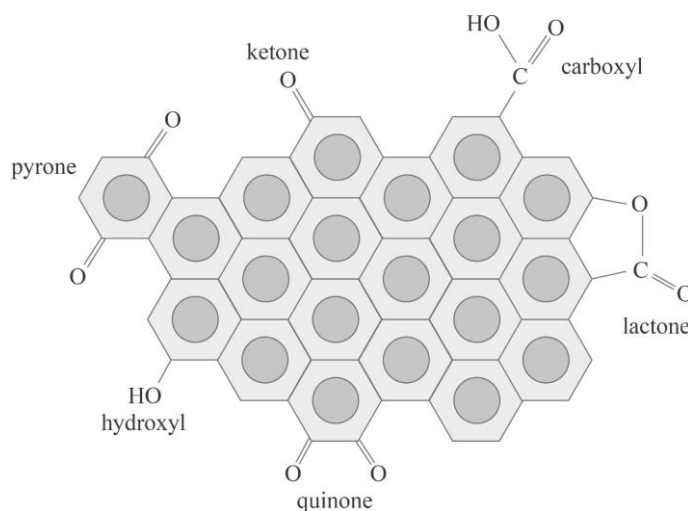


Figure I.9. Surface chemistry of carbon black.⁷¹

Carbon black is mixed with the rubber in an internal mixer or roll mill. The shear forces generated during the mixing step allow the incorporation of the filler into the polymer. The addition of carbon black increases the torque to a maximum followed by a dropping while the temperature inside the chamber continuously increase.¹ The maximum torque is occurring during the incorporation of CB because the rubber is filling voids between the carbon black structures i.e. aggregates and agglomerates until a coherent rubbery composite is obtained. After that, the torque decreases together with a reduction of agglomerate sizes so-called deagglomeration. Finally, a distribution of the filler throughout the rubber matrix takes place. The final dispersion of the filler into the polymer is critical and it is affected by the mixing conditions, carbon black type, and characteristic of the rubber matrix.⁷² Generally, the better the dispersion, the better the mechanical performance of the carbon black-filled rubber compound.

It is possible to assess the level of dispersion from two different perspectives: 1) macrodispersion usually refers to several micrometers to millimeters, or 2) microdispersion, nanometers to fractions of micrometers. In general, the term macrodispersion is used to refer to slightly dispersed carbon black existing as lumps of filler that were not fully deagglomerated. This is normally related to problems with rupture properties and appearance. The macrodispersion can be characterized following the ASTM (American Society for Testing and

Materials) standard method.¹ On the other hand, microdispersion relates the level at which the aggregates and agglomerates have been dispersed. This has a direct influence on the amount of interfacial area between the carbon black and polymer, related to polymer-filler interactions, and the formation extent of the filler-filler network held together by van der Waals forces.¹ The filler-filler network has a prominent role in the dynamic properties of the compound at low strain and will be discussed in more detail in the following paragraphs. The microdispersion can be observed qualitatively in a 2D model such as transmission electron microscope (TEM) or determined quantitatively by electrical resistivity measurements.⁷²

After the mixing of rubber and carbon black, the resulting filled compound is subjected to further processing such as calendaring, extrusion, and molding. The incorporation of the carbon black significantly increases the viscosity of the green compounds.¹ These changes in viscosity affect the ability to flow and allows further the processing of the filled rubber. It is noteworthy that when the typical polymer is made to flow at low shear rates, will show shear stress proportional to the shear rate known as Newtonian flow. However, the carbon black-filled polymers exhibit a highly increased non-Newtonian behavior.⁶⁸ This effect is mainly because the incorporation of fillers in rubbers reduces the extent of the deformable phase. Consequently, when filled compounds are subjected to shear forces exhibit much higher deformation than in unfilled materials due to the lower deformable volume.⁷³⁻⁷⁴ This phenomenon is usually called the strain amplification effect.¹ Additionally, at low shear rates, filled compounds show an additional increase of viscosity that cannot be justified by this phenomenon and is commonly attributed to the existence of the filler network.

Once the carbon-black filled compounds have been molded, the curing process takes place to produce the final tire. Carbon black particles can impact the physical properties of the cured rubber in different extents depending on their concentration.⁷⁵ At low filler content, the particles do not interact with each other and contribute only by their volume usually known as hydrodynamic reinforcement.⁷⁶ When the filler particles form clusters, the reinforcement is stronger, becoming structure-dependent.⁷⁵ The most important cases are at high concentration in which the fillers interact to form cluster-cluster aggregates and a percolated network. Therefore, at filler contents larger than a specific value, known as percolation threshold, the clusters form an irregular network supported by van der Waals forces. The filler network is not stable and might break up into smaller structures with increasing mechanical strain.⁷⁵

Generally, the deformation behavior of carbon black filled rubbers is commonly divided into two domains: at low strain (<10%) and at high strain (>10%). At low strain, filled vulcanized samples present a specific viscoelastic behavior and it is usually studied by dynamic viscoelastic measurements.¹ A schematic illustration of the response of the elastic or storage modulus (G') and the viscous or loss modulus (G'') as a function of strain amplitude at a specific frequency and temperature for a carbon black compound is depicted in Figure I.10. A decrease of the storage modulus occurs from G'_0 to a plateau value (G'_∞) when the strain amplitude is increased.⁷⁷ This decline of the storage modulus results from a dynamical break-up of the filler network and is usually known as the Payne effect.⁷⁸ The CB aggregates that form the filler network are continuously broken and reformed when strain is applied. At low deformations, the effect of the rigid filler network is dominant, whereas at high deformations the filler has only a slight remaining impact mainly hydrodynamic and caused by the rubber-filler interaction.⁷⁹

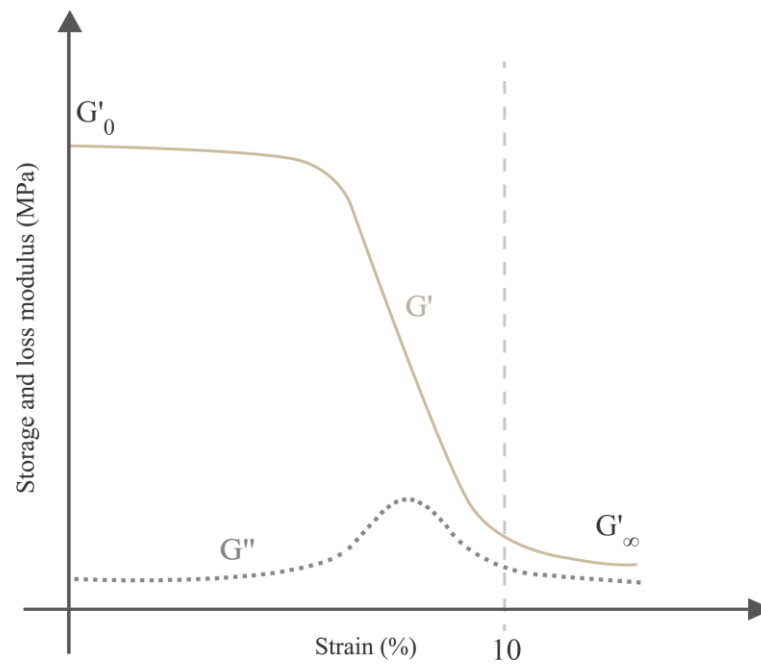


Figure I.10. Schematic representation of G' and G'' for a carbon black compound.⁶⁸

The different contributions to the storage modulus of the filled rubber network are displayed in Figure I.11 as a function of strain amplitude.⁷⁵ At small strains, rubber network, rubber-filler interactions, hydrodynamic contribution and filler network contributions are added up to the zero shear modulus, G'_0 . At larger strain amplitudes, the filler network successively breaks down and the modulus reaches a plateau at large deformation (G'_∞). At this moment, the modulus is no longer affected by the filler network but only by the rubber matrix, hydrodynamic contribution, and the interaction between filler and rubber.⁷⁵

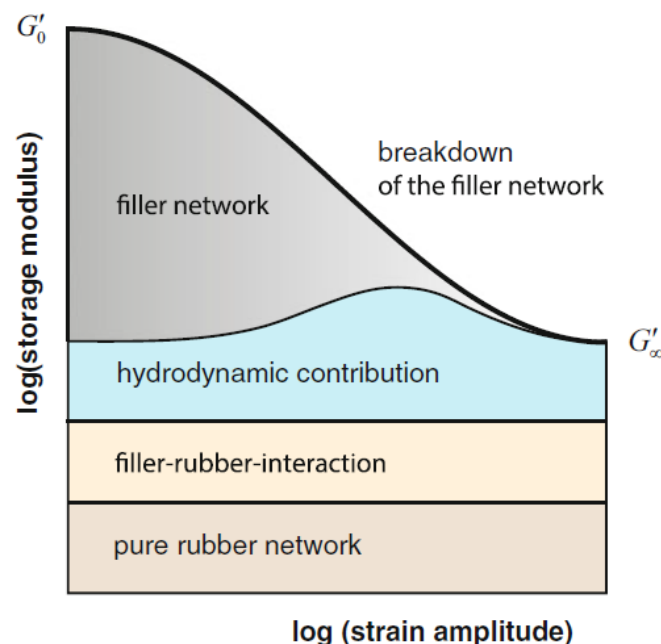


Figure I.11. Different contributions to the storage modulus as a function of the strain.⁷⁵

Furthermore, the change in G' also corresponds to an important change in G'' (Figure I.10). As the network breaks, energy is dissipated as heat leading to the increase of G'' that passes through

a maximum value before decreasing.⁶⁸ This maximum in viscous modulus at low strain (G''_{\max}) is related to the energy loss of the final rubber product. Additionally, the ratio between G'' and G' , known as loss factor or $\tan\delta$, is commonly used for the correlation to energy loss or hysteresis. This energy loss is at the same time related to the rolling resistance behavior of tires.¹

Finally, at high strain, the properties of the rubber compound are usually determined by uniaxial extension showing highly nonlinear behavior characterized by hysteresis loops when unloading and under cyclic loading conditions, loss of stiffness leading to cyclic stress softening.⁸⁰ The stress softening effect is also known as the Mullins effect and it is observed when the sample is stretched up to a certain strain, unloaded, and then reloaded.⁸¹ The stress required on reloading is less than the one needed for the initial stretching reflecting damage incurred during the previous loading. This effect is dependent on the initial strain. Additionally to the Mullins effect, when the strain amplitude is constant, the stress drops between successive loading cycles.⁸⁰ This phenomenon is especially important during the first cycles and becomes negligible after several cycles ($\sim 5-10$) when a stationary state with constant stress amplitude and stabilized hysteresis loop is then reached (Figure I.12).⁸⁰

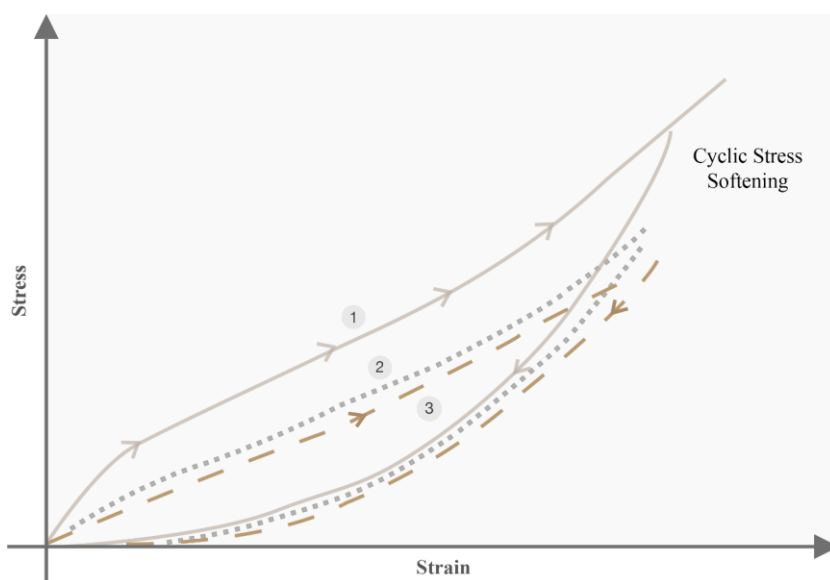


Figure I.12. Schematic illustration of cyclic stress softening behavior of elastomers.⁸⁰

The scope of this thesis is to find alternatives to phenolic resins as reinforcing agents in carbon black filled compounds. It is noteworthy another major family of filled compounds also exists using silica (SiO_2) as a filler to produce silica-reinforced materials. As these materials are out of the scope of the current study, they are not detailed. However, further information can be found in the literature.^{68, 82}

2.5.4 Special compounding ingredients

In addition to the rubbers, fillers, and curing agents, an important class of other materials are used in rubber formulations such as processing aids and resins. They are discussed in the following paragraphs.³

Processing oils serve primarily as a processing aid, i.e. they are used to promote the interactions of the rubber with the particulate fillers, helping their de-agglomeration and their dispersion. They can be divided into three categories: paraffinic, naphthenic, and aromatic.³ A careful

selection of the oil for each rubber formulation is essential to ensure a good compatibilization with the polymer. Otherwise, the oil will migrate out of the polymer leading to a loss of the physical and surface properties, and a deterioration of the adhesion between different components of the tire.³

Resins used in rubber have been classified into two categories: hydrocarbons and phenolic resins.² They serve many functions in rubber compounds.¹ In uncured rubbers, they work as processing aids and tackifiers, which are chemical compounds that act as adhesives between the different rubber layers. In cured rubber, they function as plasticizers and reinforcing agents. Reinforcing agents are materials that improve tensile strength, stiffness, hardness, and tear and abrasion resistance. Additionally, resins can be used to cure a specific type of rubbers.⁸³

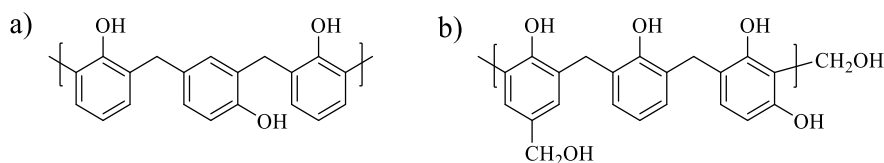
Several types of hydrocarbon resins are available today: terpene-based resins, coumarone-indene resins, petroleum-based (aliphatic and aromatics), and polymers and copolymers of styrene.⁸⁴ They tend to have high glass transition temperatures and melt during the compounding, thereby reducing the viscosity of the compound and thus improving the flow. Then, the resins will harden at room temperature and therefore, they will maintain compound hardness and moduli. Regarding hydrocarbons resins, aromatic resins are commonly employed as reinforcing agents, aliphatic resins improve the tack, and resins with intermediate properties improve both features.² Particularly, petroleum resins are a byproduct of oil refining and a wide range of grades are produced. Aliphatic resins that can contain isoprene oligomers are usually used as tackifiers, whereas aromatic resins tend to be classified as reinforcing systems.² In general terms, hydrocarbon resins provide an improvement of the tensile strength as a result of stiffening at room temperature.² They also increase the fatigue resistance because of the improved dispersion of the fillers. Additionally, they provide retardation of cut growth by the dissipation of stress at the crack tip as a result of a decrease in compound viscosity.²

Phenolic resins are classified into three main groups according to their function, type, and effects: curing resins, tackifiers resin, and reinforcing resins.⁸ This topic will be developed more in detail in the following chapter.

3 Phenolic resins as additives in the rubber industry

3.1 Introduction

Phenolic resins were the first synthetic resin exploited commercially. This class of thermosets is prepared by step-growth polymerization of phenol, or phenol derivative, with formaldehyde, using an acid or a base as a catalyst.^{85,86} Phenolic resins fall into two broad classes, novolac and resole resins (Scheme I.3).

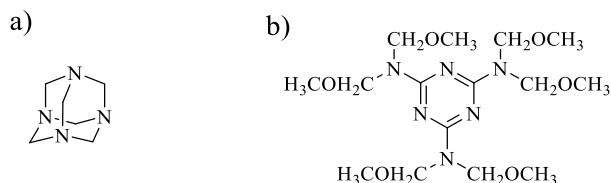


Scheme I.3. Schematic structure of phenol-formaldehyde resins a) novolac resin b) resole resin.

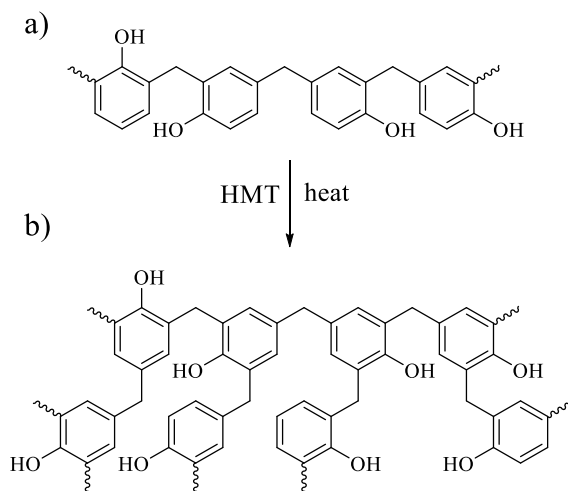
The first one, novolac, is a thermoplastic that can be used directly or can be cured to get a crosslinked structure. Novolac resins are produced by the reaction of formaldehyde with an

excess amount of phenol in the presence of an acid catalyst.⁸⁵ The second type, resol, is a multifunctional reactive compound that can be cured thermally without a catalyst. It is produced by the reaction of phenol with an excess amount of formaldehyde in the presence of a base catalyst.⁸⁵

Novolac can be cured in the presence of methylene donors such as hexamethylenetetramine (HMT) or hexamethoxymethylmelamine (HMMM) (Scheme I.4).⁸³ HMT is a condensation product from formaldehyde and ammonia and it is commonly added at 8-15 wt%.⁸⁷ The mechanism of HMT-cured novolac has been extensively studied but the presence of several intermediates difficults the analyses. The proposed mechanism is divided in two steps. The first stage comprises the formation of initial intermediates such as benzoxazines and benzyl amines. This step is followed by the reaction of these intermediates into methylene bridges with residual traces of amines, imides, imines, and methyl phenol, among others.⁸⁷⁻⁸⁸ Particularly, the use of HMT forms predominantly methylene bridges between phenolic rings making possible the formation of a crosslinked network (Scheme I.5).^{4, 89} A different network is obtained when HMMM is used with methylene bridges formed between the melamine structure and the phenyl ring.^{1, 90}



Scheme I.4. Chemical structures of commonly used curing agent for novolac resin a) HMT b) HMMM.



Scheme I.5. Crosslinking of novolac phenolic resin with hexamethylenetetramine (HMT), a) novolac resin, b) crosslinked novolac with HMT.

These systems are used in rubber formulations of specific compounds with different purposes that are described in detail in the following sections.

3.2 Phenolic resins used in rubber formulation

Phenolic resins are one of the most important resins used in the rubber industry.⁴⁻⁵ They are used to improve the processing and performance of a wide variety of rubber products and

specifically, they are important ingredients in rubber components for the automotive industry including tires, belts, and hoses.⁹¹

Reactive resins, resole type, are utilized as curing agents thanks to the presence of free methylol groups in their structure that can react and thus cure the rubber.⁴ These reactive methylol groups will crosslink with the unsaturated sites of the rubber molecule at an elevated temperature. For this reason, they are suitable for the vulcanization of low unsaturated rubbers such as butyl rubber.⁵ They form covalent carbon-carbon crosslinking enhancing heat, steam, oxidation, and aging resistance. Additionally, they act as plasticizers until the curing, improving the processing of green compounds.

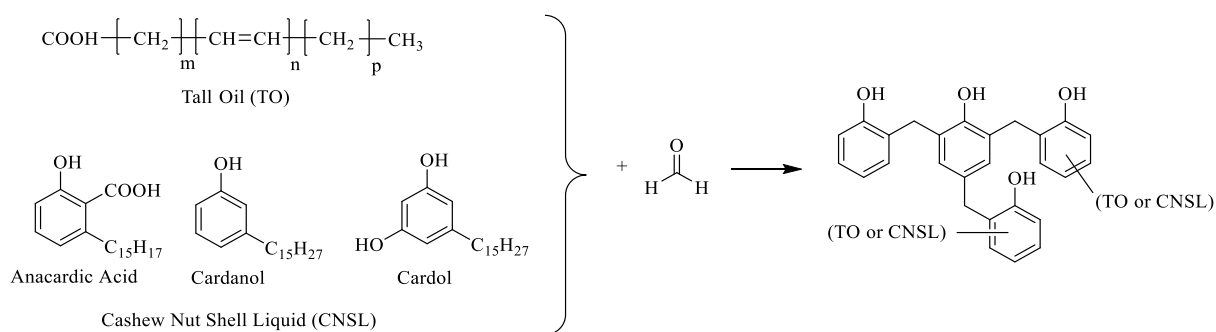
Novolac resins are unable to react further without the addition of a crosslinking agent and thus are considered non-reactive resins. They are used as tackifier resins. Alkylphenolic resins, a type of novolacs with a *para*-alkyl group ranging from C₄ to C₉, can be used for this purpose.⁴ They create strong hydrogen bonds with the rubber surface providing the rubber mixes with the desired tack.⁹² Additionally, when a curing agent is added to novolac resin they improve the cured materials hardness, acting as reinforcing resin.⁴

3.3 Novolac phenolic resins used for rubber reinforcement

Novolac phenolic resin (PR) are well-known thermosets used to reinforce rubber compounds. The first phenolic reinforcing resin was tested as early as the end of the 1940s, and that phenolic novolac cured with hexamethylenetetramine afforded good results.⁸ For enhanced compound properties, it is found to be more advantageous to incorporate novolac and let them react *in-situ* during rubber vulcanization.^{7,9} During rubber vulcanization, a parallel reaction occurs between the resin and the methylene donors. The reaction forms a crosslinked phenolic polymer that reinforces the final rubber. Moreover, the phenolic resins are considered not to crosslink with the rubber, the assumption being that interpenetrating networks are formed.⁹¹⁻⁹²

Regarding the processing of the green compound, this resin is a thermoplastic with a softening point of about 100 °C so it can easily be incorporated in the rubber matrix. Furthermore, the reinforcing network is formed only during the rubber curing stage allowing the uncured rubber to remain soft compared to conventional filled compounds. In green compounds the phenolic resins behave as softeners, they improve building tack and guarantee a good flow in the molds.⁴ Once the rubber is cured, they increase its hardness, the toughness, the stiffness, the abrasion and tear resistance and the resistance to oxidation and chemicals.⁹³ In general terms, by adding these resins, the cured rubber improves its stiffness while preserving a good processability.⁴⁹

Reinforcing resins can be used in practically all types of rubber. However, they are polar compounds and thus, less compatible with non-polar rubber. Babak *et al.* reported the formation of incompatible blends exhibiting a two-phase microstructure in which rigid spherical particles of PR were embedded in a soft rubber matrix.⁹⁴ Several strategies have been developed to decrease the polarity of PR to improve its miscibility within rubbers. The polarity can be reduced by reaction with tall oil (TO) or cashew nut shell liquid (CNSL) (Scheme I.6). The long hydrocarbon chain present in the modifiers increases miscibility with elastomers and gives to the cured phenolic resin more flexibility, especially at high temperatures compared to unmodified resins.⁹⁵⁻⁹⁶



Scheme I.6. Modification of phenolic resins with tall oil (TO) or cashew nut shell liquid (CNSL).

Phenolic reinforcing resins are commonly used in combination with fillers such as carbon black. In contrast to the unfilled system, Nigam *et al.* reported high compatibility between the novolac-type resin system in nitrile rubber in the presence of CB.⁹⁷ In this case, a combination of CB and PR improved tensile strength, dynamic mechanical properties as well as thermal stability. They assumed that the resin acts in synergy with carbon black and leads to better structural integrity. Presumably, PR is adsorbed onto the CB surface leading to higher compatibility and thus, to a uniform distribution of filler agglomerates.⁹⁷

Miyake *et al.* were granted a patent with similar results for natural rubber or diene series rubber were reported.⁹⁸ They claimed that CB and PR act in synergy, with an increased reinforcement, in comparison to rubber systems with either just resin or CB. This synergistic effect is strongly dependent on the ratio between CB and resin, as well as the type of CB. Besides, when the amount of resin was high i.e. more than 45 phr (parts per hundred rubber), excess of resin forms agglomerates that cause phase separation in the resulting rubber composition deteriorating noticeably the physical properties of the rubber composition.⁹⁸

Only recently the mechanism of the reinforcing resin with regards to the structure and the mechanical properties of CB-filled polyisoprene rubber was described.⁷ The authors claim that the resin introduces a synergistic effect with CB to strengthen the system, promoting the CB dispersion and helping the fillers to reach the percolation at a lower amount. A similar phenomenon is observed when the surface area of CB is increased.⁷ For this reason, the phenolic resin was proven to influence the formation of the filler network acting as a mediator by activating the filler-filler interface and creating resin domains at the interface. Furthermore, the resulting filler-filler bonds are much stiffer, i.e., showing higher brittleness compared to those bonds in a non-resin containing system. It is important to highlight that the resin requires a percolated system to exhibit significant reinforcing behavior.⁷ Besides, the resin was deemed to be producing a more compacted CB network, with higher density and stiffness, promoting the rubber compound mechanical properties at a level not reached with CB or PR alone.

Even though the reinforcing effect of phenolic resins in rubber compositions has been demonstrated, several shortcomings are arising from their use. One of the main drawbacks of reinforcement systems based on novolac resins is the large network breakdown on dynamic cycling, increasing the hysteresis. In addition to performance considerations, safety European regulations such as REACH (registration, evaluation, authorization and restriction of chemicals) are more and more challenging traditional phenolic resins.¹⁰⁻¹¹ Finally, phenolic resins are mainly produced from petroleum-based reagents being also challenged by society

and European institutions. The development of more sustainable alternatives has become desirable.

Among the different alternatives, polybenzoxazines have emerged as a promising substitute for phenolic resins with the possibility to overcome the shortcomings mentioned before. One of the reasons is that these thermosets are not subjected to the release of byproducts during the polymerization.¹² Besides, polybenzoxazines have rich molecular design flexibility making it feasible to tailor their chemical structure toward good performance in rubber compounds and, potentially, without compromising the hysteresis of the system.

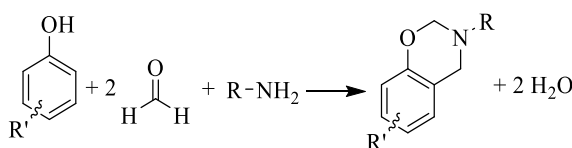
4 Benzoxazine resins

Polybenzoxazines (polyBz) are a new class of thermosets under continuous development.¹² PolyBz are high-performance monocomponent thermosets considered as an attractive candidate to replace traditional thermosets such as phenolic resins and epoxies. PolyBz have a wide range of mechanical and physical properties making them attractive alternatives to current applications.⁹⁹ These properties can be tailored to required needs, reflecting their extremely rich molecular design flexibility. In comparison to phenolic resins, polyBz show better modulus, strength, and elongation at break allowing the investigation of polybenzoxazines as reinforcing resins for tire applications.^{12,15}

Furthermore, polyBz are not only deemed a promising substitute for commercial thermosets, but also a new class of materials that goes far beyond due to its outstanding properties. In addition to properties similar to phenolic or epoxy resins, polyBz have unique features compared to other well-known polymers. They include near-zero shrinkage upon polymerization,¹⁰⁰ fast development of mechanical properties as a function of conversion,¹⁰¹ one of the highest char yield among processable resins,¹⁰² glass transition temperatures much higher than curing temperatures,¹⁰² low water absorption despite having many hydrophilic groups¹⁰³, and excellent dielectric and mechanical properties. One of the current efforts is to focus on the development of benzoxazine monomers with minimal environmental and health impact. Additionally, the development of polyBz has been linked to petroleum-based feedstocks. However, for the last ten years, the number of studies related to bio-based benzoxazines is growing rapidly as a consequence of the versatile design of their monomers chemical structure.¹⁰⁴

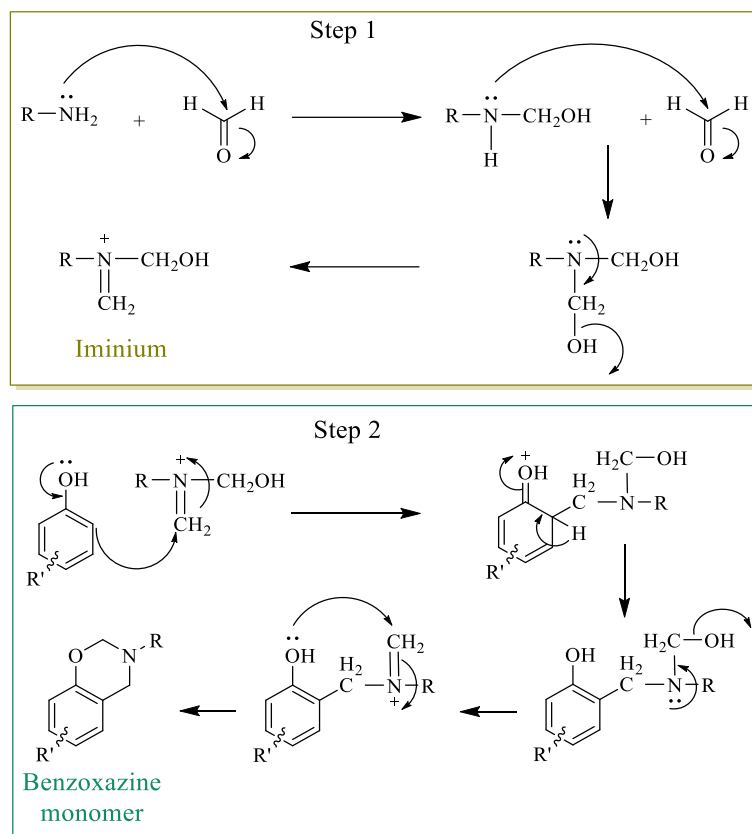
4.1 Synthesis of benzoxazine monomers

Benzoxazine resins (Bz), typically 1,3-benzoxazines, can be readily synthesized through a Mannich-like condensation of phenolic derivatives, formaldehyde, and primary amines (Scheme I.7).¹²



Scheme I.7. Synthesis of benzoxazine resin.

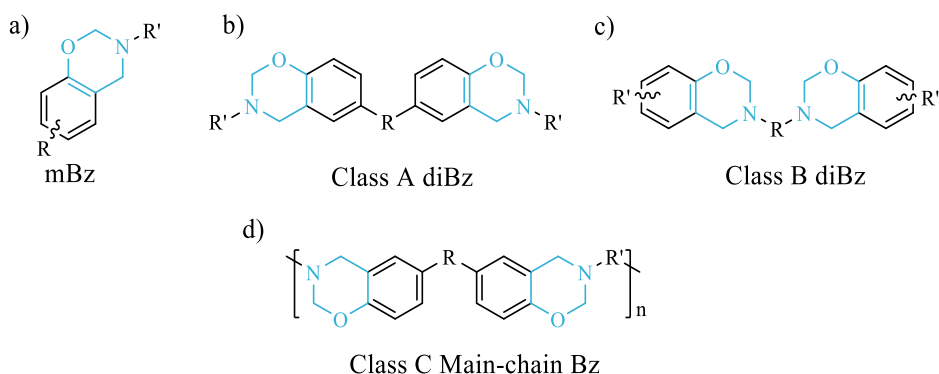
A possible mechanism for the synthesis of Bz is displayed in Scheme I.8. In a first step, the iminium is formed followed by a ring-closure process.¹⁰⁵



Scheme I.8. Two-step mechanism for the synthesis of monobenzoxazine monomers.¹⁰⁵

Depending on the reactants, reaction conditions, and synthetic procedure, the reaction yield ranges from 70 to 95%. The synthesis can be carried out with or without solvent.^{13, 106} The bulk approach is applicable for raw materials when the mixture of the reactants is liquid or in the molten state at working temperature.

The general chemical structure of the different classes of benzoxazine monomers is depicted in Scheme I.9. This scheme shows the great molecular design versatility of benzoxazines.



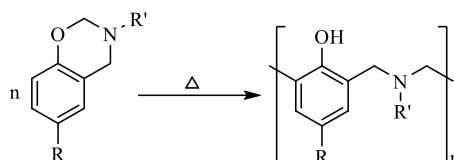
Scheme I.9. Schematic representation of benzoxazine monomers.

First, there are monobenzoxazines (mBz) which are monomers composed of one benzoxazine group (Scheme I.9a), in contrast to dibenzoxazine monomers (diBz), composed of two benzoxazine groups. DiBz monomers prepared from a diphenolic compound with a primary

amine and formaldehyde are called Class A (Scheme I.9b). If they are synthesized from a diamine compound with a phenol derivative and formaldehyde, they are defined as Class B (Scheme I.9c). A more recent concept of benzoxazine monomers involves the use of diphenolic compound(s) and diamine(s), yielding linear polymers having oxazine rings in the main chain known as Class C or main-chain Bz (Scheme I.9d).¹⁰⁷

4.2 Benzoxazine polymerization

Benzoxazine monomers are subjected to thermally accelerated, cationic ring-opening polymerization (ROP) (Scheme I.10).



Scheme I.10. Ring-opening polymerization of benzoxazines.

The ring-opening polymerization is readily achieved by heating the monomer at temperatures in the range between 160 and 250 °C.¹⁰⁸ The polymerization can take place upon heating because Bz monomers contain a small number of impurities, such as phenolic raw materials or benzoxazine oligomers. The ROP is then auto-catalyzed by the formation of phenolic compounds through the monomer oxazine ring-opening. However, the polymerization rate, as well as the applied temperature for curing, depends on the purity of the benzoxazine monomer produced.¹² In addition, the release of byproducts during the polymerization of benzoxazine resins is substantially lower than those released during the polymerization process of traditional resins. Besides, the ROP of Bz monomers does not produce water in comparison to the polycondensation of phenolic resins.

Monofunctional Bz commonly leads to a linear and low molecular weight polymer, from a few hundred to few thousand. However, if the benzene ring is sufficiently reactive, meaning additional positions such as *para* positions are available, even a monofunctional Bz can lead to a crosslinked polymer.¹⁰⁹ On the contrary, difunctional or polyfunctional benzoxazine monomers lead to crosslinked structures due to their higher functionality.¹³ Thus, Bz monomers with two or more functionalities are preferred for the elaboration of high-performance polyBz materials.

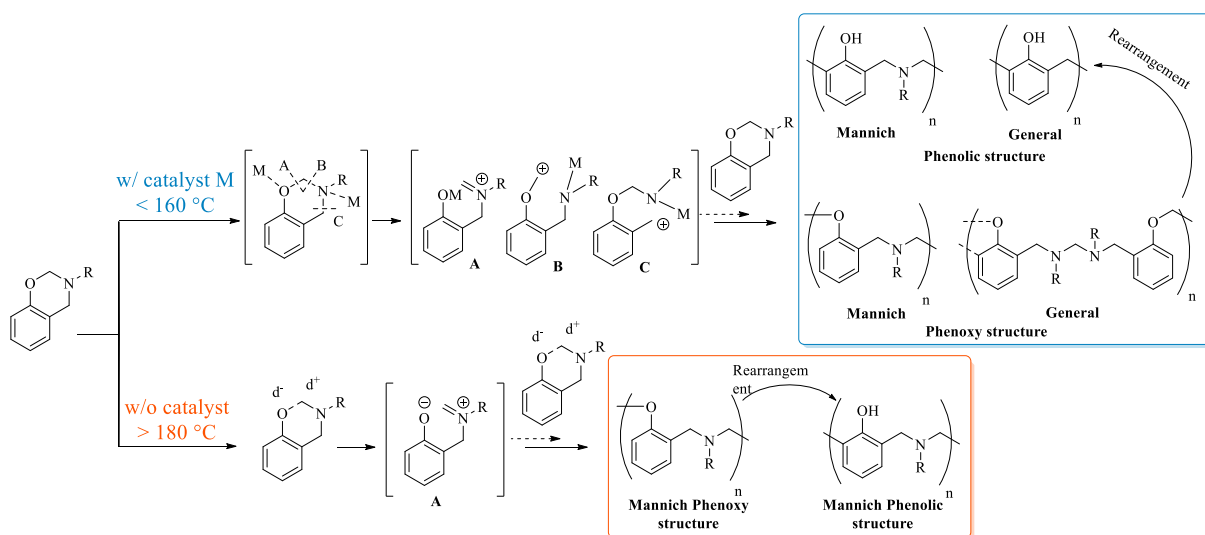
Even though the polymerization of benzoxazines is thermally accelerated and auto-catalyzed, the curing of some monomers requires high temperatures and long reaction times for its completion. In these cases, the polymerization can be accelerated or triggered to lower temperatures with the use of initiators or catalysts.^{33, 110}

Acidic catalyst are the most reported catalysts due to the effectiveness, as ROP is a cationic process. Wang *et al.*¹¹¹ studied the use of acidic catalysts for reducing the polymerization temperature of bisphenol A based monomers (BA-a). Their polymerization was performed at room temperature for 20 h with 5 mol% of several Lewis acids (PCl₅, PCl₃, POCl₃, and TiCl₄). The resulting polyBz exhibited glass transition temperatures (T_g) higher than 200 °C.

A variety of phenolic compounds originated from the ROP or benzoxazine oligomers can act as catalysts for further ring-opening polymerization reactions, resulting in the auto-catalyzed

nature of benzoxazines polymerization.¹¹⁰ In addition, the presence of phenolic structures with free *ortho* positions in the Bz monomer has a catalytic effect on the curing reaction, thus reducing the reaction induction time and increasing the reaction rate.¹¹²

Besides, Ishida and co-workers proposed a polymerization mechanism and inner structures of polybenzoxazines in the presence and absence of a catalyst.³³ As shown in Scheme I.11, the ROP of benzoxazines performed at lower temperatures (typically <160 °C) under a catalyst provides polyBz with more complex inner structures. At lower temperatures and in the presence of a catalyst, more ring-opening patterns seem to be available, resulting in three main intermediates: A, B, and C. The polyBz obtained commonly possesses relatively poor properties because less Mannich phenolic structure units are generated. On the contrary, when the benzoxazines are polymerized at higher temperatures (typically >180 °C), O-CH₂ bonds of Bz selectively generate the thermodynamically more stable intermediate A. The following aromatic electrophilic substitution reactions of intermediate A provide only Mannich phenoxy and Mannich phenolic structures.



Scheme I.11. Proposed polymerization temperature and catalyst effect on benzoxazine polymerization mechanism and inner structure of polybenzoxazines.³³

The polymerization of benzoxazines can also be catalyzed by the use of strong acids and/or carboxylic acids. Ishida *et al.*¹¹² highlighted the effect of adipic acid as a catalyst to reduce the polymerization rate of BA-a monomer. Indeed, the maximum of the exotherm appears 1 hour earlier than for the pure monomer. In summary, a broad variety of catalysts may be used for the ring-opening polymerization of Bz monomers at moderate temperatures.

Besides the use of an external catalyst, other approaches to achieve lower polymerization temperatures have been reported including the addition of initiator or catalyst-containing benzoxazines^{113,114} and strong intermolecular association without the addition of an initiator or catalyst.^{115,116} In applications where the addition of such an initiator or catalyst is undesirable, the last approach is to modify the structure of benzoxazines to achieve high reactivity and/or lower ROP temperature. The addition of functional groups on the benzoxazine monomers such as carboxylic acids that can act as a catalyst has been studied leading to the reduction of the polymerization temperature. A small amount of monocarboxylic monomer induced a reduction of about 60 to 80 °C of the polymerization temperature. In addition, it has been shown that

elemental sulfur can catalyze the ROP of benzoxazine resins. As sulfur is the main ingredient employed for rubber vulcanization this topic is discussed in detail in a separate section.

Finally, the crosslinked polybenzoxazines exhibit glass transition temperatures ranging from 160 to 400 °C, in most cases, higher than the polymerization temperatures. The presence of active sites available combined with a sufficient mobility of polymer chains allows further polymerization beyond the curing temperatures as previously reported.¹²

4.3 Structure-to-property relationship

Dibenzoxazine monomers are preferred for the elaboration of high-performance polyBz. They are divided into two main classes Class A and Class B (Scheme I.9). This chapter will provide an overview of diBz design flexibility emphasizing the relationship between the chemical structure and their properties similarly than previously reported.¹¹⁷

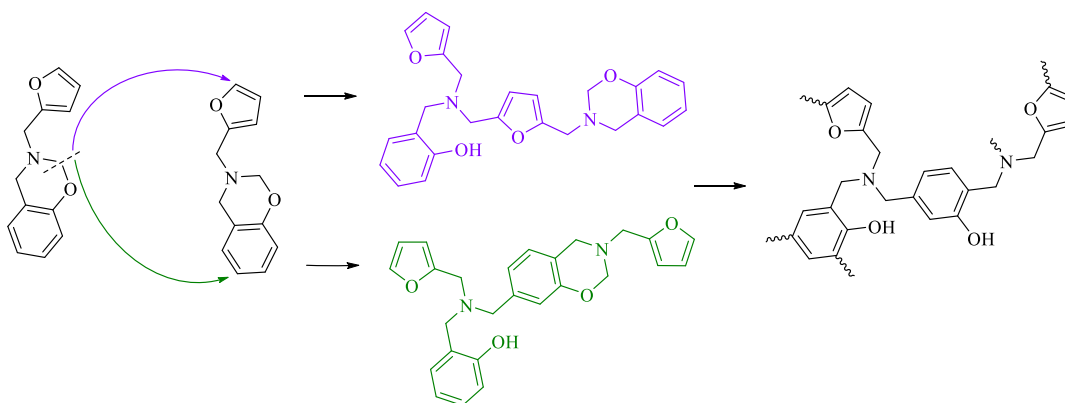
4.3.1 Class A

Class A diBz is the earliest studied and the most appealing type of diBz monomers due to its properties and the availability of a wide range of diphenolic compounds in the market. A summary of the thermal properties is listed in Table I.2. The effect of the structural features of the monomers and the substitution groups on these properties is described below.

The nature of the bridging group in diphenolic compounds has a huge impact on the synthesis and polymerization of benzoxazines. Wang *et al.* studied the influence of the electronic effects of different bisphenols on the ring-closing and ring-opening of six diBz using aniline as primary amine (Table I.2: BA-a, BF-a, BO-a, BP-a, BS-a, BZ-a).¹¹⁸ The electron-donating effect of the bridging groups of BA ($-\text{C}(\text{CH}_3)_2-$) or BP (single bond) boots the formation of oxazine rings. However, even if this type of Bz is easy to synthesize, its polymerization remains challenging. By contrast, the withdrawing effect of BZ ($-\text{CO}-$) or BS ($-\text{SO}_2-$) stabilizes the mesomeric form of the phenolic group and decreases the ability of the bisphenol to close the oxazine ring. Additionally, the presence of an electron-withdrawing group in the monomers can reduce the charge density of oxygen and destabilize the C–O bond and therefore, promote the ring-opening polymerization. Furthermore, the flexibility of the bridging group has an impact on the melting temperatures (T_m). The bridging groups of BA ($-\text{C}(\text{CH}_3)_2-$), BF ($-\text{CH}_2-$), and BO ($-\text{O}-$) lead to Bz with low melting points (around 122 °C) in comparison to benzoxazines with rigid bridges such as BZ ($-\text{CO}-$) and BP (single bond), for which higher melting temperatures are obtained (>200 °C).¹¹⁸ The impact of the flexibility could be also observed by analyzing two additional Bz from aniline using di-hydroxynaphthalene¹¹⁹ and resorcinol¹²⁰ (Table I.2: 1,5DHN-a and R-a respectively). The low flexibility of the bridging group of 1,5DHN yielded a monomer with high T_m (195 °C) compared to the low melting point obtained for R-a (14 °C). For a better understanding of the effect of the flexibility of the bridging group, Patton and co-workers prepared aliphatic-bridged bisphenol-based Bz monomers comprising four to ten methylene unit spacers that were reacted with 4-hydroxybenzaldehyde (Table I.2: 1,4BOP-ba, 1,6BOP-ba, 1,8BOP-ba, 1,10BOP-ba, respectively).¹²¹ Even though melting and polymerization temperatures remained only slightly affected, an increase in the aliphatic chain length has a clear impact on the glass transition temperature (T_g), shifting from 100 °C for a four-carbon chain length to 66 °C with a 10 carbon of the aliphatic bridge.

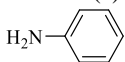
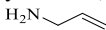
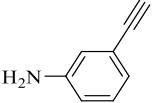
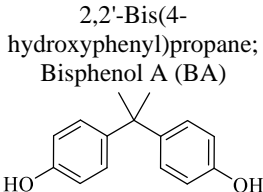
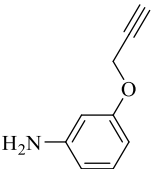
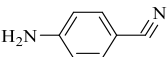
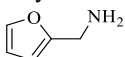
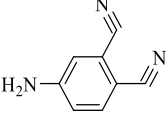
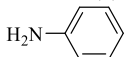
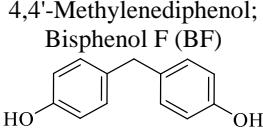
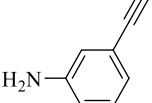
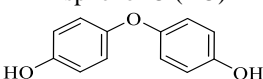
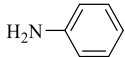
In addition to the effect of the bridging group, the impact of the type of amine used has been reported. Among the tested monoamine aniline and allylamine have been the most employed primary amine for the synthesis of polyBz. Particularly allylamine brings to the benzoxazine an allyl group responsible for the decrease of the polymerization temperature ($<150\text{ }^{\circ}\text{C}$) and at the same time introduce additional crosslinks leading to materials with high T_g (Table I.2: BA-ala, BS-ala, 1,5DHN-ala, BPBA-ala).^{119, 122-124} In comparison to the use of aniline, the absence of the benzene group reduces the energy necessary for the thermal activation of the ROP. Besides, acetylene-containing Bz were shown to increase even more the T_g of polyBz ($320\text{-}370\text{ }^{\circ}\text{C}$) due to the participation of this chemical group on the polymerization process incrementing crosslinking density of the system (Table I.2: BA-apa, BF-apa, BS-apa, BZ-apa, 1,5DHN-apa).¹²⁵⁻¹²⁷ The use of phthalonitrile or p-aminobenzonitrile to synthesize Bz leads to the incorporation of nitrile groups in the system (Table I.2: BA-ph, BZ-ph, BA-abn).¹²⁸⁻¹³⁰ In addition, some attempts to add functionalities onto the diphenolic compounds were studied. Aniline was reacted with allyl functionalized diphenol (Table I.2: DABA-a). The resulting material exhibit particularly high T_g values around $300\text{ }^{\circ}\text{C}$.¹³¹

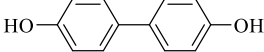
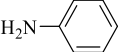
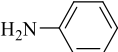
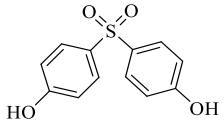
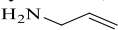
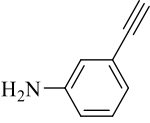
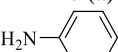
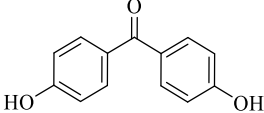
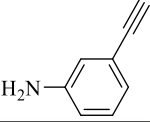
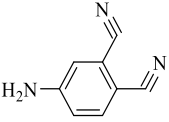
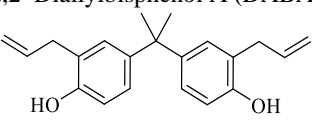
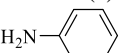
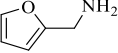
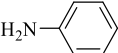
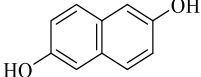

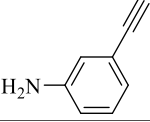
Nowadays, the development of more sustainable materials is becoming more important. In this context, the use of renewable resources for the synthesis of polyBz is augmenting. In the last years, a clear increase in the use of furfurylamine (fa), a bio-based amine, for the elaboration of polyBz has been experienced. This bio-based amine has focused the attention of the research community not only for its renewable origin but also for the involvement of the furan ring in the network formation (Scheme I.12).¹³² This additional crosslinking site leads to polyBz with excellent properties showing higher values of T_g ($308\text{ }^{\circ}\text{C}$) than the respective polyBz with aniline ($170\text{ }^{\circ}\text{C}$) (Table I.2: BA-fa).¹³² Besides, bio-based diphenolic compounds have been also targeted for the synthesis of Bz. The first example reported was diphenolic acid that was reacted with both aniline and furfurylamine. In addition to its sustainability, the compound has a carboxylic acid function in the bridging group acting as an inherent catalyst of benzoxazines ROP. Thanks to this, the polymerization temperatures are triggered around $190\text{ }^{\circ}\text{C}$ and the polybenzoxazines have a T_g of $208\text{ }^{\circ}\text{C}$ and $303\text{ }^{\circ}\text{C}$, with aniline and furfurylamine respectively (Table I.2: DPA-a, DPA-fa).¹³³⁻¹³⁴ Additionally, furfurylamine was reacted with other bio-based phenolics such as daidzein¹³⁵, resveratrol¹³⁶, catechol¹³⁷, and magnolol¹³⁸, and their properties are listed in Table I.2 (DZ-fa, RES-fa, CT-fa, M-fa).

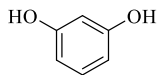
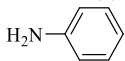
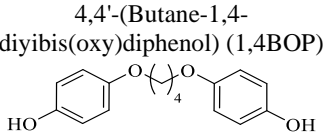
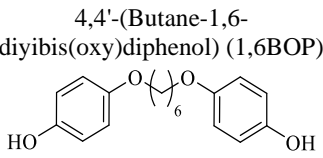
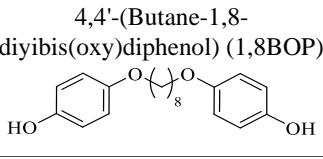
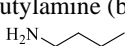
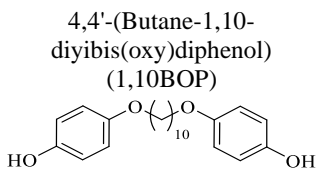
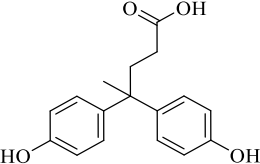
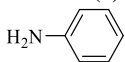
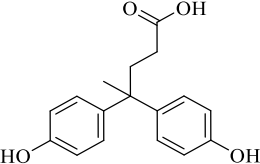
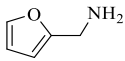
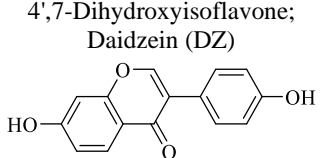
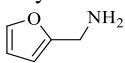
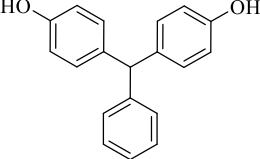
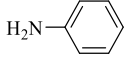
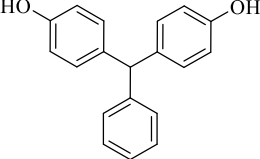
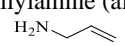
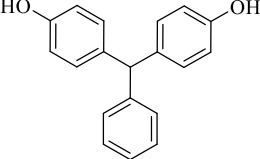
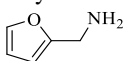


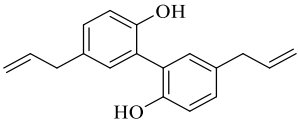
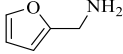
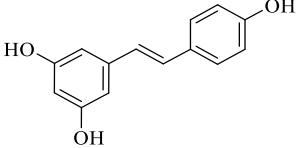
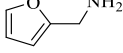
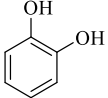
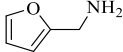
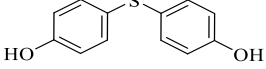
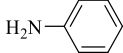
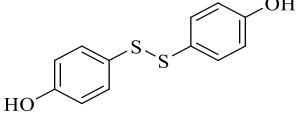
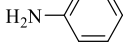
Scheme I.12. Polymerization routes of furan-containing benzoxazines.

Table I.2. Summary of the chemical features of the diphenols and monoamines used for the synthesis of Class A diBz and their thermal properties.

Abbr.	Diphenol	Monoamine	T _m ^a (°C)	T _{poly} ^b (°C)	T _g ^c (°C)	T _{5%} ^d (°C)	Ref.
BA-a		Aniline (a) 	123	267	170	310	118, 122
BA-ala		Allylamine (ala) 	-	265	298	343	122
BA-apa		Aminophenyl acetylene (apa) 	-	180	356	458	125-127
BA-appe	2,2'-Bis(4-hydroxyphenyl)propane; Bisphenol A (BA) 	Propargyl ether aniline (appe) 	-	241	295	352	139
BA-abn		4-Aminobenzonitrile (abn) 	-	259	190	-	129-130
BA-fa		Furfurylamine (fa) 	110	240	308	347	132
BA-ph		Phthalonitrile (ph) 	-	227	-	423	128
BF-a		Aniline (a) 	122	264	173	-	118, 126
BF-apa	4,4'-Methylenediphenol; Bisphenol F (BF) 	Aminophenyl acetylene (apa) 	-	-	368	470	125, 127
BO-a	4,4'-Dihydroxydiphenyl ether; Bisphenol O (BO) 	Aniline (a) 	122	260	-	-	118

Abbr.	Diphenol	Monoamine	T _m ^a (°C)	T _{poly} ^b (°C)	T _g ^c (°C)	T _{5%} ^d (°C)	Ref.
BP-a	4,4'-Dihydroxybiphenyl; Bisphenol P (BP) 	Aniline (a) 	205	257	-	-	118
BS-a		Aniline (a) 	183	215	-	300	118
BS-ala	4,4'-Sulfonyldiphenol; Bisphenol S (BS) 	Allylamine (ala) 	-	227	254	335	118
BS-apa		Aminophenyl acetylene (apa) 	-	180	-	440	125-127
BZ-a		Aniline (a) 	206	239	340	290	118
BZ-apa	4,4'-Dihydroxybenzophenone; Bisphenol Z (BZ) 	Aminophenyl acetylene (apa) 	-	180	-	478	125, 127
BZ-ph		Phthalonitrile (ph) 	-	234	-	544	128
DABA-a	2,2'-Diallylbisphenol A (DABA) 	Aniline (a) 	52- 55	270	300	395	131
DABA-fa		Furfurylamine (fa) 	-	252	-	390	140
1,5DHN-a		Aniline (a) 	195	216	220	260	119
1,5DHN-ala	1,5-Dihydroxynaphtalene (1,5DHN) 	Allylamine (ala) 	169	199	303	340	119
1,5DHN-apa		Aminophenyl acetylene (apa) 	-	185	-	448	127

Abbr.	Diphenol	Monoamine	T _m ^a (°C)	T _{poly} ^b (°C)	T _g ^c (°C)	T _{5%} ^d (°C)	Ref.
R-a	Resorcinol (R) 	Aniline (a) 	146	229	179	-	120
1,4BOP-ba	4,4'-(Butane-1,4-diyibis(oxy)diphenol) (1,4BOP) 		83.9	253	-	236	
1,6BOP-ba	4,4'-(Butane-1,6-diyibis(oxy)diphenol) (1,6BOP) 		71.5	252	-	228	
1,8BOP-ba	4,4'-(Butane-1,8-diyibis(oxy)diphenol) (1,8BOP) 	Butylamine (ba) 	76.5	254	76	231	121
1,10BOP-ba	4,4'-(Butane-1,10-diyibis(oxy)diphenol) (1,10BOP) 		79.4	257	67	231	
DPA-a	4,4'-Bis(4-hydroxyphenyl)valeric acid (DPA) 	Aniline (a) 	-	192	208	350	133, 141
DPA-fa		Furfurylamine (fa) 	-	184	303	317	134
BZ-fa	4',7-Dihydroxyisoflavone; Daidzein (DZ) 	Furfurylamine (fa) 	164	204	391	462*	135
BPBA-a	Benzaldehyde-based bisphenol (BPBA) 	Aniline (a) 	-	229	194	378	
BPBA-ala		Allylamine (ala) 	-	267	234	364	124
BPBA-fa		Furfurylamine (fa) 	-	237	240	379	

Abbr.	Diphenol	Monoamine	T _m ^a (°C)	T _{poly} ^b (°C)	T _g ^c (°C)	T _{5%} ^d (°C)	Ref.
M-fa	5,5'-Diallyl-2,2'-biphenyldiol; Magnolol (M) 	Furfurylamine (fa) 	100	229	303	440	138
RES-fa	5-[(1E)-2-(4-Hydroxyphenyl)ethenyl]-1,3-benzenediol; Resveratrol (RES) 	Furfurylamine (fa) 	126	229	312	346	136
CT-fa	Catechol (CT) 	Furfurylamine (fa) 	198	220	-	-	137
4DTP-a	4,4'-Thiodiphenol (4DTP) 	Aniline (a) 	-	-	206	-	142
4DPDS-a	4,4'-Dihydroxydiphenyldisulfide (4DPDS) 	Aniline (a)** 	-	-	-	-	143-144

^aMelting temperature of the monomers. ^bMaximum temperature of the exothermic peak corresponding to the ROP of the monomers. ^cGlass transition temperature of the polyBz. ^dTemperature of 5% of weight loss by thermogravimetric analyses, *values correspond to 10% weight loss; **cyclocondensate of aniline and formaldehyde was used (1,3,5-triphenyl-1,3,5-triazine)

4.3.2 Class B

Class B benzoxazines are composed of phenolic compounds bridged with a diamine. They are interesting due to their versatile synthesis and the numerous monophenolic and diamine compounds available. Besides, the nature of the bridging group from the diamine strongly affects the synthesis conditions and the thermal properties of the benzoxazines and their respective polyBz. Moreover, the nature of the substitution of the phenolic compound brings particular behaviors in the monomers, such as the promotion of the thermal activation of the ROP or the increase of the crosslinking density through additional reactions.¹⁴⁵⁻¹⁴⁷

PolyBz are mainly intended for high-performance applications, thus aromatic diamines that stand as rigid bridges have been used for their design. Monophenolic compounds were reacted with 1,4-phenylenediamine (pd), 4,4'-diaminodiphenylmethane (ddm), (4-aminophenyl)ether (dde), 4,4'-diamino diphenyl sulfone (dds), 4,4'-diamino diphenyl sulfone (dds), 1,4[bis(4'-aminophenoxy) phenyl sulfone] (ddps), (4-(4-aminophenoxy)phenyl)ether (44appe), bis-(3-(4-aminophenoxy)phenyl)ether (34 appe), 4,4'-(p-Biphenylenedioxy) dianiline (ddpo), 2,7-bis(4-aminophenoxy)naphtalene (npda), and 2,2-bis(4-(4-aminophenoxy)phenyl)propane

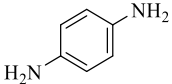
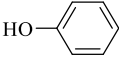
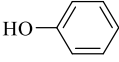
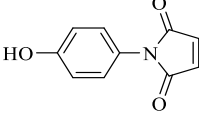
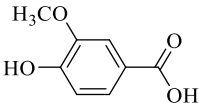
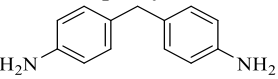
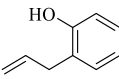
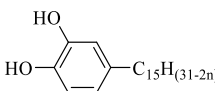
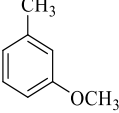
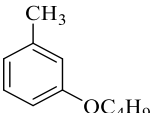
(app). The thermal properties and the references of diBz monomers prepared with the above-mentioned aromatic diamines, and their corresponding polyBz are listed in Table I.3.

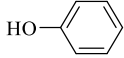
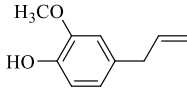
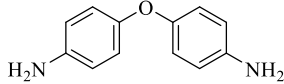
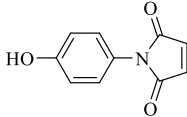
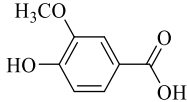
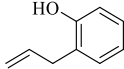
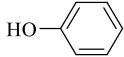
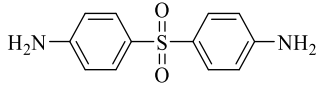
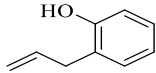
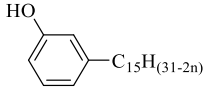
The incorporation of linear aliphatic diamines was considered as a strategy to reduce the brittle nature of Bz. Allen *et al.* studied the effect of diamines chain length, from 2 to 12 aliphatic CH₂, on the synthesis of benzoxazine monomers and their polymerization.¹⁴⁸ This work shown that the shorter the length of the diamines, the faster and the easier monomer formation was. Besides, melting and glass transition temperatures were proportionally reduced with the increasing of the length of the bridging group of the diamines (Table I.3: P-da, P-1,4da, P-1,6da, P-1,8da, P-1,12da).

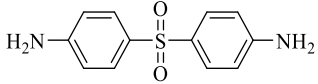
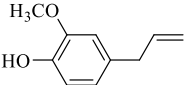
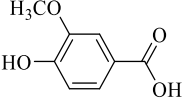
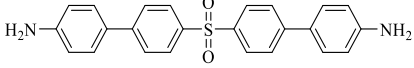
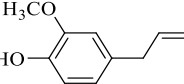
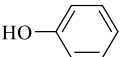
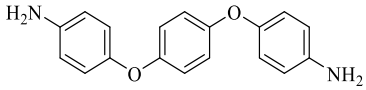
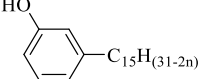
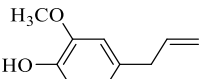
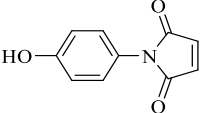
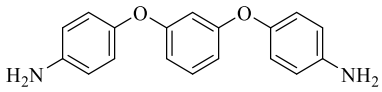
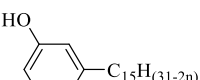
In a similar way as for Class A, the incorporation of special functionalities into Bz monomers has been extensively considered to reduce polymerization temperatures or to improve the properties of the resultant polyBz. Additionally, the design of Class B Bz brings the possibility to replace petroleum-based phenols by bio-based phenolic compounds and therefore, develop high-performance materials from renewable resources. For this reason, vanillin¹⁴⁹, eugenol¹⁵⁰⁻¹⁵¹, cardanol¹⁵²⁻¹⁵⁴, and urushiol¹⁵⁵ have been bridged with a wide set of aromatic and aliphatic diamines. Cardanol and urushiol have a long hydrophobic alkyl chain linked to a phenolic ring, abbreviated as C₁₅H_(31-2n) to refer to their variable unsaturation degree (Table I.3). Their side chain leads to monomers with wide processing windows (low T_m) and the ability to toughen polymers (Table I.3: CAR-dds, CAR-44appe, CAR-34appe, CAR-app, U-ddm). Some of the highlights of cardanol-based benzoxazines include polymers with high thermal stability and low viscosity of benzoxazines enhancing the range of possible applications.¹⁵⁶ However, there are some limitations such as high curing temperature and materials with low T_g. On the contrary, in the absence of a long alkyl chain, eugenol and vanillin-based diBz exhibit very high thermal properties and T_g (Table I.3: E-dde, E-dds, E-ddps, E-44appe, V-ddm, V-dde, V-dds, V-app). The glass transition temperature can reach 255 °C with vanillin and is ranging from 125 to 140 °C when eugenol is used.¹⁴⁹⁻¹⁵¹ Eugenol is a phenolic compound with a methoxy and an allyl group at *ortho* and *para* positions respectively. Consequently, due to blocked *ortho* and *para* positions, only the *meta* positions with low reactivity are available, impeding the formation of a highly crosslinked eugenol-based network.¹⁵⁷

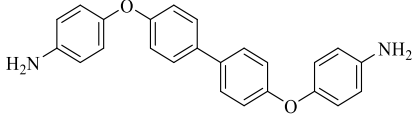
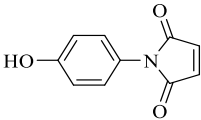
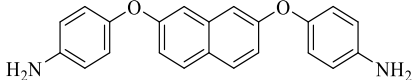
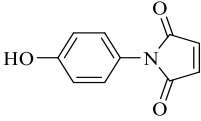
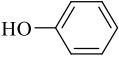
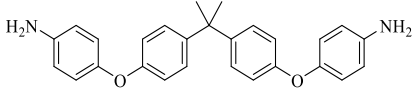
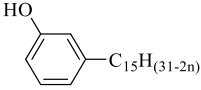
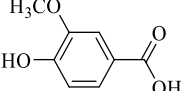
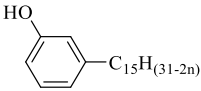
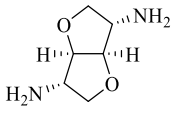
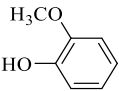
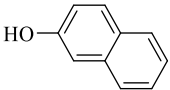
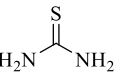
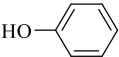
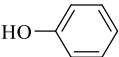
In conclusion, the rich molecular design flexibility of benzoxazines allows the synthesis of several di-benzoxazines. The characteristics of the monomer and polymer will depend on the nature and flexibility of the bridging groups and the additional functionalities that are introduced. It is important to highlight the possibility to replace partially or totally petroleum-based reagents by bio-based ones, making polyBz of high interest. Finally, the properties of each polyBz change upon the selection of the suitable starting ingredients giving the alternative to tailor the final features of the materials depending on the target application.

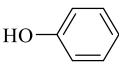
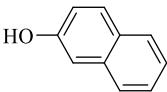
Table I.3. Summary of the chemical features of the diamines and monophenols used for the synthesis of Class B diBz and their thermal properties.

Abbr.	Diamine	Monophenol	T _m ^a (°C)	T _{poly} ^b (°C)	T _g ^c (°C)	T _{5%} ^d (°C)	Ref
P-pd	1,4-Phenylenediamine (pd) 	Phenol (P) 	180	260	220	372	158
P-ddm		Phenol (P) 	123	244	208	425	159
HPPDI O-ddm		1-(4-Hydroxyphenyl)-1h-pyrrole-2 5-dione (HPPDIO) 	100	211	300	379	146
V-ddm		Vanillin (V) 	177	234	231	352	149
oAP-ddm	4,4'-Diaminodiphenylmethane (ddm) 	o-Allylphenol (oAP) 	-	265	139	324	160
U-ddm		Urushiol (U) 	120	212	132	350	155
3,MO-ddm		3-Methoxyphenol (3,MO) 	106	216	-	-	161
3,BO-ddm		3-Butoxyphenol (3,BO) 	131	205	-	-	161

Abbr.	Diamine	Monophenol	T _m ^a (°C)	T _{poly} ^b (°C)	T _g ^c (°C)	T _{5%} ^d (°C)	Ref
P-dde		Phenol (P) 	128		194	376	158
E-dde		Eugenol (E) 	145	225	125-140	240	151
HPPDI O-dde	(4-Aminophenyl)ether (dde) 	1-(4-Hydroxyphenyl)-1h-pyrrole-2,5-dione (HPPDIO) 	100	218	301	383	146
V-dde		Vanillin (V) 	145	234	227	322	149
oAP-dde		o-Allylphenol (oAP) 	-	265	143	310	160
P-dds		Phenol (P) 	209	261	184	382	158
oAP-dds	4,4'-Diamino diphenyl sulfone (dds) 	o-Allylphenol (oAP) 	98	223	193	370	145
CAR-dds		Cardanol (CAR) 	-	251		299	162-163

Abbr.	Diamine	Monophenol	T _m ^a (°C)	T _{poly} ^b (°C)	T _g ^c (°C)	T _{5%} ^d (°C)	Ref
E-dds	4,4'-Diamino diphenyl sulfone (dds) 	Eugenol (E) 	130	195	125-140	295	151
V-dds		Vanillin (V) 	229	277	255	339	149
E-ddps	1,4[Bis(4'-aminophenoxy) phenyl sulfone] (ddps) 	Eugenol (E) 	145	250	125-140	275	151
P-44appe		Phenol (P) 	164	239	172	417	158
CAR-44appe	(4-(4-Aminophenoxy)phenyl)ether (44appe) 	Cardanol (CAR) 	114	233	-	348	162-163
E-44appe		Eugenol (E) 	115	250	125-140	260	151
HPPDI O-44appe		1-(4-Hydroxyphenyl)-1h-pyrrole-2 5-dione (HPPDIO) 	100	214	303	376	146
CAR-34appe	Bis-(3-(4-aminophenoxy)phenyl)ether (34appe) 	Cardanol (CAR) 	70	267	-	354	162-163

Abbr.	Diamine	Monophenol	T _m ^a (°C)	T _{poly} ^b (°C)	T _g ^c (°C)	T _{5%} ^d (°C)	Ref
HPPDI O-ddpo	4,4'-(p-Biphenylenedioxy) dianiline (ddpo) 	1-(4-Hydroxyphenyl)-1h-pyrrole-2,5-dione (HPPDI) 	100	221	289	374	146
HPPDI O-npda	2,7-Bis(4-aminophenoxy)naphtalene (npda) 	1-(4-Hydroxyphenyl)-1h-pyrrole-2,5-dione (HPPDI) 	100	232	307	379	146
P-appp		Phenol (P) 	152	249	170	412	158
CAR- appp	2,2-Bis(4-(4-aminophenoxy)phenyl)propane (appp) 	Cardanol (CAR) 	-	263	-	323	162- 163
V-appp		Vanillin (V) 	-	228	202	488	149
CAR- ima		Cardanol (CAR) 	103	266	83	358 *	
G-ima	Isomannide diamine (ima) 	Guaiacol(G) 	177	261	128	318 *	164
BN-ima		β-Naphthol (BN) 	203	253	-	324 *	
P-tu	Thiourea (tu) 	Phenol (P) 	-	-	-	-	165
P-da	Ethylenediamine (da) H ₂ N-(CH ₂) ₂ -NH ₂	Phenol (P) 	112	185	179	291	148

Abbr.	Diamine	Monophenol	T _m ^a (°C)	T _{poly} ^b (°C)	T _g ^c (°C)	T _{5%} ^d (°C)	Ref
P-1,3da	1,3-Diaminopropane (1,3da) H ₂ N-(CH ₂) ₃ -NH ₂	Phenol (P)	-	185	282	-	166
							
BN-1,3da	1,3-Diaminopropane (1,3da) H ₂ N-(CH ₂) ₃ -NH ₂	β-Naphthol (BN)	-	208	231	-	166
							
P-1,4da	1,4-Diaminobutane (1,4da) H ₂ N-(CH ₂) ₄ -NH ₂	Phenol (P)	94	225	169	270	148
P-1,6da	1,6-Hexanediamine (1,6da) H ₂ N-(CH ₂) ₆ -NH ₂	Phenol (P)	83	225	171	280	148
oAP-1,6da		o-allylphenol (oAP)	-	238	87	242	145
TYM-1,6da		Thymol (TYM)	-	275	-	126	167
P-1,8da	1,8-Diaminooctane (1,8da) H ₂ N-(CH ₂) ₈ -NH ₂	Phenol (P)	73	236	137	287	148
P-1,12da	1,12-Diaminododecane (1,12da) H ₂ N-(CH ₂) ₁₂ -NH ₂	Phenol (P)	49	241	105	286	

^aMelting temperature of the monomers. ^bMaximum temperature of the exothermic peak corresponding to the ROP of the monomers. ^cGlass transition temperature of the polyBz. ^dTemperature of 5% of weight loss by thermogravimetric analyses, *values correspond to 10% weight loss; *values correspond to 10% weight loss.

5 State of the art of benzoxazine resins and rubber

The project aims to use benzoxazine resins in rubber compounds. For this reason, this part will be focused on the previous work regarding the combination of benzoxazine resins and rubber.

5.1 Blends of benzoxazine resins and rubber

One of the most reported strategies to incorporate benzoxazine moieties in rubber is the production of blends. The properties of blends between model Bz monomers and rubbers are listed in Table I.4.

Nitrile butadiene rubber (NBR) has been reinforced with bisphenol F based benzoxazine resins by Rajesh *et al.*¹⁶⁸ aiming at forming composites by a co-curing process using prepregs. They found the Bz resin is existing in the form of a localized, interpenetrating network structure in

the NBR matrix. The composite showed improvements in mechanical properties such as tensile strength, tear strength, and elongation at break and in thermal resistance compared to non-reinforced NBR.

Table I.4. Type of benzoxazine and rubber used for the elaboration of blends and their properties.

Rubber	Benzoxazine	Approach	Properties	Ref
NBR	Bisphenol F and aniline (BF-a)	Composite - prepreg	Improvement of tensile strength, tear strength, tensile set, modulus and elongation at break	168
ATBN and CTBN	Bisphenol A and aniline (BA-a)	Melt mixing (120 °C)	Increase in fracture toughness and flexural strength. Accelerate cure rate	16
HTBD	Phenol and 1,12-diaminododecane (P-1,12da)	Melt mixing (100 °C)	Phase-separated domains	17
LEBD	Phenol and 1,12-diaminododecane (P-1,12da)	Melt mixing (100 °C)	Dispersed domains	17
HEBD	Phenol and 1,12-diaminododecane (P-1,12da)	Melt mixing (100 °C)	No phase separation	17
HTBD	Phenol and 1,12-diaminododecane (P-1,12da)	Melt mixing (100 °C)	Superhydrophobic rubber-Bz/SiO ₂ nanocomposite	169
ATBN, CTBN and ETBN	Bisphenol A and aniline (BA-a)	Solvent casting	Lowering ROP, improvement in toughness, and thermal stability. Increase T _g	18
SEBS	Bisphenol A and cyclohexylamine (BA-ca)	Blending mixed solvent and electrospinning	Nanospherical thermoset resins controllable size	170
ATBN	Bisphenol A and aniline (BA-a)	Melt mixing (80 °C)	Lowered curing temperature and improvement of mechanical properties	19

To overcome the brittleness of polybenzoxazines, elastic modifiers have been incorporated into the polybenzoxazine matrix. Reactive liquid rubbers are suitable for this purpose because of their low viscosity, and the polarity of rubber can be controlled by changing the ratio of polybutadiene and acrylonitrile rubber. Besides, Bz has many functional groups that can react with the reactive functional group of commercial liquid rubber.²⁰ For instance, amine-terminated butadiene/acrylonitrile rubber (ATBN),^{68,19} epoxy-terminated liquid nitrile rubber (ETBN),¹⁸ and carboxyl terminated butadiene/acrylonitrile rubber (CTBN),^{68,18} hydroxyl-terminated butadiene rubber (HTBD),¹⁷ and low and high epoxy content butadiene rubber (LEBD and HEBD),¹⁷ have been used with this objective. The combination of ATBN with benzoxazine resin based on bisphenol A and aniline (BA-a) was carried out by adding liquid rubber to molten Bz monomer at 120 °C. The molten mixture was cast in a silicone rubber mold and cured.¹⁶ The presence of ATBN resulted in a significant enhancement of the fracture toughness properties. Furthermore, the T_g of the fully cured poly(BA-a)/ATBN copolymers showed values ranging from 172 to 162 °C with increasing ATBN content. ATBN affected the T_g of the blend as well as its curing temperature. The influence of amine groups to reduce ROP temperature as nucleophiles is worth highlighting.^{18,19}

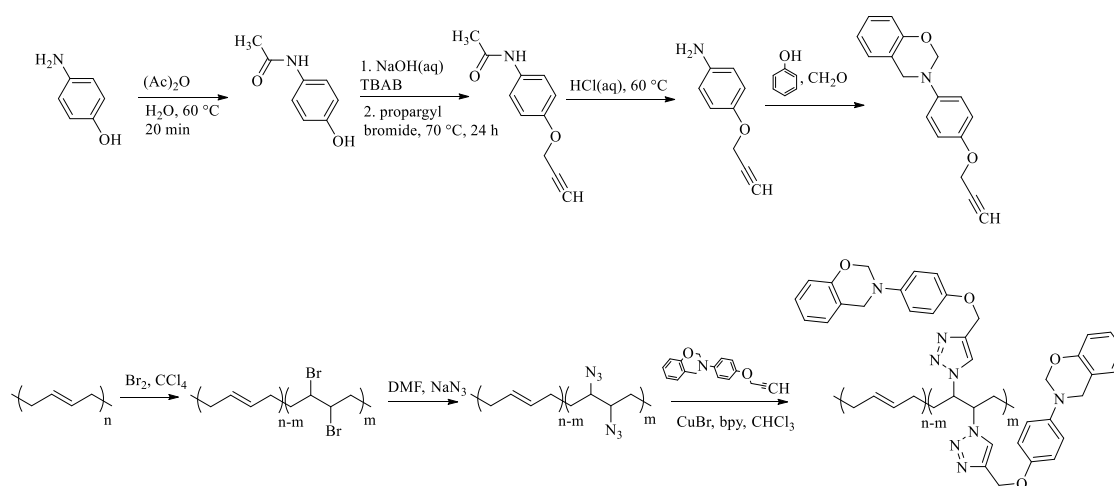
Rungswang *et al.*¹⁷⁰ investigated the blend of benzoxazine monomer from bisphenol A with a thermoplastic elastomer (polystyrene-block-poly(ethylene-*co*-1-butene)-block-polystyrene triblock copolymer). The curing of Bz in the blend not only resulted in polyBz but also formed nanoparticles in a controllable size from one hundred to a few nanometers, resulting in a simple way to prepare size-controllable nanospheres. The authors attributed the formation of nano spherical thermoset resins to the interaction between polystyrene segments and Bz followed by curing of Bz under polystyrene.

In 2017, Calcona and co-workers¹⁶⁹ applied the work of Lee *et al.*¹⁷ to produce superhydrophobic rubber-modified polybenzoxazine/SiO₂ nanocomposite coatings with anti-corrosion, anti-ice, and super-oleophilic properties.

In summary, polybenzoxazines have been used for the reinforcement of rubbers. Additionally, the elaboration of blends has also been investigated for the improvement of the brittleness of benzoxazine resins.

5.2 Functionalization of rubbers with benzoxazines

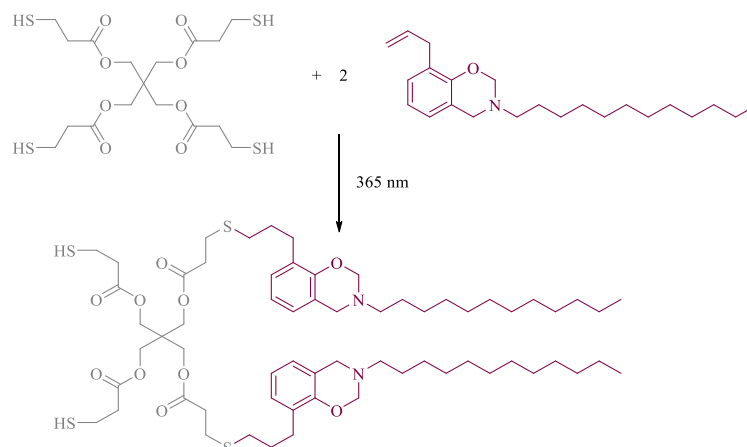
Another possible approach is to functionalize rubber with benzoxazine groups. For this aim, Kukut *et al.*²¹ functionalized polybutadiene rubber with side-chain benzoxazines by incorporating Bz groups into a polymer backbone by a simple click reaction route (Scheme I.13). They studied the polymerization behavior of the final system showing that benzoxazine groups could undergo thermal ring-opening in the absence of a catalyst to form crosslinked polymer networks. The final polymer has higher char yield compared to commercial polybutadiene. The authors support that this approach will pave a way toward the synthesis of thermally curable rubbers that can be used as intermediates for the design of more complex macromolecular systems, such as interpenetrating networks and high-performance thermoset polymers.



Scheme I.13. Synthesis of functionalized polybutadiene with side-chain Bz.²¹

Benzoxazine-functionalized poly(styrene-*b*-butadiene-*b*-styrene) was successfully synthesized *via* thiol-ene click reaction.²² Thiol containing benzoxazine monomers were synthesized following the procedure depicted in Scheme I.14. After that, the thiol-functionalized Bz was directly grafted on the polybutadiene part using UV-light. Finally, a thermal treatment was carried out to polymerize Bz moieties and, thus, improve the mechanical properties and solvent

resistance of the elastomer. The stress at break of functionalized polymer was nine times greater than that of the pure sample with only 0.5 wt% thiol functionalized Bz. The elongation at break was surprisingly even improved, contrary to traditional reinforced polymer systems.



Scheme I.14. Thiol functionalized benzoxazine.

Jubsilp *et al.* also studied the modification of BA-a with ATBN. The copolymers of polybenzoxazine modified with ATBN showed enhancement in the friction coefficient and wear resistance compared to those of the polyBz. Furthermore, the mechanical and thermal properties of the copolymers were maintained with the addition of ATBN at an amount lower than 10 wt%.

In 2018, Ren *et al.*²³ reported the use of a flexible polysulfide rubber chain to bridge benzoxazines. The approach followed relies on the ring-opening addition of thiol-capped liquid polysulfide rubber and a commercial diBz from bisphenol A and aniline.

In summary, several strategies have been developed to either incorporate benzoxazine groups to modify properties of rubbers or use these elastomers to improve the features of benzoxazines. In the next section, the effect of rubber ingredients on benzoxazines will be studied.

5.3 Interactions between benzoxazines and rubber ingredients

This section gathers a literature review concerning the interactions, functionalization, and use of benzoxazines in combination with each of the above-mentioned ingredients. The interactions between sulfur and benzoxazines are very specific and, due to their importance, will be discussed in a separate section.

The incorporation of fiber and nanoparticles into polybenzoxazines has been studied to produce novel materials with potential for commercial applications. To this aim, a variety of new polyBz-based materials have been developed using clays, carbon fibers, and carbon nanotubes. However, carbon black has not been extensively used to reinforce polybenzoxazines matrix and just a few studies have reported the preparation of nanocomposites or fibers with CB and polybenzoxazines. In 2014, the surface of carbon black was functionalized with carboxyl and hydroxyl functional groups to be used as conducting fillers for polyBz.¹⁷¹ The functionalized CB was then mixed with bisphenol A-aniline benzoxazine and polymerized obtaining nanocomposites. The formation of chemical bonds, as well as hydrogen bonding between polyBz and CB, were confirmed to give rise to enhanced electrical properties. Ahn *et al.*

functionalized carbon black with benzoxazine to produce polyacrylonitrile fibers with improved strength and conductivity.¹⁷² In a first step CB was reacted with 4-aminobenzoic acid to produce amino-terminated CB that was further reacted with phenol and paraformaldehyde yielding to benzoxazine-terminated carbon black. Tiptipakorn *et al.* studied the thermal properties of benzoxazine filled with carbon black and the effect of gamma radiation.¹⁷³ They reported an increase in the curing temperature as well as the T_g with increasing CB content.

Regarding the interaction of benzoxazines and accelerators, in July 2019 was granted a patent concerning the use of benzothiazole sulfonamides such as TBBS, CBS, and DCBS as a latent catalyst for benzoxazine resins.¹⁷⁴ Benzothiazoles reduce the energy required to cure benzoxazine as well as the temperature needed. The onset of the exothermic peak corresponding to ROP was reduced from 212 to 160 °C with a slight reduction of the T_g of the system (from 142 to 120 °C). This catalytic effect could be an asset allowing the polymerization of Bz at the same time than the vulcanization of rubber.

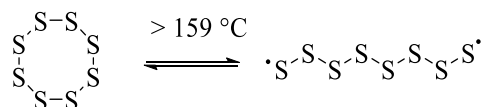
Additionally, functionalized ZnO was combined with Bz to produce polybenzoxazine nanocomposites.¹⁷⁵ The authors report the modification of the ZnO surface using monobenzoxazine terminated with silane. After that, they used it to reinforce a polyBz matrix made of BA-a. The resulted nanocomposites have a homogeneous and uniform distribution and improve both UV shielding behavior and photoluminescence at a certain wavelength.

Although the number of studies related to the use of tire components with polybenzoxazine is not very extensive, there is enough information regarding benzoxazine composites. These data highlight the importance of the interactions between the filler and the matrix. Even though tire composites are not binary systems, the interactions between the benzoxazine monomer and the rubber compound before and after curing might be of high importance.

6 Interactions between benzoxazine resins and sulfur

Sulfur is the main ingredient employed for rubber vulcanization as mentioned above.¹⁷⁶ Consequently, the interactions between benzoxazine and sulfur are of major interest. Few papers have reported these interactions, as it is a recent field of investigation. Different studies about the relationship between sulfur and benzoxazines, as well as the synthesis of sulfur-containing copolymers or benzoxazines, are gathered in the following sections.

Elemental sulfur, although it has many allotropes, is mainly present as an eight-membered ring (S_8). It melts at temperatures around 120 °C, and above 159 °C undergoes ring-opening to form a linear oligomer with di-radical chain end (Scheme I.15).¹⁷⁷ These generated radicals are reactive and could potentially react with benzoxazines.

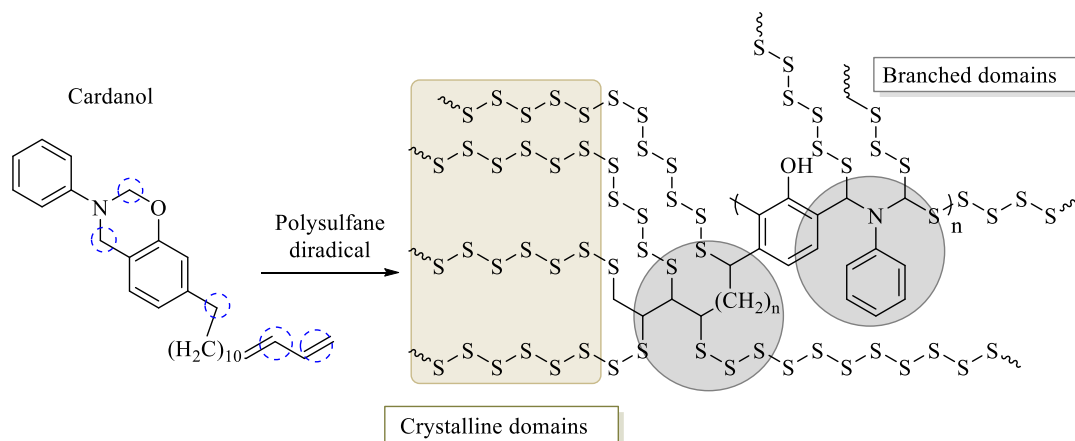


Scheme I.15. The reversible ring-opening reaction of sulfur.

Besides, thiols are organosulfur compounds with the form R-SH, where R represents an organic substituent. They can also be involved in the ring-opening polymerization of benzoxazines. Accordingly, a specific section will be dedicated to this topic.¹⁷⁸

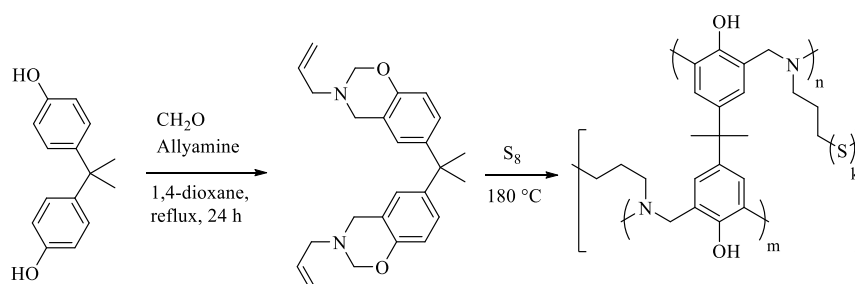
6.1 Inverse vulcanization

It is well known that sulfur can be processed in melt generating radicals on the sulfur atom. Although sulfur can polymerize alone, polysulfides are unstable at ambient conditions and depolymerize to form cyclo-octasulfur (S_8). Inverse vulcanization is the treatment of molten sulfur at temperatures above 159 °C with vinylic monomers leading to the formation of stable copolymers with a high loading of sulfur (~99%).¹⁷⁷ In the last years, inverse vulcanization has been applied to synthesize copolymers using benzoxazine monomers as a linker to chemically bind elemental sulfur. Shukla and co-workers used a cardanol benzoxazine as a sustainable linker for elemental sulfur-based random copolymer *via* inverse vulcanization (Scheme I.16).¹⁷⁹ The temperature of the ring-opening reaction was lowered from 242 to 185 °C due to the effect of elemental sulfur. Under the reaction conditions, the thiol-ene reaction and benzoxazine ring-opening occur simultaneously resulting in the creation of sulfur bonds between the methylene protons of benzoxazines and the unsaturation of cardanol. The use of this copolymer as a sustainable cathode active material in Li-S battery was also shown.¹⁸⁰



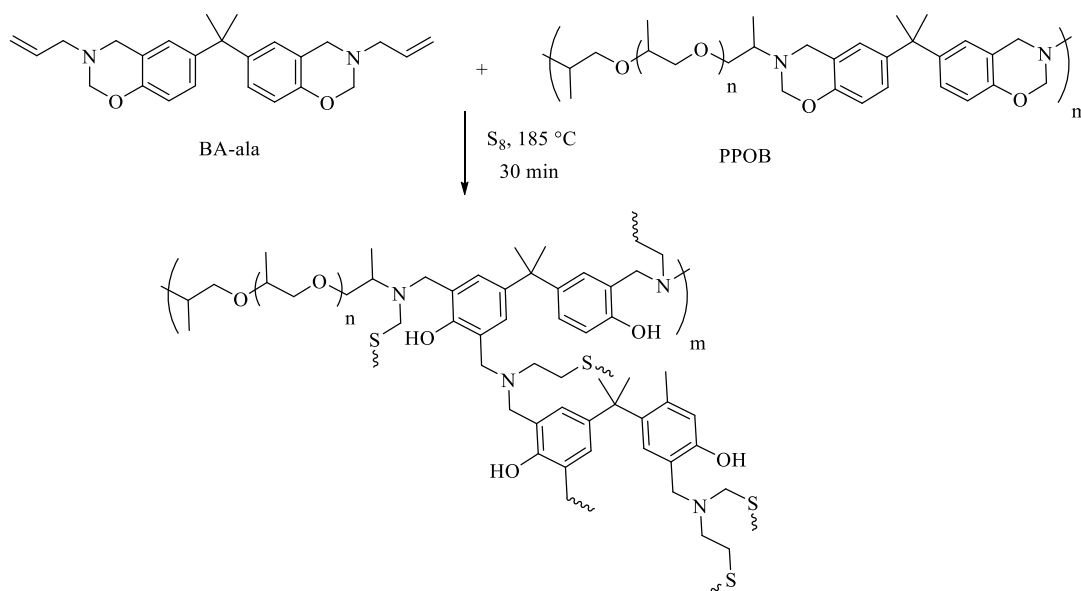
Scheme I.16. Pictorial depiction of the structure of random copolymer of sulfur and cardanol based benzoxazine.¹⁷⁹

A similar investigation was carried out by Arslan *et al.*¹⁸¹ They synthesize polybenzoxazine copolymers by reacting allyl functional benzoxazine and elemental sulfur (S_8) in a proportion ranging from 50 to 70 wt% of S_8 . Simultaneous inverse vulcanization and ring-opening reactions of benzoxazine generated copolymers at 180-185 °C. They described a relatively simple synthetic methodology that can be achieved in 30 min by a simple melt process. The curing of benzoxazine and inverse vulcanization took place simultaneously and/or sequentially producing copolymers with high sulfur content. Additionally, Akay *et al.*¹⁸² used the resulting copolymers as an efficient sorbent for mercury removal from aqueous solution.



Scheme I.17. Synthesis of polyBz copolymers with bisphenol A and allylamine benzoxazine and sulfur.

Recently, Arslan *et al.*¹⁸³ synthesize polybenzoxazines with dynamic sulfide linkages using the process mentioned above. In this case, inverse vulcanization of poly(propylene oxide)benzoxazine (PPOB) and diallylbenzoxazine (BA-ala) with elemental sulfur was performed at 185 °C (Scheme I.18), the ring-opening polymerization of the benzoxazines occurring concomitantly. The obtained crosslinked polymer films exhibited thermally driven recycling ability up to 5 cycles and the self-healing property of the film was demonstrated.



Scheme I.18. Synthesis of self-healing polyBz by using PPOB, B-al, and S₈ with various mixing ratios.

In summary, copolymers of polybenzoxazine and sulfur have been developed by inverse vulcanization following different approaches and targeting several applications, thus, valorizing a byproduct of the petrochemical industry.

6.2 Elemental sulfur and benzoxazines

There are two main elements reported in the literature concerning sulfur and benzoxazines. The first one considers sulfur as a catalyst for ROP, and in the second approach, sulfur acts as a co-reactant.

6.2.1 Elemental sulfur as a catalyst

Rodriguez Arza *et al.*³⁰ studied the reduction of the polymerization temperature caused by elemental sulfur. For this purpose, elemental sulfur (S₈) was mixed with several benzoxazines that were then reacted at 120 °C. It is important to highlight that this temperature is below the temperature for the formation of di-radical sulfur. The introduction of S₈ into benzoxazines generated new structures bearing a Schiff base and a phenolic –OH within the reactive system, which then triggered the reduction of the polymerization temperature by about 15% (up to a limit of around 220 °C) when 5 mol% of S₈ was added (Figure I.13). They found that the more basic the amine used to form the benzoxazine, the higher the extent of the reaction toward the formation of Schiff bases. It is worthwhile to note that the radical pathway for the reaction between S₈ and the monomers can be neglected because no differences were found when a radical inhibitor was introduced in the system. This result strongly suggests that the interactions between benzoxazines and sulfur occur through the amine portion of the Bz.

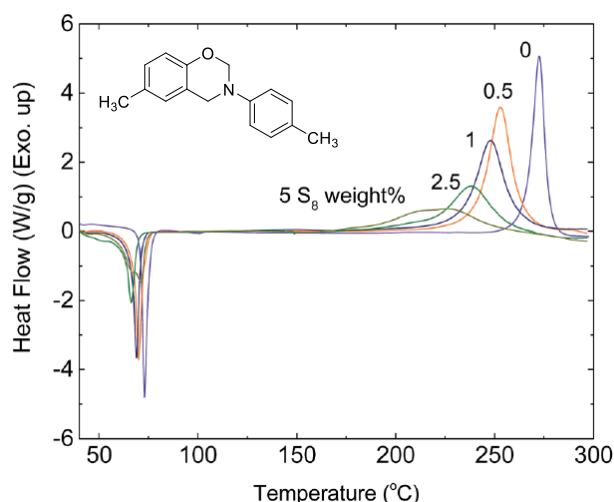
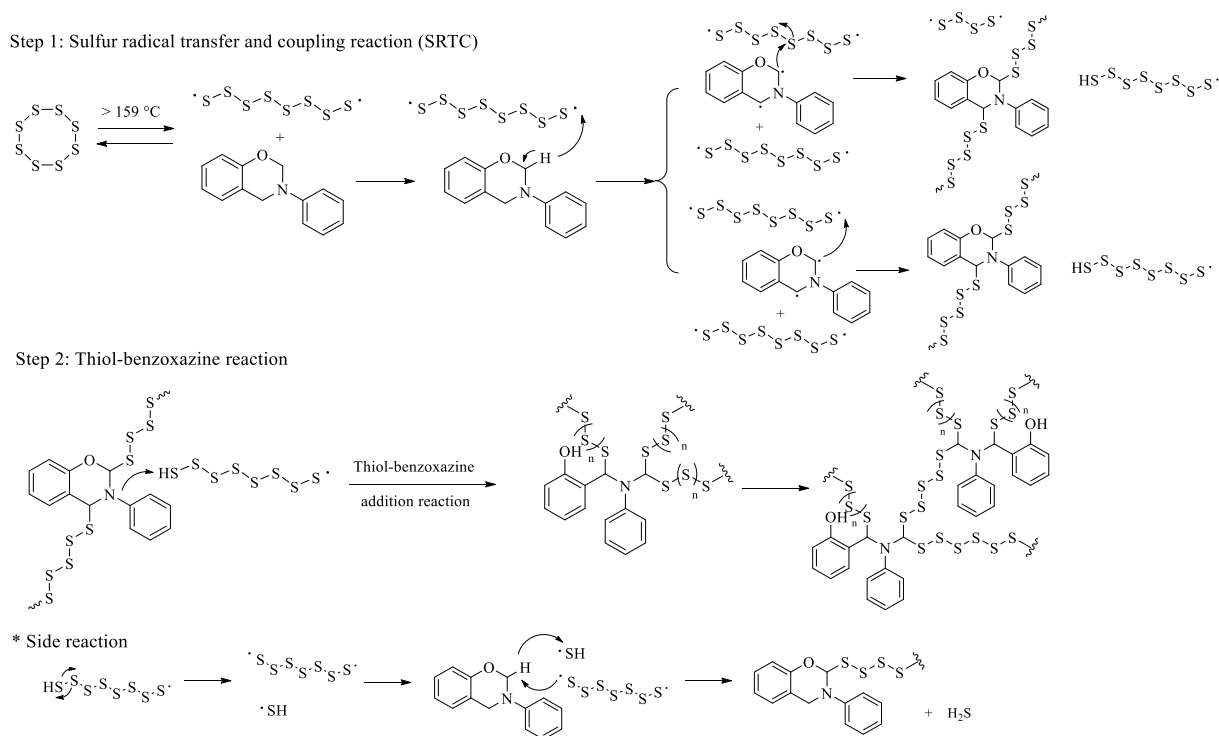


Figure I.13. DSC thermograms of Bz containing 0, 0.5, 1, 2.5 and 5 wt%.³⁰

To conclude, elemental sulfur appears to be a suitable catalyst for the ROP of benzoxazines. It could help to trigger the formation of the benzoxazine network at temperatures suitable for the vulcanization process of rubbers.

6.2.2 Elemental sulfur as a co-reagent

In 2018, Lin *et al.* reported a new reaction between sulfur and benzoxazine groups called sulfur radical transfer and coupling reaction (SRTC).³¹ They studied in detail the reaction between sulfur and a monobenzoxazine from phenol and aniline (P-a). After the study, they concluded that the reaction between elemental sulfur and benzoxazines occurs via a sequential SRTC reaction followed by thiol-benzoxazine addition reaction (explain in the following section). In Scheme I.19 is displayed the mechanism reaction.



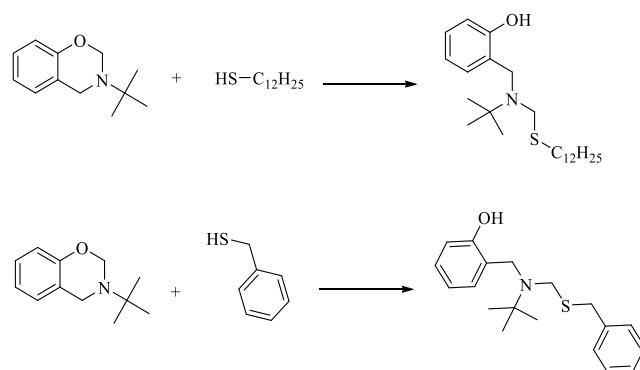
Scheme I.19. Reaction mechanism between S_8 and benzoxazines through the SRTC reaction and thiol-benzoxazine addition reaction.³¹

In the first step, the ring-opening of sulfur above 159 °C generates polysulfide chains with radicals at the end of the chain. Then, a radical transfer takes place from the polysulfide to the benzoxazine with a generation of thiols (–SH) and the formation of C–S bonds as well as radical addition to S–S bonds. In the last step, the generated thiols react with benzoxazines, opening the rings and forming a stable network between sulfur and benzoxazines. In conclusion, the SRTC reaction provides an easy route for the preparation of sulfur-containing polymers.

It is noteworthy that this study is not considering the option that benzoxazine could open before its reaction with sulfur, while sulfur has been proven to catalyze ROP of benzoxazines.³⁰

6.3 COLBERT reaction

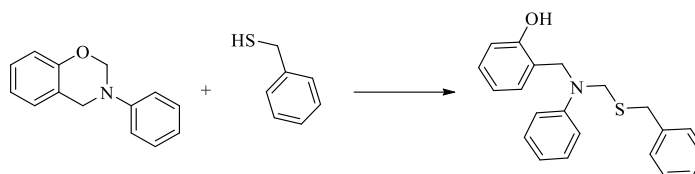
The catalytic opening of the lateral benzoxazine rings by thiols, known as COLBERT reaction, was found to proceed under ambient conditions to completion without releasing any byproducts.¹⁷⁸ This reaction made possible the polymerization of specific benzoxazines at room temperature and under solventless conditions. Gorodisher and co-workers studied the reaction between aliphatic and aromatic thiols with different kinds of benzoxazines. Three model benzoxazines were synthesized, one from *tert*-butyl amine and phenol, and the others from aniline or 4-methoxy-2-methyl-aniline and phenol. Several thiols with a simple chemical structure were selected for the study: 1-dodecanethiol, 4-nitrophenyl thiol, and benzyl thiol. The progress of the COLBERT reaction was followed by ¹H NMR (nuclear magnetic resonance). Benzoxazine monomers have a characteristic peak corresponding to the methylene group between the oxygen and the nitrogen that appear between 4.8 and 5.2 ppm. Thus, the progress of the reaction was monitored by tracking the disappearance of this peak around 5 ppm as the peak at 3.9 ppm appears due to the formation of the thioether linkage. Firstly, they studied the reactivity of benzoxazine derived from aliphatic amines (Scheme I.20).



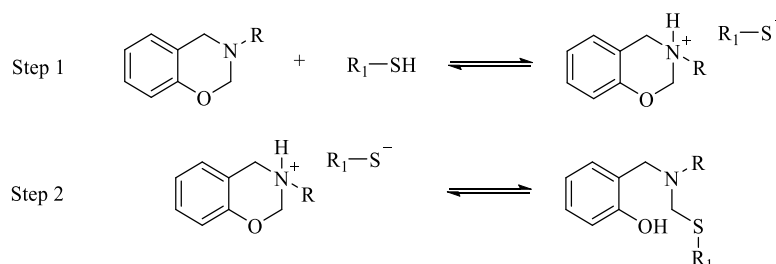
Scheme I.20. The reaction of benzoxazine derived from aliphatic amines with aromatic and aliphatic thiols.

The authors highlighted the importance of the miscibility between the thiol and Bz because this influences directly the reaction rate. The reaction between 1-dodecanethiol and *t*-butyl Bz took around 5 hours to finish, while benzyl thiol and *t*-butyl Bz finished in 15 minutes due to a higher miscibility of the system. The reactivity of benzoxazines derived from aromatic amines was also studied (Scheme I.21) showing an appreciably slower reaction rate reaching the end after 1 day. Furthermore, they proposed a mechanism that follows a two-step acid-catalyzed nucleophilic addition (Scheme I.22). During the first step, the benzoxazine amine is protonated by either an acid catalyst or a thiol. A sulfide attack on the methylene group (between the

nitrogen and the oxygen in the oxazine ring) is immediately triggered forming a new thioether bond resulting in the ring-opening polymerization of the benzoxazine.

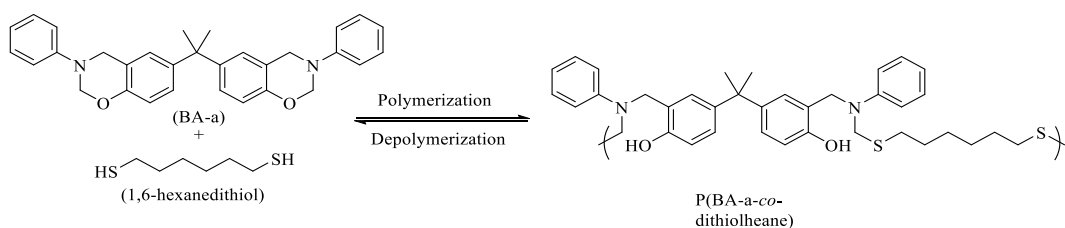


Scheme I.21. The reaction of benzoxazine derived from aromatic amines with aromatic thiol.



Scheme I.22. Proposed mechanism for the ring-opening of benzoxazines by thiols.

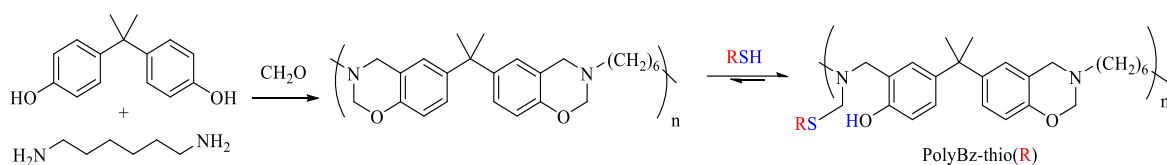
Further studies based on the COLBERT reaction were investigated by William Kawaguchi *et al.*¹⁸⁴ They discovered that the addition reaction of benzoxazine and thiols at room temperature was reversible by a polymerization-depolymerization reaction (Scheme I.23). This study highlighted the strong effect of the solvent.



Scheme I.23. Reversible polymerization-depolymerization of BA-a and 1,6-hexanedithiol.

Recently, Semerci *et al.*¹⁸⁵ modified main-chain polybenzoxazine using thiol-Bz chemistry. Benzoxazine resins synthesized from bisphenol-A and 1,6-diaminehexane, were reacted at room temperature with various thiol compounds, namely, thiophenol, 2-ethanethiol, and 1-butanethiol in $\text{CH}_3\text{OH}/\text{CHCl}_3$ (1:0.56 v:v) for 24 hours (Scheme I.24). As a consequence of the reversible nature of the reaction reported previously,¹⁸⁴ the obtained polybenzoxazine precursors remained closed oxazine rings, readily available for the subsequent curing. In the subsequent heat treatment, both ring-opening polymerization of the oxazine ring and the crosslinking reaction took place. It is known that ring-opening polymerization temperatures of benzoxazines generally ranges from 160 to 220 °C, depending on the substituents. In the studied cases, the maximum of exothermic peak ranged from 170 to 190 °C depending on the thiol used. Moreover, functionalization had a direct effect on the ring-opening polymerization temperatures. The obtained polymers by successive COLBERT reactions exhibited comparable thermal stability to classical polyBz precursors.

In 2017, a more recent study was reported by Urbaniak *et al.*¹⁸⁶ They investigated in detail the reversibility of the reaction both in a solvent and in bulk. In particular, they shown that 92% of the benzoxazine rings could be recovered while heating the mixtures above 90 °C.

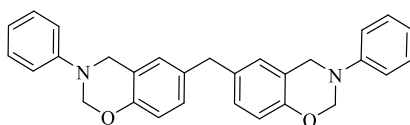
Scheme I.24. Synthesis of polybenzoxazine precursor and its modification with thiols.¹⁸⁵

In conclusion, thiols and elemental sulfur have been described to be involved in the opening of oxazine rings. In the case of elemental sulfur, the ROP is triggered at lower temperatures, getting closer to the range of rubber vulcanization. Besides, sulfur can react with benzoxazines to obtain sulfur-containing polymers. It is important to highlight that in the reported studies; the amount of sulfur is generally very high compared to the traditional recipe of rubber curing and it was difficult to predict if this will be an asset or a drawback for the topic of this project. Thiols are also particularly effective, and some studies have even demonstrated that the oxazine ring cleavage can occur at room temperature and the reaction can be reversible in bulk upon heating. Even though thiols could be formed during rubber vulcanization, in most of the formulations they are not primary ingredients, so this aspect remains of less importance. These notions are particularly important as the co-reactivity of the rubber and the benzoxazine network will strongly affect the morphology and properties of the resulting materials.

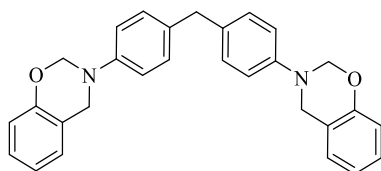
7 Application of benzoxazine resins in the tire industry

As mentioned previously, polybenzoxazines have attracted the attention of the industry as a suitable alternative for phenolic resin. More precisely, the tire industry has developed a few examples of benzoxazines to achieve this objective. The content of the patents that can be found in the literature regarding this topic is summarized in the following paragraphs and in the Table below (Table I.5).

In 2010, a rubber composition was patented consisting of a rubber component with a filler and a resin system composed of benzoxazines and novolac phenolic resins.²⁴ Two benzoxazines commercially available by Shikoku Chemicals were used in combination with phenolic resins. Specifically, a Class A diBz from bisphenol F and aniline (BF-a) (Scheme I.25), and a Class B diBz from phenol and 4,4'-diaminodiphenylmethane (P-ddm) (Scheme I.26) were employed.



Scheme I.25. Dibenzoaxazine monomer from bisphenol F and aniline (BF-a).

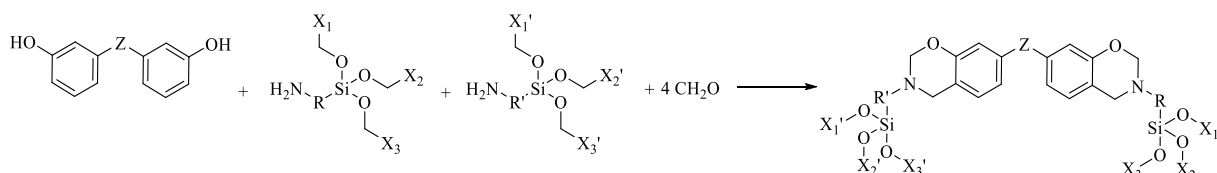


Scheme I.26. Dibenzoaxazine from phenol and 4,4'-diaminodiphenylmethane (P-ddm).

Five years later, another patent providing a rubber composition was granted in Japan, reporting improvement of the grip performance from intermediate temperature to high temperature, and its use in a pneumatic tire.²⁵ The rubber composition was comprised of a rubber component, a

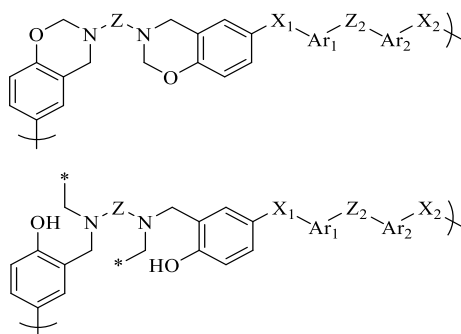
nitrogen compound selected from a group consisting of piperidine derivatives, imidazoles and caprolactam, and a dibenzoxazine. The diBz used were the same ones as for the previous patent mentioned above.

In 2020, a patent was granted in Korea about the use of benzoxazines in silica filled compounds.²⁶ Benzoxazine compounds were used in silica-containing compounds leading to an improvement of the mechanical properties while improving processability. The benzoxazines developed maximized the compatibility with silica promoting the tire reinforcement. The reaction scheme is displayed in Scheme I.27 where Z, X_i, and X_i' (with i equal to 1,2, or 3) could be any organic compound.



Scheme I.27. DiBz from bisphenol and silicon-containing amine.

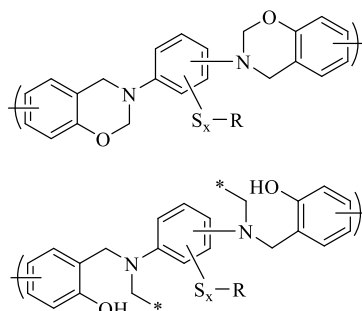
In 2015, Michelin described the use of polybenzoxazines as an adhesive between a metallic substrate and rubber aimed at tire application in a patent application.²⁷ This patent application covers polybenzoxazines that contain at least one of the following chemical structures (Scheme I.28).



Scheme I.28. Polybenzoxazines for adhesion between metallic cord and rubber.

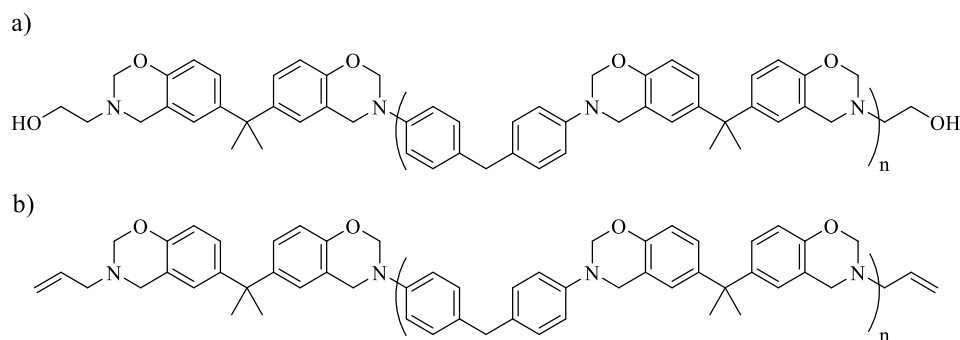
In Scheme I.28, Z represents a group of bonds at least one divalent, aliphatic, cycloaliphatic or aromatic, composed of at least one carbon atom and eventually, at least one heteroatom selected from O, S, N, and P. X₁ and X₂ identical or different representing O or S. Ar₁ and Ar₂ identical or different representing a phenylene group substituted or unsubstituted. Z₂ represents O or (S)_n where n is equal or higher than 1.

In 2020, Michelin filed another patent application regarding a sulfurized polybenzoxazine for coating metallic substrate and bonding it to rubber.²⁸ They claimed the use of benzoxazines with at least one unit corresponding to the following formulas (Scheme I.29). The two oxazine rings from Scheme I.29 are connected to another by a central aromatic group whose benzene ring carries one, two, three or four groups of formula -S_x-R in which "x" is an integer from 1 to 8 and R represents hydrogen or a hydrocarbon group containing 1 to 10 carbon atoms and optionally a heteroatom selected from O, S, N, and P.



Scheme I.29. Sulfurized polybenzoxazines for coating metallic cord and bonding to rubber.

Recently, in 2020 a patent was granted to Kolon Industries regarding the use of main chain benzoxazines for the rubber reinforcement aiming at tire application.²⁹ The rubber composition containing main chain benzoxazines does not generate byproducts during vulcanization and can be used as a replacement of phenol novolac resin. Specifically, the use of high molecular weight main-chain benzoxazines (Scheme I.30) is capable of maintaining excellent mechanical properties and exhibiting high flexibility. For the main chain synthesis, bisphenol A and 4,4'-diaminodiphenylmethane were used and monoamines such as ethanolamine (ea) and allylamine were included to add further functionalities at the end of the polymer chain.



Scheme I.30. Main chain benzoxazines from bisphenol A and 4,4'-diaminodiphenylmethane (BA-ddm) where n is a number from 0 to 10 a) BA-ddm end-capped with ethanolamine, b) BA-ddm end-capped with allylamine.

In Table I.5 is summarized the content of the patents that can be found in the literature regarding this topic.

Table I.5. Summary of the content of the patent literature related to tires and benzoxazines.

Patent	Year	Benzoxazine	Application	Ref
JP 4616187	2010	BF-a; P-ddm	High elasticity and high breaking strength	24
JP 5005609	2012	BF-a; P-ddm and nitrogen compounds	Improvement of gripping performance	25
KR102066167	2020	BA and silicon-containing amine	Reinforcing resin in SiO ₂ compounds	26
FR1562499	2015*	Containing heteroatoms (S, P, O or N)	Adhesion between a metallic substrate and rubber	27
EP3638745A1	2020*	Benzoxazine containing sulfur	Coating metallic substrate and bonding to rubber	28
US 10,538,648	2020	Main chain BA-ddm terminated with ala and ea	Reinforcing resin in CB compounds	29

*Patent application

In the last years, benzoxazines have gained the attention of the industry as a candidate to replace phenolic resin in tire applications. Different chemical structures and approaches were developed thanks to one of the main advantages of benzoxazines, their rich molecular design flexibility. This feature allowed the design of several benzoxazines with different properties. At the same time, the design flexibility provide scope to create new molecules not covered by prior art. Besides, no understanding of the mechanism of reinforcement has been disseminated or explained in the case of benzoxazines. In-depth analyses should be carried out to find a reliable alternative to phenolic resins based on polybenzoxazine systems.

8 Conclusion

This project aims to investigate and develop new polymeric reinforcements with controlled morphology, allowing a full replacement of classical phenolic reinforcing resins in tire compounds. An alternative resin system to replace today's reinforcing resin technology based on polybenzoxazines will be investigated.

It is important to highlight the interactions and the competition that could occur between rubber curing additives and benzoxazine ring-opening polymerization. Elemental sulfur is able to trigger the polymerization and even to react with benzoxazine monomers. However, the reported work employs a very high content of sulfur and it is thus difficult to conclude if a similar behavior could happen in rubber compounds. Nevertheless, triggering the benzoxazine curing at lower temperatures could be a clear asset. Similarly, thiols are also particularly effective to react with benzoxazines and even though they can be formed during the rubber curing, they are not commonly introduced as primary ingredients in rubber formulations, remaining of less importance.

Regarding the use of benzoxazines for tire applications, only a few patents were found. Thanks to the rich molecular design flexibility of Bz resins, different chemical structures and approaches were developed to replace phenolic resin such as dibenzoxazines monomer, main-chain benzoxazines, and silicon-functionalized benzoxazines. This feature brings at the same time the possibility to create new molecules not covered by prior art. Besides, no understanding of the mechanism of reinforcement has been disseminated or explained in the case of benzoxazines. In-depth analyses should be made to find a reliable alternative to phenolic resins based on polybenzoxazine systems.

**Chapter II:
Synthesis, molecular
and thermal
characterization of
benzoxazine resins**

II Synthesis, molecular and thermal characterization of benzoxazine resins

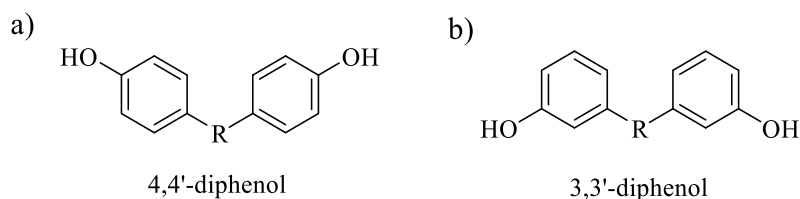
1 Introduction

This chapter relates the design of novel dibenzoxazines to be used as potential reinforcing resins of rubber compounds. Among the different types of dibenzoxazines, Class A monomers, prepared from diphenolic compounds with primary amines and formaldehyde, were studied in this project. This type of benzoxazines was selected because of the high availability of diphenolic compounds in the market and the easy synthetic pathway leading to products with high yields.¹¹⁷ For this purpose, several diphenolic compounds with different bridging groups were employed. Firstly, conventional diphenols were used such as bisphenol A (BA) and 4,4'-thiodiphenol (4DTP). However, the application of benzoxazines from these diphenols in tire compounds was already covered by prior art. Thanks to the rich molecular design flexibility, two new diphenolic compounds containing disulfide bonds (S–S) were used to produce new monomers. For this reason, 4,4'- and 3,3'-dihydroxydiphenyl disulfides (4DPDS and 3DPDS, respectively) were selected. The impact of the position of the oxazine ring was assessed due to the selection of 4,4'- and 3,3'-dihydroxylated structures. In addition, the effect of the amine was investigated by employing monoamines with different functionalities such as benzene or furan rings, or long aliphatic alkyl chains. Aniline (a), the most commonly used petroleum-based monoamine, and two bio-based amines, furfurylamine (fa) and stearylamine (ste), were reacted with the diphenols to yield novel dibenzoxazines. It is noteworthy that the incorporation of reagents from natural resources will allow to produce more sustainable precursors.

In the first part of this chapter, the synthesis of the set of monomers and the characterization of their structural features are addressed. Secondly, their thermal and thermo-mechanical properties, and polymerization kinetics are described. Finally, the impact of the different functional groups on the final properties of the materials was assessed as well as the selection of the precursors act as reinforcing resins.

2 Synthesis and characterization of the structural features of benzoxazines

The design of Class A dibenzoxazines have been focused on the use of 4,4'-dihydroxylated structures for their synthesis due to the availability of a wide variety of 4,4'-diphenols in the market (Table I.2). These diphenols have a common feature where the hydroxyl group (O–H) is in *para* position of the bridging group in between phenolic moieties, as depicted in Scheme II.1a.



Scheme II.1. Chemical structures of the diphenols.

The use of diphenolic compounds of different structures has been previously reported to design Bz.¹⁸⁷ 2,2'-, 2,4'- and 4,4'-substituted isomers from bisphenol F were employed showing the position of the oxazine ring impacts the reactivity and the cured properties of the resulting molecules. Considering this conclusion, 3,3'-dihydroxylated compounds were employed in the frame of this work as a new reagent for the design of benzoxazines. The particularity of this molecule is the relative position of the hydroxyl group (O–H) to the bridging group as the substituents are in *meta* position (Scheme II.1b).

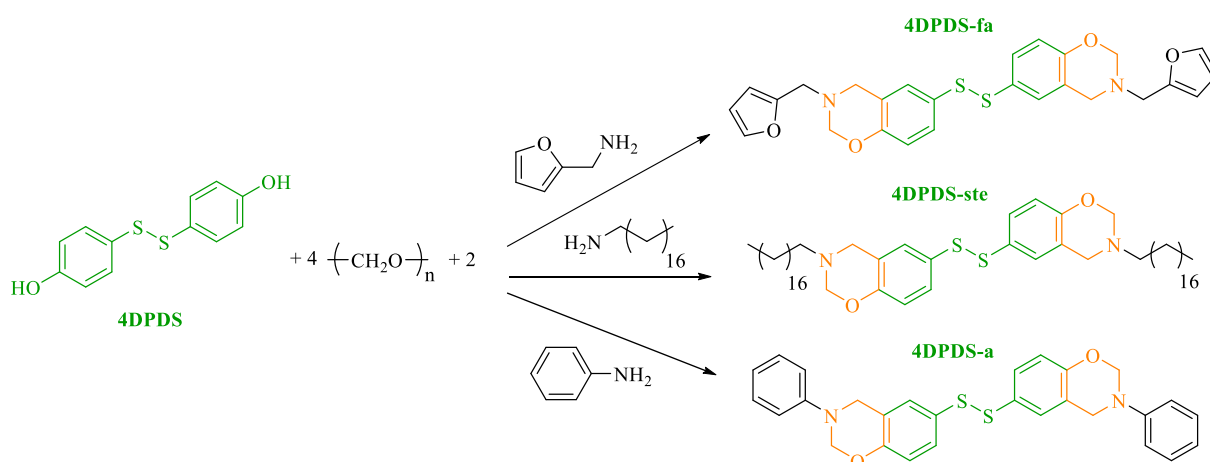
For this reason, this part of the chapter is divided in two sections. The first part comprises the synthesis and characterization of the dibenzoxazine monomers from 4,4'-dihydroxylated structures. The second section focuses on the study of 3,3'-dihydroxylated compounds, due to the more complex characterization of its molecular structure.

2.1 4,4'-substituted benzoxazines

The diphenolic compounds were selected between 4,4'-dihydroxydiphenyl disulfide (4DPDS), 4,4'-thiodiphenol (4TDP), and bisphenol A (BA). 4DPDS was selected as a reference example due to its novelty and peculiarities reflected by the presence of a disulfide bond (S–S) between the phenolic moieties and its limited use for the synthesis of diBz.¹⁴³ Therefore, the following sections relate a detailed description of the synthesis and molecular characterization of dibenzoxazines prepared from 4DPDS. At the end of this sub-section the characterization of the structural features of the molecules prepared from BA and 4DTP are tabulated.

2.1.1 Synthesis pathway

Disulfide-containing diBz were synthesized through a Mannich-like condensation of 4,4'-dihydroxydiphenyl disulfide (4DPDS), a primary monoamine, and paraformaldehyde in stoichiometric ratio 1:2:4 in toluene (Scheme II.2). The monoamines were chosen from the group composed of aniline (a), furfurylamine (fa), and stearylamine (ste). Aniline is the most reported monoamine used for the design of Bz but is detrimentally affected by its non-renewable origin and toxicity. On the contrary, furfurylamine is a non-toxic bio-based amine. Stearylamine is also produced from natural resources and combines the amine functionality with a long alkyl chain.

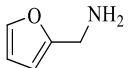
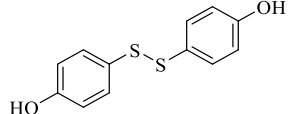
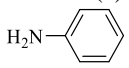
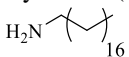


Scheme II.2. Synthesis of 4,4'-substituted benzoxazine monomers containing disulfide bond.

After the reaction, the solvent was evaporated under reduced pressure. The resulting products were solubilized in CHCl_3 and three liquid-liquid extractions with 2 N NaOH and three with distilled water were performed. The organic layer was dried over magnesium sulphate, filtered and the solvent evaporated under reduced pressure. The final materials were dried overnight under reduced pressure.

A summary of the reagents, abbreviations (abbr.), reaction conditions, and yields are gathered in Table II.1.

Table II.1. Abbreviations, chemical structure of the diphenols and the monoamines used for the synthesis of 4,4'-substituted Bz containing disulfide, reaction conditions, and yields.

Abbr.	Diphenol	Monoamine	Reaction time (h) / Temperature ($^{\circ}\text{C}$)	Yield (%)
4DPDS-fa	4,4'-Dihydroxydiphenyl disulfide (4DPDS)	Furfurylamine (fa) 	5 h / 110 $^{\circ}\text{C}$	90
4DPDS-a		Aniline (a) 	5 h / 110 $^{\circ}\text{C}$	80
4DPDS-ste		Stearylamine (ste) 	4 h / 110 $^{\circ}\text{C}$	76

The structural features of the monomers were characterized by nuclear magnetic resonance (NMR), Fourier transform infrared spectroscopy (FTIR), Raman spectroscopy and elemental analysis (EA). A detailed description of each characterization technique is gathered in Annex A (sections A.1.2-A.1.5).

2.1.2 Characterization by NMR

This section reports the molecular characterization of 4DPDS-fa, 4DPDS-a, and 4DPDS-ste by ^1H and ^{13}C NMR.

NMR characterization of 4DPDS-fa

The structural features of 4DPDS-fa were substantiated by ^1H NMR (Figure II.1).

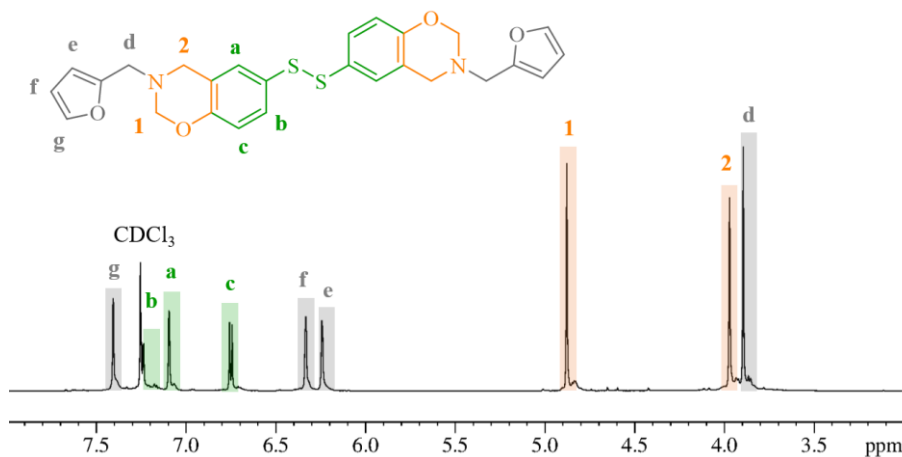


Figure II.1. ^1H NMR spectrum in CHCl_3 of 4DPDS-fa.

The success of the reaction was confirmed by the characteristic peaks of benzoxazine structure at 3.97 and 4.88 ppm corresponding to the protons from Ar-CH₂-N [2] and O-CH₂-N [1] respectively. Moreover, one singlet [a] and two doublets [b, c] attributed to the aromatic protons from the benzoxazine structure are present between 6.75 and 7.24 ppm. The signal at 3.89 ppm corresponding to the methylene group of furfurylamine, N-CH₂ [d], together with the presence of three singlets [e, f, g] at 6.24, 6.33, and 7.41 ppm attributed to the protons from the furan ring, confirmed the presence of the amine.

The peak corresponding to O-CH₂-N [1] was chosen as the reference for the integration. The integrations corresponding to Ar-CH₂-N [2] and N-CH₂ [d] were found to be 2.02 H and 2.02 H respectively (theoretical 2.00 H each peak). The aromatic peaks from the diphenol [a, c] integrated 2.13 H (theoretical 2.00 H), and from the furan ring [e, f, g] 3.17 H (theoretical 3.00 H). It is noteworthy that the doublet at 7.24 ppm is overlapped with the solvent peak centered at 7.26 ppm impeding its integration. However, the signal integrations confirmed the structure of 4DPDS-fa.

The ¹³C NMR spectrum of 4DPDS-fa is reported on Figure II.2. The characteristic peaks of the oxazine ring were found at 49.4 and 82.0 ppm attributed to N-CH₂-Ar, [2] and O-CH₂-N [1] respectively. The quaternary carbons from the benzoxazine structure, CH₂-C(=C)-CH [i] and O-C(=C)-CH [h], are observed at 120.3 and 154.3 ppm respectively. Moreover, the quaternary carbon from furan ring, CH₂-C(=C)-O [k], is present at 151.2 ppm. Finally, the peak corresponding to C-S [j] bond is located at 128.5 ppm. The full assignment of the carbon signal further demonstrates the structure of 4DPDS-Fa.

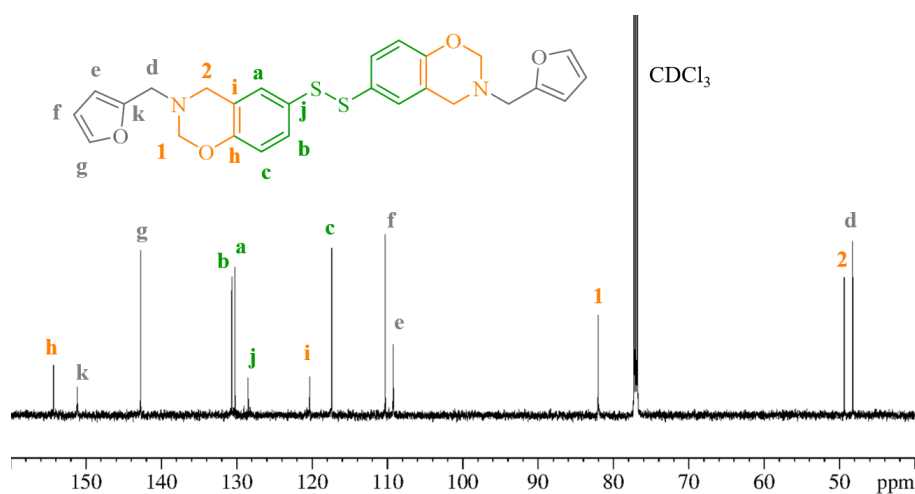


Figure II.2. ¹³C NMR spectrum in CHCl₃ of 4DPDS-fa.

Proton-carbon correlations were done with the aid of 2D NMR. For this purpose, ¹H-¹³C heteronuclear single quantum coherence (HSQC) and ¹H-¹³C heteronuclear multiple bond correlation (HMBC) were carried out. In HSQC and HMBC spectra the ¹H spectrum is shown on the horizontal axis while ¹³C spectrum is on the vertical axis (Figure II.3). HSQC spectrum of 4DPDS-fa shows the correlation of the protons that are directly attached to carbon atoms as depicted in Figure II.3a. HMBC complements this information by showing the correlation between protons and carbons that are separated by multiple bonds while the direct one-bond correlation are suppressed (Figure II.3b). This technique was used for the assignment of quaternary carbons of 4DPDS-fa, i.e. carbons that have no protons attached.

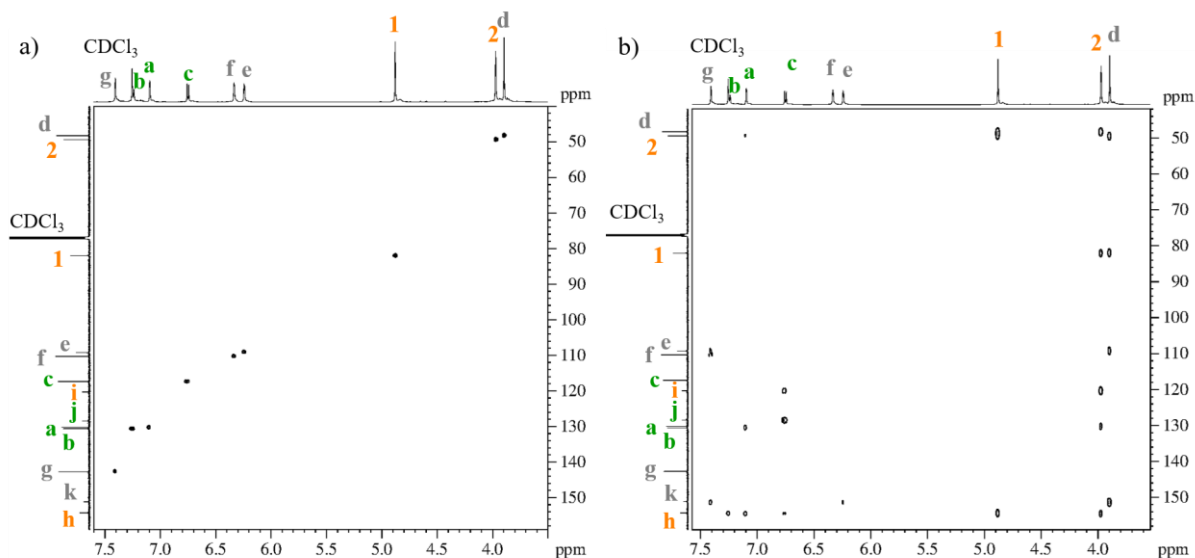


Figure II.3. 2D NMR spectra in CHCl_3 of 4DPDS-fa a) HSQC, b) HMBC.

NMR characterization of 4DPDS-a

The ^1H NMR spectrum of 4DPDS-a is depicted in Figure II.4. The characteristic protons from the oxazine rings were observed at 4.65 and 5.48 ppm attributed to $\text{Ar}-\text{CH}_2-\text{N}$ [2] and $\text{O}-\text{CH}_2-\text{N}$ [1] respectively. Additionally, two doublets at 6.74 ppm [c], and 7.20 ppm [b], and one singlet at 7.28 ppm [a] were found in the aromatic region confirming the formation of the benzoxazine. Moreover, the aromatic protons from the benzene of aniline were shown as one doublet at 7.12 ppm [d, e], and two triplets at 6.87 ppm [h], and 7.23 ppm [g, f] giving an additional proof of the reaction success. As previously, the peak from the oxazine $\text{O}-\text{CH}_2-\text{N}$ [1] was used as a reference for the integrations. Consistently, the integrations of the proton signals confirmed the chemical structure of 4DPDS-a.

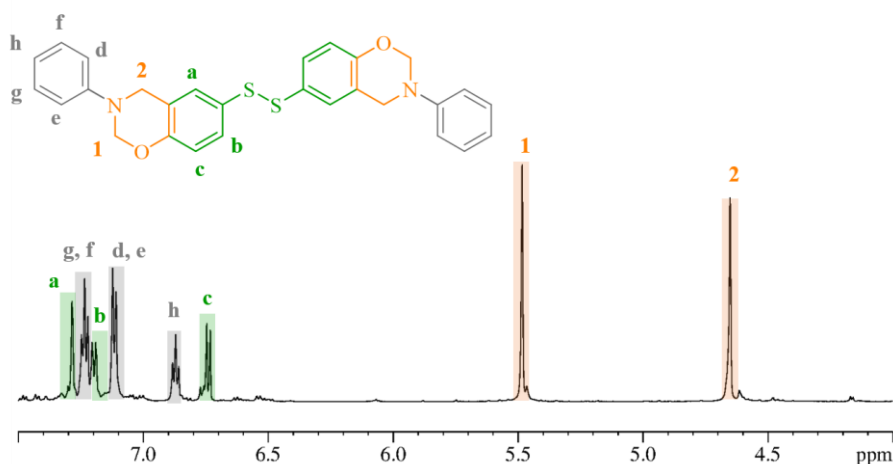


Figure II.4. ^1H NMR spectrum in DMSO of 4DPDS-a.

In Figure II.5 is depicted the ^{13}C NMR spectrum of 4DPDS-a. Peaks corresponding to $\text{N}-\text{CH}_2-\text{Ar}$ [2], and $\text{O}-\text{CH}_2-\text{N}$ [1] are found at 48.5, and 78.9 ppm respectively. The quaternary carbons are observed at 155.1, 147.9 and 122.9 ppm attributed to $\text{O}-\text{C}(=\text{C})-\text{CH}$ [k], $\text{C}-\text{C}(=\text{C})-\text{N}$ [m], and $\text{CH}_2-\text{C}(=\text{C})-\text{CH}$ [i] respectively. Moreover, the peak corresponding to $\text{C}-\text{S}$ [j] bond is

present at 127.2 ppm. The full assignment of the carbon signal further demonstrates the structure of 4DPDS-a.

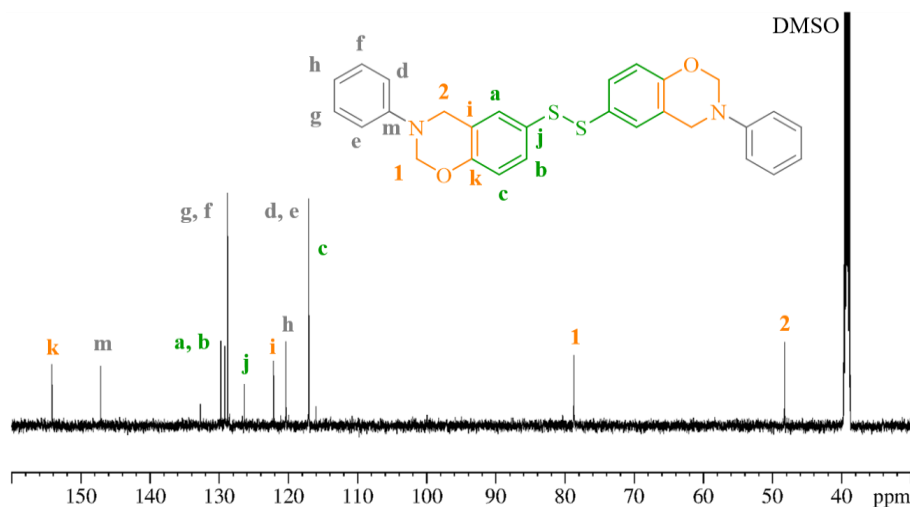


Figure II.5. ^{13}C NMR spectrum in DMSO of 4DPDS-a.

NMR characterization of 4DPDS-ste

The structural features of 4DPDS-ste were also assessed by ^1H and ^{13}C NMR (Figure II.6 and Figure II.7, respectively).

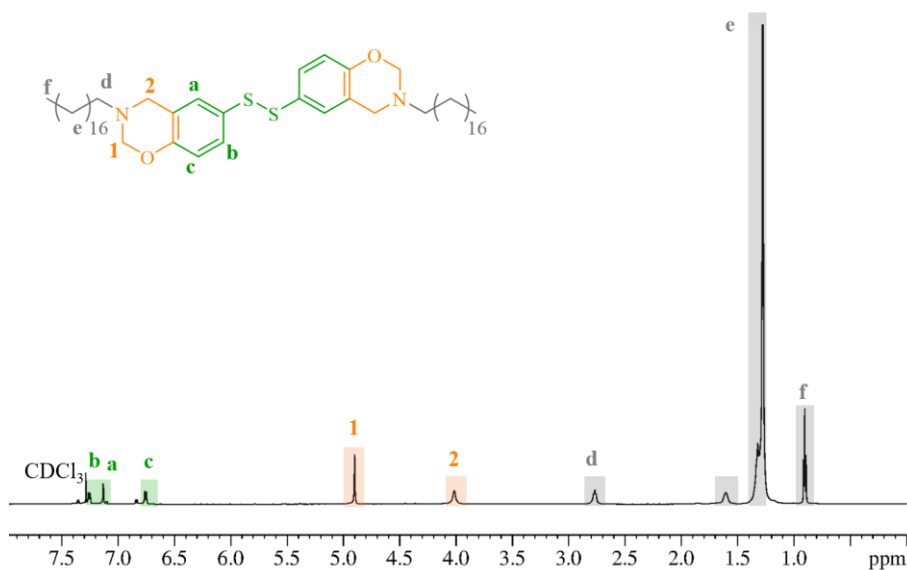


Figure II.6. ^1H NMR spectrum in CHCl_3 of 4DPDS-ste.

The formation of the target molecule was confirmed by the presence of the oxazine proton peaks at 3.99 and 4.87 ppm and carbon signal at 50.2 and 82.4 ppm attributed to $\text{Ar}-\text{CH}_2-\text{N}$ [2] and $\text{O}-\text{CH}_2-\text{N}$ [1], respectively. The peaks corresponding to the alkyl chain of stearylamine are also present. A large signal at 1.25 and a peak at 1.58 ppm attributed to the methylene groups of the side chain [e], together with a triplet at 0.89 ppm from the methyl group ($-\text{CH}_3$) and the peak at 2.74 ppm from the methylene connected to the nitrogen from the oxazine ($-\text{CH}_2-\text{N}$) [d]. Additionally, the carbon signal corresponding to stearylamine was observed between 22.6 and 32.4 attributed to the methylene groups of the alkyl chain [e] (Figure II.7). Moreover, methyl end group [f] was found at 14.1 ppm and the methylene next to the nitrogen from the oxazine

group [d] at 51.9. These peaks confirmed the incorporation of the amine into the benzoxazine structure and together with the integrations of the proton peaks confirm the structure of 4DPDS-ste.

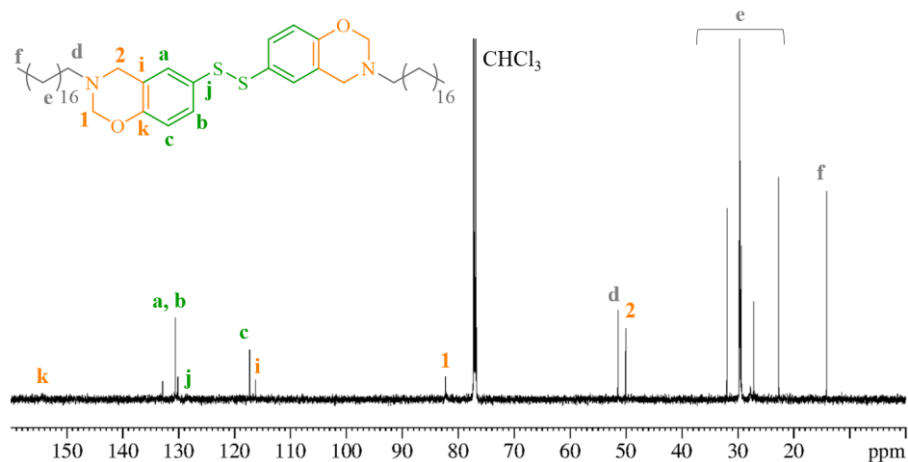


Figure II.7. ^{13}C NMR spectrum in CHCl_3 of 4DPDS-ste.

To conclude, the combination of ^1H NMR and ^{13}C NMR together 2D NMR spectra confirmed the chemical structures of 4DPDS-fa, 4DPDS-a, and 4DPDS-ste. A summary of the characteristic peaks corresponding to the oxazine rings is given in Table II.2.

Table II.2. Structural characteristics by NMR of 4,4'-substituted Bz containing disulfide bond.

Abbr.	diBz	^1H NMR (ppm) Ar-CH ₂ -N / O-CH ₂ -N	^{13}C NMR (ppm) Ar-CH ₂ -N / O-CH ₂ -N
4DPDS-fa		3.97 / 4.88	49.4 / 82.0
4DPDS-a		4.65 / 5.48	48.5 / 78.9
4DPDS-ste		3.99 / 4.87	50.0 / 82.5

2.1.3 Characterization by FTIR

The FTIR spectrum of 4DPDS-fa is depicted in Figure II.8. The presence of the absorption bands at 929 (out-of-plane vibration of the benzoxazine ring), at 1013 (symmetric C–O–C stretching), at 1150 (symmetric C–N–C stretching), at 1227 (asymmetric C–O–C stretching), and at 1481 (trisubstituted benzene) cm^{-1} confirmed the formation of the benzoxazine ring after the reaction. Additionally, the characteristic peaks attributable to the furan ring are observed at 1571, 987, and 750 cm^{-1} (identified with dash lines in Figure II.8) further supporting the chemical structure of 4DPDS-fa.

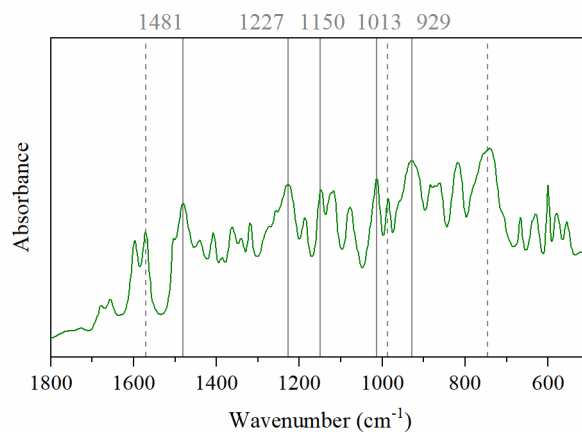


Figure II.8. FTIR transmission spectrum of 4DPDS-fa.

4DPDS-a and 4DPDS-ste were also analyzed by FTIR and their corresponding spectra are gathered in Annex B (Figure B.2 and Figure B.3, respectively). Similar absorption peaks were observed confirming the formation of the oxazine ring in both cases.

The characteristic bands of the benzoxazines structures of 4DPDS-based monomers are summarized in Table II.3.

Table II.3. Characteristic IR absorption bands from 4,4'-substituted Bz containing disulfide bond.

Abbr.	Benzoxazine related mode (cm ⁻¹)	Symmetric C–O–C stretching (cm ⁻¹)	Symmetric C–N–C stretching (cm ⁻¹)	Asymmetric C–O–C stretching (cm ⁻¹)	Trisubstituted benzene ring (cm ⁻¹)
4DPDS-fa	929	1013	1150	1227	1481
4DPDS-a	936	1030	1148	1231	1480
4DPDS-ste	936	1013	1152	1224	1471

2.1.4 Characterization by Raman

The Raman spectrum of 4DPDS-fa is displayed in Figure II.9. The appearance of a band from 420 to 544 cm⁻¹, centered at 484 cm⁻¹, confirmed the presence of the disulfide bond after the reaction. An additional band at 742 cm⁻¹ attributed to C–S stretch was also observed on the spectra. Interestingly, a peak of small but wide intensity located between 2550 and 2600 cm⁻¹ also appeared. This band is attributed to a thiol stretch (S–H). Specifically, for 4DPDS-fa this band represents approximately 2% of the total S–S bonds in the molecule. This value was determined using the relative area between the band corresponding to the disulfide bond and the thiol band. This means that around 2% of the S–S bonds of 4DPDS-fa cleaved. The presence of these small bands attributed to thiols indicates the disulfide bond from 4DPDS-fa can be reduced under relatively mild conditions. This could be considered as an asset as they could accelerate the ROP of the benzoxazine.^{144, 188} Their impact on the curing behavior of 4DPDS-fa is described later in this manuscript.

A similar band was observed on the Raman spectrum of 4DPDS-ste, but not for 4DPDS-a (Figure II.10a and b, respectively). The reduction of the disulfide bond to thiols seems consistently to be related to the basicity of the amine used for the benzoxazine. Indeed, the pK_a

of furfurylamine and stearylamine are high (9.12 and 10.65, respectively), whereas the pK_a of aniline is 4.6.

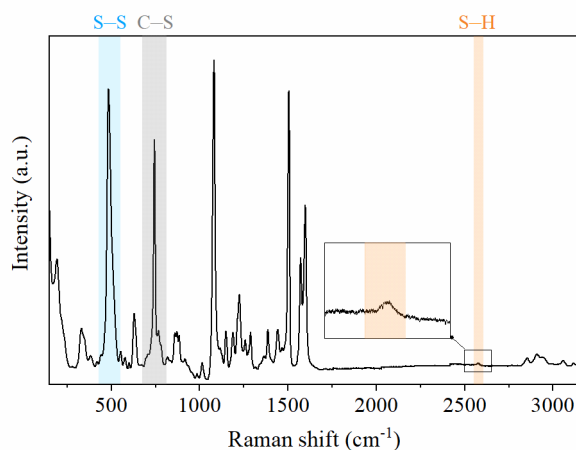


Figure II.9. Raman spectrum of 4DPDS-fa.

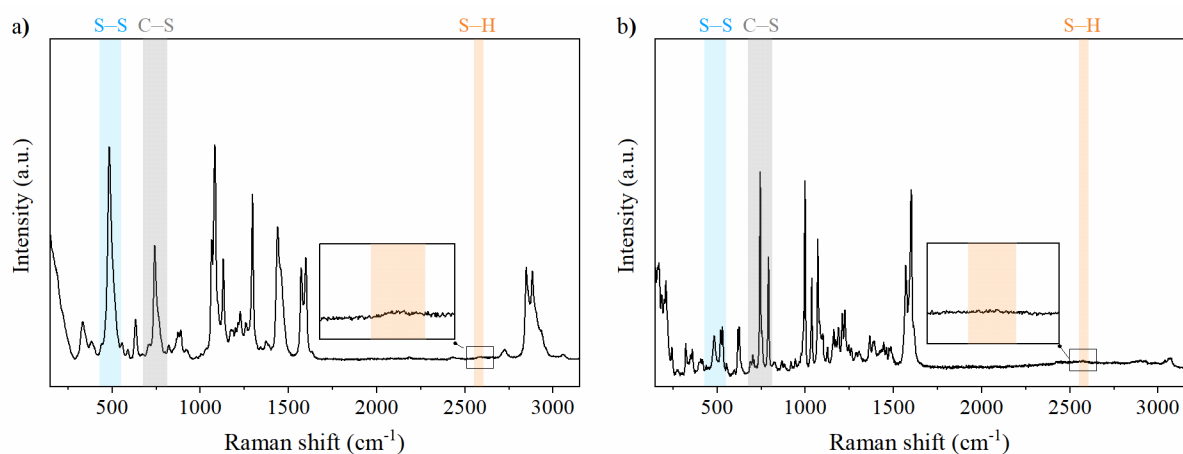
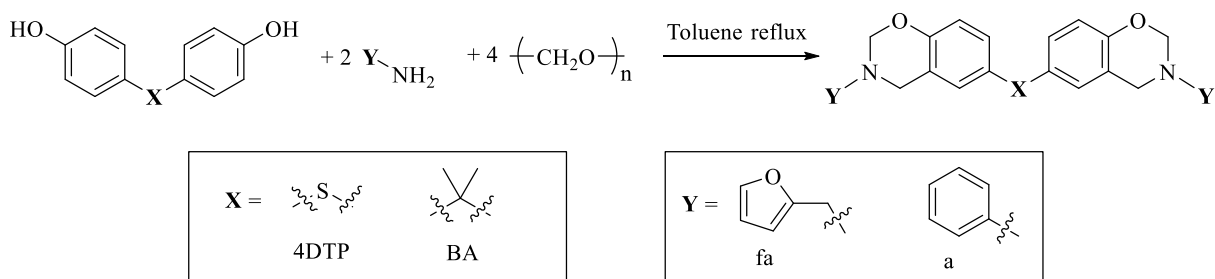


Figure II.10. Raman spectra of a) 4DPDS-ste, and b) 4DPDS-a.

2.1.5 Synthesis and structural features of additional benzoxazines

In addition, a set of dibenzoxazines prepared either with 4,4'-thiodiphenol (4TDP) or bisphenol A (BA) was synthesized with aniline or furfurylamine, and paraformaldehyde in stoichiometric ratio 1:2:4 in toluene as depicted in Scheme II.3. After the reaction, the solvent was evaporated under reduced pressure and the samples were purified following the procedure described in section 2.1.1. Their respective abbreviations, reaction conditions, and yields are gathered in Table II.4.



Scheme II.3. Synthesis of 4,4'-substituted benzoxazine monomers from bisphenol A and 4,4'-thiodiphenol.

Table II.4. Abbreviations, chemical structure of the diphenols and the monoamines used for the synthesis of 4,4'-substituted Bz, reaction conditions, and yields.

Abbr.	Diphenol	Monoamine	Reaction time (h) / Temperature (°C)	Yield (%)
4DTP-fa	4,4'-Thiodiphenol (4DTP) 	Furfurylamine (fa) 	4 h / 110 °C	88
4DTP-a		Aniline (a) 	4 h / 110 °C	75
BA-fa	Bisphenol A (BA) 	Furfurylamine (fa) 	6 h / 110 °C	85
BA-a		Aniline (a) 	6 h / 110 °C	87

The set of synthesized benzoxazines was characterized by NMR and FTIR and their corresponding spectra are displayed in Annex B (from Figure B.4 to Figure B.17). The structural features were confirmed, and a summary of the main peaks is gathered in Table II.5. The purity of the compounds was also confirmed by elemental analyses (Annex B, sections B.4-B.7).

Table II.5. Structural features of 4,4'-substituted Bz by NMR and FTIR.

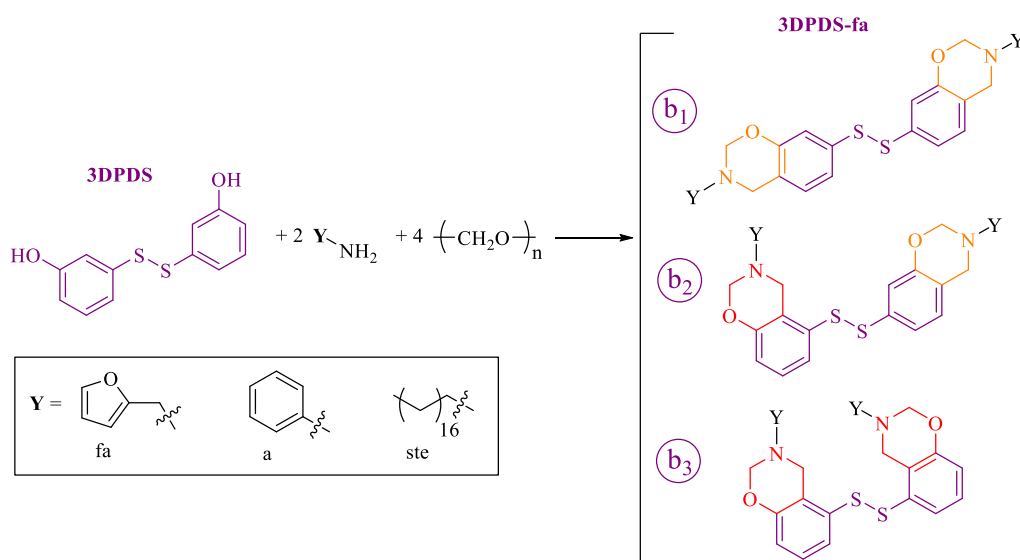
Abbr.	diBz	¹ H NMR and ¹³ C NMR (ppm) ^a	FTIR (cm ⁻¹) ^b
4DTP-fa		3.97 / 4.87 49.4 / 82.0	930 / 1013 / 1150 / 1226 / 1480
4DTP-a		4.64 / 5.46 49.1 / 79.3	937 / 1030 / 1160 / 1231 / 1483
BA-fa		3.99 / 4.85 50.1 / 81.8	936 / 1013 / 1150 / 1230 / 1500
BA-a		4.57 / 5.32 50.7 / 79.1	949 / 1031 / 1152 / 1233 / 1499

^a Ar-CH₂-N / O-CH₂-N. Proton shifts above, carbon shifts below. ^b Benzoxazine related mode (out-of-plane vibration of the benzoxazine ring) / Symmetric C-O-C stretching / Symmetric C-N-C stretching / Asymmetric C-O-C stretching / Trisubstituted benzene ring.

2.2 3,3'-substituted benzoxazines

2.2.1 Synthesis pathway

3,3'-Dihydroxydiphenyl disulfide (3DPDS) was used to yield diBz with structural features not reported before. The particularity of this molecule is the relative position of the hydroxyl group (O–H) to the disulfide bond (S–S) as the substituents are in *meta* position (Scheme II.4). The use of this diphenol to synthesize Bz precursor leads to a mixture of diBz depending on the relative position of the oxazine ring from the S–S as depicted in Scheme II.4. The mixture is composed of two symmetric monomers depending if the resulting benzoxazine rings are closed in *para* position (b_1 in Scheme II.4) or in *ortho* position (b_3 in Scheme II.4) with respect to the S–S. An asymmetric third monomer might be also present if one of the oxazine rings closes in *para* and the second one in *ortho* (b_2 in Scheme II.4). Three dibenzoxazines were synthesized from 3DPDS as diphenol and aniline, furfurylamine, and stearylamine, as monoamines. Their respective abbreviations, reaction conditions, and yields are gathered in Table II.6.



Scheme II.4. Synthesis of 3,3'-substituted benzoxazine monomers containing disulfide bond.

Table II.6. Abbreviations, chemical structure of the diphenols and the monoamines used for the synthesis of 3,3'-substituted Bz containing disulfide, reaction conditions, and yields.

Abbr.	Diphenol	Monoamine	Reaction time (h) / Temperature (°C)	Yield (%)
3DPDS-fa	3,3'-Dihydroxydiphenyl disulfide (3DPDS)	Furfurylamine (fa) 	5 h / 100 °C	91
3DPDS-a		Aniline (a) 	5 h / 100 °C	79
3DPDS-ste		Stearylamine (ste) 	4 h / 100 °C	74

The structural features of the monomers were characterized by NMR, FTIR, and Raman spectroscopy and are detailed in the sections below. The purity of the compounds was assessed by EA and it is reported in the Annex B (sections B.8-B.10).

2.2.2 Characterization by NMR

The ^1H NMR spectrum of 3DPDS-fa is depicted in Figure II.11. The formation of the oxazine ring was attested by the presence of peaks corresponding to the protons from Ar-CH₂-N [2] and O-CH₂-N [1] at 3.98 and 4.87 ppm respectively. Interestingly, new peaks were observed in the region of these protons. Specifically, peaks with lower intensity were observed at 4.07 and 4.17 ppm and at 4.84 and 4.86 ppm attributed to the Ar-CH₂-N [2' and 2''] and O-CH₂-N [1' and 1''] respectively. The main peaks [1, 2] are attributed to the symmetric monomer when both rings closed in *para* position (*b*₁ in Scheme II.4) while the others [1', 2'] and [1'', 2''] were assigned to the forms *b*₂ and *b*₃ respectively as shown in Scheme II.4. These results confirmed that a mixture of isomers was obtained with 3,3'-dyhydrodisulfide. It is noteworthy that the protons corresponding to Ar-CH₂-N showed a more pronounced shift to higher ppm explained by the significant modification of their chemical environment. Additionally, three peaks were observed for the methylene group from furfurylamine, N-CH₂ [d'', d' and d] at 3.85, 3.89, and 3.91 ppm due to the impact of the benzoxazine conformation on their chemical shift. Moreover, instead of one singlet and two doublets observed in the aromatic region for 4DPDS-fa (Figure II.1), 3DPDS-fa showed more peaks between 6.75 and 7.25 ppm further demonstrating the formation of more than one diBz structure.

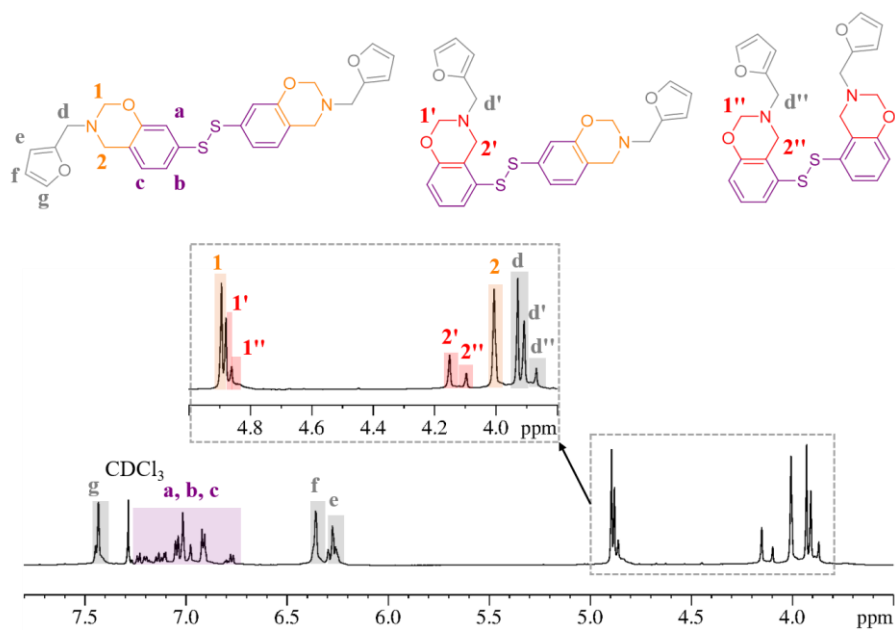


Figure II.11. ^1H NMR spectrum in CHCl_3 of 3DPDS-fa.

After the signal assignment, the peaks were integrated taking as reference the methylene group of the oxazine O-CH₂-N [1, 1', 1'']. The integrations corresponding to Ar-CH₂-N [2, 2', 2''] and N-CH₂ [d, d', d''] were found to be 2.09 H and 2.02 H respectively (theoretical 2.00 H each peak). The aromatic peaks from the diphenol [a, b, c] integrate 3.01 H (theoretical 3.00 H), and from the furan ring [e, f, g] 3.01 H (theoretical 3.00 H) confirming the structure of 3DPDS-fa. Moreover, the isomer ratios were determined using the integrations of the different peaks observed for Ar-CH₂-N [2], [2'], and [2'']. The results showed the presence of around 70% of the symmetric monomer with both rings closed in *para* position (*b*₁ in Scheme II.4) while the structures *b*₂ and *b*₃ represent 20 and 10% respectively (Scheme II.4).

Additionally, the full ^{13}C NMR spectrum signals (Figure II.12) were assigned using HSQC and HMBC NMR displayed in Annex B (Figure B.18). Similarly to 4DPDS-fa, the characteristic peaks of the benzoxazine structure were observed at 49.4 and 82.0 ppm, attributed to N-CH₂-Ar, [2] and O-CH₂-N [1] respectively. Additional peaks were also observed due the presence of the isomers of 3DPDS-fa as depicted in Figure II.12.

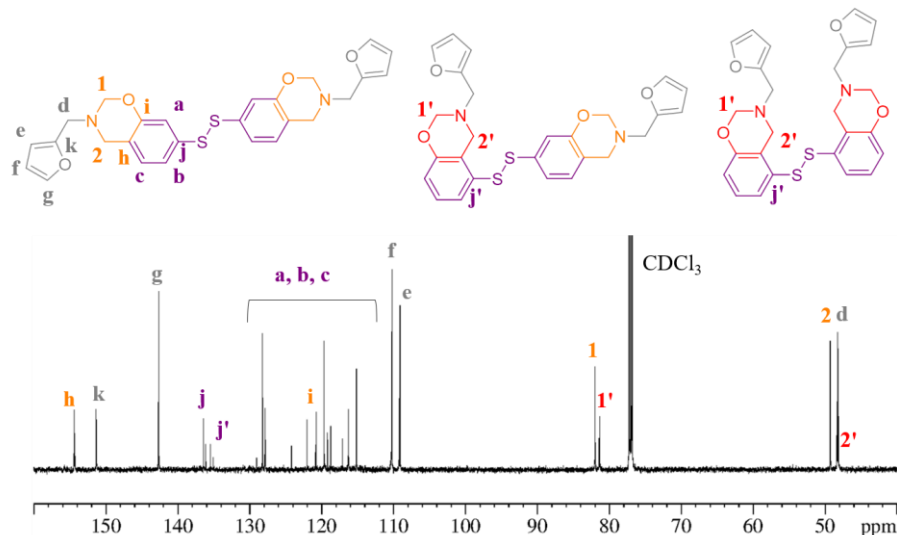


Figure II.12. ^{13}C NMR spectrum in CHCl_3 of 3DPDS-fa.

The chemical structures of 3DPDS-a, and 3DPDS-ste, were similarly demonstrated by ^1H NMR and ^{13}C NMR. A mixture of isomers was also obtained in each case as attested by the presence of more than one peak corresponding to the methylene groups of the oxazine ring and their values are gathered in Table II.7. The full attribution of all the peaks for these molecules is detailed in Annex B (sections B.9 and B.10).

Table II.7. Structural characteristics by NMR of 3,3'-substituted Bz containing disulfide bond.

Abbr.	diBz	^1H NMR (ppm) Ar-CH ₂ -N / O-CH ₂ -N	^{13}C NMR (ppm) Ar-CH ₂ -N / O-CH ₂ -N
3DPDS-fa		3.98; 4.07; 4.13 / 4.84; 4.86; 4.87	48.2; 48.4; 49.4 / 81.3; 81.4; 82.0
3DPDS-a		4.58; 4.66; 4.70 / 5.33; 5.35; 5.36	48.5; 48.7; 50.4 / 79.4; 79.6; 79.7
3DPDS-ste		3.95; 4.02; 4.08 / 4.81; 4.84	48.6; 49.9; 51.7 / 82.0; 82.5

2.2.3 Characterization by FTIR

The FTIR spectrum of 3DPDS-fa is reported in Figure II.13. The presence of the absorption bands at 936 (out-of-plane vibration), at 1013 (symmetric C–O–C stretching), at 1150 (symmetric C–N–C stretching), at 1235 (asymmetric C–O–C stretching), and at 1490 (trisubstituted benzene) cm^{-1} confirmed the formation of the benzoxazine ring after the reaction. Moreover, the characteristic peaks attributable to the furan ring were observed at 1569, 987, and 785 cm^{-1} (identify with dash lines in Figure II.13) further proving the chemical structure of 3DPDS-fa.

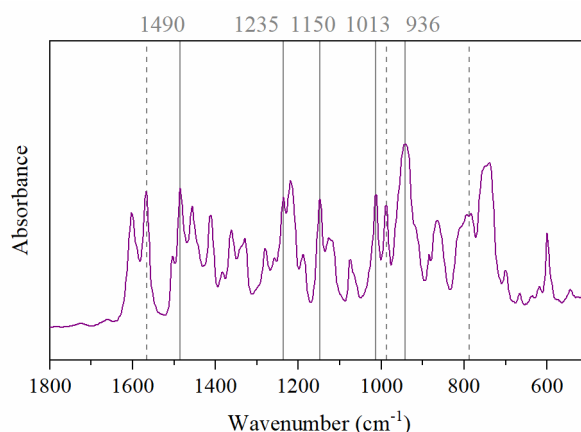


Figure II.13. FTIR transmission spectrum of 3DPDS-fa.

In addition, it could be expected to observe an impact from the different structures of the isomers (i.e. *para* and *ortho* closing). However, this effect is not visible in Figure II.13 probably due to the predominant effect of the isomer with both rings closed in *para* as it represents more than 70% of the total mixture of isomers.

Similarly, 3DPDS-a and 3DPDS-ste were analyzed by FTIR and their corresponding spectra are gathered in Annex B (Figure B.22 and Figure B.25, respectively). The formation of the benzoxazine was confirmed in both cases by the presence of the characteristic absorption peaks.

A summary of the IR absorption bands for the molecules prepared from 3DPDS is gathered in Table II.8.

Table II.8. Characteristic IR absorption bands from 3,3'-substituted Bz containing disulfide bond.

Abbr.	Benzoxazine related mode (cm^{-1})	Symmetric C–O–C stretching (cm^{-1})	Symmetric C–N–C stretching (cm^{-1})	Asymmetric C–O–C stretching (cm^{-1})	Trisubstituted benzene ring (cm^{-1})
3DPDS-fa	936	1013	1150	1235	1490
3DPDS-a	950	1031	1149	1223	1496
3DPDS-ste	938	1010	1144	1216	1495

2.2.4 Characterization by Raman

The Raman spectrum of 3DPDS-fa is displayed in Figure II.14. The appearance of a band between 430 and 550 cm^{-1} confirmed the presence of the disulfide bond. This band exhibited

three contributions further confirming the presence of a mixture of isomers. No peaks were found between 2550 and 2600 cm^{-1} on the contrary of 4DPDS-fa in spite of the exact similarity of the synthesis conditions of the two disulfide Bz. The higher stability of 3DPDS-fa toward the reduction of its disulfide bond in thiols compared to 4DPDS is difficult to justify without resorting to molecular dynamics. Nevertheless, the bond dissociation energy (BDE) of disulfide bonds is known to be strongly influenced by the chemical and electronic environments as previously reported.¹⁸⁹ Indeed, BDE of 4,4'- and 2,2'-dihydroxydiphenyl disulfide were found to be 49.5 and 51.8 $\text{kcal}\cdot\text{mol}^{-1}$ respectively.¹⁸⁹ These disparities are explained by the differences in the chemical environment of these molecules. Even though the BDE of 3,3'-dihydroxydiphenyl disulfide have never been reported, it is reasonable to expect that it may differ from its counterparts.

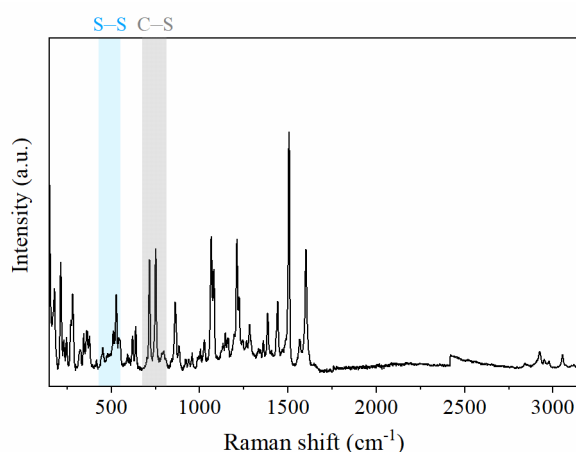


Figure II.14. Raman spectrum of 3DPDS-fa.

The Raman spectra of 3DPDS-a, and 3DPDS-ste are displayed in Figure II.15. The absorption band around 500 cm^{-1} attributed to S–S stretch confirm the presence of the disulfide bond after the reaction. Interestingly, the band characteristic of thiols (between 2550 and 2600 cm^{-1}) was not detected in any Raman spectra of the benzoxazine molecules prepared from 3DPDS. The results indicate that the reduction of the disulfide bond in 3DPDS seems to be more difficult to achieve than for its 4,4' counterparts.

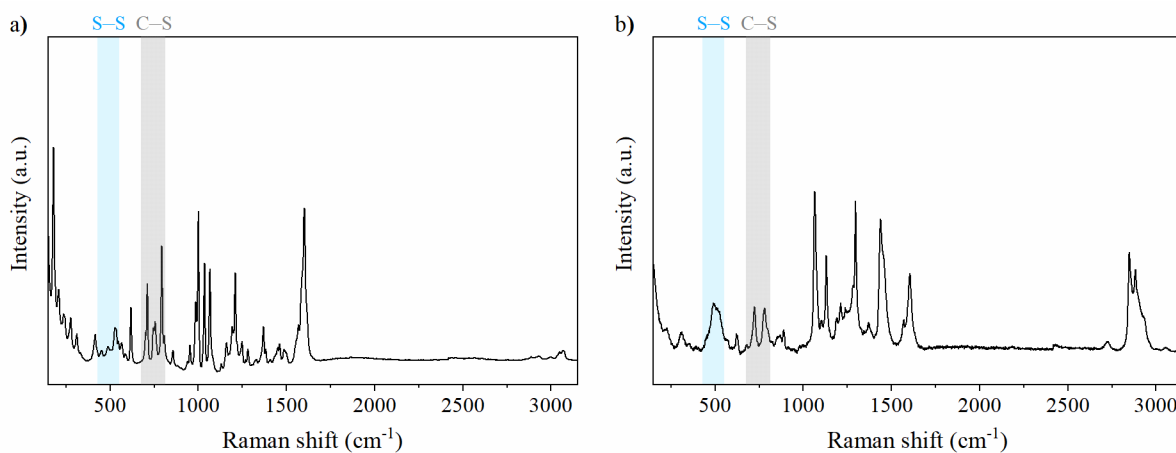


Figure II.15. Raman spectra of a) 3DPDS-a, and b) 3DPDS-ste.

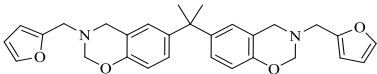
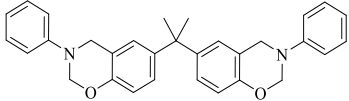
2.3 Discussion

This section describes the results of the synthesis of Class A dibenzoxazines through a Mannich-like condensation of several diphenolic derivatives with monoamines, and paraformaldehyde. The structural features were identified by FTIR and NMR spectroscopy. The peaks corresponding to the oxazine rings were detected by both techniques confirming the successful product formation. Additionally, the purity of the precursors was confirmed by elemental analysis. Following this synthetic approach, benzoxazines with a newly designed chemical structure were synthesized in a one-step reaction with high yield.

A summary of the structural features, and the purity by EA is gathered in Table II.9.

Table II.9. Summary of the structural features, and purity of the synthesized dibenzoxazines monomers.

Abbr.	diBz	¹ H NMR (ppm)	FTIR ^a (cm ⁻¹)	EA element (exp., th.)
4DPDS-fa		3.97 / 4.88	929	N (3.2, 3.5); C (44.3, 44.8); H (42.7, 41.4); S (3.4, 3.4); O (6.4, 6.9)
4DPDS-a		4.65 / 5.48	936	N (3.4, 3.4); C (48.7, 48.3); H (41.4, 41.5); S (3.6, 3.4); O (2.9, 3.4).
4DPDS-ste		3.99 / 4.87	936	-
3DPDS-fa		3.98; 4.07; 4.13 / 4.84; 4.86; 4.87	936	N (3.2, 3.5); C (44.9, 44.8); H (42.0, 41.4); S (3.9, 3.4); O (6.0, 6.9)
3DPDS-a		4.58; 4.66; 4.70 / 5.33; 5.35; 5.36	950	N (3.5, 3.4); C (49.0, 48.3); H (41.4, 41.5); S (3.5, 3.4); O (2.6, 3.4).
3DPDS-ste		3.95; 4.02; 4.08 / 4.81; 4.84	938	-
4DTP-fa		3.97 / 4.87	930	N (3.2, 3.5); C (46.4, 45.6); H (42.2, 42.1); S (1.8, 1.8); O (6.3, 7.0).
4DTP-a		4.64 / 5.46	937	N (3.5, 3.5); C (51.4, 49.1); H (40.3, 42.1); S (1.9, 1.8); O (2.9, 3.5).

Abbr.	diBz	¹ H NMR (ppm)	FTIR ^a (cm ⁻¹)	EA element (exp., th.)
BA-fa		3.99 / 4.85	936	N (3.0, 3.1); C (44.0, 44.6); H (46.1, 46.2); O (6.9, 6.1).
BA-a		4.57 / 5.32	949	N (2.8, 3.1); C (47.9, 47.7); H (46.4, 46.1); O (2.9, 3.1).

^a Benzoxazine related mode (out-of-plane vibration of the benzoxazine ring)

Additionally, the presence of the disulfide bond was confirmed by Raman for diBz prepared from 4DPDS and 3DPDS. It is important to highlight that small amounts of thiols were found in 4DPDS-fa whereas no thiols were detected for 3DPDS-fa. These results could indicate that the disulfide bond of 4DPDS representatives is less stable and could cleave in relatively mild conditions compared to 3DPDS derivatives.

Finally, the employment of furfurylamine and stearylamine led to benzoxazine precursors with a bio-based content ranging from 35 to 60%, respectively. The bio-based content was determined considering the full amount of biomass in the material. These results spotlight the possibility to partially replace petroleum-based reagents to produce materials more sustainable.

3 Thermal and thermomechanical characterizations

This chapter relates the thermal and polymerization behaviors of the benzoxazine monomers described in the previous section by differential scanning calorimetry (DSC), thermogravimetric analysis (TGA), and rheological measurements. A detail description of the measurement conditions can be found in Annex A (sections A.1.6-A.1.8).

3.1 Thermal behavior by DSC

3.1.1 General comments about the characterization of benzoxazines by DSC

The study of the thermal behavior of benzoxazines is usually carried out by non-isothermal DSC. This method is commonly used because the data can be obtained in relatively short time with high reliability. The thermogram of benzoxazines shows a typical exothermic peak (T_{poly}) in the range of 200-250 °C attributed to the ring-opening polymerization (ROP).¹² The heat of polymerization considered as the enthalpy of the exothermic peak (ΔH) is regularly in the range of 150-600 J·g⁻¹ for pure monomers.¹²

The apparent activation energy (E_a) of polymerization can be determined using the well-known Kissinger and Ozawa methods.¹⁹⁰ For this purpose, DSC is performed at different heating rates. According to the Kissinger method, the activation energy is calculated as follows:

$$\ln\left(\frac{\beta}{T_{poly}^2}\right) = \ln\left(\frac{AR}{E_a}\right) - \frac{E_a}{RT_{poly}}, \quad (I.1)$$

where β is the heating rate (K·min⁻¹), T_{poly} is the maximum temperature of the exothermic peak

(K), A pre-exponential factor, E_a the apparent activation energy ($\text{kJ}\cdot\text{mol}^{-1}$), and R is the ideal gas constant ($\text{kJ}\cdot\text{mol}^{-1}\cdot\text{K}^{-1}$). This method is based on a linear relationship between the $\ln(\beta/T_{poly}^2)$ with the inverse of T_{poly} and E_a is calculated from the slope of this plot.

The Ozawa method relates the logarithm of the heating rate and the inverse of T_{poly} . Therefore, activation energy can be calculated from the slope of this plot following Eq. (I.2):

$$\ln(\beta) = -1.052 \frac{E_a}{RT_{poly}} + C, \quad (\text{I.2})$$

where C is a constant.

The study of the polymerization reaction and the determination of the kinetic parameters by a non-isothermal method are reported in the following section. For the sake of clarity, the section is divided in three parts depending on the amine used for the synthesis: furfurylamine, aniline, and stearylamine.

3.1.2 DSC of benzoxazine monomers prepared from furfurylamine

In Figure II.16 the DSC thermograms of 4DPDS-fa, 3DPDS-fa, 4DTP-fa, and BA-fa are gathered. An endothermic peak corresponding to the melting point (T_m) is observed for each precursor. For 4DTP-fa, 4DPDS-fa, and BA-fa, this peak is centered at 99, 74, and 100 °C respectively. In the case of 3DPDS-fa, the endotherm shows two main contributions, with a first peak at 90 °C and a second at 115 °C as it is a mixture of isomers.

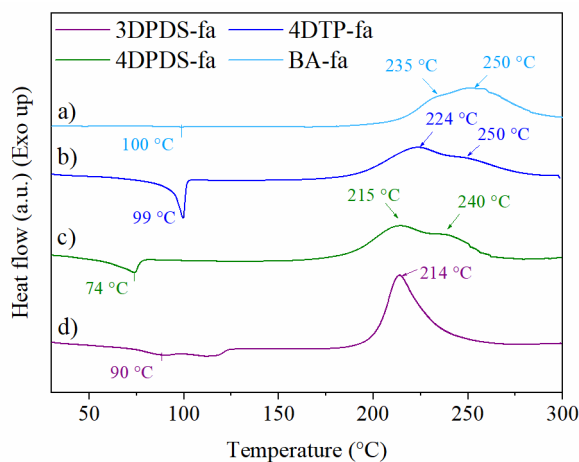


Figure II.16. DSC thermograms at $10 \text{ K}\cdot\text{min}^{-1}$ of diBz: a) BA-fa, b) 4DTP-fa, c) 4DPDS-fa, and d) 3DPDS-fa.

An exothermic peak is observed for each Bz corresponding to the thermally activated ROP. 3DPDS-fa shows a single exothermic peak centered at 214 °C. Even though 3DPDS-fa is a mixture of isomers, it exhibits the sharpest ROP transition. One possible explanation is the presence of one dominant curing process (Figure II.16d). On the contrary, 4,4'-substituted benzoxazines exhibit two curing processes signified by a clear split of the exothermic peak (Figure II.16a, b and c). The first exothermic peak is located at 215, 224, and 235 °C for 4DPDS-fa, 4DTP-fa, and BA-fa, respectively and it was attributed to the benzoxazine ring opening reaction. The exothermic peak located higher temperature, centered between 240 and 250 °C, was assigned to the post-polymerization reaction of the furan rings, in agreement with research works reported previously.^{109, 132, 191-193}

The involvement of this group in the polymerization was double-checked by FTIR (Figure II.17) by characterizing the monomers before and after a thermal treatment at 170 °C for 1 hour. 4DPDS-fa shows a broadening of absorption between 1570 and 1700 cm^{-1} , indicating that electrophilic substitutions occurred on the furfuryl groups. Moreover, the double-peak pattern is present for 4DTP-fa, and BA-fa as well as the widening of the FTIR peak around 1620 cm^{-1} . Even though the DSC profile of 3DPDS-fa just revealed one exothermic peak, the furan rings seem to be also involved in the polymerization process as attested by FTIR. An increase of the absorption peak located at 1580 cm^{-1} confirms also the reaction occurred.

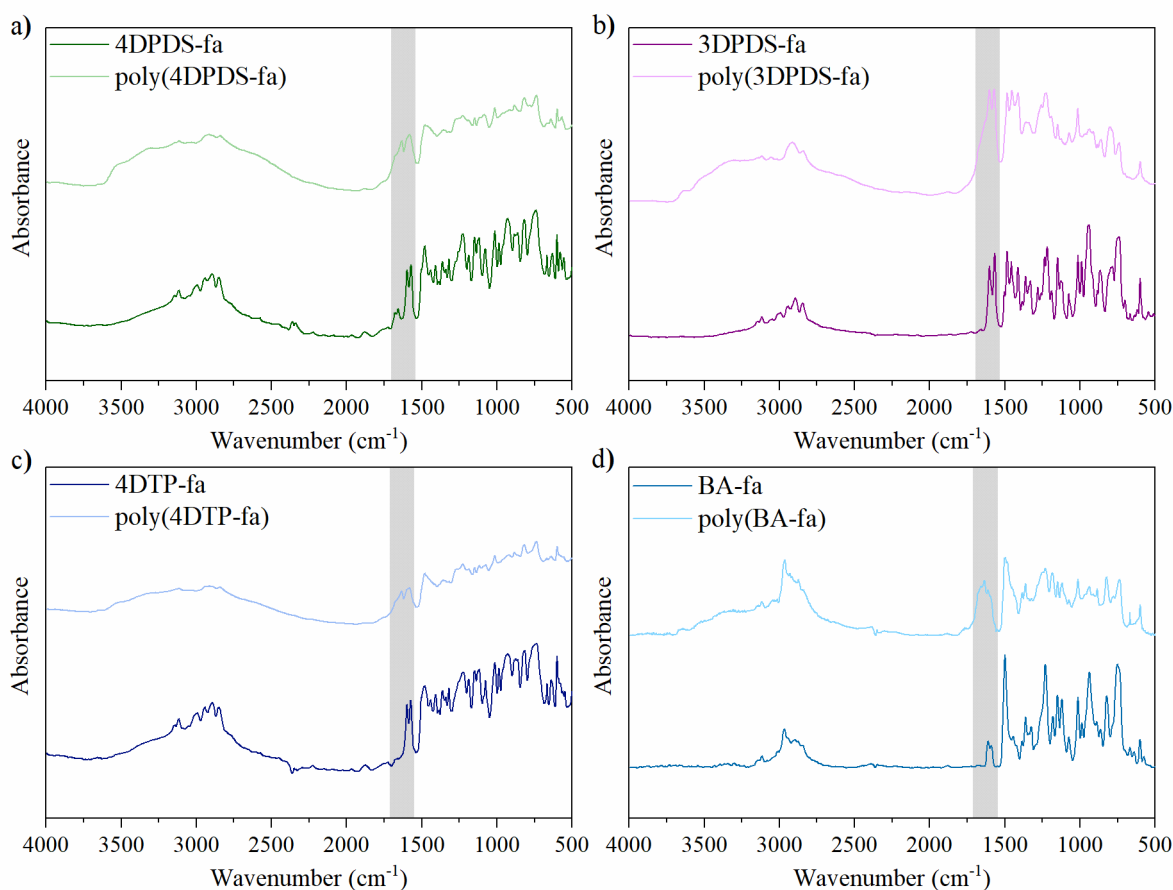


Figure II.17. FTIR transmission spectra of diBz a) 4DPDS-fa, b) 3DPDS-fa, c) 4DTP-fa, and d) BA-fa before and after curing at 170 °C for 1 hour.

Additionally, the reaction enthalpies of ROP (ΔH) were determined and decreased as follows: 3DPDS-fa > 4DPDS-fa > BA-fa > 4DTP-fa with values ranging from 178 to 148 $\text{kJ}\cdot\text{mol}^{-1}$ in agreement with previously reported similar diBz.¹³²

Furthermore, the apparent activation energies were calculated using Kissinger and Ozawa methods. For this reason, non-isothermal DSC tests were carried out at different heating rates (5, 10, and 20 $\text{K}\cdot\text{min}^{-1}$). The corresponding DSC thermograms, and Kissinger and Ozawa plots are gathered in Annex C (from Figure C.1 to Figure C.4). It is important to highlight that for 4,4'-substituted benzoxazines, E_a were determined from the exothermic peak located at the low temperature. 3DPDS-fa exhibit an activation energy of 109.3 $\text{kJ}\cdot\text{mol}^{-1}$ closely followed by 4DTP-fa and 4DPDS-fa (116.9 and 120.6 $\text{kJ}\cdot\text{mol}^{-1}$ respectively) using Kissinger method. For BA-fa, E_a was found to be 87.1 $\text{kJ}\cdot\text{mol}^{-1}$ similar to previously published.¹³² Comparable results

were obtained from both methods.¹⁹⁰ The results obtained are summarized in Table II.10 together with the thermal and polymerization parameters determined from DSC.

Table II.10. Thermal behavior and polymerization kinetic parameters of furfurylamine-containing diBz.

Abbr.	T _m ^a (°C)	T _{onset} ^b (°C)	T _{poly} ^c (°C)	ΔH ^d (kJ·mol ⁻¹)	E _a (kJ·mol ⁻¹)	
					Kissinger*	Ozawa*
4DPDS-fa	74	146	215 / 240	172	120.6	122.3
3DPDS-fa	90 / 115	155	214	178	109.3	111.5
4DTP-fa	99	151	224 / 250	148	116.9	119.1
BA-fa	100	170	235 / 250	156	87.1	90.8

^a Melting temperature from the endotherm at 10 K·min⁻¹. ^b Onset temperature of the exotherm at 5 K·min⁻¹.

^c Maximum temperature of the exothermic peak at 10 K·min⁻¹. ^d Enthalpy of the exothermic peak at 10 K·min⁻¹.

*T_{poly} maximum of first exothermic peak.

An additional important outcome from DSC technique, is the onset temperature of the ROP (T_{onset}). This parameter corresponds to the temperature at which the oxazine rings starts to open, and thus, indicates the minimum polymerization temperature at one specific heating rate. Even though, in real applications the polymerization of benzoxazine is carried out following isothermal processes, T_{onset} can guide the range of temperatures that can potentially be used for the curing. For this reason, these values were determined from the DSC curves at the lowest heating rate i.e. 5 K·min⁻¹ to have a better approximation to an isothermal curing. A summary of the T_{onset} is gather in Table II.10. The highest polymerization onset is found for BA-fa around 170 °C while for sulfur-containing diBz these values range from 146 to 155 °C. Interestingly, for 4DPDS-fa, 3DPDS-fa, and 4DTP-fa, the polymerization temperatures fit to the temperatures commonly applied to vulcanize rubber compounds in the tire industry (ca. 150 °C). The curing kinetics of the benzoxazine monomers will be reported later by rheological analysis at 150 °C.

3.1.3 DSC of benzoxazine monomers prepared from aniline

DSC thermograms of 4DPDS-a, 3DPDS-a, 4DTP-a, and BA-a are reported in Figure II.18. Each monomer exhibits an endothermic and an exothermic peak. For 3DPDS-a and 4DPDS-a, the endothermic peaks related to the melting are found at 103 and 129 °C, respectively. 4DTP-a and BA-a show their melting points at 114 and 100 °C respectively.

Regarding the ring-opening temperatures, they exhibit just one exothermic peak because of the presence of one dominant autocatalytic curing process.¹⁹⁰ The maximum of the exothermic peak ranges from 194 °C for 4DPDS-a to 201 and 221 °C for 3DPDS-a and 4DTP-a, respectively. BA-a exhibit the highest T_{poly} at 225 °C in agreement with the literature.¹⁹⁰ The polymerization onsets were determined from the DSC thermograms at 5 K·min⁻¹. 4DPDS-a and 3DPDS-fa exhibit similar T_{onset} around 160 °C. By contrast, for 4DTP-a and BA-a, the onsets are approximately located at 177 and 172 °C, respectively.

The polymerization enthalpies, ranging from 90 to 143 kJ·mol⁻¹, decreased as follows: 3DPDS-a > 4DTP-a > BA-a > 4DPDS-fa. Relatively lower enthalpies were determined for aniline-containing diBz compared to their counterparts with furfurylamine (from 106 to 178 kJ·mol⁻¹).

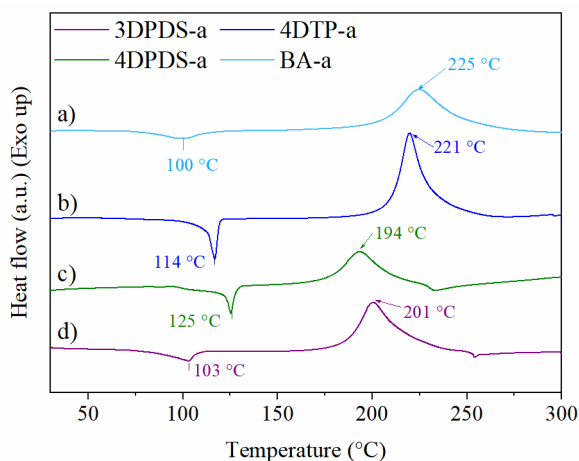


Figure II.18. DSC thermograms at 10 K·min⁻¹ of diBz: a) BA-a, b) 4DTP-a, c) 4DPDS-a, and d) 3DPDS-a.

The apparent activation energies were calculated using Kissinger and Ozawa methods. Additional DSC thermograms, and Kissinger and Ozawa plots are gathered in Annex C (from Figure C.5 to Figure C.8). The activation energies range from 79.7 kJ·mol⁻¹ for 4DTP-a, to 90.0 kJ·mol⁻¹ for 4DPDS-a, by Kissinger method. BA-a shows an apparent activation energy of 87.7 kJ·mol⁻¹ similar than previously reported.¹⁹⁰ Moreover, both methods lead to comparable results that are gathered in Table II.11.

Table II.11. Thermal behavior and polymerization kinetic parameters of aniline-containing diBz.

Abbr.	T _m ^a (°C)	T _{onset} ^b (°C)	T _{poly} ^c (°C)	ΔH ^d (kJ·mol ⁻¹)	E _a (kJ·mol ⁻¹)	
					Kissinger	Ozawa
4DPDS-a	129	158	194	90	90.0	93.0
3DPDS-a	103	159	201	143	84.3	87.7
4DTP-a	114	177	221	102	79.7	83.6
BA-a	100	172	225	141	87.8	91.3

^a Melting temperature from the endotherm at 10 K·min⁻¹. ^b Onset temperature of the exotherm at 5 K·min⁻¹.

^c Maximum temperature of the exothermic peak at 10 K·min⁻¹. ^d Enthalpy of the exothermic peak at 10 K·min⁻¹.

Finally, the thermal properties and kinetic parameters are summarized in Table II.11. In conclusion, aniline-containing diBz exhibit lower E_a than furfurylamine diBz. However, they required higher temperatures to polymerize. The feasibility of these diBz to polymerize at 150 °C will be studied later by rheological analyses.

3.1.4 DSC of benzoxazine monomers prepared from stearylamine

The DSC thermograms of 4DPDS-ste and 3DPDS-ste are displayed in Figure II.19. These monomers melt at low temperature (between 40 and 65 °C) compared to their derivatives with furfurylamine and aniline. The exothermic peaks are centered at 223 °C for 3DPDS-ste and at 233 °C for 4DPDS-ste. Due to a dilution effect of the long alkyl chain of stearylamine group, 3DPDS-ste and 4DPDS-ste have low polymerization enthalpies, around 40 kJ·mol⁻¹ for both diBz.

Finally, a summary of their thermal properties and the kinetic parameters is gathered in a Table II.12

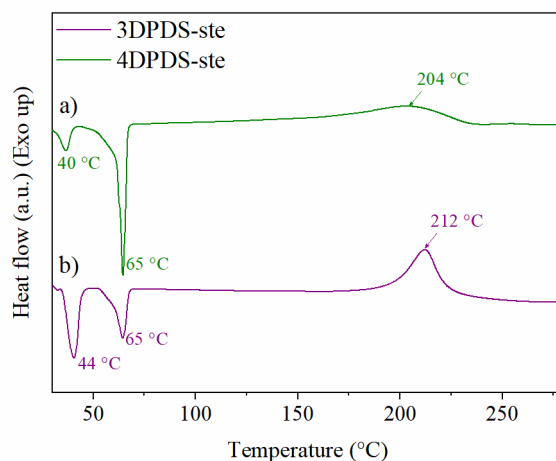
Figure II.19. DSC thermograms at 10 K·min⁻¹ of diBz: a) 4DPDS-ste, and b) 3DPDS-ste.

Table II.12. Thermal behavior and polymerization kinetic parameters of stearylamine-containing diBz.

Abbr.	T _m ^a (°C)	T _{onset} ^b (°C)	T _{poly} ^c (°C)	ΔH ^d (kJ·mol ⁻¹)	E _a (kJ·mol ⁻¹)	
					Kissinger	Ozawa
4DPDS-ste	40 / 65	152	204	39	92.0	95.0
3DPDS-ste	44 / 65	165	212	40	107.8	110.0

^a Melting temperature from the endotherm at 10 K·min⁻¹. ^b Onset temperature of the exotherm at 5 K·min⁻¹.

^c Maximum temperature of the exothermic peak at 10 K·min⁻¹. ^d Enthalpy of the exothermic peak at 10 K·min⁻¹.

3.2 Thermal stability by TGA

For the sake of clarity, TGA and DSC thermograms of benzoxazines containing furfurylamine are plotted together (Figure II.20). All the precursors remain stable at least up to 225 °C as indicated by the temperatures of 5% of weight loss (T_{5%}). It is not before 250, 260 and 264 °C that 4DPDS-fa, 4DTP-fa, and 3DPDS-fa release 5% degradation products, respectively. For BA-fa T_{5%} is found at 225 °C. These results highlight that the dibenzoxazines can polymerize before degrading. Regarding the char yield, 3DPDS-fa exhibits the highest value, 61%, followed by 4DTP-fa with 57%, 4DPDS-fa with 55%, and BA-fa with 45%. It is noteworthy the sulfur containing molecules lead to higher char yields compared to bisphenol A counterparts.

Similarly, TGA thermograms of aniline-containing diBz are overlapped with the DSC curves (Annex C, Figure C.11). Likewise, all the benzoxazines show stability at polymerization temperatures as the exothermic peaks are located before the T_{5%}. Indeed, this value ranges from 215 to 288 °C, the lowest corresponding to 4DPDS-a and the highest to 4DTP-a. Char yield (CY) increases as follows 27% (BA-a) > 52% (4DTP-a) > 49% (4DPDS-a) > 56% (3DPDS-a). The use of sulfur-containing diphenols leads to higher CY compared to bisphenol A molecules. Additionally, the usage of furfurylamine is preferable to obtain compounds with high char yields.

The thermal stability of stearylamine-containing precursors was also assessed by TGA and is reported in Annex C (Figure C.12). Both molecules, 3DPDS-ste, and 4DPDS-ste, exhibit 5% of weight loss above 220 °C, thus they could polymerize without degrading under the testing conditions.

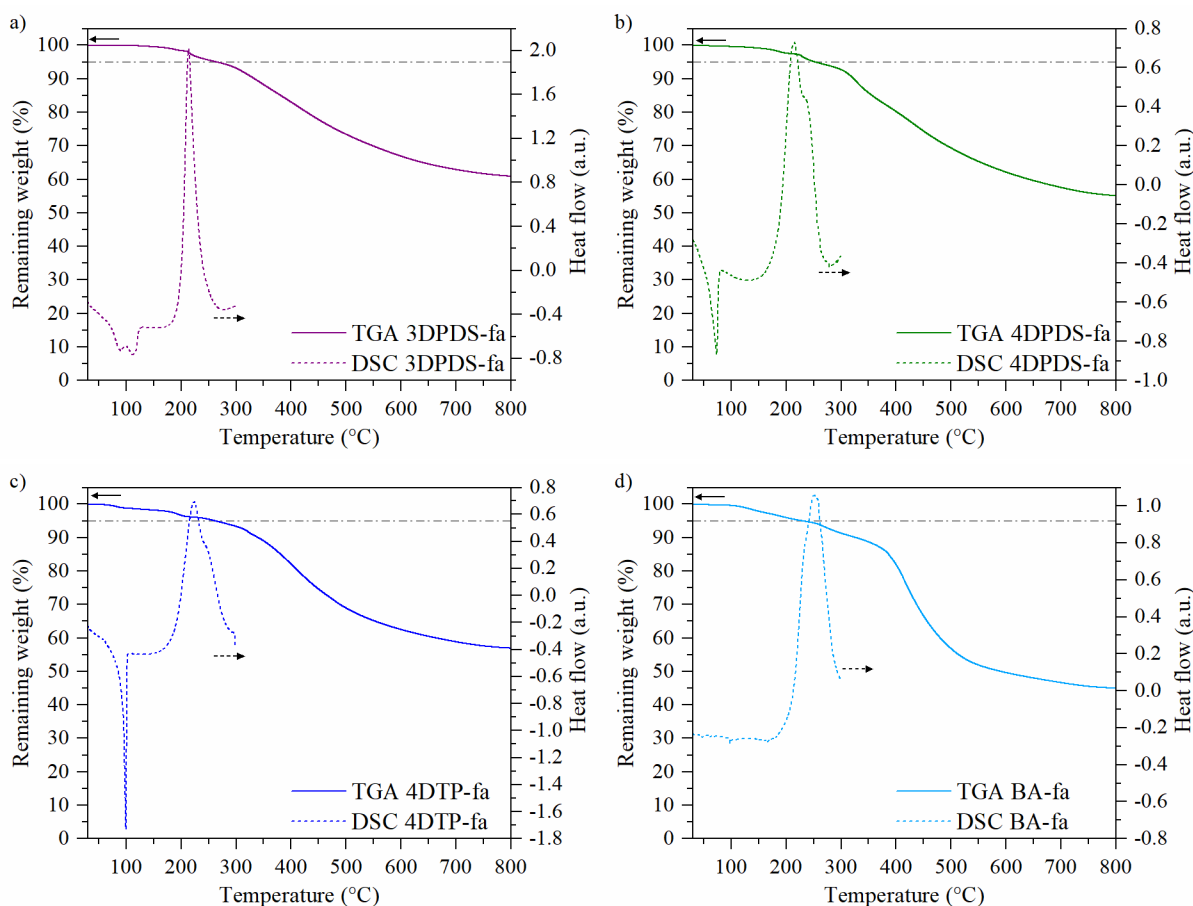


Figure II.20. TGA thermograms of dibenzoxazines from furfurylamine: a) 3DPDS-fa, b) 4DPDS-fa, c) 4DTP-fa, and d) BA-fa.

A summary of the results obtained by TGA is gathered in Table II.13. All the synthesized benzoxazines are thermally stable in the range of polymerization temperatures under the testing conditions.

Table II.13. Thermal stability of diBz by TGA.

Abbr.	T _{5%} ^a (°C)	CY ^b (%)
4DPDS-fa	250	55
3DPDS-fa	264	61
4DTP-fa	262	57
BA-fa	225	45
4DPDS-a	215	49
3DPDS-a	260	56
4DTP-a	288	52
BA-a	228	27
4DPDS-ste	234	10
3DPDS-ste	223	19

^a Temperature of 5% of weight loss by TGA at 10 K·min⁻¹ under N₂. ^b Char yield at 800 °C by TGA under N₂.

3.3 Polymerization behavior by rheology

The rheo-kinetics of the dibenzoxazines monomers were studied by following the evolution of their complex viscosity (η^*), and their storage (G') and loss moduli (G'') under isothermal conditions at 150 °C. This temperature was selected because it is commonly applied to vulcanize rubber compounds in the tire industry (i.e. ≥ 150 °C). For this reason, the feasibility of the diBz to polymerize at 150 °C is assessed in this section. Even though, this temperature is significantly lower than the T_{poly} values determined by DSC, the polymerization onsets at low heating rate demonstrated that the diBz can cure at much lower temperatures.

The evolution of η^* of the furfurylamine-containing dibenzoxazines is displayed in Figure II.21a. In the molten state, the monomers exhibit very low values of η^* , between $6 \cdot 10^2$ and $11 \cdot 10^2$ mPa·s. After several minutes, η^* noticeably increases indicating the curing of the monomers. Additionally, the evolution of G' and G'' is depicted in Figure II.21b. The gelation times (t_{gel}), defined as the crossover point of G' and G'' , are observed after 17, 34, 40 and 41 minutes, for 4DPDS-fa, 4DTP-fa, BA-fa, and 3DPDS-fa, respectively.

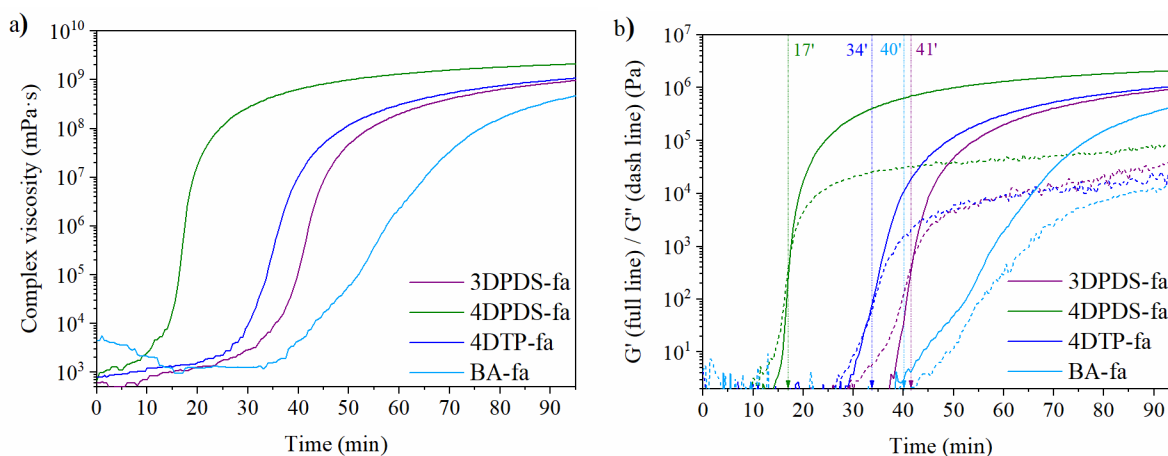


Figure II.21. Polymerization of furfurylamine-containing diBz followed by rheology over time at 150 °C: a) complex viscosity; b) G' (full line) and G'' (dash line).

Surprisingly, 3DPDS-fa takes more than twice the time to cure in comparison to 4DPDS-fa (41 min and 17 min, respectively). The significant difference in the curing kinetics could be attributed to the small amount of thiol groups identified by Raman spectroscopy for 4DPDS-fa (Figure II.9). Indeed, the catalytic opening of the lateral benzoxazines ring by thiol, the so-called COLBERT reaction, has been reported^{144, 188} and described in Chapter I, section 6.3. This reaction between thiols and benzoxazines could happen under ambient conditions but is highly influenced by the nature and number of thiols as well as the nature of the amine used for the synthesis of diBz. In the case of 4DPDS-fa, the higher reactivity might be explained by the formation of catalytic species through the COLBERT reaction (Scheme I.21) that are able to further catalyze the ROP. This could explain why its reactivity is so high in comparison to 3DPDS-fa. The polymerization behavior of 4DTP-fa confirms this assumption. Indeed, this benzoxazine, which contains mono-heteroatom of sulfur and cannot form thiols due to the absence of a disulfide bond, cures in the same range than 3DPDS-fa.

Furthermore, the curing kinetics of dibenzoxazines prepared with aniline were also assessed. The rheo-kinetic characterizations at 150 °C are displayed in Figure II.22. The crosslinking of

the monomers is shown by the increase of the complex viscosity over time. For 4DPDS-a, the gelation time is reached after 16 minutes followed by 3DPDS-a (19.5 minutes). Interestingly, 4DPDS-a does not exhibit the catalytic effect observed for its counterpart with fa (4DPDS-fa) due to the absence of thiol groups attested by Raman (Figure II.10). In fact, 4DPDS-fa and 3DPDS-fa has similar reactivity at 150 °C. On the contrary, 4DTP-a and BA-a cure in 34 and 47 minutes respectively showing the lower reactivity of these monomers. These values are in agreement with results obtained by DSC, as their T_{onset} are approximately 10 °C higher than the ROP onsets for 3DPDS-a and 4DPDS-a.

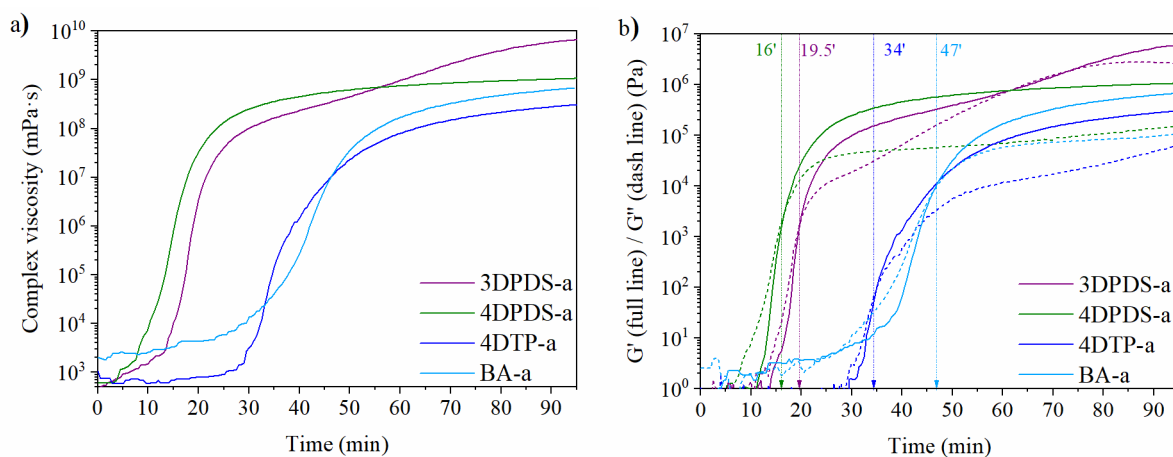


Figure II.22. Polymerization of aniline-containing diBz followed by rheology over time at 150 °C: a) complex viscosity; b) G' (full line) and G'' (dash line).

The crosslinking ability of 3DPDS-ste and 4DPDS-ste was also studied by rheo-kinetic measurements and the corresponding rheograms are displayed in Figure II.23. 4DPDS-ste and 3DPDS-ste show in the molten state low values of η^* , $6.7 \cdot 10^2$ and $5.6 \cdot 10^2$ mPa·s, respectively. The gelation times of both monomers are reached after approximately 1 hour at 150 °C. These values reflect the low reactivity of these precursors due the presence of a long alkyl chain from stearylamine.

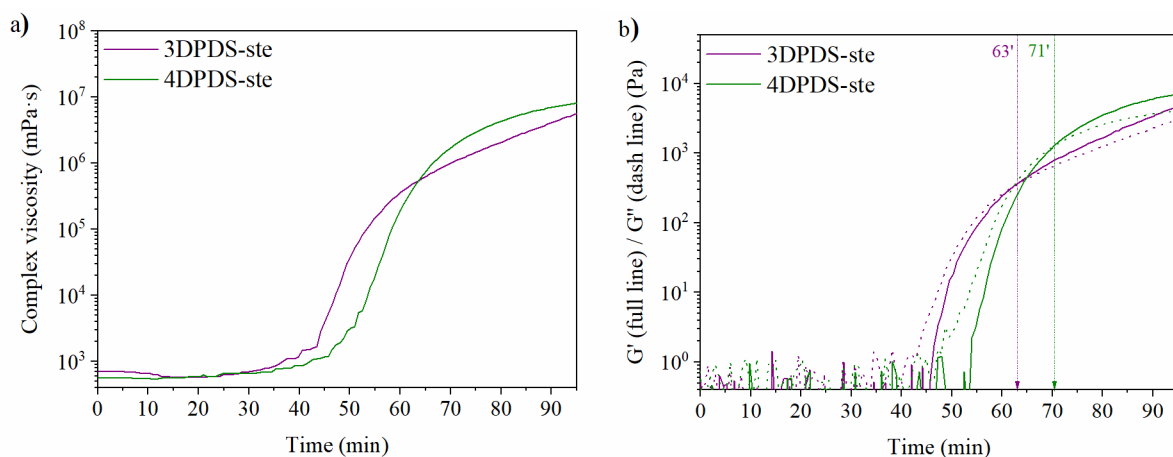


Figure II.23. Polymerization of stearylamine-containing diBz followed by rheology over time at 150 °C: a) complex viscosity; b) G' (full line) and G'' (dash line).

The gelation times at 150 °C of each benzoxazine precursor are gathered in Table II.14. The curing times of benzoxazines monomers prepared either with furfurylamine or aniline are in an appropriate range for use in the tire industry.

Table II.14. Gelation time of diBz by rheological measurements at 150 °C.

Abbr.	t_{gel} (min)	Abbr.	t_{gel} (min)
4DPDS-fa	13	4DPDS-a	16
3DPDS-fa	41	3DPDS-a	19.5
4DTP-fa	34	4DTP-a	34.5
BA-fa	40	BA-a	47
4DPDS-ste	71	3DPDS-ste	63

3.4 Viscoelastic properties of polybenzoxazine

Polybenzoxazines (polyBz) were formed by curing their precursors. The curing was performed at 170 °C for 1 hour, at 190 °C for 1 hour and at 210 °C for 1 hour (see more details in Annex A, section A.1.9). It is important to keep in mind that the vulcanization process is commonly done in shorter times and at lower temperatures. For this reason, the properties of the polyBz inside the rubber compounds will differ from the ones that will be reported in the following paragraphs. Nevertheless, the viscoelastic properties of the polyBz were studied after a complete curing to fully characterized the molecules.

The evolution of the storage (G') and loss moduli (G''), and loss factor ($\tan\delta$) as a function of the temperature of poly(3DPDS-fa), poly(4DPDS-fa), poly(4DTP-fa), and poly(BA-fa) are displayed in Figure II.24.

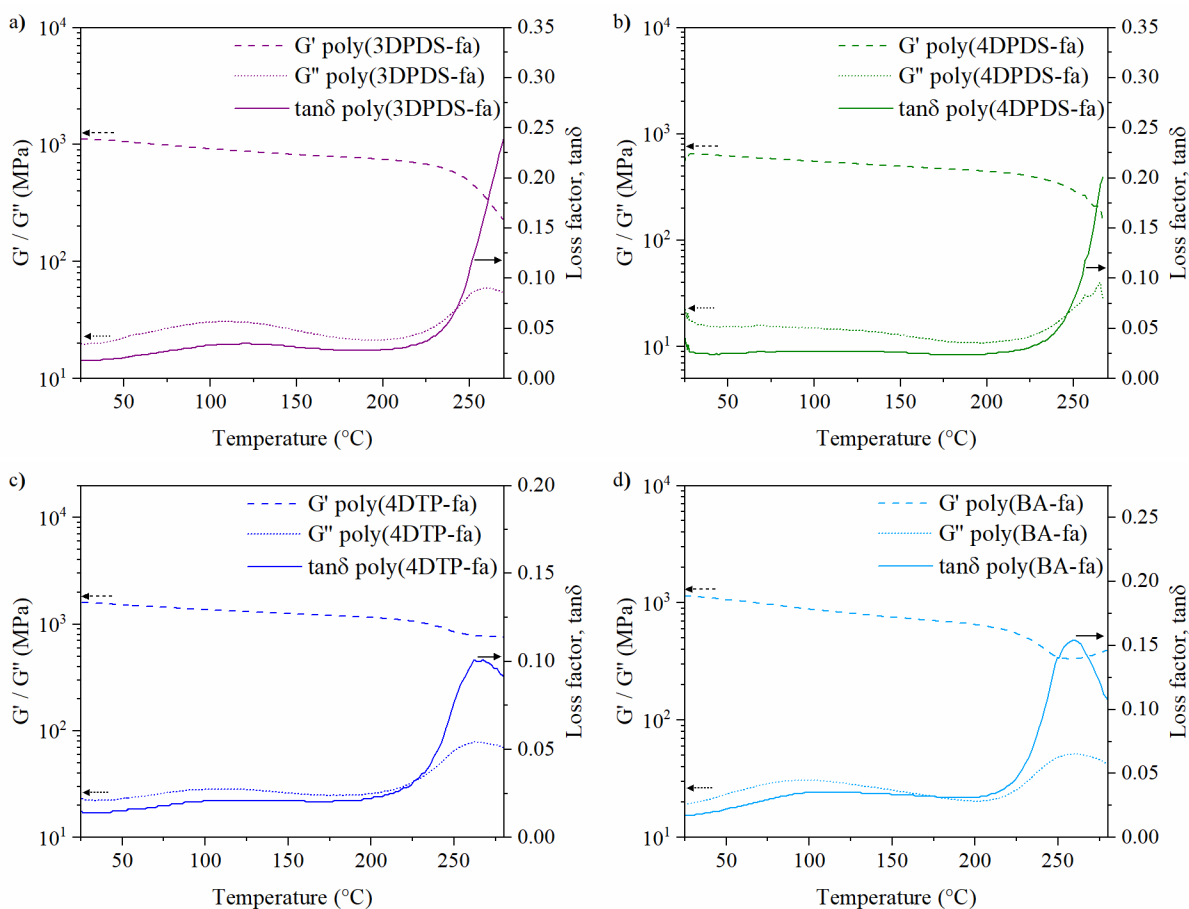


Figure II.24. Rheology curves in temperature sweep mode of a) poly(3DPDS-fa), b) poly(4DPDS-fa), c) poly(4DTP-fa), and d) poly(BA-fa).

The α -relaxation temperatures (T_α) were determined for each polyBz from the maximum of the G'' . Polybenzoxazines containing furan groups exhibited T_α around 260 °C. These high values of T_α are explained by the involvement of the furan ring in the network as previously reported.^{132, 191}

The viscoelastic properties of poly(4DTP-a) and poly(BA-a) are shown in Figure II.25. The glass transition temperatures are found to be 200 and 150 °C, respectively. These values are lower than the results obtained for their derivatives with furfurylamine. The use of furfurylamine is more desirable to produce high T_α materials. No curves are displayed for 4DPDS-a and 3DPDS-a because they degraded before being fully cured preventing the formation of polyBz in these cases.

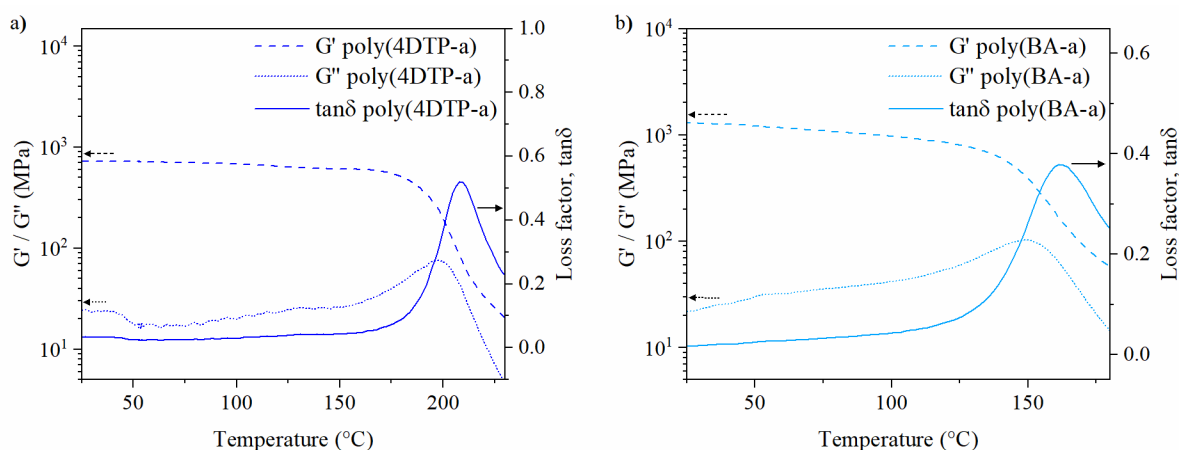


Figure II.25. Rheology curves in temperature sweep mode of a) poly(4DTP-a), and b) poly(BA-a).

Finally, the α -relaxation temperatures are gathered in Table II.15.

Table II.15. The α -relaxation temperatures of polyBz by rheological measurements.

Abbr.	T_α ^a (°C)	Abbr.	T_α ^a (°C)
Poly(4DPDS-fa)	260	Poly(3DPDS-fa)	260
Poly(4DTP-fa)	263	Poly(4DTP-a)	200
Poly(BA-fa)	260	Poly(BA-a)	150

^a α -Relaxation temperature determined from the maximum of G'' .

3.5 Discussion

This section described the thermal and polymerization behaviors of the benzoxazine precursors by DSC, TGA, and rheological measurements, and the viscoelastic properties of their polyBz.

Precursors prepared with furfurylamine exhibit melting points below 100 °C while aniline counterparts melt above 100 °C. The ring-opening polymerizations were characterized by the maximum of the exothermic peak, ranging from 190 to 235 °C. Additionally, all synthesized monomers were thermally stable in the range of polymerization temperatures.

Despite the high polymerization temperatures found by DSC, the benzoxazine precursors were able to cure at lower temperatures. Isothermal rheological measurement showed all the diBz polymerized at 150 °C. Dibenzoxazines prepared from furfurylamine and aniline exhibited gelation points between 13 and 41 minutes. These results demonstrated the possibility to use

these benzoxazines to reinforce rubber compounds. Indeed, they could polymerize at the same time than the rubber vulcanization and thus, potentially act as reinforcing resin.

Finally, T_{α} of the polybenzoxazines were also characterized. Polybenzoxazines with furan groups exhibited T_{α} around 260 °C thanks to the involvement of the furan ring in the 3D network confirmed by FTIR. These results together with the cure kinetics show the feasibility to use these dibenzoxazine precursors to reinforce rubber compounds.

To conclude, a summary of the main properties is gathered in Table II.16.

Table II.16. Summary of thermal and curing properties of the synthesized diBz monomers and their polyBz.

Abbr.	T_m^a (°C)	T_{onset}^b (°C)	t_{gel}^c (min)	T_{α}^d (°C)
4DPDS-fa	74	146	13	260
3DPDS-fa	90 / 115	155	41	260
4DTP-fa	99	151	34	263
BA-fa	100	170	40	260
4DPDS-a	129	158	16	-
3DPDS-a	103	159	19.5	-
4DTP-a	114	177	34.5	200
BA-a	100	172	47	150
4DPDS-ste	40 / 65	152	71	-
3DPDS-ste	44 / 65	165	63	-

^aMelting temperature from the endotherm at 10 K·min⁻¹ by DSC. ^bOnset temperature of the exotherm at 5 K·min⁻¹ by DSC. ^cGelation time at 150 °C by rheology. ^d α -Relaxation temperature determined from the maximum of G'' by rheological measurements of polyBz.

4 Conclusion

This chapter described the design and successful synthesis of Class A dibenzoxazines (diBz). Disulfide-containing diBz were prepared from the reaction of 4,4'-dihydroxydiphenyl disulfide (4DPDS) and 3,3'-dihydroxydiphenyl disulfide (3DPDS) with furfurylamine (fa), aniline (a), and stearylamine (ste). 4,4'-thiodiphenol (4TDP) and bisphenol A (BA) were employed in combination with furfurylamine and aniline to yield diBz monomers with one or non-heteroatom of sulfur respectively. The benzoxazine monomers were readily synthesized through a one-step Mannich-like condensation reaction leading to high yields. The chemical features of the monomers were supported by FTIR and NMR, and their purity was confirmed by elemental analyses. Moreover, the presence of the disulfide bonds in benzoxazines from 3DPDS and 4DPDS was attested by Raman.

The thermal properties and polymerization kinetics of each benzoxazine precursor were fully characterized by DSC, TGA, and rheological measurements. The results demonstrated that diBz prepared from furfurylamine shown an interesting combination of thermal and mechanical properties. They exhibit relatively low melting points below 100°C as assessed by DSC. In addition, they polymerize in relatively short times (between 13 and 41 minutes at 150 °C). These polymerization times and temperatures are in the same range as vulcanization times and temperatures in the tire industry. Additionally, polybenzoxazines with furan groups exhibited

the highest T_{α} around 260 °C showing the potential of these diBz to be used as reinforcing resins. Indeed, they exhibit higher T_{α} than currently used phenolic resins (i.e. ~170 °C). These values together with the reactivity of the monomers make them suitable candidates as reinforcing resins for rubber applications.

To conclude, among the set of resins synthesized and characterized, diBz prepared from furfurylamine were selected to be tested into rubber formulations as reinforcing resins as they are the best compromise between thermomechanical and processing properties. In particular, 4DPDS-fa, 3DPDS-fa, and 4DTP-fa will be investigated in detail. In addition to exhibit the best properties, these precursors have a bio-based content of about 35% resulting at the same time in a suitable and more sustainable approach when compared to traditional resins.

**Chapter III:
Application of
benzoxazine resins in
unfilled compounds**

III Application of benzoxazine resins in unfilled compounds

1 Introduction

The project aims to develop new polymeric reinforcements based on polybenzoxazines to replace phenolic reinforcing resins in tires. This topic has been investigated using for instance model dibenzoxazines monomers as previously described in Chapter I, section 7. The rich molecular design flexibility of polybenzoxazines brings the possibility to design new molecules with interesting features and not covered by previous patents.

In this chapter the performance of the newly synthesized sulfur-containing benzoxazine in rubber compound is investigated. The feasibility of 4DPDS-fa, 3DPDS-fa, and 4DTP-fa as potential reinforcing resins is reported. The potential of each benzoxazine was tested in a simplified recipe in the absence of a filler, so-called unfilled compounds. This approach allows the development of a proof of concepts by the investigation of the performance of each benzoxazines in unfilled rubber compounds.

The chapter is divided in three sections: (1) the investigation of the polymerization behavior of the monomers in the presence of the curing package, (2) the application of sulfur-containing dibenzoxazines on unfilled rubber compounds, and (3) the comparison of the reinforcement effect of 3DPDS-fa with a model dibenzoxazine and traditional phenolic resins.

2 Investigation of benzoxazine curing in the presence of curing system

The ring-opening polymerization (ROP) of benzoxazines is known to be catalyzed by a variety of inorganic or organic compounds.³³ Among them, sulfur and carboxylic acids, which are ingredients of conventional tire recipe, have been described to be efficient. The rubber recipe that has been used in this work is composed of polyisoprene and a curing system constituted of sulfur (S_8), N,N'-dicyclohexyl benzothiazole-2-sulfenamide (DCBS), zinc oxide (ZnO) and stearic acid. Among the different synthesized benzoxazines, 3DPDS-fa was used as a model molecule to assess the impact of the curing system on the ROP. Therefore, the curing behavior of 3DPDS-fa was studied in the presence of each ingredient of the curing system (Figure III.1 a).

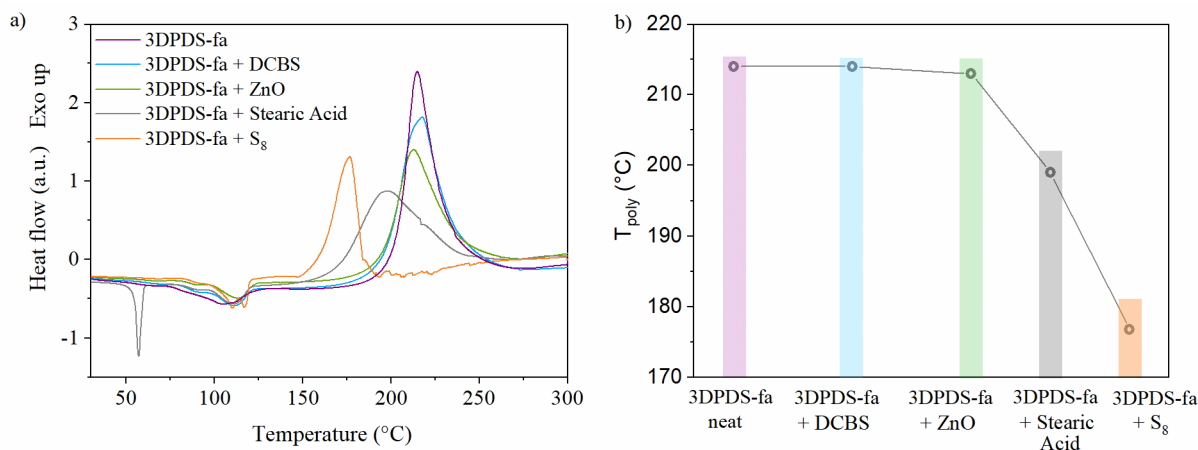
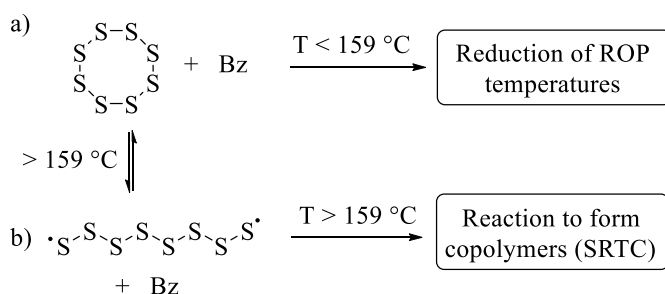


Figure III.1. a) DSC thermogram of 3DPDS-fa with DCBS, ZnO, stearic acid, and sulfur; b) Evolution of T_{poly} with the presence of curing system.

The impact of each ingredient on the polymerization temperature is plotted in Figure III.1b. The main ingredient that lowers T_{poly} of 3DPDS-fa is sulfur, as attested by the shift of the maximum from 214 to 175 °C. Stearic acid also affects the curing of 3DPDS-fa, but to a significantly lower extent compared to sulfur. For this reason, the study of the effect of sulfur in the curing of diBz will be further investigated.

Sulfur has been previously reported to trigger the ROP reaction, as previously discussed in Chapter I, section 6.2. Ishida *et al.* demonstrated that elemental sulfur (S_8) is an efficient catalyst to decrease the polymerization temperature of benzoxazines.³⁰ This triggering effect was reported to happen at temperatures below the thermally induced homolytic cleavage of sulfur (Scheme III.1a). Additionally, sulfur can react with benzoxazine monomers to form a copolymer at temperatures above 159 °C as reported by Liu *et al.* (Scheme III.1b).³¹ This reaction was initiated by sulfur radicals formed after the cleavage of sulfur ring and it is known as sulfur radical transfer and coupling reaction (SRTC).



Scheme III.1. Schematic representation of the effect of sulfur on benzoxazine monomers previously reported: a) Triggering effect of sulfur on the ROP of benzoxazines³⁰; b) Reaction between sulfur and benzoxazines to form copolymers³¹.

In the following sections, the effect of sulfur on the polymerization of 4DPDS-fa, 3DPDS-fa, and 4DTP-fa is studied by DSC and rheological measurements.

2.1 Effect of sulfur on the thermal behavior of the benzoxazine precursors.

Each benzoxazine was mixed with different amounts of sulfur ranging from 1 to 30 wt% and non-isothermal DSCs were carried out (see in Annex D, Figure D.1 and Figure D.2). DSC thermograms of 4DPDS-fa, 3DPDS-fa, and 4DTP-fa, without and with 30 wt% of sulfur are depicted in Figure III.2a. For all the tested benzoxazines, when sulfur is added, the maximum temperature of the exothermic peak is reduced. In the case of 3DPDS-fa the maximum of the exotherm is highly shifted from 214 to 175 °C as mentioned before. On the other hand, the exothermic peak of 4DPDS-fa was converted from a double wide peak located around 215 °C to a single narrow peak centered at 187 °C. Similar results were observed for 4DTP-fa with a decrease of T_{poly} of about 36 °C. However, for this monomer, the double wide peak around 224 °C was slowly converted to a single peak with the increase of the amount of sulfur (Figure D.2 in Annex D). A single narrow peak centered at 188 °C was obtained after the addition of 20 wt% of sulfur.

The evolution of the T_{poly} as a function of the sulfur content is displayed in Figure III.2b. For all the benzoxazines precursors, the increase of the amount of sulfur results in the lowering of the polymerization temperature, in agreement with previous works.^{14, 30} A plateau is reached with 20 wt% of sulfur. The lowest T_{poly} for 3DPDS-fa and 4DTP-fa are reached at 142 and

150 °C, respectively. It is worthy to note that the differences observed in the trend of 4DTP-fa depicted in Figure III.2b should be considered carefully, since it is mainly due to the DSC profile (i.e. the merging of the two peaks).

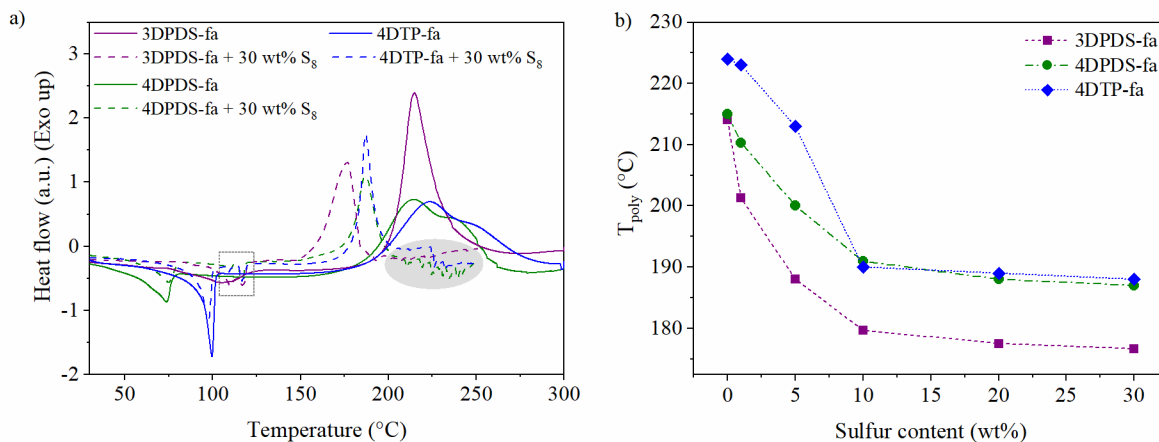


Figure III.2. a) DSC thermogram of 3DPDS-fa, 4DPDS-fa, and 4DTP-fa with and without 30 wt% of sulfur; b) Evolution of T_{poly} of 3DPDS-fa, 4DPDS-fa, and 4DTP-fa as a function of sulfur content. Dash lines serve to guide the eye.

The apparent activation energies of polymerization (E_a) were calculated using Kissinger and Ozawa plots as described in Chapter II, section 3.1.1. The additional DSC thermograms required for the calculations as well as the resulting plots are gathered in Annex D (from Figure D.3 to Figure D.6). Similar E_a were obtained for each benzoxazine. In the case of 4DPDS-fa and 4DTP-fa the addition of 30 wt% of sulfur slightly lowers E_a (113.5 kJ·mol⁻¹ determined by Kissinger). On the contrary, the incorporation of sulfur to 3DPDS-fa results in an increase of E_a (120.7 kJ·mol⁻¹) compared to 109.3 kJ·mol⁻¹ for the neat 3DPDS-fa; combined with a decrease of the polymerization temperatures. This could indicate that a side reaction could occur in these conditions, this will be discussed in the following sections.

The thermal properties and kinetic parameters of the precursor in the presence of sulfur are summarized in Table III.1. The parameters for the neat benzoxazines are displayed in Table II.10 in Chapter II.

Table III.1. Thermal behavior and polymerization kinetic parameters of 3DPDS-fa, 4DPDS-fa, and 4DTP-fa with 30 wt% of sulfur.

Abbr.	T_{onset}^a (°C)	T_{poly}^b (°C)	ΔT_{poly}^c (°C)	E_a (kJ·mol ⁻¹)	
				Kissinger	Ozawa
3DPDS-fa + 30 wt% of S ₈	142	175	39	120.7	121.8
4DPDS-fa + 30 wt% of S ₈	144	187	28	113.9	115.5
4DTP-fa + 30 wt% of S ₈	150	188	36	113.4	115.0

^a Onset temperature of the exotherm at 5 K·min⁻¹. ^b Maximum temperature of the exothermic peak at 10 K·min⁻¹. ^c Difference of T_{poly} between diBz with and without sulfur.

2.2 Effect of sulfur on the polymerization of benzoxazine precursors

Rheo-kinetic analyses were carried out to detail the catalytic effect of sulfur on the polymerization of the benzoxazine precursors from a viscoelastic perspective. For this purpose, each precursor was mixed with 1 and 5 wt% of sulfur and analyzed under isothermal conditions

at 150 °C (see in Annex D, Figure D.7 and Figure D.8). The evolution of the complex viscosity of 3DPDS-fa, 4DPDS-fa, and 4DTP-fa, without or with 5 wt% of sulfur, is displayed in Figure III.3a. For these tests lower amount of sulfur was employed than for DSC due to the high catalytic effect observed with the addition of only 5 wt% of S₈.

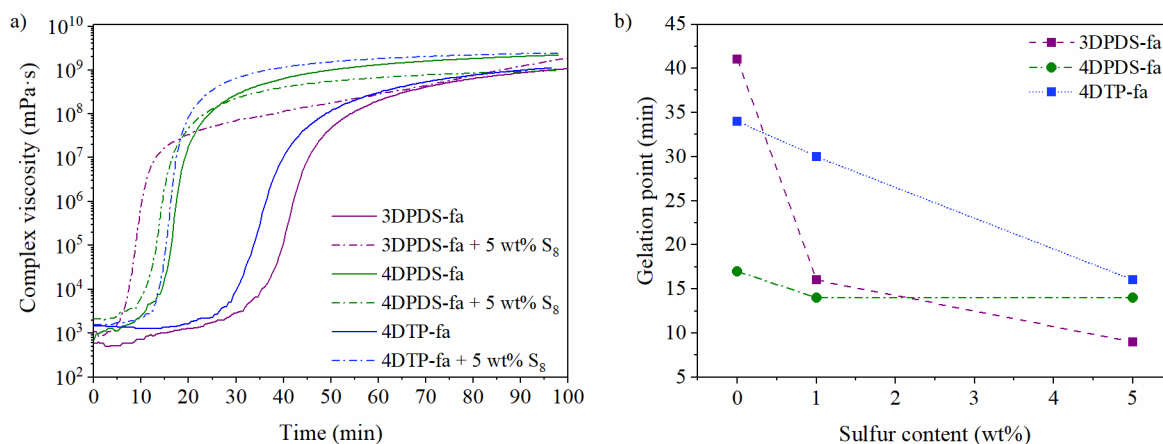


Figure III.3. a) Curing behavior of 3DPDS-fa, 4DPDS-fa, and 4DTP-fa with and without 5 wt% of sulfur by rheo-kinetics measurement at 150 °C followed by complex viscosity over time; b) Gelation times of 3DPDS-fa, 4DPDS-fa, and 4DTP-fa as a function of sulfur content. Dash lines are drawn to guide the eye.

The polymerization of 3DPDS-fa is strongly catalyzed by sulfur, even if it is added in small amounts. For this molecule the gelation time shifted from 41 to 17 min just with the addition of 1 wt% of sulfur and to 9 min with 5 wt% of S₈. On the contrary, the polymerization of 4DPDS-fa is almost not affected by the presence of sulfur. As previously mentioned, this might be due to the small amount of thiolated forms of cleaved 4DPDS-fa, which already catalyze its polymerization. This assumption is also confirmed by the curing behavior of 4DTP-fa in the presence of sulfur as a high catalytic effect is also observed. This mono-sulfide benzoxazine precursor exhibits a shift of the t_{gel} from 34 min to 16 min with 5 wt% of sulfur.

To conclude, the addition of a low amount of sulfur (i.e. 5 wt%) to the diBz results in a decrease of the curing times which are ranging from 9 to 16 min for 3DPDS-fa and 4DTP-fa, respectively (Table II.14). The presence of sulfur could be considered as an asset because it could act like an inherent catalyst for the polymerization of diBz inside most of the rubber compounds. Moreover, it might overcome the long times commonly required to cure benzoxazine monomers and therefore, allow them to efficiently crosslink at the same time than the rubber vulcanization.

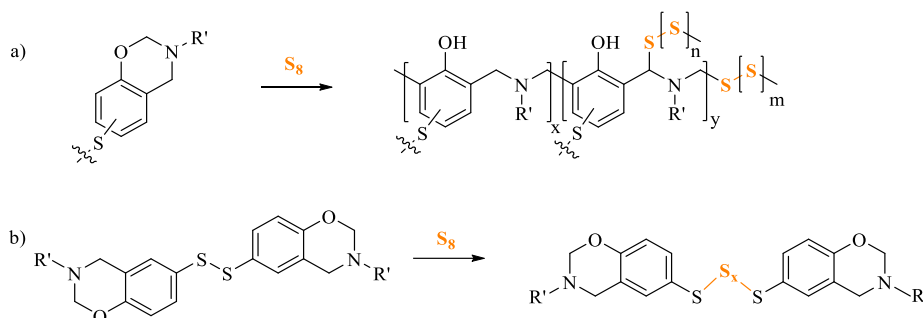
Table III.2. Gelation time of 3DPDS-fa, 4DPDS-fa, and 4DTP-fa with 1 and 5 wt% of sulfur by rheological measurements at 150 °C.

Abbr.	t_{gel} (min)	Abbr.	t_{gel} (min)
3DPDS-fa + 1 wt% of S ₈	16	3DPDS-fa + 5 wt% of S ₈	9
4DPDS-fa + 1 wt% of S ₈	14	4DPDS-fa + 5 wt% of S ₈	14
4DTP-fa + 1 wt% of S ₈	30	4DTP-fa + 5 wt% of S ₈	16

2.3 Solubility of polybenzoxazines in the presence of sulfur

Additionally, each precursor was polymerized in the absence and presence of sulfur following the procedure described in the Annex A (section A.2.8) and their solubility was tested in

dimethylformamide (DMF). For the sake of clarity, cured benzoxazine precursors will be annotated as poly(“precursor”). When cured in the presence of sulfur, they will be annotated poly(“precursor”)/S₈. Poly(3DPDS-fa), poly(4DPDS-fa), and poly(4DTP-fa) were insoluble, as expected from polybenzoxazine networks. On the contrary, poly(4DPDS-fa)/S₈ was fully soluble in DMF even when it was cured in the same conditions. A partial solubility was also observed for poly(3DPDS-fa)/S₈ and poly(4DTP-fa)/S₈, for which a solid fraction of about 60% of the initial mass was recovered after the test. The partial solubility of poly(3DPDS-fa)/S₈ and poly(4DTP-fa)/S₈ could be explained by a co-reaction occurring between sulfur and the oxazine rings, in these specific conditions as previously reported (Scheme III.2a).^{14, 31}



Scheme III.2. Schematic representation of possible reactions between elemental sulfur and benzoxazines a) through the oxazine ring SRTC reaction^{14, 31}, and b) through the disulfide bond forming a polysulfide (in the case of 4DPDS-fa).

The full solubility of poly(4DPDS-fa) in DMF indicates an additional reaction is occurring between S₈ and 4DPDS-fa otherwise its solubility should remain the same than poly(4DTP-fa)/S₈. The only structural difference between these molecules is the disulfide bond. Therefore, the other side-reaction taking place could be through this bond as reported in other works and described in Scheme III.2b, with the formation of a polysulfide.^{32, 194-195} Interestingly, the disulfide bond in 3DPDS-fa does not undergo a similar side-reaction. Indeed, poly(3DPDS-fa)/S₈ shows a similar solubility than poly(4DTP-fa)/S₈, meaning their curing in the presence of sulfur are also similar. The two different curing behaviors between poly(3DPDS-fa)/S₈ and poly(4DPDS-fa)/S₈ may be explained by the lower stability of the disulfide bond of 4DPDS-fa, as mentioned in Chapter II.

2.4 Discussion

The thermal behavior of the benzoxazines precursors was studied in the presence of the curing system. Sulfur was the ingredient with the highest impact on the cure kinetics by greatly decreasing the polymerization times. This behavior is a clear asset for the application of diBz in rubber compounds as it is acting as an inherent catalyst for their polymerization and thus, is overcoming the long curing times usually required for diBz. Furthermore, a reaction between sulfur and benzoxazine could also take place as previously reported. However, it is important to highlight that it is not possible to predict if this reaction will occur inside the rubber compounds in a similar fashion.

To conclude, due to their curing kinetic in the presence or absence of sulfur, 4DPDS-fa, 3DPDS-fa, and 4DTP-fa are three suitable candidates to be used for the reinforcement of rubber compounds. For this reason, they were incorporated in unfilled rubber compounds and tested

as reinforcing agents. The performance of each precursor on the curing behavior and the final properties of the materials will be reported in the following section.

3 Application of dibenzoxazines precursors in unfilled compounds

The potential of each benzoxazine to act as a reinforcing resin in rubber compounds has been tested in a recipe composed of polyisoprene and a curing system constituted of sulfur, DCBS, ZnO, and stearic acid. Unfilled polyisoprene materials were prepared using the formulation displayed in Table III.3. All the values are indicated in weight percentage as well as in phr (parts per hundred rubber), which is commonly used in the rubber industry. For the sake of clarity, the term “unfilled compound” will be employed in the rest of this chapter to designate cured rubber composed of a mixture of polyisoprene and curing system with or without benzoxazine precursors while “unfilled green compound” will refer to the uncured materials.

Table III.3. Formulation of unfilled polyisoprene compounds with 3DPDS-fa, 4DPDS-fa, and 4DTP-fa system and carbon black

Ingredients	Amount (phr)		Amount (wt%)		
	3DPDS-fa	4DPDS-fa	3DPDS-fa	4DPDS-fa	4DTP-fa
Polyisoprene	100	86.6	83.0	76.6	68.7
Benzoxazines	0 / 5 / 15 / 30	0	4.1	11.5	20.6
Sulfur	5.5	4.3	4.1	3.8	3.4
Zinc oxide (ZnO)	5	1.7	1.7	1.5	1.4
Stearic acid	2	4.8	4.6	4.2	3.8
DCBS^a	3	2.6	2.5	2.3	2.1

^a N,N'-Dicyclohexyl benzothiazole-2-sulfenamide.

Unfilled green compounds were mixed in an internal mixer in a two-step process. In the first stage, so-called non-productive step (NP1), polyisoprene, ZnO, stearic acid, and each benzoxazine were mixed. In the final step so-called productive step (PD) sulfur and the accelerator were incorporated to the mixture from the previous process. The temperature in this last process should remain below 110 °C to avoid early vulcanization of the unfilled compounds. Further details about the mixing procedure are described in Annex A (section A.2.2).

It should be noted that the benzoxazines mixed with the rubber are introduced as precursors. Their curing occurs simultaneously with the curing of the rubber. All the experiments described in the section above demonstrated that each benzoxazine precursor would be able to crosslink in the same time as the rubber during the curing step. Their ability to efficiently cure inside each unfilled compound will also be investigated.

The benzoxazine precursors were added to the polyisoprene formulations at different loading. For the sake of clarity, unfilled compounds containing a benzoxazine are annotated as PI(precursor)_{phr}. For instance, an unfilled compound containing 10 phr of 3DPDS-fa is called PI(3DPDS-fa)₁₀. Moreover, PI(precursor) refers to a compound containing a Bz in whatever quantity; for example, an unfilled compound with 4DPDS-fa is named PI(4DPDS-fa).

The following sections report the performance of benzoxazine precursors in unfilled compounds and is split in three main parts: (1) their impact on the curing of unfilled green compounds and (2) the morphological characterization by Atomic Force Microscopy (AFM) and (3) mechanical properties by tensile test of unfilled compounds.

3.1 Curing of unfilled green compounds containing benzoxazine precursors

The curing process of the materials containing the benzoxazine precursors was followed by using a moving die rheometer (MDR). In this method, the curing of the rubber is followed thanks to the evolution of the torque. The torque increases as the material is crosslinking, being more resistant to the torsional strength applied. A detailed description of this measurement can be found in Annex A (section A.2.3). The cure curves of the unfilled compounds were plotted separately depending on the amount of benzoxazine as shown in Figure III.4.

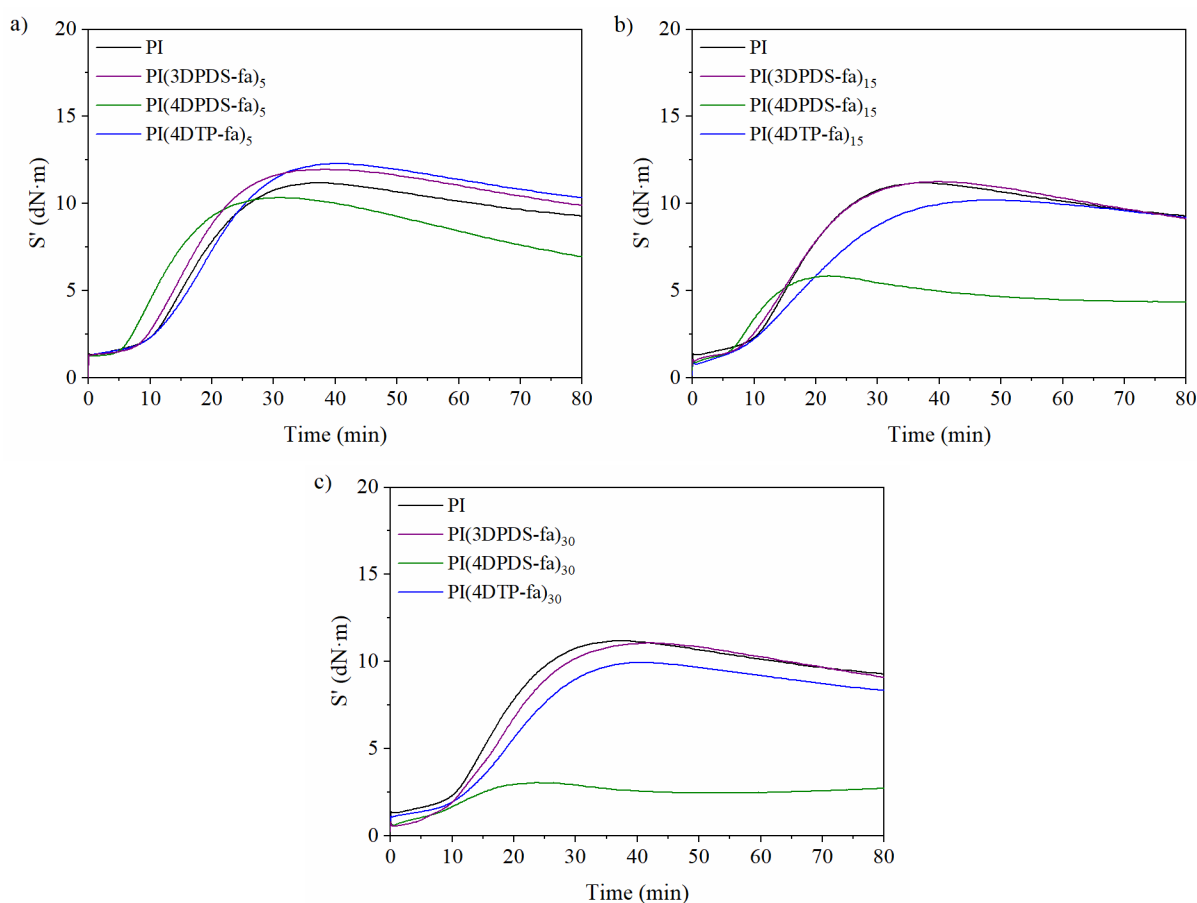


Figure III.4. MDR cure curves of unfilled compounds without diBz and with a) 5 phr of diBz, b) 15 phr of diBz, and c) 30 phr of diBz.

The impact of the benzoxazines precursors on the curing of the unfilled compounds depends on the chemical structure of the resin as well as the amount employed. Similar cure curves are observed when 3DPDS-fa and 4DTP-fa are used in comparison to the neat polyisoprene compound (PI), so-called reference. On the contrary, the incorporation of 4DPDS-fa leads to faster curing together with lower achieved torque.

To evaluate the impact of each benzoxazine on the curing profile, the optimum cure times (t_{90}) were determined as the time required to reach 90% of the change from minimum torque toward

maximum achieved torque. The t_{90} values and the maximum achieved torques (S'_{\max}) for each unfilled compound were plotted as a function of diBz content for each precursor (Figure III.5).

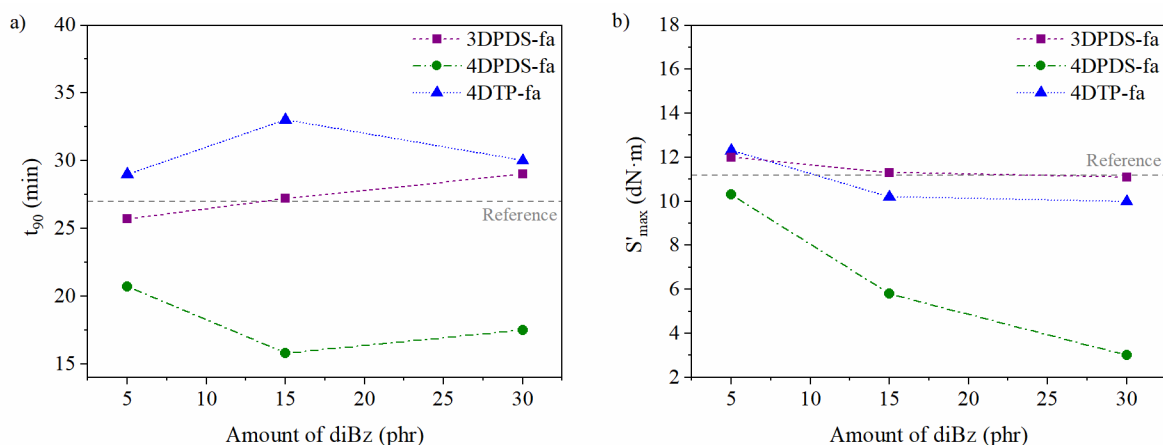


Figure III.5. a) Evolution of t_{90} and b) evolution of S'_{\max} as a function of the amount of the diBz for unfilled compounds.

In the case of the reference, t_{90} was reached after 27 min at 150 °C. PI(3DPDS-fa) cured in a similar duration than the reference ranging between 26 and 29 minutes, depending on the amount of benzoxazine. Additionally, PI(4DTP-fa) cured in a slightly longer period ranging from 29 to 33 min for different contents of diBz. This small increase of t_{90} could be explained by the lower reactivity of this precursor, as reported in Chapter II. The incorporation of 3DPDS-fa and 4DTP-fa led to comparable S'_{\max} than the reference. By contrast, the curing time of PI(4DPDS-fa) was strongly affected, t_{90} being reached after only 16 min with 15 phr of the resin. In this case, the t_{90} decrease was also accompanied by a significant drop of the maximum achievable torque, up to 73% (Figure III.5b). The lowering of the achieved torque could be explained by a decrease of the crosslinking density of the network.

For this reason, unfilled compounds with and without diBz were cured at 150 °C at the determined optimum curing times. After that, the crosslinking density (v_c) of the materials was determined by swelling tests and using the Flory Rehner equation (see in Annex A section A.2.5 for detail of the calculation). The results are plotted as a function of diBz content in Figure III.6.

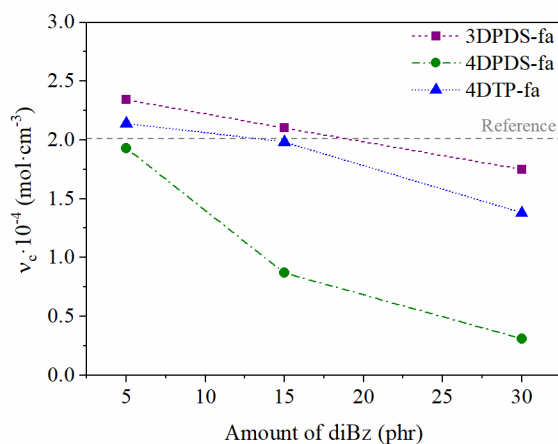


Figure III.6. Evolution of v_c as a function of the amount of the diBz for unfilled compounds.

The crosslinking densities follow a similar trend than the maximum achieved torques obtained by MDR (Figure III.5b). Unfilled compounds containing 5 and 15 phr of 3DPDS-fa and

4DTP-fa exhibit comparable crosslinking densities than the reference. Additionally, when the content of these benzoxazines is higher, i.e. 30 phr, the values of v_c are slightly lower ($\sim 1.4\text{--}1.8 \cdot 10^{-4} \text{ mol}\cdot\text{cm}^{-3}$) than for PI ($\sim 2.0 \cdot 10^{-4} \text{ mol}\cdot\text{cm}^{-3}$). This slight decrease of the crosslinking density for these samples could be explained by a dilution effect or a potential co-reaction occurring between sulfur and the oxazine rings leading to a possible consumption of sulfur (Scheme III.2a). Nevertheless, the values of v_c and S'_{\max} for samples with lower content of diBz, i.e. <30 phr, indicate that the curing of 3DPDS-fa and 4DTP-fa precursors, simultaneously to polyisoprene, does not consume sulfur and, if it happens, does not affect the curing of the rubber network.

On the contrary, the incorporation of 4DPDS-fa resulted in a drastic decrease of the v_c for these unfilled compounds in comparison to the reference. Indeed, the crosslinking density decreased to $0.3 \cdot 10^{-4} \text{ mol}\cdot\text{cm}^{-3}$ compared to $\sim 2.0 \cdot 10^{-4} \text{ mol}\cdot\text{cm}^{-3}$ for PI. The decrease of the maximum achievable torque together with the drop of the crosslinking density when 4DPDS-fa is used can be explained by the lower stability of the disulfide bond. The disulfide bond from 4DPDS seems to be easier to reduce than its counterpart 3DPDS. In the event of the reduction of the disulfide, thiols are formed, as observed by Raman (see Figure II.9 in Chapter II). Another option is that they could trap other sulfur radicals coming from the opening of the elemental sulfur ring (S_8). Therefore, polysulfide chains would be formed in between the phenolic moieties as previously reported (Scheme III.2b).^{32, 194-195} If such competitive reactions occur during the curing of PI(4DPDS-fa), less sulfur would be accessible for the curing of polyisoprene and thus, the properties of the unfilled compounds would be affected. This hypothesis is supported by the maximum torque reduction observed by MDR as well as the drop of the crosslinking density for materials containing 4DPDS-fa.

Additionally, the solubility test of poly(4DPDS-fa) with and without sulfur described above revealed that a fully soluble network was formed in the presence of sulfur. These results are a further proof that a reaction is occurring between 4DPDS-fa and sulfur. On the contrary, when 3DPDS-fa was employed, the values of maximum torque and crosslinking density remained similar to the reference and to PI(4DTP-fa), emphasizing the absence of such a reaction between 3DPDS-fa and S_8 . This provides additional evidence that the low stability of the S–S bond in 4DPDS-fa is the reason for the low curing extent of its materials with polyisoprene and the low crosslinking density.

Finally, a summary of the MDR parameters and crosslinking densities is gathered in Table III.4.

Table III.4. Summary of the curing properties and crosslinking densities of unfilled compounds with and without dibenzoxazines.

Abbr.	t_{90}^a (min)	S'_{\max}^b (dN·m)	$v_c \cdot 10^{-4}^c$ (mol·cm ⁻³)
PI	27	11	2.01
PI(3DPDS-fa) ₅	26	12	2.34
PI(3DPDS-fa) ₁₅	27	11	2.10
PI(3DPDS-fa) ₃₀	29	11	1.75
PI(4DPDS-fa) ₅	21	10	1.93
PI(4DPDS-fa) ₁₅	16	6	0.87

Abbr.	t_{90}^a (min)	S'_{max}^b (dN·m)	$v_c \cdot 10^{-4}^c$ (mol·cm ⁻³)
PI(4DPDS-fa) ₃₀	18	3	0.31
PI(4DTP-fa) ₅	29	12	2.14
PI(4DTP-fa) ₁₅	33	10	1.98
PI(4DTP-fa) ₃₀	30	10	1.38

^a Optimum cure time. ^b Maximum achieved torque. ^c Crosslinking density calculated from Flory-Rehner equation (see in Annex A section A.2.5 for additional information).

3.2 Morphological characterization and nanomechanical properties of unfilled compounds by AFM

The morphology of the unfilled compounds containing 15 phr of benzoxazine was explored by AFM. A detailed description of the sample preparation and the measurement conditions can be found in Annex A (section A.3.8). The mapping of the mechanical properties of the materials with and without benzoxazine precursors in areas of 20×20 μm² are depicted in Figure III.7a.

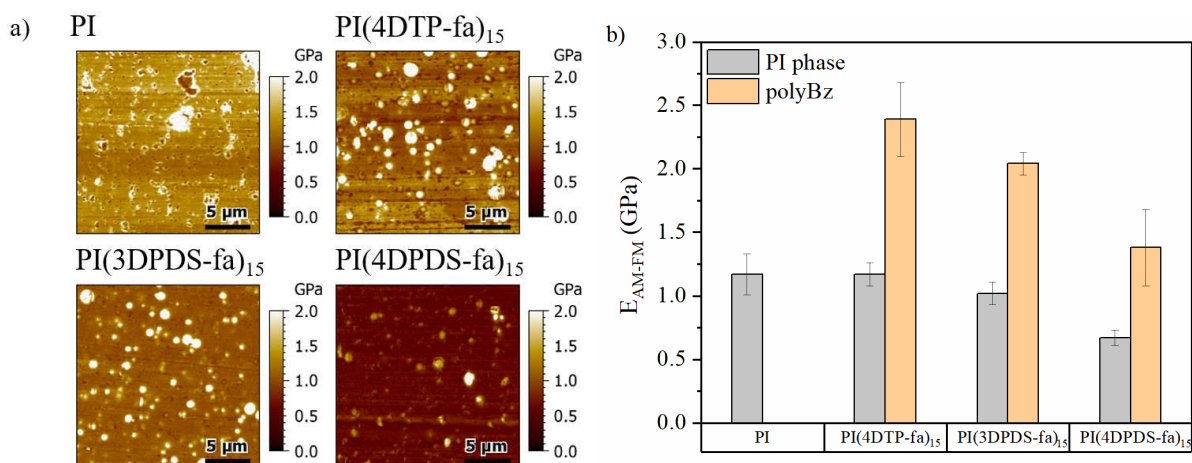


Figure III.7. a) AFM-AM-FM images of the modulus of unfilled compounds with and without 15 phr of polyBz, b) Measurements of the moduli in each of the phases in the materials.

The morphologies of the unfilled compounds are revealed by the contrast in nanomechanical properties. In the reference sample, small stiff irregular particles were observed (white contrast), probably related to zinc oxide particles present in the composition. In the unfilled compounds containing benzoxazine, round shape domains with high modulus can be seen well dispersed in the matrix. Despite a high dispersity of nodules sizes, there is a clear trend where 4DPDS-fa nodules are almost not detectable as shown in Figure III.7a. The presence of smaller benzoxazine nodules in the case 4DPDS-fa (~440 nm) compared to the nodules of 3DPDS-fa and 4DTP-fa (~550 nm) is aligned with the previous observations. Indeed, 4DPDS-fa is cleaving through the S–S bond, with a polysulfide chain growing between the phenolic moieties, as illustrated on Scheme III.2b. This cleavage leads to a dilution of the resin within the polyisoprene matrix. In these conditions, the scattered benzoxazine groups from 4DPDS-fa have a lower probability to meet with each other and thus, to form a network, in comparison to 3DPDS-fa and 4DTP-fa. This hypothesis is supported by the small size of polyBz domains found in PI(4DPDS-fa)₁₅.

The evaluation of the quantitative nanomechanical measurements acquired with the images follows the same conclusions. The average modulus for the rubber and polybenzoxazine phases in each sample are plotted in Figure III.7b. The modulus of the rubber matrix in the reference sample was measured as 1.17 ± 0.16 GPa. It is noteworthy that the apparent high modulus of the rubber matrix is related to the high frequency used in the analysis (~ 1.6 MHz), since the viscoelastic properties of the rubber are frequency dependent. Nevertheless, a clear trend can be observed when considering the materials containing benzoxazines as the modulus of the polyisoprene phase (E_{PI}) is decreasing as follows: $4DTP-fa > 3DPDS-fa > 4DPDS-fa$. In $PI(4DTP-fa)_{15}$ and $PI(3DPDS-fa)_{15}$, E_{PI} s are similar than the E_{PI} values for neat crosslinked polyisoprene, in agreement with the crosslinking density measurements reported in the section above. The quantitative nanomechanical measurements are also in line with the drastic reduction of the crosslinking density for $PI(4DPDS-fa)_{15}$, since E_{PI} significantly decreased by 43%. AM-FM also allows the simultaneous measurement of the loss tangent of each phase, complementarily to the modulus measurements. Results showed equivalent trends and are in accordance with the modulus measurements (see Figure E.1 in Annex E). These measurements, together with the lower crosslinking density, are well aligned with the hypothesis of a consumption of sulfur as stated previously due to a reaction with the disulfide bond from 4DPDS-fa.

Finally, the moduli of the polybenzoxazine nodules (E_{polyBz}^{PI}) within the unfilled compounds were measured and compared to the moduli of neat polyBz (E_{polyBz}) (Figure III.8). In $PI(3DPDS-fa)_{15}$ and $PI(4DTP-fa)_{15}$, E_{polyBz}^{PI} are slightly lower than E_{polyBz} , but they remain in the same range (around 2.1 GPa instead of 3 GPa). These values show the successful crosslinking of the benzoxazine precursors simultaneously with the rubber curing. On the contrary, for $PI(4DPDS-fa)_{15}$, moduli of both rubber and polybenzoxazine phases are lower than their corresponding references (0.67 and 1.4 GPa for E_{PI} and E_{polyBz}^{PI} respectively, compared to 1.17 and 3 GPa for neat rubber and polyBz references). This agrees also with the assumption that sulfur is consumed by this benzoxazine, this last one being diluted and unable to efficiently crosslink and preventing at the same time a proper curing of polyisoprene.

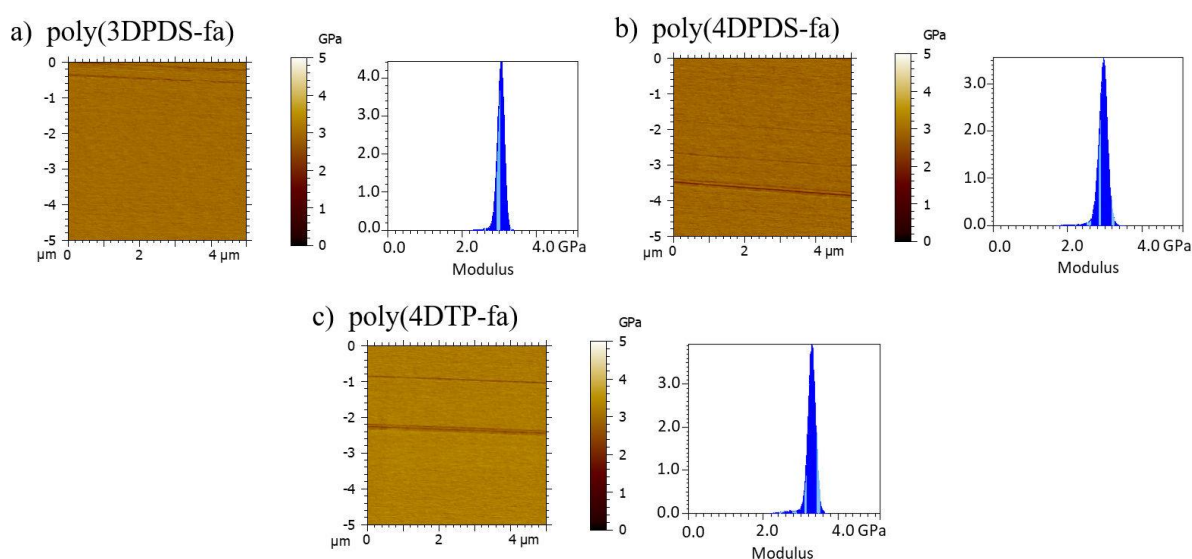


Figure III.8. AFM-AM-FM modulus images and respective histograms of a) poly(3DPDS-fa), b) poly(4DPDS-fa), and c) poly(4DTP-fa). Images depict an area of $5 \times 5 \mu m^2$.

3.3 Mechanical properties of unfilled compounds by tensile test

Tensile tests were performed to assess the mechanical properties of the unfilled compounds of polyisoprene and benzoxazine precursor. A detailed description about the testing conditions can be found in Annex A (section A.3.6) as well as the stress-strain curves are gathered in Annex E (Figure E.2). A summary of the mechanical properties by tensile test are gathered in Table III.5.

Table III.5. Summary of the mechanical properties of unfilled compounds with and without dibenzoxazines.

Abbr.	E ^a (MPa)	$\sigma_{200\%}$ ^b (MPa)	$\sigma_{600\%}$ ^c (MPa)	σ_{break} ^d (MPa)	ϵ_{break} ^e (%)
PI	2.6 ± 0.1	2.28 ± 0.02	10.9 ± 1.1	11.3 ± 1.4	551 ± 67
PI(3DPDS-fa) ₅	2.7 ± 0.7	2.86 ± 0.04	-	4.3 ± 0.8	284 ± 42
PI(3DPDS-fa) ₁₅	2.8 ± 0.2	2.57 ± 0.04	12.8 ± 0.3	18.3 ± 0.6	691 ± 3
PI(3DPDS-fa) ₃₀	3.1 ± 0.1	2.39 ± 0.04	9.84 ± 0.14	13.7 ± 3.3	710 ± 70
PI(4DPDS-fa) ₅	1.7 ± 0.3	2.22 ± 0.03	-	7.8 ± 1.4	499 ± 46
PI(4DPDS-fa) ₁₅	1.8 ± 0.1	1.12 ± 0.02	3.71 ± 0.04	19.0 ± 0.8	1032 ± 9
PI(4DPDS-fa) ₃₀	1.8 ± 0.1	0.87 ± 0.01	3.00 ± 0.06	13.9 ± 0.8	1060 ± 20
PI(4DTP-fa) ₅	2.7 ± 0.2	2.54 ± 0.01	-	5.8 ± 1.0	391 ± 42
PI(4DTP-fa) ₁₅	2.9 ± 0.1	2.50 ± 0.03	-	4.7 ± 0.6	346 ± 35
PI(4DTP-fa) ₃₀	2.8 ± 0.2	2.21 ± 0.09	9.3 ± 0.4	11.6 ± 3.2	650 ± 80

^a Young modulus. ^b Stress at 200% of strain. ^c Stress at 600% of strain. ^d Stress at break. ^e Elongation at break.

The cured material PI(4DPDS-fa) exhibits poor mechanical properties, below the reference for all the compositions tested (Figure III.9). These results were expected because of the low curing extent of this compound, shown by the low crosslinking density and low E_{PI} and E_{PI}^{polyBz} measured by AFM due to the sulfur consumption.

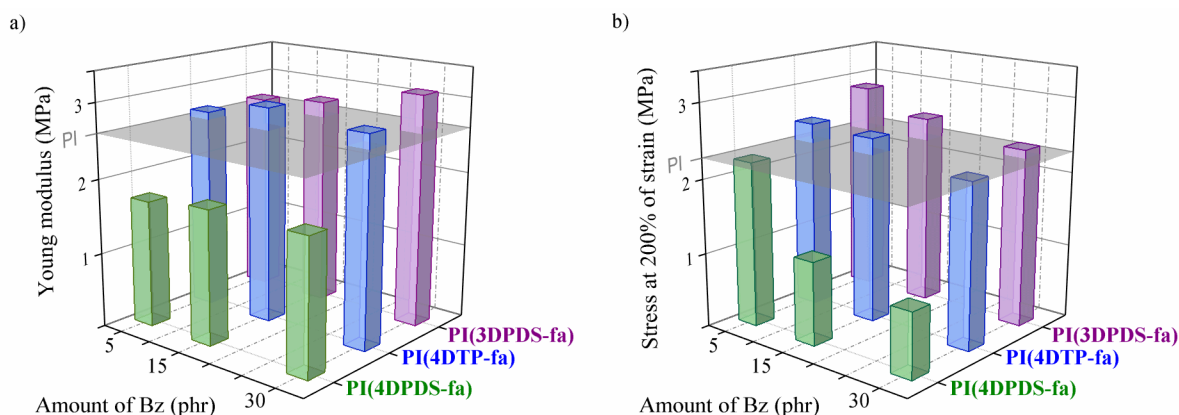


Figure III.9. a) Young modulus as a function of the amount of benzoxazine; b) Stress at 200% of strain as a function of the amount of benzoxazine.

On the contrary, for PI(3DPDS-fa) and PI(4DTP-fa), a reinforcement of the mechanical properties was observed as attested by the highest values of Young modulus (E), up to 3.1 and 2.9 MPa respectively compared to the reference (2.6 MPa) (Figure III.9a). Furthermore, the stresses measured at 200% of strain ($\sigma_{200\%}$) also increased for these unfilled compounds

(Figure III.9b). Nevertheless, when 30 phr of 3DPDS-fa or 4DTP-fa were incorporated in the polyisoprene materials the improvements at low strain were combined with a decrease of the tensile stress at high strain i.e. above 400% (Figure E.2 in Annex E). These unfilled compounds also showed slightly lower crosslinking density than the reference. The lower values of v_c together with the tensile results could be explained by a co-reaction occurring between sulfur and the benzoxazine resulting in a sulfur consumption. However, this behavior was only visible when high content of 3DPDS-fa and 4DTP-fa was employed. In case this reaction is also happening with lower content of diBz, it does not adversely affect the mechanical properties of the unfilled compounds.

From an overall perspective, PI(3DPDS-fa)₁₅ is the material with the most significant improvement of the stress at low elongation ($\sigma_{200\%}$) and high elongation ($\sigma_{600\%}$) as well as enhancing its tensile strength. The ultimate mechanical properties of PI(3DPDS-fa)₁₅ were improved compared to the reference, with a higher elongation and stress at break up to ~700% and 15.1 MPa respectively, compared to ~500% and 11.3 MPa for the reference.

3.4 Discussion

3DPDS-fa, 4DPDS-fa, and 4DTP-fa were incorporated in unfilled compounds and tested as reinforcing resins. The chemical structures of the monomers appeared to be a major parameter to consider in the elaboration of reinforced rubber compounds resulting in two distinctive behaviors.

4DPDS-fa did not show any reinforcement at any content. This precursor interfered with the curing of the unfilled compounds by reducing t_{90} and the maximum achieved torque. It leads to materials with lower crosslinking densities than the reference. It was assumed that the low stability of the disulfide bond in 4DPDS-fa yielded a side-reaction when heated in the presence of sulfur, driving the consumption of this essential element for the crosslinking of polyisoprene. Additionally, the decrease of the moduli of both rubber and polyBz network, determined by AFM, supported the assumption that sulfur is consumed by this diBz. This prevented an efficient curing of the polyisoprene network and resulted in a detrimental impact on the polybenzoxazine explaining the lack of reinforcement when 4DPDS-fa is employed.

On the contrary, 3DPDS-fa and 4DTP-fa reinforced unfilled compounds. The incorporation of 15 phr of these diBz did not interfere with the curing of polyisoprene showing similar t_{90} and crosslinking densities than the reference. Moreover, the moduli of the rubber and polyBz phases determined by AFM were similar than their respective references. These results confirmed the feasibility to employ benzoxazines precursors to reinforce rubber compounds.

Finally, PI(3DPDS-fa)₁₅ was the material where the most significant improvement of the mechanical properties was observed. For this reason, the reinforcement effect of 3DPDS-fa will be compared with the effect of traditional resins.

4 Comparison of 3DPDS-fa to other resin-reinforced unfilled compounds

The aim of this work is to develop a new reinforcing system based on polybenzoxazines. This topic has been investigated using model benzoxazines from bisphenol A (BA) as previously reported in Chapter I, section 7.²⁴⁻²⁵ For this reason, the performance of the newly synthesized

sulfur-containing benzoxazine proposed in this work is compared to a model benzoxazine from BA. Additionally, the feasibility to replace traditional phenolic resin is studied.

4.1 Comparison to model dibenzoxazine monomers

The model benzoxazine from bisphenol A and furfurylamine (BA-fa) was tested in the rubber formulation. The curing of the unfilled green compounds was followed by MDR and their t_{90} determined (see Figure E.3 in Annex E). The stress-strain curves are displayed in Figure E.4 in Annex E and the mechanical properties are gathered in Table III.6. This compound exhibits higher values of Young modulus than the reference demonstrating a reinforcement with this molecule is also feasible. However, at higher strain, the reinforcement observed in PI(BA-fa) is lower than for PI(3DPDS-fa) and PI(4DTP-fa), whatever the content of benzoxazine precursor.

Table III.6. Summary of the mechanical properties of unfilled compounds with BA-fa.

Abbr.	E ^a (MPa)	$\sigma_{200\%}$ ^b (MPa)	$\sigma_{600\%}$ ^c (MPa)	σ_{break} ^d (MPa)	ϵ_{break} ^e (%)
PI(BA-fa) ₅	2.8 ± 0.1	2.49 ± 0.04	-	7.7 ± 2.5	450 ± 90
PI(BA-fa) ₁₅	2.6 ± 0.1	2.1 ± 0.1	-	7.1 ± 4.2	568 ± 135
PI(BA-fa) ₃₀	2.8 ± 0.2	1.13 ± 0.09	3.4 ± 0.2	13.9 ± 1.1	1058 ± 24

^a Young modulus. ^b Stress at 200% of strain. ^c Stress at 600% of strain. ^d Stress at break. ^e Elongation at break.

4.2 Comparison to traditional phenolic compounds

In order to evaluate the reinforcement effect of polybenzoxazine in comparison to traditional phenolic resins, the mechanical properties of a compound containing phenolic resin (PR) were assessed. For that purpose, a phenolic system composed of a precondensed novolac resin and hexamethylenetetramine, as *in-situ* crosslinker, was mixed with the polyisoprene formulation (see more details about the formulation in Annex E, Table E.1).

Mechanical properties of phenolic resin compounds (PI(PR)₁₅) were compared to the compound containing 3DPDS-fa (PI(3DPDS-fa)₁₅) and the results are summarized in Table III.7 and displayed in Figure III.10. Comparable results were obtained regarding Young modulus and stress at low strain i.e. $\sigma_{200\%}$. Nevertheless, PI(3DPDS-fa)₁₅ exhibited higher stress at high strain ($\sigma_{600\%}$) with an additional improvement of the ultimate tensile properties showing higher elongation and stress at break than PI(PR)₁₅ and the reference PI and therefore, combining high stiffness with high elasticity. In conclusion, these results support the suitability to employ benzoxazines precursors to replace phenolic resins as reinforcing agents for rubber applications.

Table III.7. Summary of the mechanical properties of unfilled compounds with PR.

Abbr.	E ^a (MPa)	$\sigma_{200\%}$ ^b (MPa)	$\sigma_{600\%}$ ^c (MPa)	σ_{break} ^d (MPa)	ϵ_{break} ^e (%)
PI(PR) ₁₅	2.8 ± 0.1	2.7 ± 0.1	10.7 ± 0.2	12.7 ± 1.9	630 ± 40

^a Young modulus. ^b Stress at 200% of strain. ^c Stress at 600% of strain. ^d Stress at break. ^e Elongation at break.

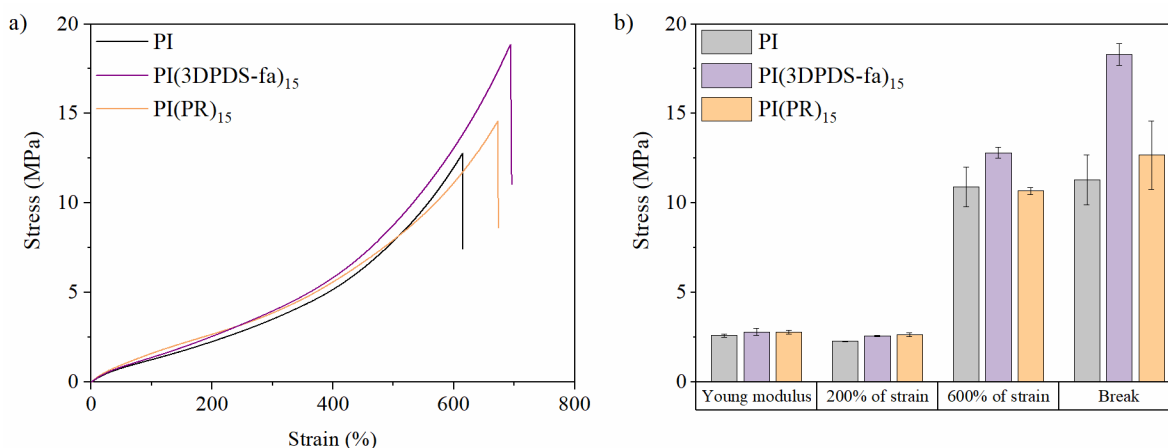


Figure III.10. a) Stress-strain curves and b) Stress (MPa) (\pm SD): Young modulus, $\sigma_{200\%}$ of strain, $\sigma_{600\%}$ of strain, and σ_{break} (from left to right), of reference compound (PI) and compounds containing 3DPDS-fa, and phenolic resin.

4.3 Discussion

In conclusion, the reinforcement of the mechanical properties of the compounds containing 3DPDS-fa was shown to be more significant than the reinforcing of mechanical properties of the compounds prepared with a model benzoxazine or a commonly employed phenolic resin. These results confirmed the feasibility to employ benzoxazines precursors to reinforce rubber compounds and likewise replace phenolic resins for rubber applications.

5 Conclusion

This chapter described the application of the newly designed benzoxazines 4DPDS-fa, 3DPDS-fa, and 4DTP-fa in unfilled compounds.

In the first part, the investigation of the polymerization behavior of the monomers in the presence of the curing package was carried out. The curing of the dibenzoxazines was shown to occur between 9 and 16 min thanks to the efficient catalytic effect of sulfur, overcoming the long curing times commonly required. Even though it could also lead to a side-reactions with the benzoxazines, the presence of an inherent catalyst in rubber compounds is a clear asset for the use of reinforcing systems based on polybenzoxazines. Due to their cure kinetics, 4DPDS-fa, 3DPDS-fa, and 4DTP-fa are three suitable candidates to be used for the reinforcement of rubber compounds. For this reason, each benzoxazine precursor was subsequently compounded with polyisoprene and a curing system, so-called PI(precursor), and their performance was investigated.

The incorporation of 15 phr of 3DPDS-fa and 4DTP-fa did not interfere with the curing of polyisoprene. Indeed, similar t_{90} and crosslinking densities were measured for the compounds cured in the presence or absence of these benzoxazines. On the contrary, the compounds prepared with 4DPDS-fa exhibited lower values of t_{90} and crosslinking densities together with the decrease of the maximum achieved torque. These results showed the samples with 4DPDS-fa did not reach the same extent of curing compared to the PI reference. It was assumed that the low stability of the disulfide bond in 4DPDS-fa yielded a side-reaction when heated in the presence of sulfur, driving the consumption of this essential element to the crosslinking of polyisoprene.

The morphology and nanomechanical properties of the compounds were explored by AFM. The formation of stiffer nodules dispersed in the rubber matrix demonstrated the crosslinking of the benzoxazine precursors simultaneously with the rubber curing. In PI(3DPDS-fa)₁₅ and PI(4DTP-fa)₁₅ benzoxazine nodules of about 550 nm were observed and the moduli of each phase was similar to their respective reference. By contrast, AFM images of PI(4DPDS-fa)₁₅ exhibited nodules of smaller sizes (around 440 nm) and lower moduli of both benzoxazine and rubber phases in comparison to their corresponding references. This supports the assumption that sulfur is consumed by 4DPDS-fa, preventing an efficient curing of polyisoprene and leading to a detrimental impact on the polybenzoxazine network.

Finally, the performance of the cured compounds was assessed by tensile test. These results were aligned to the previous observations showing a lack of reinforcement for 4DPDS-fa while 3DPDS-fa and 4DTP-fa reinforced rubber compounds. PI(3DPDS-fa)₁₅ exhibited the most significant improvement of the mechanical properties combining high stiffness with high elasticity. Furthermore, the reinforcement of the mechanical properties of the compound when using 3DPDS-fa was shown to be more significant than compounds prepared with a model benzoxazine or a commonly employed phenolic resin. These results confirmed the feasibility to employ benzoxazine precursors to reinforce rubber compounds and likewise replace phenolic resins for rubber applications. Additionally, this study spotlights the possibility to use partially bio-based precursors leading to a more sustainable alternative than traditional resins.

Finally, by this approach, the development of a proof of concept was performed by understanding the effect of each benzoxazine in a simplified rubber system. These investigations highlight the importance of considering the chemical structure and the curing kinetics of the precursors in the presence of the sulfur as major factors for the reinforcement of rubber compounds with benzoxazines. The work presented in this chapter was published in a peer-reviewed journal.¹⁹⁶

**Chapter IV:
Application of
benzoxazine resins in
filled compounds**

IV Application of benzoxazine resins in filled compounds

1 Introduction

The apex is a triangular extruded profile, also known as bead filler, that provides a cushion between the rigid bead and the flexible inner liner and body ply assembly (see Chapter I for more details). The rubber compound is formulated to have good dynamic stiffness, hardness and durability thanks to the combination of a high loading of carbon black together with a high content of sulfur. To reach the demanding high levels of stiffness and hardness, conventional reinforcing polymeric resins are also employed, generally resorcinol-methylene donor systems.⁶

The feasibility to reinforce rubber compounds with dibenzoxazines was demonstrated on unfilled polyisoprene formulations in Chapter III. The level of reinforcement was linked to the structural features of the benzoxazine precursor, which were driving their curing properties. The results highlighted that polybenzoxazines are a possible alternative to traditional phenolic resins in rubber industry. Among them, 3DPDS-fa is the precursor which leads to the most significant reinforcement of the mechanical properties of unfilled compounds. The next step is to investigate the effect of this benzoxazine in tire compounds i.e. rubber compounds filled with carbon black. For this reason, filled rubber materials were prepared with different amounts of 3DPDS-fa and with different loadings of carbon black to map the formulation-to-properties relationship. Therefore, the feasibility of this benzoxazine to act as reinforcing resin can be checked by testing the mechanical properties of the resulting compounds.

This chapter is divided in two parts: (1) the investigation of the effect of 3DPDS-fa on the properties of rubber compounds by its incorporation in carbon black containing formulations and (2) the comparison of the reinforcing effect of 3DPDS-fa with other dibenzoxazines and conventional phenolic resins are reported.

2 Application of 3DPDS-fa in filled compounds

Compounds containing 3DPDS-fa were prepared by using a recipe composed of polyisoprene (PI), carbon black (CB) and the same curing package employed for the curing of the unfilled materials described in the previous chapter. It is constituted of sulfur (S₈), N,N'-dicyclohexyl benzothiazole-2-sulfenamide (DCBS) as accelerator, and zinc oxide (ZnO) and stearic acid as activators. The formulation commonly employed in apex compounds is shown in Table IV.1. All the values are indicated both in phr and weight percentage. For the sake of clarity, the term "compound" will be employed in the rest of the chapter to designate a cured mixture of polyisoprene, carbon black and the curing system, independently of the introduction of the benzoxazine precursors while "green compound" will refer to the uncured materials.

Green compounds were prepared in an internal mixer in a three-step process. In the first process, so-called non-productive step (NP1), polyisoprene, ZnO, stearic acid, half of the carbon black, and two thirds of the oil were mixed. The first step was common for all the compounds. The second step (NP2), for which the initial temperature set at 110 °C to allow the melting of the

resin, was different for the compounds with and without 3DPDS-fa. In both cases, this step was subdivided in three parts:

- For the reference compound, 1/6 of the CB and 1/3 of the remaining oil were progressively added in each substep.
- For the compounds with 3DPDS-fa, in the first two substeps, 1/6 of the CB and 1/2 of remaining the oil were mixed. In the last substep, the precursor was added with the remaining 1/6 of CB.

Finally, in the final step so-called productive step (PD) sulfur and the accelerator were mixed with the compound from the NP2. The temperature in this last process should remain below 110 °C to avoid early vulcanization of the compounds. Further details about the mixing procedure are described in Annex A (section A.3.2).

Table IV.1. Recipe of a model formulation for apex compounds.

Ingredients	Amount (phr)	Amount (%wt)
Polyisoprene	100	46.4
Carbon black (CB)	80	37.1
TDAE oil ^a	5	2.3
Reinforcing resin	15	7.0
Sulfur (S ₈)	5.5	2.6
Zinc oxide (ZnO)	5	2.3
Stearic acid	2	0.9
DCBS ^b	3	1.4

^a Treated distillate aromatic extracted, commonly used processing rubber oil. ^b N,N'-Dicyclohexyl benzothiazole-2-sulfenamide.

The first part of this section relates a comprehensive investigation of the potential of 3DPDS-fa to reinforce filled compounds. This section is followed by the study of their dynamic mechanical properties and, finally, the morphology and nanomechanical properties are reported.

2.1 Understanding the reinforcing mechanism of 3DPDS-fa in filled compounds

2.1.1 Preparation of green compounds with 3DPDS-fa

Different amounts of 3DPDS-fa were incorporated into the carbon black polyisoprene formulations as shown in Table IV.2. Several loadings of CB (20, 50 and 80 phr) were employed keeping constant the ratio between carbon black and the processing oil (equal to 16). The main recipe includes 5.5 phr of sulfur, however, for the sake of comparison the content of this ingredient was also varied in the formulation (2.8 and 6.9 phr).

The following nomenclature has been employed to avoid any confusion between the different materials. Polyisoprene compounds mixed with carbon black and the curing package are annotated as PI(CB)_{phr}, phr corresponding to the amount of CB. When a reinforcing resin is used, whatever it is, the formulations is noted PI(CB)_{phr}(precursor)_{phr1}, where phr1 corresponds

to the amount of reinforcing resin (i.e. Bz or PR). For instance, a polyisoprene compound containing 50 phr of carbon black and 15 phr of 3DPDS-fa is called PI(CB)₅₀(3DPDS-fa)₁₅. For the compounds constituted of an amount of sulfur other than 5.5 phr, the exact phr of this ingredient is indicated after the PI as: PI_{2.8}(CB)₅₀(3DPDS-fa)₁₅ when 2.8 phr of sulfur is used, for example.

Table IV.2. Summary of the formulations of compounds with 3DPDS-fa and carbon black.

Ingredients	Amount (phr)		
Polyisoprene	100	100	100
Carbon black (CB)	20	50	80
TDAE oil ^a	1.25	3.12	5
3DPDS-fa	0 / 15 / 30	0 / 5 / 10 / 15 / 20 / 30	0 / 10 / 15 / 30
Sulfur	5.5	5.5	2.8* / 5.5 / 6.9*
Zinc oxide (ZnO)	5	5	5
Stearic acid	2	2	2
DCBS ^b	3	3	3

^a Treated distillate aromatic extracted, commonly used processing rubber oil. ^b N,N'-Dicyclohexyl benzothiazole-2-sulfenamide. *Just mixed with 15 phr of 3DPDS-fa.

2.1.2 Effect of 3DPDS-fa on the curing of the green compounds

The curing of the green compounds was studied under isothermal conditions at 150 °C by using a moving die rheometer (MDR). A detailed description of the measurement can be found in Annex A (section A.3.3). It should be noted that the benzoxazines mixed with the rubber were introduced as precursors, i.e. as monomers and their curing will occur simultaneously with the curing of the rubber.

The curing profiles of the compounds prepared with 20, 50 or 80 phr of CB are displayed in Figure IV.1. A pronounced increase of the maximum torque (S'_{\max}) is observed with increasing the amount of carbon black, as expected (Figure IV.1d). The incorporation of 3DPDS-fa to the compounds leads to an additional increase of S'_{\max} for almost all the samples. This increment was more pronounced when the benzoxazine was used in combination with 50 and 80 phr of CB indicating the reinforcing mechanism of 3DPDS-fa might be affected by the filler content. Furthermore, the increase of S'_{\max} with 3DPDS-fa confirms that the precursor cured simultaneously to the vulcanization of the rubber, leading to the formation of polyBz as reported in Chapter III.

The presence of 3DPDS-fa affects not only S'_{\max} but the overall curing profile of filled rubber compounds as shown in Figure IV.1. 3DPDS-fa has an impact on the minimum torque achieved (S'_{\min}), on the scorch time (t_{s1}), and on the optimum cure time (t_{90}). The evolution of these characteristic curing parameters as a function of the benzoxazine content for compounds with 50 phr of CB is displayed in Figure IV.2.

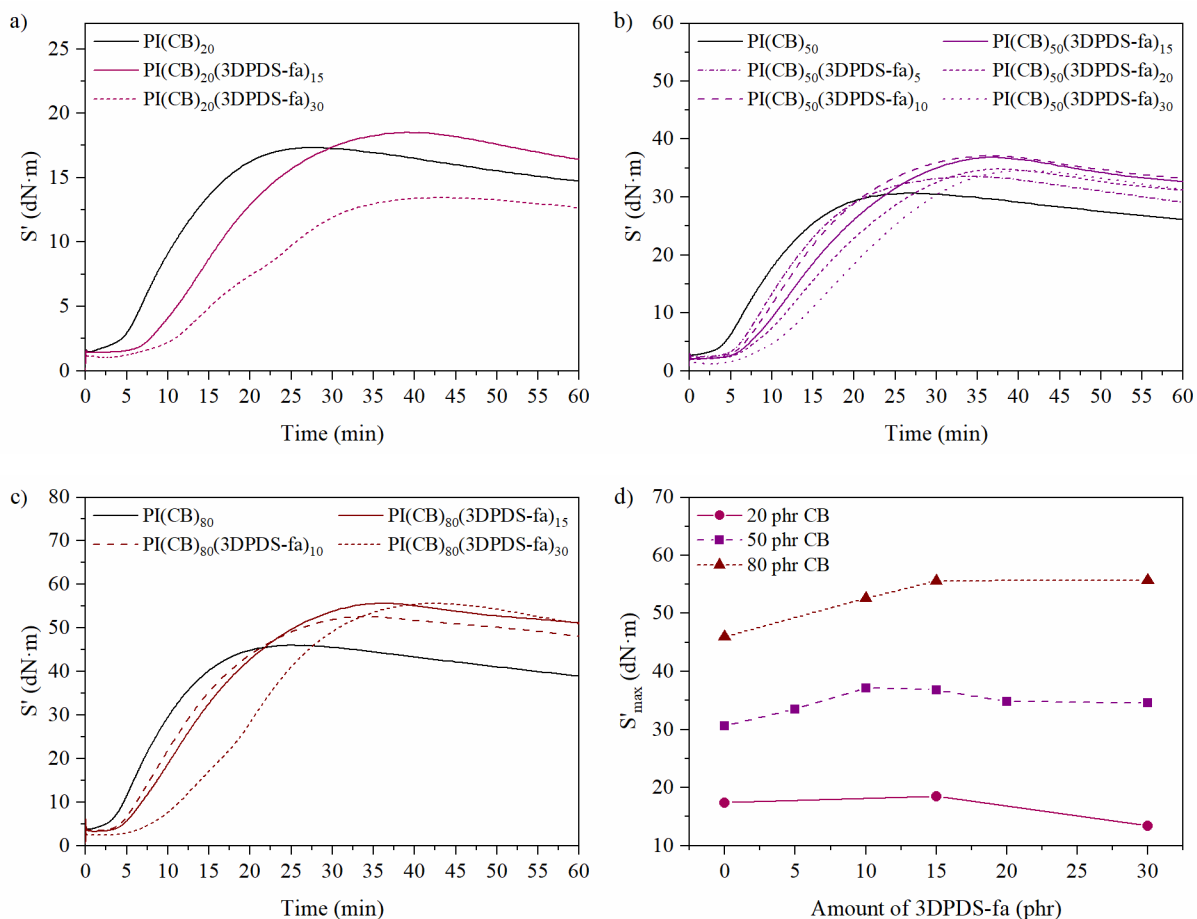


Figure IV.1. MDR cure curves of compounds with a) 20 phr of CB, b) 50 phr of CB, and c) 80 phr of CB; d) evolution of S'_{max} as the function of 3DPDS-fa.

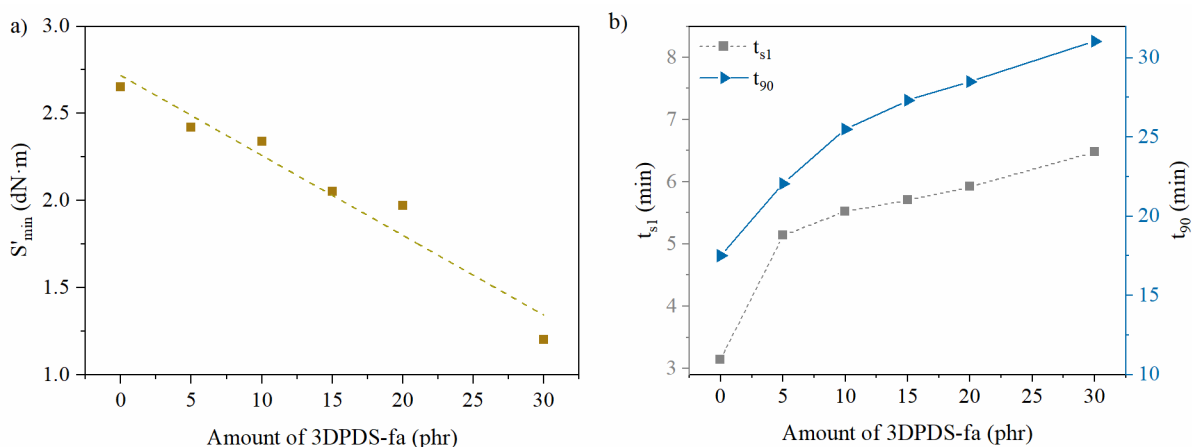


Figure IV.2. a) Evolution of S'_{min} and b) evolution of t_{s1} and t_{90} as a function of the amount of 3DPDS-fa for compounds with 50 phr CB.

The minimum torque decreases linearly with the incorporation of 3DPDS-fa (Figure IV.2a) and thus, to the decrease of the viscosity of the green compounds. At 150 °C, 3DPDS-fa is molten and might act as a processing aid before crosslinking resulting in a decrease of the torque and therefore, may improve the processability of the tire parts before the curing step. Once the benzoxazine starts to crosslink, the effect is annihilated due to the formation of a polyBz.

Additionally, the scorch time of the compounds increases with the amount of 3DPDS-fa as depicted in Figure IV.2b. Indeed, t_{s1} increased from 3 minutes to 6.5 minutes for the reference

(PI(CB)₅₀) and the compound with 30 phr of 3DPDS-fa (PI(CB)₅₀(3DPDS-fa)₃₀) resulting in an increase by around 100%. Similarly, t_{90} increases with the amount of 3DPDS-fa. PI(CB)₅₀ cures in 17.5 min while the optimum curing of PI(CB)₅₀(3DPDS-fa)₁₅ and PI(CB)₅₀(3DPDS-fa)₃₀ is reached after 27 and 31 min, respectively.

In conclusion, 3DPDS-fa influences the curing profile of the green compounds as attested by the increase of t_{s1} and t_{90} . The maximum torque is also enhanced by the addition of 3DPDS-fa, confirming the simultaneous curing of the Bz precursors with the rubber. Moreover, the addition of 3DPDS-fa leads to a decrease of the viscosity of the green compounds potentially improving the processability of the tire parts before the vulcanization. A summary of the MDR data is gathered in Table IV.3.

Table IV.3. MDR data for compounds with carbon black and 3DPDS-fa.

Abbr.	S'_{\min} (dN·m)	S'_{\max} (dN·m)	t_{s1} (min)	t_{90} (min)
PI(CB) ₂₀	1.5	17.4	4.3	18.7
PI(CB) ₂₀ (3DPDS-fa) ₁₅	1.4	18.5	7.7	28.0
PI(CB) ₂₀ (3DPDS-fa) ₃₀	1.0	13.4	9.4	30.9
PI(CB) ₅₀	2.7	30.7	3.1	17.5
PI(CB) ₅₀ (3DPDS-fa) ₅	2.4	33.5	5.1	22.1
PI(CB) ₅₀ (3DPDS-fa) ₁₀	2.3	37.2	5.5	25.5
PI(CB) ₅₀ (3DPDS-fa) ₁₅	2.1	36.8	5.7	27.3
PI(CB) ₅₀ (3DPDS-fa) ₂₀	2.0	34.8	5.9	28.5
PI(CB) ₅₀ (3DPDS-fa) ₃₀	1.2	34.6	6.5	31.0
PI(CB) ₈₀	3.7	46.0	2.2	16.2
PI(CB) ₈₀ (3DPDS-fa) ₁₀	3.4	52.6	3.8	23.4
PI(CB) ₈₀ (3DPDS-fa) ₁₅	3.3	55.6	4.1	25.7
PI(CB) ₈₀ (3DPDS-fa) ₃₀	2.4	55.7	5.9	31.0

2.1.3 Reinforcing effect of 3DPDS-fa in filled compounds

In this section, the study of the quasi-static mechanical properties of cured compounds is reported. A detailed description about the testing conditions can be found in Annex A (section A.3.6). Compounds with and without 3DPDS-fa were cured at 150 °C at the determined optimum curing times (see section 2.1.2). The impact of the loading of carbon black, the content of 3DPDS-fa and the amount of sulfur on the mechanical properties of the samples is reported in the following paragraphs.

Determination of the relationship between CB and 3DPDS-fa in filled compounds

The stress-strain curves of compounds with 15 phr of 3DPDS-fa and either 20, 50 and 80 phr of CB are displayed in Figure IV.3.

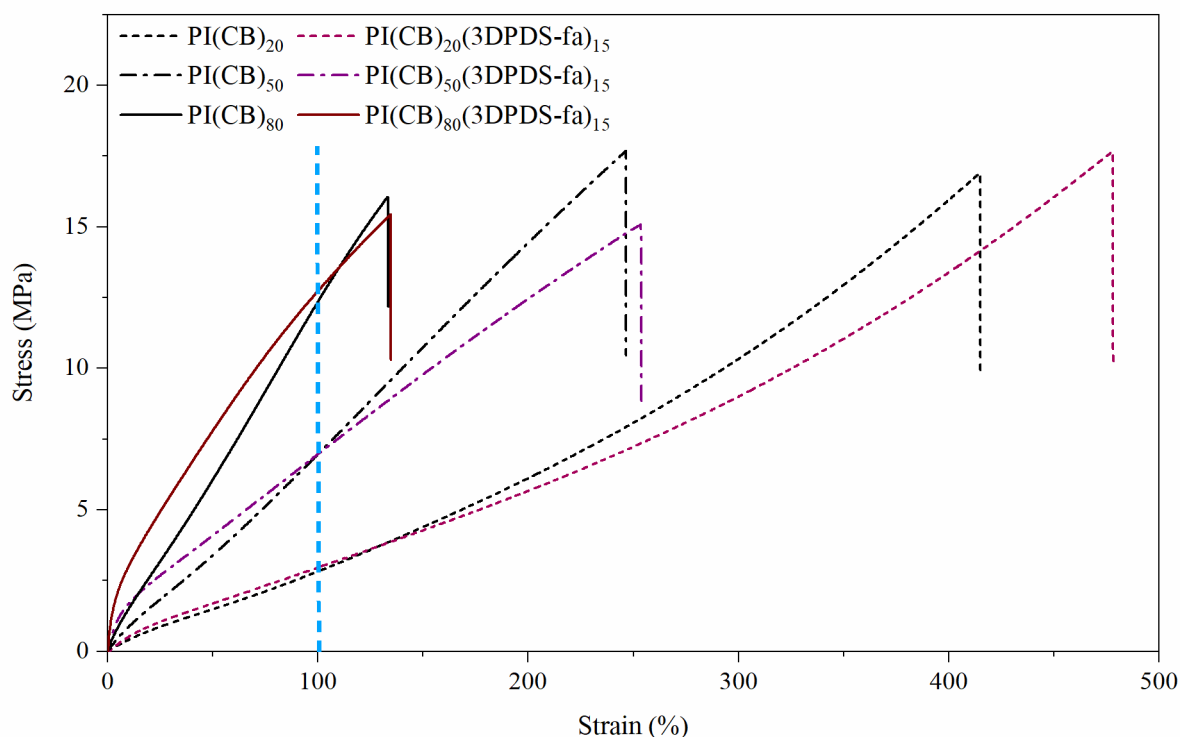


Figure IV.3. Stress-strain curve of filled compounds with and without 15 phr of 3DPDS-fa.

The strain at break is substantially reduced with increasing the amount of CB, as expected. Additionally, the effect of 3DPDS-fa on the stress-strain curves of the compounds can be described in two different ranges, i.e. below and above 100% of strain (Figure IV.3). Below 100%, all the compounds with 3DPDS-fa exhibit higher tensile modulus and stresses than the reference. Above 100%, the stress of the reference is above the materials with 3DPDS-fa.

The increase of stress reflects the enhancement of the stiffness of the materials with the incorporation of 3DPDS-fa and therefore, confirms the ability of this benzoxazine to reinforce tire compounds. These improvements can be explained by the formation of a polyBz i.e. poly(3DPDS-fa) simultaneously with the curing of the rubber also confirmed by the increase of S'_{max} by MDR tests.

Furthermore, it can be observed that the impact of 3DPDS-fa on the reinforcement depends on the amount of carbon black resulting in a higher percentage of improvement for highly filled systems. To visualize these differences, Young moduli (E) and stresses at 50 % of strain ($\sigma_{50\%}$) are plotted as a function of the content of CB in Figure IV.4a and b, respectively. In highly filled CB systems (i.e. ≥ 50 phr) the impact of 3DPDS-fa is more pronounced than for lowly filled CB materials (i.e. 20 phr).

In summary, the incorporation of 3DPDS-fa in filled materials results in an improvement of their mechanical properties. These results show 3DPDS-fa is acting as a reinforcing resin thanks to the formation of poly(3DPDS-fa) together with the rubber curing. Additionally, the reinforcement of 3DPDS-fa is affected by the amount of carbon black being more pronounced in highly filled systems while for low filler loadings it is almost negligible. These differences could be explained by the influence of the benzoxazine in the formation of the filler network, and therefore, leading to a synergistic mechanism between CB and 3DPDS-fa. This indicates

the formation of a polybenzoxazine could be only one part of the reinforcing mechanism of 3DPDS-fa in the system.

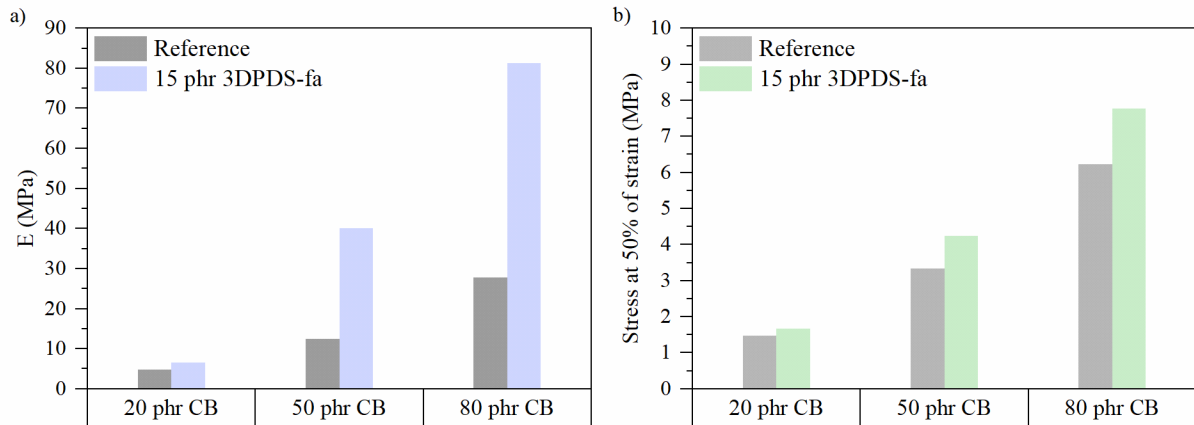


Figure IV.4. a) E and b) $\sigma_{50\%}$ as a function of CB loading for the compounds with and without 15 phr of 3DPDS-fa.

To further understand the impact of 3DPDS-fa on the materials, the mechanical properties of lowly and highly filled compounds with different content of 3DPDS-fa were analyzed.

The addition of 3DPDS-fa to compounds with 20 phr of CB leads to a weak improvement of the mechanical properties as shown in Figure IV.5. Indeed, even when doubling the amount of the benzoxazine (from 15 to 30 phr), the reinforcement at low strain is not improved and even reduced the stress at high strain ($>75\%$). These results showed that the effect of 3DPDS-fa is almost negligible in lowly filled compounds.

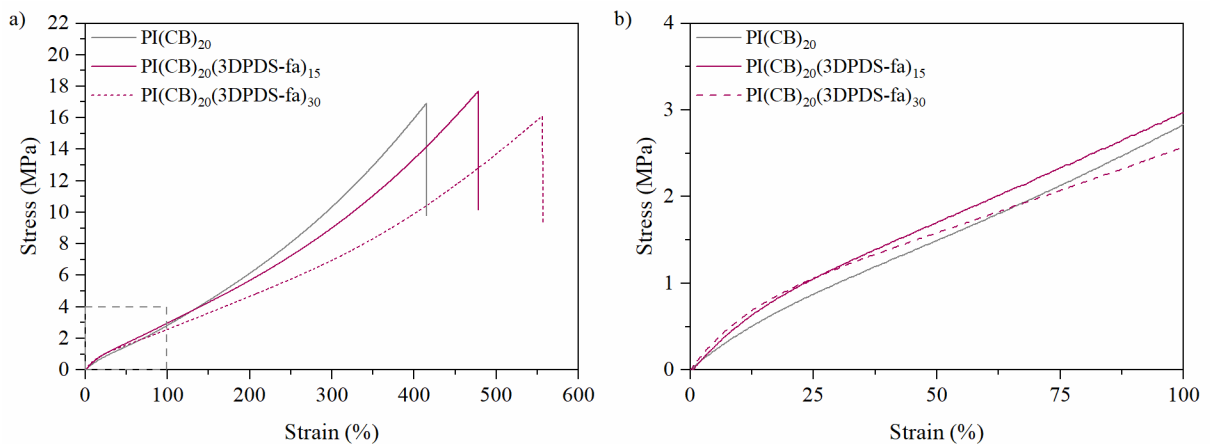


Figure IV.5. a) Full stress-strain curve and b) stress-strain curve up to 100% of strain of rubber compound with 20 phr of CB and with 0, 15, and 30 phr of 3DPDS-fa.

On the contrary, the impact of the content of 3DPDS-fa in highly filled systems (i.e. ≥ 50 phr of CB) is more pronounced as shown Figure IV.6. The effect is observed with a significant enhancement of the Young modulus and stress at low strain revealing higher stiffness with increasing the amount of 3DPDS-fa. Meanwhile, the evolution of the stresses at high strain and at break follows an opposite behavior due to an inversion of the stress-strain curves with the content of this Bz. To visualize these differences, the evolution of the stress at low ($\leq 25\%$) and high ($\geq 75\%$) strain are displayed as a function of the amount of 3DPDS-fa in Figure IV.6b and d, for compounds with 50 and 80 phr of CB respectively.

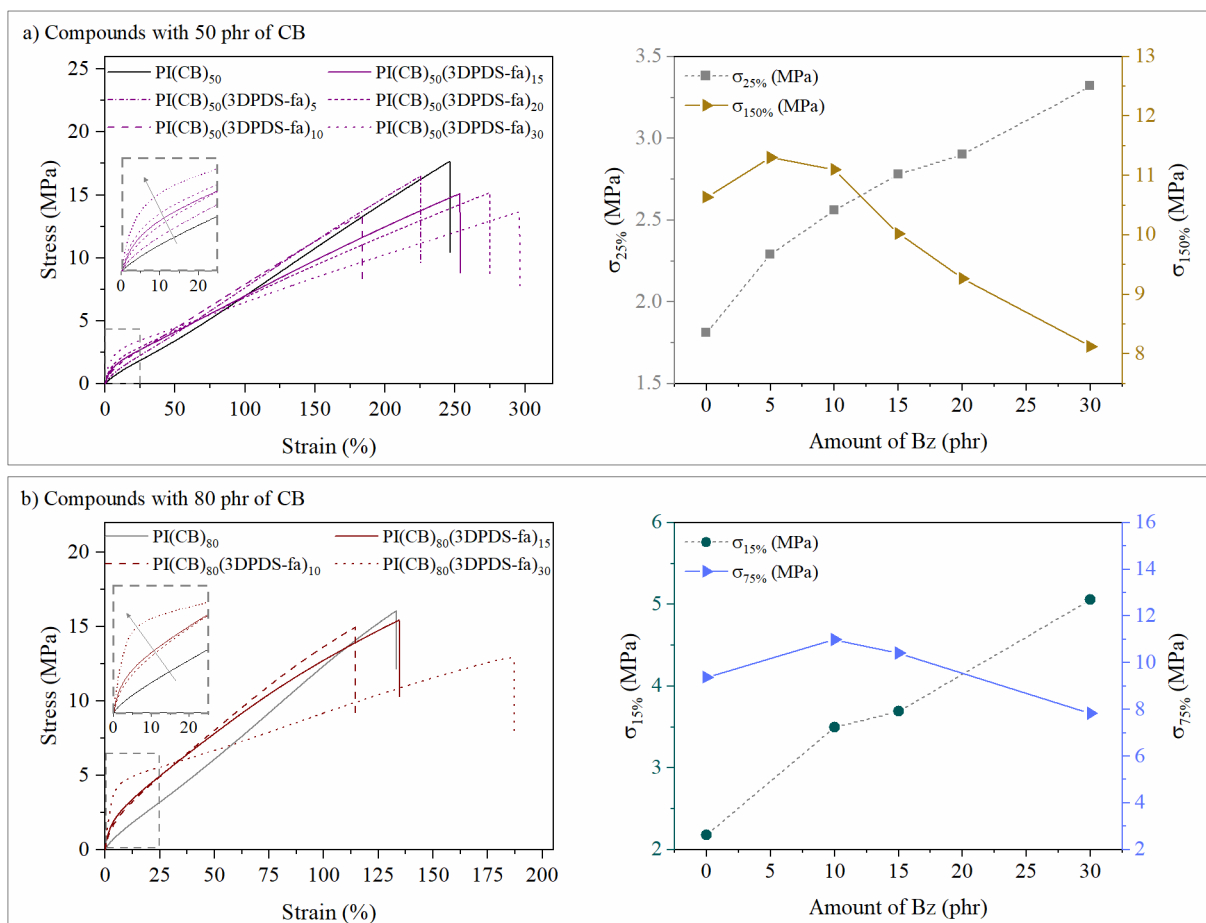


Figure IV.6. a) Stress-strain curve of rubber compound with 50 phr of CB and with 0, 5, 10, 15, 20, and 30 phr of 3DPDS-fa (on the left); Evolution of $\sigma_{25\%}$ and $\sigma_{150\%}$ as a function of the amount of 3DPDS-fa (on the right); b) Stress-strain curve of rubber compound with 80 phr of CB and with 0, 10, 15, and 30 phr of 3DPDS-fa (on the left); Evolution of E , $\sigma_{15\%}$ and $\sigma_{75\%}$ as a function of the amount of 3DPDS-fa (on the right).

Interestingly, for samples with 50 phr of CB, $\sigma_{150\%}$ reaches its maximum with 10 phr of 3DPDS-fa and decreases above this amount, even to values lower than the reference (PI(CB)₅₀) (Figure IV.6b). For the compound with 80 phr of CB and 15 phr of 3DPDS-fa, this inversion takes place just before the breaking ($\epsilon_{\text{break}} \sim 133\%$) avoiding a detrimental impact on the properties at high strain. Indeed, this compound exhibits improved stress at low strain combined with similar stress and elongation at break than the reference (PI(CB)₈₀). Therefore, PI(CB)₈₀(3DPDS-fa)₁₅ shows the best overall performance among the tested compounds.

In conclusion, the stiffness of highly filled compounds is enhanced by increasing the amount of 3DPDS-fa while a reduction of the mechanical properties at high strain occurs. It is worth mentioning that in unfilled compounds (Chapter III) this behavior was just observed with high content of diBz (i.e. 30 phr). This lowering of the stress with the increase of the strain could be explained by a decrease of the crosslinking density of the network. In order to further elucidate this behavior, the crosslinking density of the samples as well as additional tests were carried out and are reported in the following section.

Understanding the behavior at high strain of filled compounds with 3DPDS-fa

The observed behavior at high strain is generally the sign of a reduction of the crosslinking density of the network. For this reason, the crosslinking density (ν_c) of each compound was

checked by swelling test and calculated using the Flory Rehner equation (see in Annex A, section A.3.5 for detail of the calculation). The obtained values are plotted as a function of the benzoxazine amount in Figure IV.7.

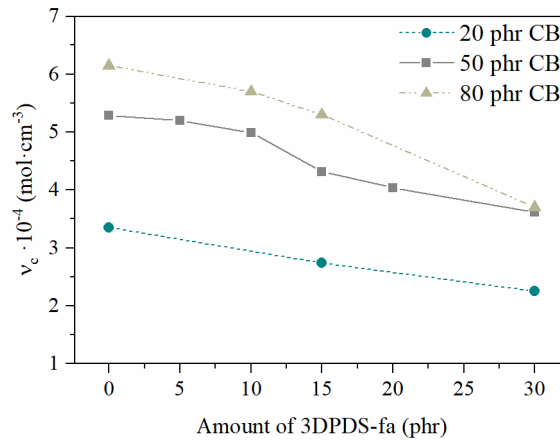


Figure IV.7. Crosslinking density of filled compound as a function of the amount of 3DPDS-fa.

A clear tendency is observed with a decrease of the crosslinking density with increasing the amount of 3DPDS-fa. For example, the addition of 30 phr 3DPDS-fa to compounds with 80 phr of CB reduces the v_c by 40% while 15 phr of the Bz by 14% compared to the reference (PI(CB)₈₀). A possible explanation for this phenomenon would be a sulfur consumption by 3DPDS-fa during the vulcanization previously reported and discussed in Chapter III.³¹

In order to verify this hypothesis, the performance of compounds with lower and higher content of sulfur was tested. To this aim, two samples with 80 phr of CB and 15 phr of 3DPDS-fa were prepared with an increase of the amount of sulfur of 25% (i.e. 6.9 phr) and a reduction of 50% (i.e. 2.8 phr). It should be noted that the amount of the other ingredients of the curing package was not changed to be able to isolate the effect of sulfur. The stress-strain curves are depicted in Figure IV.8.

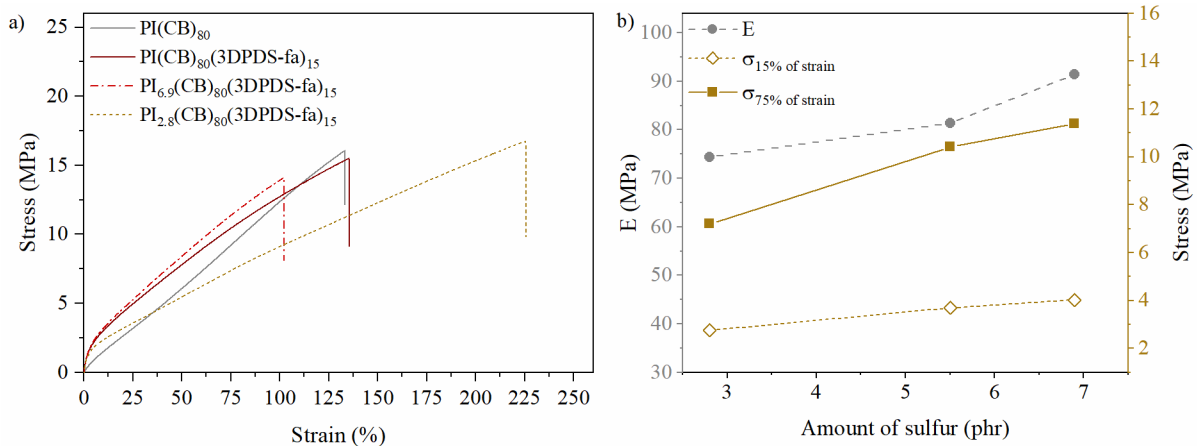


Figure IV.8. a) Stress-strain curve of rubber compounds with 15 phr of 3DPDS-fa and 80 phr of CB with varying sulfur content (2.8, 5.5 and 6.9 phr); b) Evolution of E , $\sigma_{15\%}$ and $\sigma_{75\%}$ as a function of the sulfur content.

The decrease of sulfur content leads to a decrease of the stress at high strain as shown in Figure IV.8a similarly to previously observed in compounds with high amount of 3DPDS-fa. These results show that the loss of reinforcement is due to a reduction of the available sulfur to crosslink the rubber network, therefore, demonstrate a sulfur consumption by 3DPDS-fa.

Indeed, a potential co-reaction between the oxazine rings from 3DPDS-fa and sulfur could take place during the vulcanization similar to what was observed for unfilled materials when a high content of 3DPDS-fa was used (Chapter III, section 3.3). Nevertheless, in the case of PI(CB)₈₀(3DPDS-fa)₁₅ just a small amount of sulfur is consumed. Otherwise, the stress-strain curve would be closer to the one with lower amount of sulfur and thus, it will not be able to reinforce it the way it does. Additionally, it is important to highlight that it is possible to overcome the sulfur consumption with an increase of the amount of sulfur in the formulation as observed for PI_{6,9}(CB)₈₀(3DPDS-fa)₁₅ in Figure IV.8a.

The mechanical properties and the crosslinking densities are summarized in Table IV.4.

Table IV.4. Summary of the tensile test data and crosslinking density for compounds with CB and 3DPDS-fa.

Abbr.	E (MPa)	$\sigma_{15\%}$ (MPa)	$\sigma_{25\%}$ (MPa)	$\sigma_{75\%}$ (MPa)	$\sigma_{150\%}$ (MPa)	σ_{break} (MPa)	$v_c \cdot 10^{-4}$ (mol·cm ⁻³)
PI(CB) ₂₀	4.9±0.4	0.57±0.01	0.85±0.01	2.09±0.03	4.34±0.05	15.9±2.2	3.35±0.03
PI(CB) ₂₀ (3DPDS-fa) ₁₅	6.6±0.4	0.71±0.01	1.03±0.01	2.29±0.02	4.33±0.03	18.1±0.8	2.74±0.01
PI(CB) ₂₀ (3DPDS-fa) ₃₀	8.3±0.4	0.78±0.01	1.07±0.01	2.08±0.02	3.62±0.03	15.8±0.8	2.25±0.03
PI(CB) ₅₀	12.5±0.3	1.18±0.02	1.81±0.03	5.03±0.09	10.64±0.09	18.0±0.3	5.29±0.01
PI(CB) ₅₀ (3DPDS-fa) ₅	22.2±0.9	1.58±0.04	2.29±0.05	5.82±0.06	11.29±0.03	15.7±0.8	5.20±0.05
PI(CB) ₅₀ (3DPDS-fa) ₁₀	29.9±0.7	1.85±0.06	2.56±0.08	5.9±0.1	11.1±0.2	12.8±1.8	4.99±0.06
PI(CB) ₅₀ (3DPDS-fa) ₁₅	40.1±1.4	2.15±0.07	2.78±0.07	5.7±0.1	10.0±0.2	14.7±0.8	4.32±0.01
PI(CB) ₅₀ (3DPDS-fa) ₂₀	46.4±0.4	2.31±0.02	2.90±0.03	5.46±0.06	9.3±0.1	14.7±0.7	4.04±0.05
PI(CB) ₅₀ (3DPDS-fa) ₃₀	64.4±1.5	2.86±0.07	3.32±0.08	5.2±0.2	8.1±0.3	12.8±0.6	3.61±0.03
PI(CB) ₈₀	27.3±1.8	2.18±0.09	3.31±0.12	9.32±0.08	-	16.2±0.8	6.15±0.07
PI(CB) ₈₀ (3DPDS-fa) ₁₀	67.9±1.3	3.50±0.08	4.81±0.09	11.0±0.1	-	14.5±0.8	5.7±0.1
PI(CB) ₈₀ (3DPDS-fa) ₁₅	81.4±1.4	3.69±0.04	4.91±0.04	10.41±0.04	-	15.3±0.1	5.27±0.03
PI(CB) ₈₀ (3DPDS-fa) ₃₀	153±3	5.06±0.09	5.53±0.08	7.84±0.05	11.4±0.09	12.5±0.4	3.69±0.03
PI _{2,8} (CB) ₈₀ (3DPDS-fa) ₁₅	70.6±0.4	2.75±0.03	3.50±0.04	7.2±0.1	12.0±0.2	16.7±0.1	3.41±0.02
PI _{6,9} (CB) ₈₀ (3DPDS-fa) ₁₅	90.3±1.4	4.03±0.06	5.36±0.06	11.39±0.04	-	13.8±0.8	6.34±0.07

The incorporation of 3DPDS-fa enhanced the stiffness of the CB loaded compounds while the addition of a high content of 3DPDS-fa resulted in a reduction of the mechanical properties at high strain. The decrease of the crosslinking density with the increase of the amount of the diBz and the resulting softening at high elongation are consistent with sulfur consumption. Nevertheless, it was demonstrated that the sulfur intake can be overcome with an increase of its amount in the formulation without impacting the overall performance. Interestingly, these materials exhibit at the same time higher elongation at break and therefore, they combine high stiffness with high elasticity. Even though this might not be desirable for tire application, the combination of these two behaviors could be interesting for other fields.

In conclusion, these results show 3DPDS-fa is acting as a reinforcing resin thanks to the formation of poly(3DPDS-fa) together with the rubber curing. The relation observed between the amount of CB and the reinforcement of 3DPDS-fa indicates that a synergistic mechanism between CB and 3DPDS-fa is occurring. It seems the presence of 3DPDS-fa influences the

formation of the filler network and, therefore, additional cyclic tensile tests were performed to further understand the effect of 3DPDS-fa on the filler network.

2.1.4 Study of the performance of filled compounds with 3DPDS-fa by cyclic tensile test

The reinforcing mechanism of 3DPDS-fa can be explained by two main contributions: (1) formation of poly(3DPDS-fa) and (2) the influence of 3DPDS-fa in the formation of the CB network structure leading to a synergistic effect between CB and the benzoxazine. Quasi-static cyclic tensile tests can be carried out to elucidate the effect of 3DPDS-fa on the reinforcement.

The cyclic stress softening behavior is a phenomenon characteristic of rubber compounds and was previously described in Chapter I, section 2.5.3. Basically, at a constant strain, the stress drops between successive loading cycles. This effect is more important during the first two cycles becoming negligible after several cycles (~5) when a steady state with a stabilized hysteresis loop is then reached. The difference between the stress reached after the first cycle and the stress at the last cycle represents the stress softening. This behavior is related to a rearrangement or breakdown of the filler network structure.¹⁹⁷

To that aim, quasi-static cyclic tensile test of compounds with and without 3DPDS-fa were performed following the procedure described in Annex A (Figure A.1). Each compound was deformed cyclically 5 times at each strain-controlled interval (i.e. 15, 30, 50, 70, and 90%). The first and the last stress-strain deformation cycles of each compound is displayed in Figure IV.9.

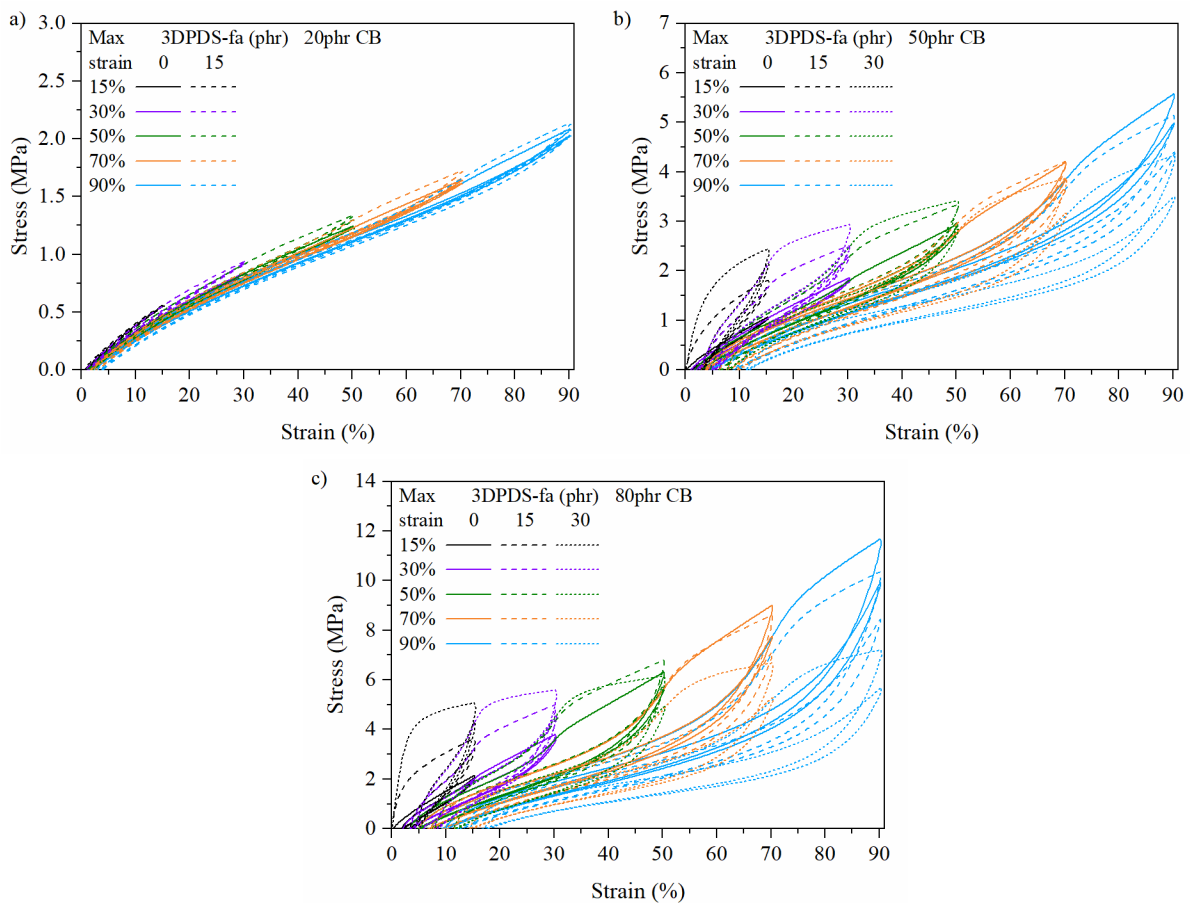


Figure IV.9. The first and last cyclic loop for different content of 3DPDS-fa in compounds with a) 20 phr CB; b) 50 phr CB; and c) 80 phr CB.

In lowly filled samples, the differences between the first and last cycle is almost negligible. On the contrary, in highly filled samples a pronounced difference is observed between these two cycles. For these compounds, a clear reduction of the hysteresis loop and the achieved stress at the end of the test occurs reflecting the cyclic stress softening phenomenon.

The outcome of the cyclic stress softening can be employed to determine the rate of modulus reduction with respect to the applied strain deformation.⁷ For example, to determine the modulus reduction at 30% strain (ϵ), the stress (σ) of the first and the last cycle curves from the following cycles are derived with respect to ϵ ($\delta\sigma/\delta\epsilon$) and plotted as a function of ϵ (Figure IV.10). The difference between the maximum point of the derivative of the first cycle (E_{1st}) and the slope of the last cycle (E_{5th}) is denoted as ΔE ($=E_{1st}-E_{5th}$). This parameter is used to quantify the relative softening of the material during the deformation cycles. Finally, ΔE obtained for each compound containing 3DPDS-fa is normalized to its corresponding reference without the benzoxazine (ΔE_{Ref}) and therefore, the outcome of this procedure ($\Delta E/\Delta E_{Ref}$) gives the contribution of 3DPDS-fa to the system. The normalized values were plotted as a function of the strain (Figure IV.11a).

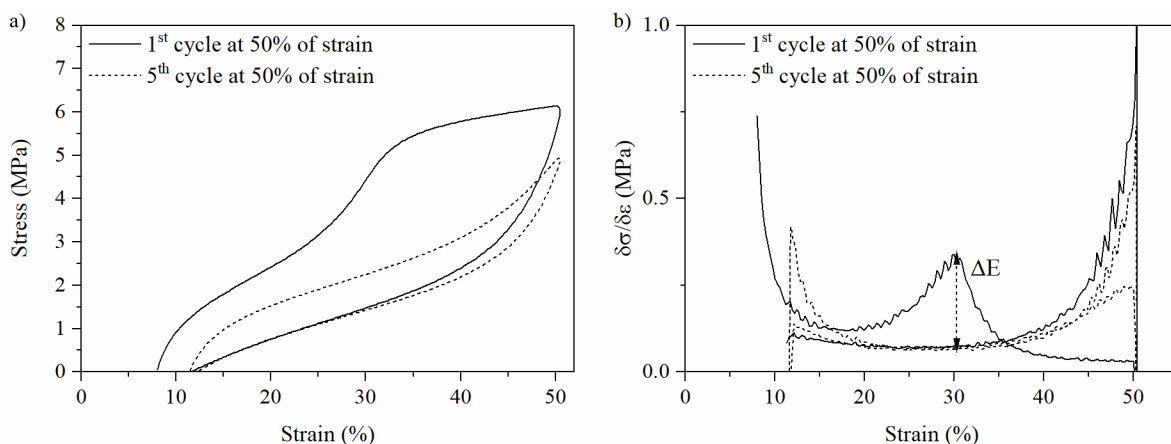


Figure IV.10. Example of the procedure followed to determine ΔE by transforming stress-strain curve into “local” modulus: a) First and last cycling curve; b) Derivative of the curves.

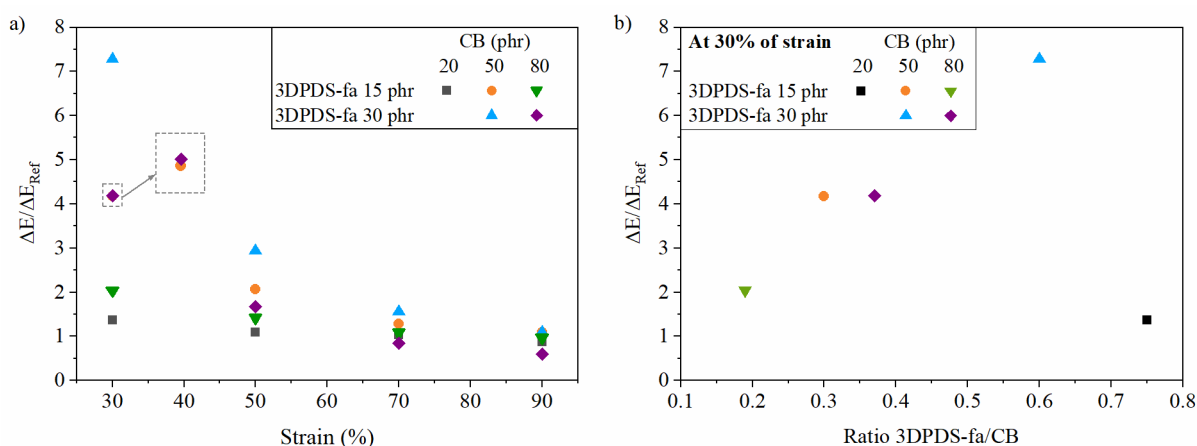


Figure IV.11. Normalized softening effect ($\Delta E/\Delta E_{Ref}$) of compounds with different content of 3DPDS-fa and loadings of CB a) as a function of the strain; b) as a function of the ratio 3DPDS-fa/CB.

The most significant softening occurs at low strain (<50%). This can be explained because of the brittle nature of polybenzoxazines that is not able to deform similarly to the rubber matrix.

PI(CB)₅₀(3DPDS-fa)₃₀, shows the most pronounced softening effect as shown in Figure IV.11. Similar softening effects were obtained for PI(CB)₅₀(3DPDS-fa)₁₅ and PI(CB)₈₀(3DPDS-fa)₃₀; compounds with comparable ratios 3DPDS-fa/CB (0.30 and 0.38, respectively). These results showed that in highly filled compounds the softening reaches its maximum not when a high content of the resin is present but when the ratio between 3DPDS-fa and CB is the highest. These results give further evidence that a synergy between the filler and the resin is occurring resulting in much stiffer filler-filler bonds. On the contrary, in lowly filled compounds such as PI(CB)₂₀(3DPDS-fa)₁₅, even if the ratio 3DPDS-fa/CB is high (0.75), the resin has almost no impact on the stress softening behavior. These results show a dependency of 3DPDS-fa and the filler loading whereby highly filled compounds (≥ 50 phr of CB) exhibit softening behavior while the effect on compounds with low CB content is negligible highlighting the existence of the synergistic effect.

In summary, the quasi-static cyclic tests showed the influence of the 3DPDS-fa in the formation of the filler network leading to a synergistic effect between CB and the benzoxazine. The resulting network exhibits much stiffer filler-filler bonds with higher brittleness compared to the filler network on the compounds without 3DPDS-fa. This behavior could be explained by the formation of a hybrid network between CB and polyBz. This hypothesis and the impact of the 3DPDS-fa on the hysteresis of the materials was investigated by dynamic mechanical analysis (DMA) and is reported in the following section.

2.2 Investigation of the effect of 3DPDS-fa on the dynamic mechanical properties of filled compounds

It is well-known that the incorporation of reinforcing resins leads to an improvement of the compound stiffness, but it is commonly combined with an undesirable increase of the energy dissipation so-called hysteresis. For this reason, in this section, stiff apex compounds with and without the incorporation of 15 phr of 3DPDS-fa were analyzed by DMA. The aim was to investigate the effect of 3DPDS-fa on the dynamic mechanical properties of the materials and therefore, on the hysteresis. DMA tests were carried out in two modes: strain sweeps at 25 and 70 °C and temperature sweep from -100 to 200 °C. By performing strain sweep tests, the maximum dissipated energy can be determined and compared to the reference while the temperature sweep tests provide its evolution as a function of the temperature. The measurement conditions and sample dimensions are described in Annex A (section A.3.7). The following subsections reports the results obtained using both modes.

2.2.1 DMA strain sweep

The evolution of the storage modulus (G'), loss modulus (G''), and loss factor ($\tan\delta$) as a function of strain at 25 and 70 °C of PI(CB)₈₀ and PI(CB)₈₀(3DPDS-fa)₁₅ is shown in Figure IV.12. The decrease of G' with increasing strain amplitude is commonly known as the Payne effect and was previously described in Chapter I, section 2.5.3. This decline of the storage modulus results from a dynamical break-up of the filler network present in most of the filled rubber systems, it is more pronounced for large filler contents and tends to disappear for small filler fractions. As the network breaks, energy is dissipated as heat leading to the increase of G'' and thus, to an increase of $\tan\delta$. The difference between G' at the lowest (0.1%) and G' at the highest strain (50%) is a measure of the magnitude of the Payne effect ($\Delta G'$). Additionally,

the dynamic stiffness for which higher values are desirable for stiff tire compounds, and hysteresis for which lower values are better for reducing the energy dissipated, were followed. The main information from this test is summarized in Table IV.5.

The incorporation of 3DPDS-fa leads to higher dynamic stiffness over the whole range of strain amplitudes. The improvement of G' is occurring together with the rise of $\Delta G'$. Indeed, at 25 °C the Payne effect is increased by 230% for PI(CB)₈₀(3DPDS-fa)₁₅. The Payne effect is less pronounced at 70 °C for both reference and compounds with 3DPDS-fa.

The Kraus model can be used to quantify the Payne effect and has often been successfully applied for the fitting of experimental data.¹⁹⁸ The model is based on the assumption that the filler network breaks and (re-)agglomerates under shear amplitude (γ). The decrease of the storage modulus G' with increasing strain amplitude follows Eq. IV.1:

$$\frac{G' - G'_\infty}{G'_0 - G'_\infty} = \frac{1}{1 + (\gamma/\gamma_c)^{2m}}, \quad (\text{IV.1})$$

where γ_c and m are fitting parameters. γ_c is the critical amplitude defining the breakdown of the filler network while the exponent m is entirely determined by the structure of the filler network showing universal features of the cluster network.⁷⁷ Using this phenomenological model, the Payne effect was approximated, and the fitting parameter determined. The obtained curves plotted in Figure IV.12 show a good fitting with the experimental data (dashed and dotted lines). The values obtained for the exponent m and γ_c are displayed in Table IV.5. The m parameter is representative of the structure of the filler network showing 3DPDS-fa has a direct impact on the formation of the CB network and confirming the assumption of a hybrid polyBz/CB network as discussed above. The main change in G' occurs at a critical strain (γ_c) at 0.2 or 0.6% for PI(CB)₈₀ at 70 and 25 °C, respectively, and around 2% for PI(CB)₈₀(3DPDS-fa)₁₅ at both temperatures. Interestingly, the dynamic modulus of the reference is more affected by temperature than for the 3DPDS-fa compound as attested by the variations of Payne effect and critical strain with increasing temperature.

Additionally, the presence of 3DPDS-fa leads to a steeper network breakdown leading to a higher dissipation of energy as attested by the increase of $\tan\delta$, up to 156% at 70 °C with respect to the reference. For the reference, the energy dissipation decreases when increasing the temperature while $\tan\delta_{6\%}$ for 3DPDS-fa compounds is found to be almost the same at both temperatures. To understand this behavior, $G''_{6\%}$ was analyzed in detail. $G''_{6\%}$ of the reference is reduced by 50% when the temperature is increased explaining the low value of $\tan\delta_{6\%}$ in this case. On the contrary, when 3DPDS-fa is incorporated, the viscous modulus, $G''_{6\%}$, is not affected by temperature being the main contribution for the increase of $\tan\delta_{6\%}$ at 70 °C. One possible explanation for this behavior might be the presence of unpolymerized benzoxazine or benzoxazine oligomers that could melt when the temperature is increased and, thus, increase the viscous portion. Another hypothesis could be the formation of a polyBz network with low relaxation temperature, due to unfinished curing or from the reaction with sulfur, that could also lead to an increase of the dissipation of energy at high temperature. To further elucidate the effect of temperature on the compounds, DMA temperature sweep tests were carried out are discussed in the following section.

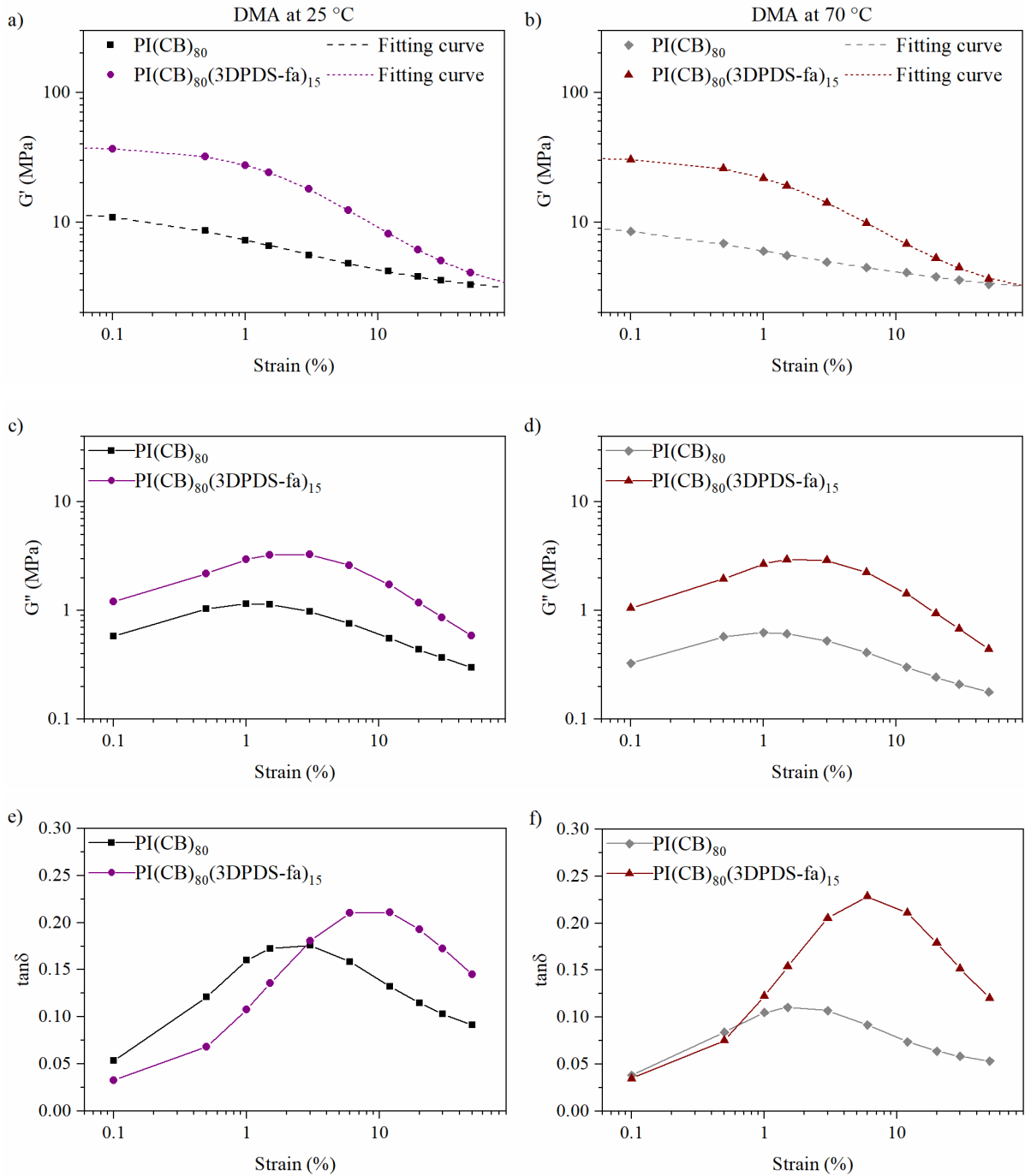


Figure IV.12. DMA strain sweep at 25 °C (on the left) and at 70 °C (on the right) of compounds with 80 phr of CB and with and without 15 phr of 3DPDS-fa; a) b) G' and fitting curve by Kraus model; c) d) G'' , and e) f) $\tan\delta$ (in G'' and $\tan\delta$ the line is to guide the eye).

Table IV.5. Viscoelastic results from DMA test in strain sweep mode for compounds with CB and 3DPDS-fa.

Abbr.	25 °C					70 °C				
	$\Delta G'$ MPa ^a	$G'_{6\%}$ MPa	$G''_{6\%}$ MPa	$\tan\delta_{6\%}$	γ_c / m^b	$\Delta G'$ MPa ^a	$G'_{6\%}$ MPa	$G''_{6\%}$ MPa	$\tan\delta_{6\%}$	γ_c / m^b
PI(CB)₈₀	7.6	4.8	0.8	0.17	0.6 / 0.3	5.2	4.5	0.4	0.09	0.2 / 0.2
PI(CB)₈₀(3DPDS-fa)₁₅	32.6	12.4	2.6	0.21	2.3 / 0.5	26.6	9.8	2.3	0.23	2.0 / 0.5

^a $\Delta G' = G'_{0.1\%} - G'_{50\%}$. ^b Fitting parameters from Kraus model.

2.2.2 DMA temperature sweep

The temperature dependence of the viscoelastic behavior of compounds with and without 3DPDS-fa in Figure IV.13. The maximum of E'' was used to quantify the T_α (reported in Table IV.6). There is a slight decrease of the T_α for $\text{PI}(\text{CB})_{80}(3\text{DPDS-fa})_{15}$ that might be associated to a lower crosslinking density. The disparities in the $\tan\delta_{\max}$ are explained by the different values of E' .¹⁹⁹ Indeed, the incorporation of reinforcing system increases the E' at the expenses of limiting the $\tan\delta$ peak height. The $\tan\delta_{\max}$ for $\text{PI}(\text{CB})_{80}$ is greater as the value of E' in the rubbery plateau is lower while the opposite behavior is observed for $\text{PI}(\text{CB})_{80}(3\text{DPDS-fa})_{15}$ with lower $\tan\delta_{\max}$ and higher E' above the T_α .

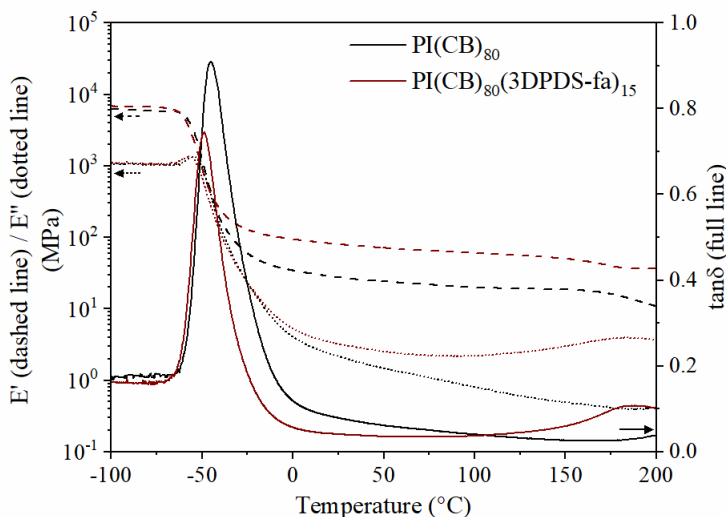


Figure IV.13. DMA temperature sweep of compounds with 80 phr of CB and with and without 15 phr of 3DPDS-fa (E' dashed line; E'' dotted line; $\tan\delta$ full line).

Table IV.6. Viscoelastic results by DMA tests in temperature sweep mode for compounds with CB and 3DPDS-fa.

Abbr.	T_α °C ^a	$\tan\delta_{\max}$ ^b	$E'_{50^\circ\text{C}}$ MPa	$\tan\delta_{50^\circ\text{C}}$	$E'_{100^\circ\text{C}}$ MPa	$\tan\delta_{100^\circ\text{C}}$
PI(CB)₈₀	-43.1	0.91	24.1	0.061	20.0	0.040
PI(CB)₈₀(3DPDS-fa)₁₅	-49.1	0.75	71.0	0.035	59.9	0.036

^a α -Relaxation from maximum of E'' peak. ^b Peak height.

The storage modulus of $\text{PI}(\text{CB})_{80}(3\text{DPDS-fa})_{15}$ is higher than the reference ($\text{PI}(\text{CB})_{80}$) over the whole range of temperatures as observed in Figure IV.13 following a similar trend over the temperature range. On the contrary, E'' of $\text{PI}(\text{CB})_{80}$ is reduced with increasing temperature while E'' of $\text{PI}(\text{CB})_{80}(3\text{DPDS-fa})_{15}$ is constant until 100 °C and above this temperature starts to increase. This increase of E'' is responsible of the high value of $\tan\delta$ at temperatures above 100 °C for $\text{PI}(\text{CB})_{80}(3\text{DPDS-fa})_{15}$. These results are in agreement with the outcome from DMA strain sweep proving the high values of $\tan\delta_{6\%}$ at 70 °C and thus, hysteresis, are due to an increment of loss modulus with temperature when 3DPDS-fa is incorporated into the compound. Indeed, the increase of the E'' and $\tan\delta$ at high temperature points the presence of a second phase around 180 °C for $\text{PI}(\text{CB})_{80}(3\text{DPDS-fa})_{15}$, most probably, corresponding to the poly(3DPDS-fa). It is noteworthy that the lower value of T_α in comparison to the fully cured neat 3DPDS-fa ($T_\alpha \sim 260^\circ\text{C}$) can be explained by the unfinished polymerization due to the short

curing time during the vulcanization, a potential sulfur reaction, or a dilution effect in the rubber matrix.

Regarding the higher hysteresis observed for the compounds with 3DPDS-fa, one possible explanation could be the formation of a hybrid network between CB and polyBz, resulting in a network with higher stiffness but combined with higher brittleness. Additionally, the phase separation observed by DMA could also explain the higher energy loss observed. In order to understand the effect of 3DPDS-fa, the morphology of the filler network as well as the nanomechanical properties of the materials with and without 3DPDS-fa was characterized by atomic force microscopy (AFM) and is reported in the following section.

2.3 Morphological characterization and nanomechanical properties of filled compounds with 3DPDS-fa

AFM was used to explore the morphology of the filler network in the presence and absence of 3DPDS-fa, and the impact of the benzoxazine on the nanomechanical properties of the filled compounds. A detail description of the sample preparation and the measurement conditions can be found in Annex A (section A.3.8).

2.3.1 Morphological characterizations

The morphology of compounds with 80 phr of CB were first characterized and the phase shift images of the compounds with and without 15 and 30 phr of 3DPDS-fa in areas of $5 \times 5 \mu\text{m}^2$ are shown in Figure IV.14. The morphologies of the compounds are revealed by the contrast in the phases with the dispersion of particles (low phase/black contrast) in the polymer matrix (high phase/light grey contrast). The particles are composed of only carbon black, for the reference sample, and a combination of both: CB and 3DPDS-fa for the compounds containing the diBz. A percolated filler network is observed in all the samples containing 80 phr of CB. Similar CB distribution is observed for the reference and the compound with 15 phr of 3DPDS-fa. On the other side, the addition of 30 phr of 3DPDS-fa leads to an agglomeration of the CB particles as observed in Figure IV.14. It is worth mentioning that it is well-known that the dispersion of fillers is affected by the shearing forces during the mixing step. As observed by MDR, the incorporation of 30 phr of 3DPDS-fa to the compounds decreased the viscosity of the compounds at 150 °C (Table IV.3). However, 3DPDS-fa is introduced at the last step of the mixing, while CB has already been masticated for 8 minutes. Thus, even if 3DPDS-fa reduces the viscosity of the green compound, CB has been deagglomerated during the first part of the mixing and the impact of 3DPDS-fa during the mixing might be slight or negligible. Therefore, the observed agglomeration is more likely due to the interactions between polyBz and CB particles with a formation of a hybrid network. In order to elucidate this hypothesis, samples with lower amount of CB (i.e. 20 and 50 phr of CB) were also analyzed by AFM.

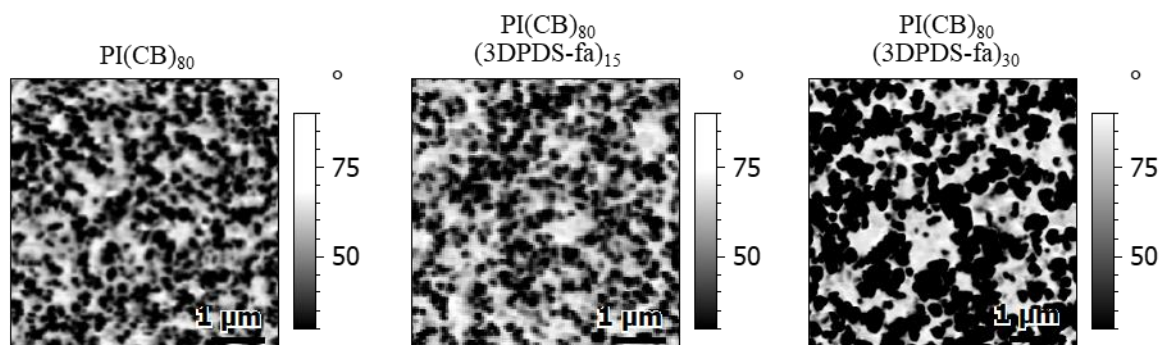


Figure IV.14. AFM-AM-FM phase images of rubber compounds with and without 15 and 30 phr of 3DPDS-fa with 80 phr of CB.

The phase images in areas of $5 \times 5 \mu\text{m}^2$ of compounds with 20 phr of CB containing 15 and 30 phr of 3DPDS-fa are depicted in Figure IV.15a.

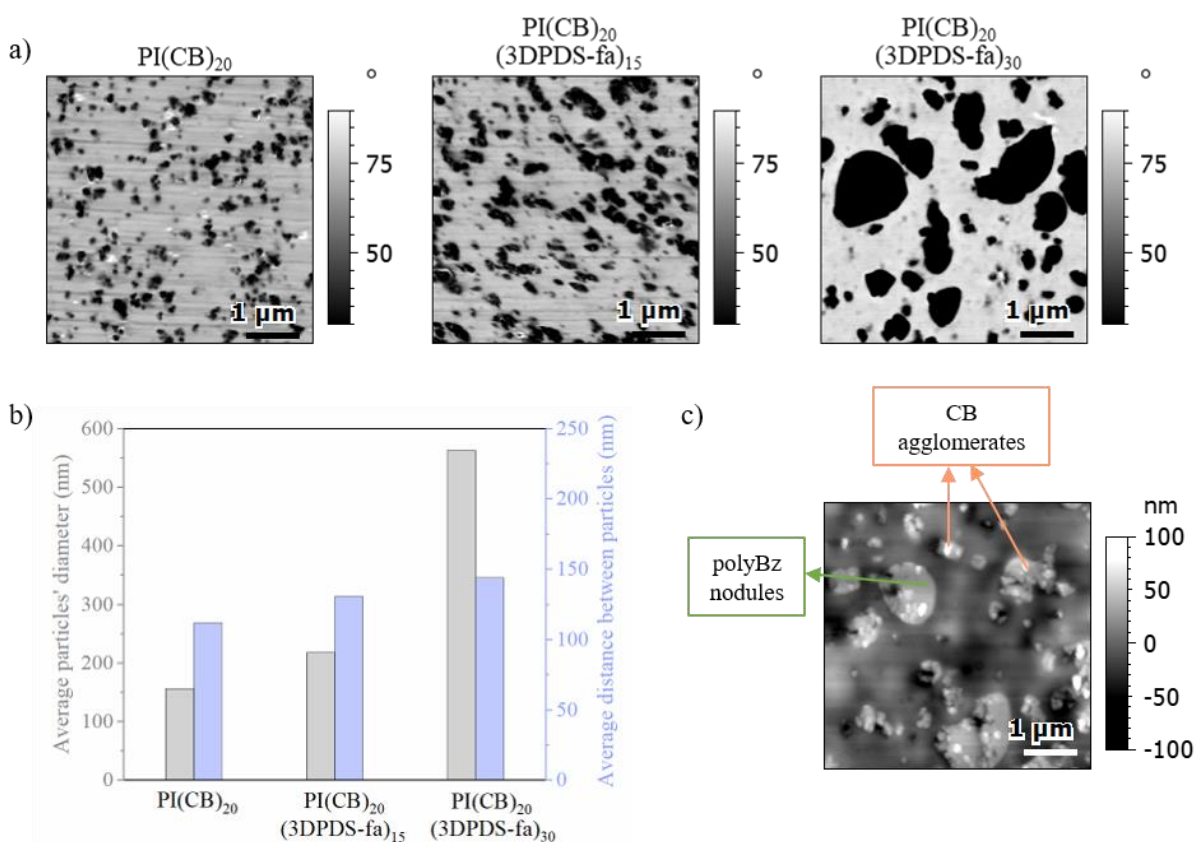


Figure IV.15. a) AFM-AM-FM phase images of compounds with 20 phr of CB and with and without 15 and 30 phr of 3DPDS-fa, b) average particles' diameter and distance between particles, and c) AFM-AM-FM topography image of PI(CB)₂₀(3DPDS-fa)₃₀.

In lowly filled compounds, a percolated network was not observed. The reference, PI(CB)₂₀, exhibits an even dispersion of CB while the incorporation of 15 phr of 3DPDS-fa leads to a slight aggregation of the particles. In this compound (PI(CB)₂₀(3DPDS-fa)₁₅), the amount of CB is higher than the content of 3DPDS-fa. On the contrary, the addition of 30 phr of 3DPDS-fa results in a pronounced increase of the particle size. In fact, the average particle size increased from 150 and 200 nm (for the reference and the compound with 15 phr of 3DPDS-fa, respectively) to 550 nm when 30 phr of Bz were employed as displayed in Figure IV.15b. In this last compound, i.e. PI(CB)₂₀(3DPDS-fa)₃₀, the content of 3DPDS-fa is higher than the

amount of CB allowing to distinguish the polyBz nodules from the carbon black agglomerates using the topography images as displayed in Figure IV.15c. The round flat particles with clear delimited borders are attributed to the polyBz while the small white and irregular particles correspond to small CB agglomerates. It can be observed that the carbon black particles are situated alongside the polyBz nodules showing the affinity between the resin and the filler. This observation tends to confirm the assumption of a hybrid polyBz/CB network deduced from DMA and cyclic tensile tests.

For PI(CB)₅₀ a percolated filled network was achieved with a uniform distribution of CB observed in phase images of compounds with 50 phr of CB in areas of 5×5 μm² (Figure IV.16). The addition of 15 phr of benzoxazine leads to the slight formation of aggregates while keeping a good distribution of the filler in the polymer matrix. In contrast, in systems with a high amount of 3DPDS-fa, i.e. PI(CB)₅₀(3DPDS-fa)₃₀, its incorporation causes a clear agglomeration of the carbon black particles leading to an increase in the average of particle size and therefore in the average distance between particles. The average size of carbon black network agglomerates for PI(CB)₅₀ is 150±95 nm while for PI(CB)₅₀(3DPDS-fa)₃₀ is 230±180 nm as displayed in Annex F (Figure F.3). Although these values could be considered the same within the error, the impact of the resin on the filler network is clearly observed in Figure IV.16 indicating the incorporation of high content of 3DPDS-fa results in a detrimental impact on the carbon black distribution.

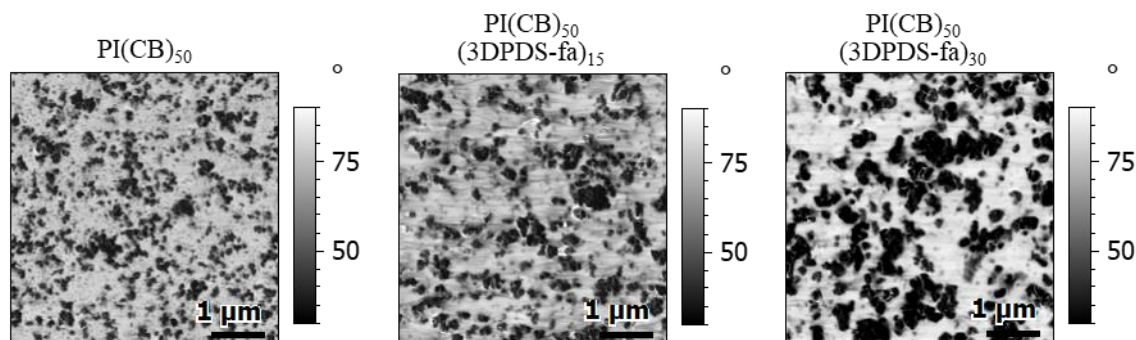


Figure IV.16. AFM-AM-FM phase images of rubber compounds with 50 phr of CB and with and without 15 and 30 phr of 3DPDS-fa.

In conclusion, the morphological assessment of the compounds showed that 3DPDS-fa has an impact on the formation of the filler network. 3DPDS-fa and CB may tend to agglomerate together during the mixing certainly due to their closer polarities as compared to polyisoprene, and the curing step would fix the morphology of the compounds. In lowly filled compounds, large aggregates of hybrid polyBz/CB particles are observed while in highly filled compounds (i.e. CB ≥50phr) a hybrid percolated network is detected.

2.3.2 Nanomechanical properties

The morphologies of the compounds with 80 phr of CB were also revealed by the contrast in nanomechanical properties with a clear distinction of two phases: rubber with low modulus (dark brown) and filler network with high modulus (light yellow) (Figure IV.17a). Unfortunately, it is not possible to distinguish polyBz and CB networks by their mechanical properties as they are similar at the scale of the measurement. Moreover, the incorporation of 3DPDS-fa to these compounds does not lead to a significant change on the moduli of the filler network as it is mainly influenced by the high content of carbon. However, the presence of

3DPDS-fa leads to a decrease of the modulus of the rubber matrix (E_{PI}) by 23% with 15 phr of the Bz for instance. These measurements, together with the lower crosslinking density, and the tensile tests (Figure IV.6c), are well aligned with the hypothesis of a consumption of sulfur as stated previously. Furthermore, the nanomechanical properties of lowly filled compounds were also analyzed and are displayed in Figure IV.18 showing a similar decrease of E_{PI} with increasing 3DPDS-fa. Additionally, the presence of 3DPDS-fa increases the modulus of the particles as shown in Figure IV.18b. This can be explained by the preferential location of the benzoxazine alongside the CB particles as previously shown and therefore, impacting the carbon black network formation. Similar results were obtained for samples with 50 phr of CB as displayed in Annex F (Figure F.4). The incorporation of high content of 3DPDS-fa led to an increase of the overall modulus of the particles by 40%. In this case, the impact of the resin is more pronounced than for samples with 80 phr of CB because the ratio between 3DPDS-fa and CB is higher for compounds with 50 phr of CB.

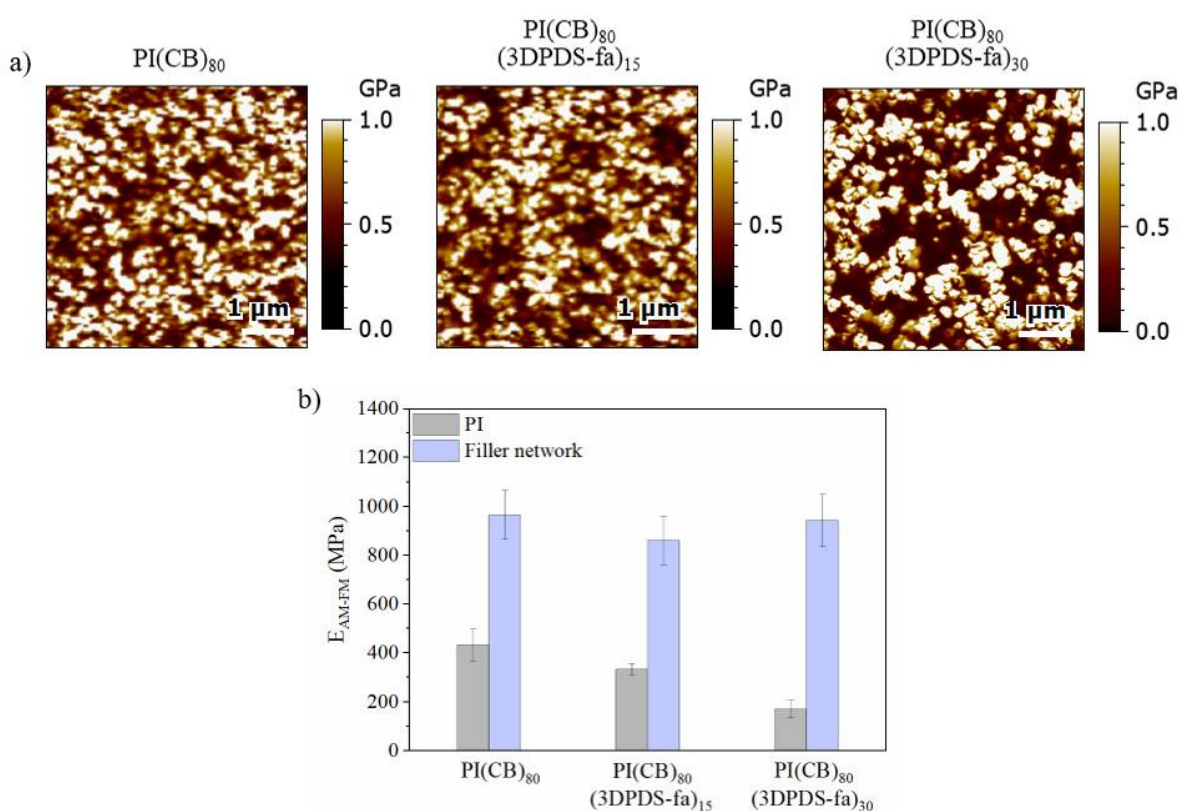


Figure IV.17. a) AFM-AM-FM images of the modulus of rubber compounds with and without 15 and 30 phr of 3DPDS-fa with 80 phr of CB; b) measurements of the moduli in each of the phases in the compounds.

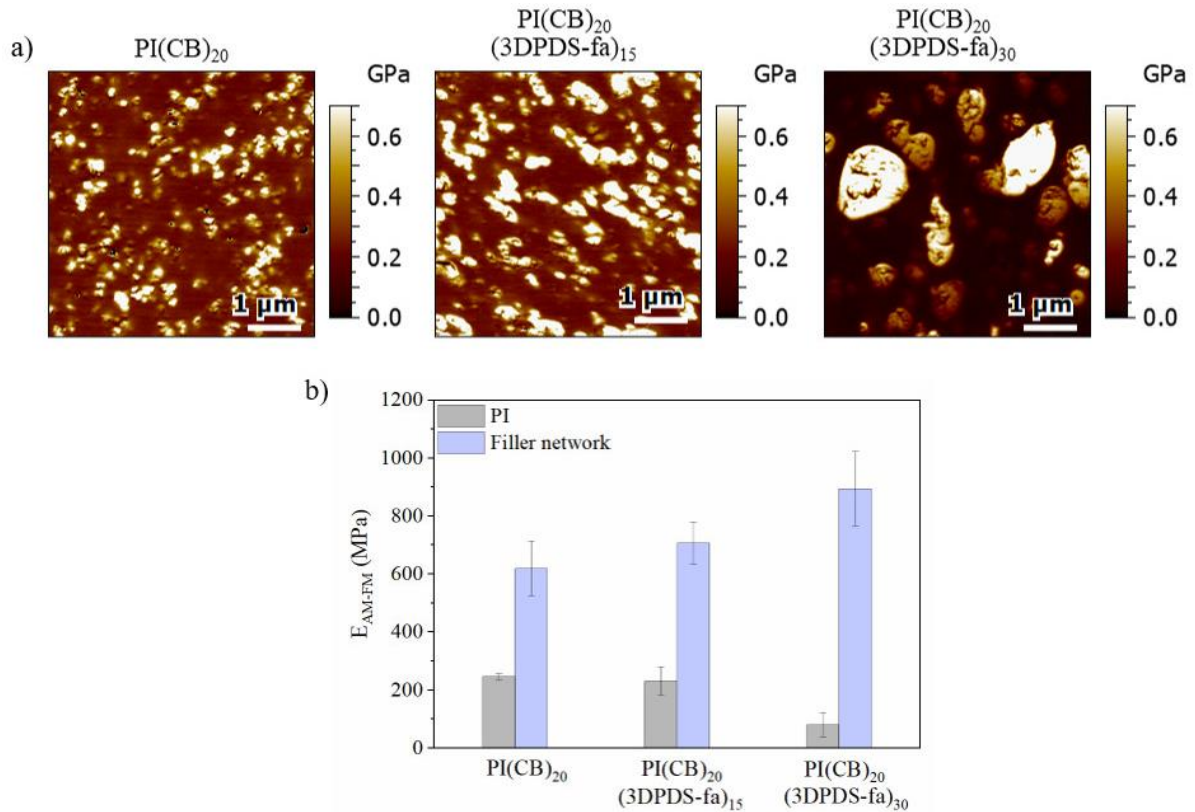


Figure IV.18. a) AFM-AM-FM images of the modulus of rubber compounds with and without 15 and 30 phr of 3DPDS-fa with 20 phr of CB; b) measurements of the moduli in each of the phases in the compounds.

To conclude, the incorporation of high contents of 3DPDS-fa leads to a detrimental impact on the nanomechanical properties of the compounds supporting the conclusion of the sulfur consumption. Finally, the increase of the modulus of the particles highlights the formation of a hybrid network between polyBz and CB, in agreement with the previous observations.

2.4 Discussion

3DPDS-fa reinforces filled rubber compounds. The addition of this diBz leads to materials with improved stiffness as observed by the increase of the Young moduli and the maximum torque. These results confirmed the simultaneous curing of the 3DPDS-fa and the rubber. Additionally, 3DPDS-fa consumes sulfur during its curing as attested by the decrease of the crosslinking density, the stress at high strain, and the modulus of the rubber phase. Even though this side-reaction takes place, it is possible to compensate it with the increment of sulfur content on the formulation without a detrimental impact on the overall mechanical properties.

The incorporation of 3DPDS-fa results in the formation of a hybrid network between the polyBz and the CB confirmed by cyclic tests and DMA, resulting in a stiffer filler network with higher brittleness. For this reason, the reinforcing effect of 3DPDS-fa exhibit a clear dependency with the filler content. The presence of 3DPDS-fa in highly filled compounds (≥ 50 phr of CB) results in improved mechanical properties, while its effect is less pronounced on lower CB content counterparts. These results are attributed to the presence or not of a hybrid percolated network as attested by morphological characterization. In its absence, the resin is almost ineffective, while in its presence, the combination of the effect of both the filler and 3DPDS-fa is synergistic.

The use of 3DPDS-fa resulted in compounds that combined a higher dynamic stiffness and a higher hysteresis than the reference. Several hypotheses could be drawn to explain this behavior. The first one is the presence of a stiffer hybrid network with higher brittleness possibly leading to an increase of the dissipation of energy. Another possibility is the presence of unpolymerized benzoxazine or benzoxazine oligomers that could melt when the temperature increases and, therefore, contribute to the increase of the viscous portion. Additionally, the formation of a polyBz network with low relaxation temperature, due to unfinished curing or from the reaction with sulfur, could also lead to an increase of the dissipation of energy at high temperature. The lower crosslinking density could potentially be another factor to be considered as it might lead to a higher polymer chain mobility. A potential increase of sulfur content could reduce to a certain extent this dissipation of energy and thus, overcome the high values of $\tan\delta$. Optimization of the formulation could be additionally carried out to be able to tackle this issue. Furthermore, thanks to the rich molecular design flexibility of polybenzoxazines, additional functionalities could be added to the diBz structure with the ability to react with the rubber during the vulcanization. The formation of covalent chemical links between the two networks could potentially help to decrease the hysteresis. However, further analyses should be done to fully understand the impact of 3DPDS-fa on the filler network and its possible impact on polymer-filler interactions.

3 Comparison of 3DPDS-fa with other resins

This chapter is divided in two subsections. The first part is dedicated to the testing of compounds prepared with the dibenzoxazines described in the previous chapters. The performance of 3DPDS-fa and phenolic resin are compared in the last subsection

3.1 Comparison with additional dibenzoxazine precursors

In this section is described the investigation of additional dibenzoxazines as potential reinforcing resins in carbon black filled compounds. Each benzoxazine was tested in the model formulation commonly employed in apex compounds shown in Table IV.1. The curing behavior of the compounds was evaluated by MDR. The cure curves are displayed in Annex F (Figure F.5) and the main data summarized in Table IV.7. Then, the samples were cured at the determined t_{90} and the mechanical properties assessed by tensile test. The stress-strain curves are displayed in Figure IV.19a.

Table IV.7. MDR data for compounds with carbon black and diBz.

Abbr.	S'_{\min} (dN·m)	S'_{\max} (dN·m)	t_{s1} (min)	t_{90} (min)
PI(CB) ₈₀	3.72	46.03	2.16	16.18
PI(CB) ₈₀ (3DPDS-fa) ₁₅	3.07	52.87	3.92	24.65
PI(CB) ₈₀ (4DPDS-fa) ₁₅	2.97	32.16	3.57	19.44
PI(CB) ₈₀ (4DTP-fa) ₁₅	3.33	41.86	4.56	34.23
PI(CB) ₈₀ (BA-fa) ₁₅	3.26	38.07	2.01	30.44

At low strain, all the tested Bz reinforce the filled compounds as attested by the increase of the Young moduli in comparison to the reference (PI(CB)₈₀). This behavior is observed until a

specific point where an inversion between the two curves occurs. This inversion takes place around 15% for the compound with 4DPDS-fa resulting in a detrimental impact of its mechanical properties. This behavior occurs at much lower strain for 4DPDS-fa compounds than for the other materials with 3DPDS-fa (~110%), 4DTP-fa (~65%), and BA-fa (~40%). The loss of reinforcement observed is presumably due to a sulfur consumption as discussed previously in section 2.1.3. The tensile test results are in accordance with the crosslinking density being higher for the compounds that show the best reinforcement at high strain (Table IV.8). The lowest v_c was obtained for PI(CB)₈₀(4DPDS-fa)₁₅ indicating the most pronounced sulfur consumption is occurring when 4DPDS-fa is used in agreement with the discussion in Chapter III.

Interestingly, the stress-strain curve of PI(CB)₈₀(4DPDS-fa)₁₅ is similar to the curve of the compound with lower amount of sulfur (2.8 phr) as shown in Figure IV.8a. Indeed, PI_{2.8}(CB)₈₀(3DPDS-fa)₁₅ exhibit similar ultimate tensile properties ($\epsilon_{\text{break}} = 225\%$ and $\sigma_{\text{break}} = 14$ MPa) than PI(CB)₈₀(4DPDS-fa)₁₅ ($\epsilon_{\text{break}} = 234\%$ and $\sigma_{\text{break}} = 15$ MPa). This gives an additional evidence that the lack of reinforcement for 4DPDS-fa compound is clearly due to the consumption of sulfur preventing an adequate vulcanization of the rubber and thus, leading to a compound with poor mechanical properties.

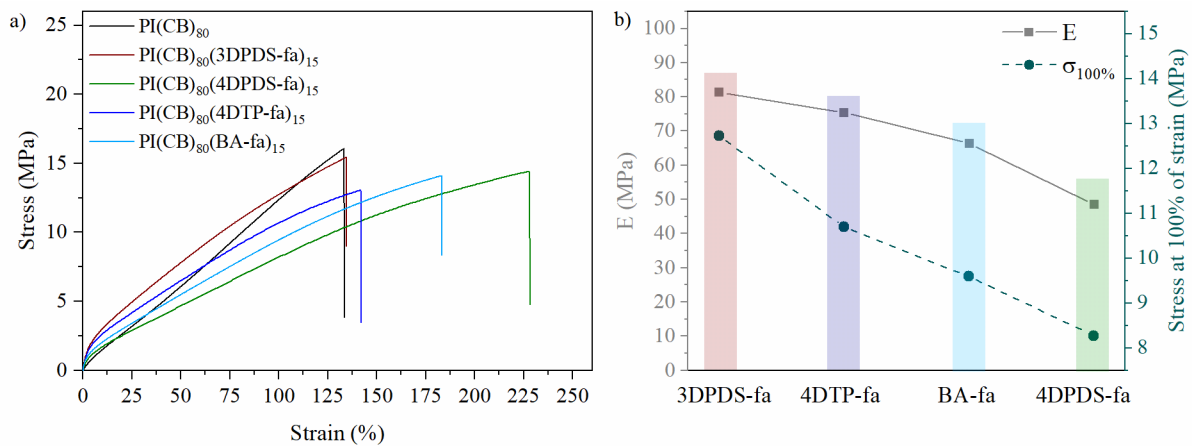


Figure IV.19. a) Stress-strain curve of rubber compounds with 15 phr of diBz and 80 phr of CB; b) Evolution of E and $\sigma_{100\%}$ for the compounds.

In conclusion, the incorporation of 3DPDS-fa leads to the most significant reinforcement and the use of 4DPDS-fa to the worst. These results are in agreement with those discussed in Chapter III. The overall reinforcing effect increases as follows PI(CB)₈₀(3DPDS-fa)₁₅ > PI(CB)₈₀(4DTP-fa)₁₅ > PI(CB)₈₀(BA-fa)₁₅ > PI(CB)₈₀(4DPDS-fa)₁₅. A summary of the mechanical properties by tensile test is gathered in Table IV.8.

Table IV.8. Summary of the tensile test data and crosslinking density for compounds with CB and diBz.

Abbr.	E (MPa)	$\sigma_{15\%}$ (MPa)	$\sigma_{25\%}$ (MPa)	$\sigma_{50\%}$ (MPa)	$\sigma_{100\%}$ (MPa)	σ_{break} (MPa)	$v_c \cdot 10^{-4}$ (mol·cm ⁻³)
PI(CB) ₈₀ (3DPDS-fa) ₁₅	81.4±1.4	3.69±0.04	4.91±0.04	7.77±0.05	12.72±0.02	15.3±0.1	5.27±0.03
PI(CB) ₈₀ (4DPDS-fa) ₁₅	48.6±0.5	2.13±0.02	2.89±0.03	4.70±0.05	8.27±0.08	14.7±0.3	3.53±0.03
PI(CB) ₈₀ (4DTP-fa) ₁₅	75.4±2.4	3.13±0.02	4.11±0.02	6.47±0.02	10.69±0.02	13.1±0.1	4.62±0.06
PI(CB) ₈₀ (BA-fa) ₁₅	66.4±0.9	2.58±0.04	3.48±0.06	5.60±0.09	9.59±0.12	14.1±0.1	4.95±0.05

3.2 Comparison with traditional phenolic resins

Finally, the effect of 3DPDS-fa as potential reinforcing resins in carbon black filled compounds is compared to traditional phenolic resins (PR). For that purpose, a phenolic system composed of a precondensed novolac resin and hexamethylenetetramine (HMT), as *in-situ* crosslinker, were mixed with the model formulation used for apex compound previously described and depicted in Table IV.9. In addition to the common recipe where 15 phr of PR are used so-called PI(CB)₈₀(PR)₁₅, another reference was prepared where 7 phr of PR are employed (PI(CB)₈₀(PR)₇). This additional compound, which contained a lower amount of PR, corresponds to the equimolar amount in relation to 15 phr of 3DPDS-fa. Like that, the number of reactive sites for both resins were kept constant.

Table IV.9. Formulation of compounds with PR system and carbon black.

Ingredients	Amount (phr)	
Polyisoprene	100	100
Carbon black (CB)	80	80
TDAE oil ^a	5	5
Phenolic resin (PR)	15	7
HMT ^b	3	1.4
Sulfur	5.5	5.5
Zinc oxide (ZnO)	5	5
Stearic acid	2	2
DCBS ^c	3	3

^a Treated Distillate Aromatic Extracted, commonly used processing rubber oil; ^b Hexamethylenetetramine, *in-situ* crosslinker; ^c N,N'-dicyclohexyl benzothiazole-2-sulfenamide.

This chapter reports a comparative analysis of the curing behavior and the mechanical properties of compounds with both resins: 3DPDS-fa and PR.

3.2.1 Curing behavior by MDR

The cure curves of the compounds with PR are displayed in Annex F (Figure F.6) and the main data summarized in Table IV.10 together with the reference without resin (PI(CB)₈₀) and with 3DPDS-fa (PI(CB)₈₀(3DPDS-fa)₁₅).

Table IV.10. MDR data for compounds with carbon black, 3DPDS-fa and PR.

Abbr.	S' _{min} (dN·m)	S' _{max} (dN·m)	t _{s1} (min)	t ₉₀ (min)
PI(CB) ₈₀	3.72	46.03	2.16	16.18
PI(CB) ₈₀ (3DPDS-fa) ₁₅	3.07	52.87	3.92	24.65
PI(CB) ₈₀ (PR) ₁₅	3.50	75.26	1.17	19.34
PI(CB) ₈₀ (PR) ₇	3.50	66.25	1.45	15.69

The incorporation of PR leads to a slight decrease of the minimum torque (S'_{\min}) and therefore, to a limited improvement in the processability of the tire parts before the vulcanization. By contrast, the presence of 3DPDS-fa resulted in a more pronounced decrease of the S'_{\min} acting as a more efficient plasticizer than the PR at 150 °C. The lower molecular weight of 3DPDS-fa in comparison to the precondensed PR could be a possible explanation for the more effective plasticization. Furthermore, the addition of the phenolic system to the compounds decreases the scorch time most probably, due to the well-known catalytic effect from HMT, the *in-situ* crosslinker.²⁰⁰ Therefore, the use of PR leads to a penalty in processing not observed in the case of 3DPDS-fa. Finally, the maximum torque (S'_{\max}) was found to be higher when the PR were incorporated.

3.2.2 Tensile test

The compounds with and without PR were cured at the determined t_{90} and the mechanical properties assessed by tensile test. The stress-strain curves of compounds without and with either PR or 3DPDS-fa are displayed in Figure IV.20a. The addition of both resins to filled materials leads to a similar increase of Young modulus and tensile modulus at low strain ($\sigma_{15\%}$) indicating a higher stiffness of the compounds, which is a characteristic behavior of reinforcing resins. At high strain (i.e. $\sigma_{50\%}$), compounds with PR show slightly higher tensile moduli than the compound with the Bz. From an overall perspective, analogous performance is observed with the use of both resins (Figure IV.20a). These results are promising and highlight the use 3DPDS-fa as a possible alternative to phenolic resins to reinforce filled compounds.

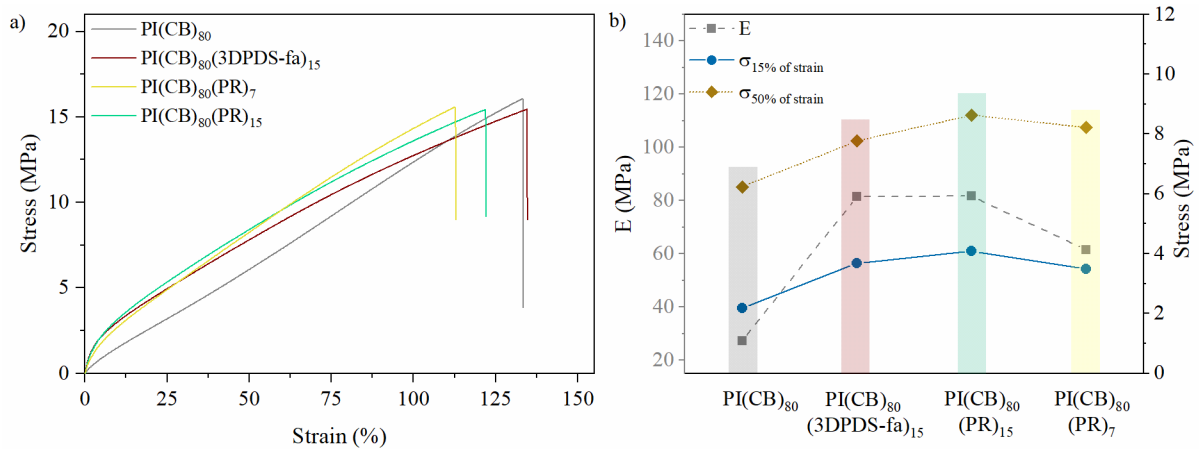


Figure IV.20. a) Stress-strain curves of rubber compound with 80 phr of CB with and without reinforcing resins; b) Evolution of E , $\sigma_{15\%}$ and $\sigma_{50\%}$ for the compounds.

One of the main parameters to be enhanced in 3DPDS-fa compounds to compensate the performance at high strain is the sulfur content. A comparison between 3DPDS-fa materials with higher sulfur amount ($PI_{6.9}(CB)_{80}(3DPDS-fa)_{15}$), the reference ($PI(CB)_{80}$), and the compound containing PR ($PI(CB)_{80}(PR)_{15}$) is shown in Figure IV.21a. The evolution of the stress over the strain range is the same for both compounds containing the resins (Figure IV.21b). These results further show the feasibility to employ benzoxazines precursors to replace phenolic resins as reinforcing agents for tire applications.

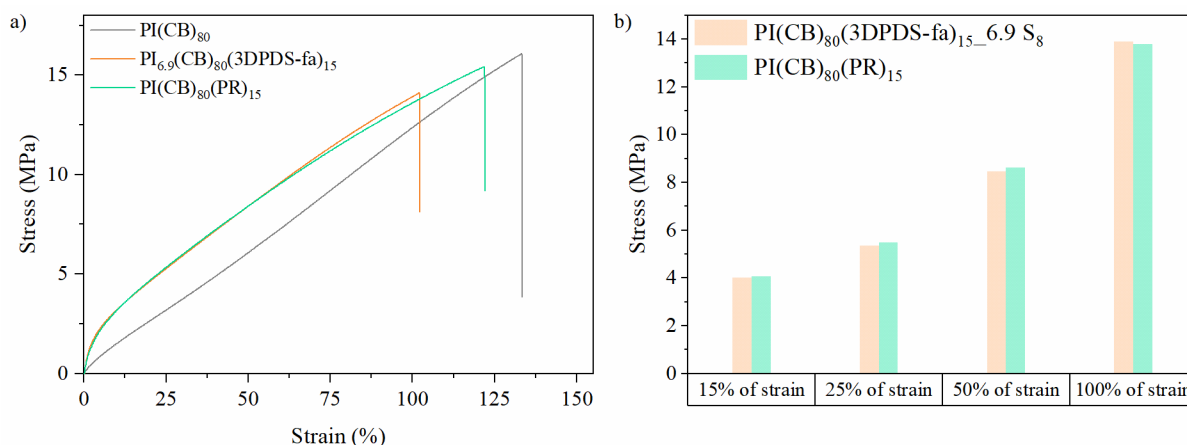


Figure IV.21. a) Stress-strain curves of rubber compound with 80 phr of CB with and without PR, and with 3DPDS-fa with 6.9 phr of sulfur; b) Stress responses at 15, 25, 50, and 100% of strain.

Finally, the mechanical properties of the compounds with phenolic resins are summarized in Table IV.11.

Table IV.11. Summary of the tensile test data and crosslinking density for compounds with CB and PR.

Abbr.	E (MPa)	$\sigma_{15\%}$ (MPa)	$\sigma_{25\%}$ (MPa)	$\sigma_{50\%}$ (MPa)	$\sigma_{100\%}$ (MPa)	σ_{break} (MPa)	ϵ_{break} (%)
PI(CB) ₈₀ (PR) ₇	61.4±1.9	3.48±0.01	4.87±0.02	8.22±0.04	14.36±0.03	14.6±0.2	123±4
PI(CB) ₈₀ (PR) ₁₅	81.7±1.9	4.09±0.09	5.5±0.1	8.62±0.15	13.81±0.15	15.4±0.1	119±2

3.2.3 Dynamic mechanical analysis

DMA tests were carried out in two modes: strain sweep at 25 and 70 °C and temperature sweep from -100 to 200 °C.

DMA strain sweep

The evolution of G' , G'' , and $\tan\delta$ as a function of strain at 25 and 70 °C of PI(CB)₈₀, PI(CB)₈₀(3DPDS-fa)₁₅ and PI(CB)₈₀(PR)₁₅ is shown in Figure IV.22.

The use of PR in combination with CB leads to higher storage moduli over the whole range of strain amplitudes when compared to the G'_{Ref} , but lower than $G'_{3DPDS-fa}$. The increment of G' is occurring together with the rise of $\Delta G'$ (Payne effect) up to 200% for PI(CB)₈₀(PR)₁₅ respect to PI(CB)₈₀. The Payne effect was quantified using Kraus model, and the fitting parameters, γ_c and m were determined. The obtained curves are plotted in Figure IV.22 showing a good fitting with the experimental data (dashed and dotted lines). Similar values of m , between 0.2 and 0.3, were obtained for the compounds with and without phenolic resin in opposition to the results obtained for compounds with 3DPDS-fa. These results might be explained by a different impact of the PR on the formation of the CB network in comparison to the effect of the benzoxazine resin ($m = 0.5$). The critical strain (γ_c) corresponds to the main change in G' which occurs around 1 and 2% for compounds containing PR similarly than for PI(CB)₈₀(3DPDS-fa)₁₅ (~2%). The main information for PI(CB)₈₀(PR)₁₅ is summarized in Table IV.12.

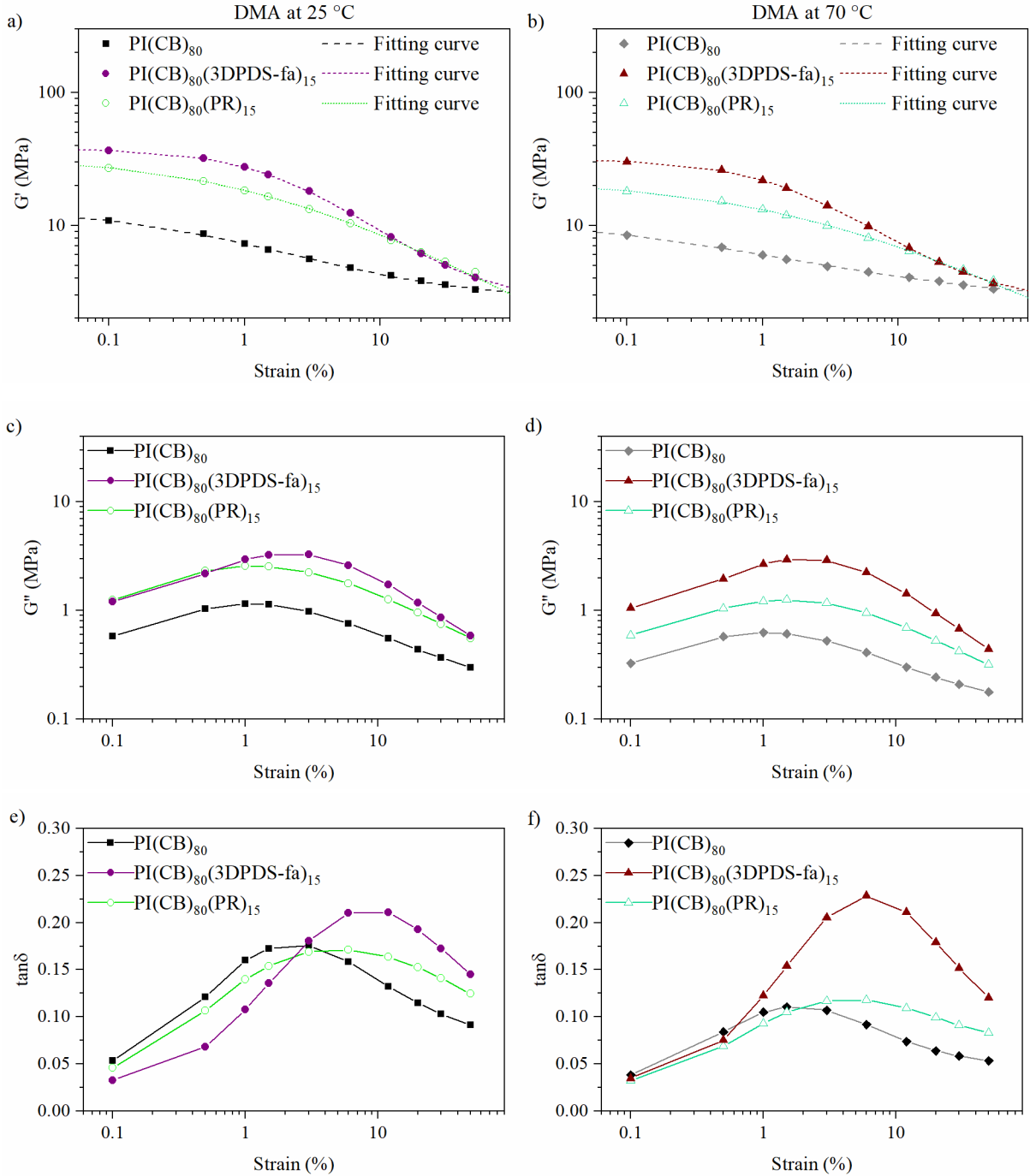


Figure IV.22. Strain sweeps at 25 °C (on the left) and at 70 °C (on the right) of compounds with 80 phr of CB and with and without 15 phr of 3DPDS-fa or PR; a) b) G' and fitting curve by Kraus model; c) d) G'' , and e) f) $\tan\delta$ (in G'' and $\tan\delta$ the line is to guide the eye).

Table IV.12. Viscoelastic results from DMA test in strain sweep mode for compounds with CB and PR.

Abbr.	25 °C					70 °C				
	$\Delta G'$ MPa ^a	$G'_{6\%}$ MPa	$G''_{6\%}$ MPa	$\tan\delta_{6\%}$	γ_c / m^b	$\Delta G'$ MPa ^a	$G'_{6\%}$ MPa	$G''_{6\%}$ MPa	$\tan\delta_{6\%}$	γ_c / m^b
PI(CB) ₈₀ (PR) ₁₅	22.64	10.4	1.8	0.17	1.4 / 0.3	14.3	8.1	1.0	0.12	2.0 / 0.2

^a $\Delta G' = G'_{0.1\%} - G'_{50\%}$. ^b Fitting parameters from Kraus model.

Furthermore, a similar dissipation of energy of the network breakdown is observed at 25 °C for the compounds with and without PR attested by the comparable values of $\tan\delta_{6\%}$ around 0.17

in both cases. At 70 °C, the $\tan\delta_{6\%}$ of $\text{PI}(\text{CB})_{80}(\text{PR})_{15}$ is 33% higher than for $\text{PI}(\text{CB})_{80}$ but 50% lower than the compound with 3DPDS-fa. The use of both resins led to an increase on the hysteresis with respect to the reference due to probably the formation of a stiffer filler network. The main difference between the performance of the PR and 3DPDS-fa that has a direct impact on the loss factor, is the evolution of G'' with temperature. Indeed, at high temperature the loss modulus of $\text{PI}(\text{CB})_{80}(\text{PR})_{15}$ decreases while for $\text{PI}(\text{CB})_{80}(3\text{DPDS-fa})_{15}$ is maintained constant leading to a comparable higher hysteresis for the compound with benzoxazine. In addition to the stiffer filler network, $\text{PI}(\text{CB})_{80}(3\text{DPDS-fa})_{15}$ exhibits greater viscous contribution leading to a higher dissipation of heat and, thus raising the hysteresis.

To further understand the observed effect of temperature, DMA temperature sweep tests are reported in the next section.

DMA temperature sweep

The temperature dependence of viscoelastic behavior from the glassy state to the rubbery state is shown in Figure IV.23 and the results are summarized in Annex F (Table F.1).

Similar tendency of E' , E'' , and $\tan\delta$ over the temperature range is observed for compounds containing PR and 3DPDS-fa. The main difference is the evolution of E'' above 50 °C. In fact, the loss modulus of $\text{PI}(\text{CB})_{80}(\text{PR})_{15}$ decreases with increasing temperature in a comparable fashion than the reference ($\text{PI}(\text{CB})_{80}$). On the contrary, as discussed previously, the E'' of $\text{PI}(\text{CB})_{80}(\text{PR})_{15}$ remains constant between 25 to 100 °C and above this temperature increases explaining the differences observed for the compounds with both resins.

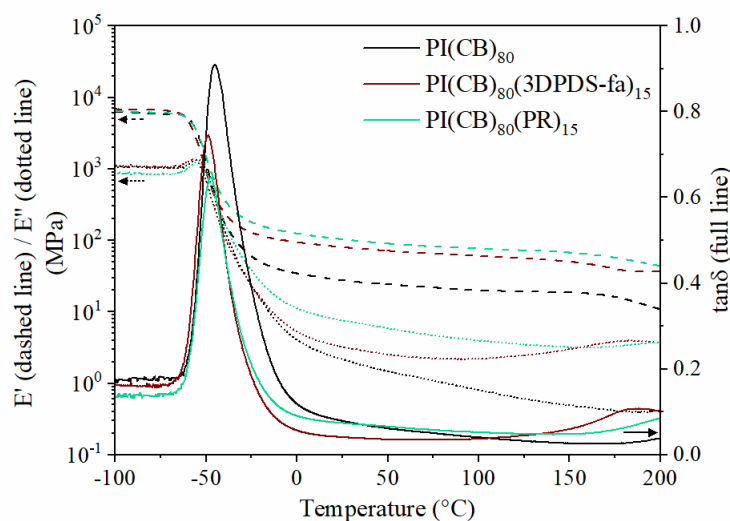


Figure IV.23. DMA temperature sweep of compounds with 80 phr of CB and with and without 15 phr of 3DPDS-fa or PR (E' dashed line; E'' dotted line; $\tan\delta$ full line).

3.2.4 Cyclic tensile test

Finally, cyclic tensile tests at 50% of strain were carried out on the final compounds with 15 phr of PR and compared to the samples with 3DPDS-fa (Figure IV.24). The stress-strain curve of rubber compounds under cyclic loading shows stress softening and hysteresis loop due to viscoelasticity.²⁰¹ The area of the loop represents the energy loss, hysteresis, per unit volume in

a deformation cycle. The energy loss is more pronounced during the first cycles until a stabilized hysteresis loop is then reached.

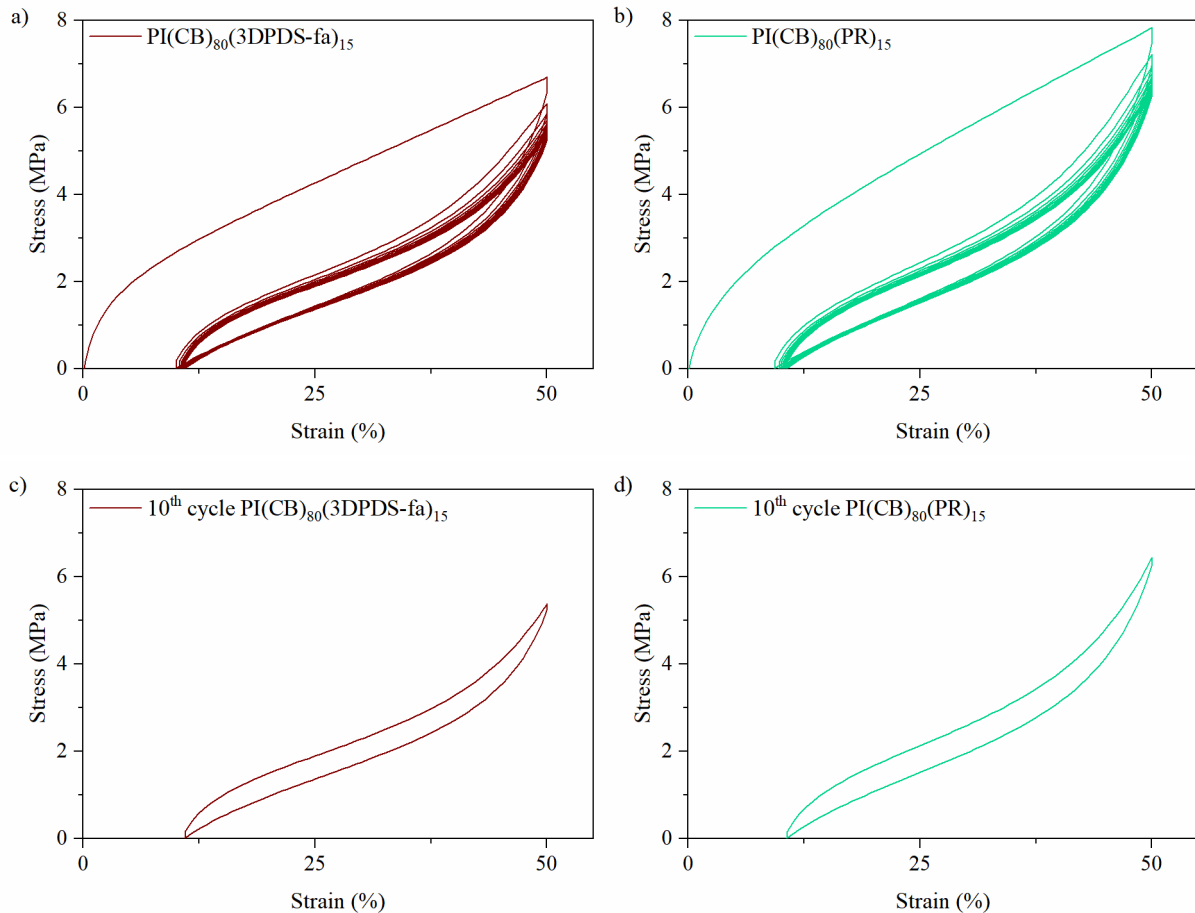


Figure IV.24. Stress-strain hysteresis loops of cyclic test of a) $\text{PI}(\text{CB})_{80}(\text{3DPDS-fa})_{15}$, and b) $\text{PI}(\text{CB})_{80}(\text{PR})_{15}$; Stabilized stress-strain hysteresis loop after 10th cycles of c) $\text{PI}(\text{CB})_{80}(\text{3DPDS-fa})_{15}$, and d) $\text{PI}(\text{CB})_{80}(\text{PR})_{15}$.

The hysteresis from the stabilized loop was used to determine the energy loss from the samples with 15 phr of resin. The incorporation of 3DPDS-fa led to an energy loss of 20 MJ/m³ while 23 MJ/m³ were found for the compound with PR. Even though a higher hysteresis was observed for the compounds with 3DPDS-fa by DMA, the energy loss after several cycles was found to be comparable with the compounds with PR. These results highlight the feasibility to use 3DPDS-fa to replace PR in tire compounds.

3.3 Discussion

In summary, the incorporation of 3DPDS-fa leads to compounds that exhibited better mechanical properties compared to the performance of the other dibenzoxazines as reinforcing resin. These results are in agreement with previously reported outcomes for unfilled rubber system.

Additionally, 3DPDS-fa showed comparable compound mechanical properties to traditional phenolic resins. It is important to highlight that PR was already optimized for use in the tire industry. For this reason, optimization of the formulation could be beneficial to enhance the performance of 3DPDS-fa. Indeed, an increase of sulfur content in compounds with 3DPDS-fa, results in materials with the same stress-strain curves than compounds containing PR. These

results confirmed the feasibility to use 3DPDS-fa to replace phenolic resins as reinforcing agents for tire applications. Finally, compounds containing 3DPDS-fa exhibited comparable hysteresis after cyclic loading than their counterparts containing PR.

4 Conclusion

This first part of the chapter is dedicated to the investigation of 3DPDS-fa on CB-filled tire compounds with a variety of filler and resin contents. After the compounding, the effect of 3DPDS-fa on the curing of the green compounds was evaluated resulting in an increase of the scorch and optimum curing time. A reduction of the viscosity of the green compounds was also observed with increasing 3DPDS-fa content indicating a potential improvement on the processability of the tire parts before the curing. The compounds were then vulcanized at their respective t_{90} values and were subjected to the study of quasi-static and dynamic mechanical properties as well as nanomechanical and morphological measurements. The full characterization of the compounds with and without 3DPDS-fa led to the following conclusions.

The addition of 3DPDS-fa in filled compounds leads to an improvement of their mechanical properties attested by the increase of the stiffness of the materials and therefore, reinforcing filled rubber compounds. Specifically, the incorporation of 3DPDS-fa results in the formation of a hybrid network between the crosslinked polyBz and the CB confirmed by cyclic tests and DMA. This hybrid network is stiffer and more brittle due to the presence of the polyBz. Therefore, there is a relation between the filler content and the reinforcing effect of 3DPDS-fa. In highly filled compounds (≥ 50 phr of CB), the addition of the diBz enhanced the mechanical properties of the materials, while it has almost no impact on lowly filled counterparts (20 phr of CB). The presence of a hybrid percolated network explained these differences as the combination of the effect of the filler and 3DPDS-fa is synergistic.

The incorporation of 3DPDS-fa also leads to a sulfur consumption demonstrated by the lower values of crosslinking densities, stress at high strain, and modulus of the rubber phase with increasing 3DPDS-fa content. However, this effect could be overcome with additional sulfur content in the formulation without a detrimental impact on the overall mechanical properties.

The use of 3DPDS-fa resulted in compounds that exhibit higher hysteresis when compared to the reference without 3DPDS-fa. Several hypotheses could explain the higher dissipation of energy: (1) the formation of a stiffer hybrid network with higher brittleness due to the presence of a polyBz, (2) the lower crosslinking density because of the sulfur consumption resulting in a decrease of the amount of covalent bonds, and (3) presence of unpolymerized benzoxazine or benzoxazine oligomers with low relaxation temperature due to unfinished curing or from the reaction with sulfur. Possible solutions could be proposed to tackle this behavior such as: (1) optimization of the formulation such as sulfur content, amount and type of accelerator, etc., and (2) the design of benzoxazine precursor with additional functionalities that could create chemical links between the resin and the rubber and therefore, decreasing the energy dissipation.

The second part of the chapter gathered the comparison of the performance of compounds with 3DPDS-fa with additional benzoxazine resins (4DPDS-fa, 4DTP-fa, and BA-fa) and traditional phenolic resin to reinforce apex compounds. 3DPDS-fa led to compounds that

exhibit the best mechanical properties among all the diBz tested. 4DPDS-fa showed the worst reinforcing effect due to a higher sulfur consumption leading to a detrimental impact similarly than observed for unfilled rubber system. Furthermore, 3DPDS-fa showed comparable reinforcing effect than traditional phenolic resins confirming the feasibility to employ 3DPDS-fa to replace phenolic systems as reinforcing resins in rubber compounds. This work also shows the possibility to replace petroleum-based resins by a more sustainable solution with around 35% of bio-based content. The results showed 3DPDS-fa is not only interesting due to its reinforcement capabilities but also for the renewable added value.

Overviewing all the results it can be concluded that polybenzoxazines are a good alternative to traditional phenolic resins to reinforce rubber compounds for tire applications. This work highlights the importance of the chemical structure of the benzoxazines to ensure the curing kinetics fit rubber vulcanization, together with the requirement of good interaction between the benzoxazines and carbon black. Moreover, thanks to the rich molecular design flexibility of benzoxazine resins, partial replacement of non-renewable resin could be performed by a careful design of the precursors resulting in enhancement of the sustainability. Finally, part of the results described in this chapter has led to the filing of a provisional patent application.²⁰²

General conclusion

This work addressed the different problematics considered for the use of polybenzoxazines as potential alternatives to phenolic resins to reinforce rubber compounds. In this context, the synthesis of traditional and new molecules was foreseen to investigate the impact of the curing package ingredients on the polymerization of the benzoxazine precursors. Novel disulfide-containing dibenzoxazines (diBz) were designed and successfully synthesized from the reaction of 4,4'-dihydroxydiphenyl disulfide (4DPDS) and 3,3'-dihydroxydiphenyl disulfide (3DPDS) with furfurylamine (fa), aniline (a), and stearylamine (ste). Moreover, additional benzoxazines were also synthesized using 4,4'-thiodiphenol (4TDP) and bisphenol A (BA) in combination with furfurylamine and aniline to yield diBz monomers with one or non-heteroatom of sulfur respectively. All the diBz were synthesized through a one-step reaction leading to high yield and high purity compounds.

The thermal properties and polymerization kinetics in the absence and presence of the curing package demonstrated that diBz prepared from furfurylamine showed the most interesting combination of properties. They exhibited relatively low melting points below 100 °C and were able to polymerize in relatively short times (between 13 and 41 minutes). Additionally, the presence of sulfur decreases more than half the curing time of the precursors (between 9 and 16 min) allowing a better fit to vulcanization times in the tire industry. These results indicated that sulfur is an efficient catalyst to overcome the long curing times commonly required for benzoxazine resins. Even though it could also lead to a side-reactions with the benzoxazines, the presence of an inherent catalyst is a clear asset for the use of reinforcing systems based on polybenzoxazines. Moreover, polybenzoxazines with furan groups exhibited higher T_g (~260 °C) than currently used phenolic resins (~170 °C) showing the potential of these diBz to be used as reinforcing resins.

Among the set of resins synthesized and characterized, precursors prepared from furfurylamine and sulfur-containing diphenols were selected (4DPDS-fa, 3DPDS-fa, and 4TDP-fa) as they are the most promising monomers. In addition, thanks to the use of furfurylamine, the carbon footprint of the monomer was significantly reduced with a bio-based content of about 35%.

The ability of the selected benzoxazines to reinforce rubber was tested in recipes without carbon black, so-called unfilled compounds. After a thorough assessment of the results, two distinctives performances were observed and the following conclusions were drawn:

- On the one side, 4DPDS-fa yields a side-reaction when heated in the presence of sulfur probably due to a low stability of the disulfide bond during the rubber curing. This side-reaction drives the consumption of sulfur impeding the effective curing of the polyisoprene network and therefore, resulting in a detrimental impact of the mechanical properties of the rubber compounds containing 4DPDS-fa.
- On the other hand, 3DPDS-fa and 4TDP-fa reinforce unfilled compounds. The incorporation of 15 phr of these precursors does not interfere with the curing of polyisoprene, but the presence of sulfur significantly catalyzes their polymerization. AFM reveals the appearance of nodules dispersed in the rubber matrix confirming the

formation polyBz simultaneously with the rubber curing and thus, improving the mechanical properties of the unfilled compounds. Nevertheless, high content of these precursors (≥ 30 phr) leads to a slightly consumption of sulfur not observed with lower amounts of these monomers.

- Among the tested precursors, 3DPDS-fa exhibited the most significant improvement of the mechanical properties combining high stiffness with high elasticity. The unfilled compounds with 3DPDS-fa showed better mechanical properties than materials prepared with resins reported in the prior art such as a model benzoxazine or a traditional phenolic resin.

The results obtained from the characterization of unfilled compounds prepared with benzoxazine show the feasibility to employ novel precursors with the objective of mechanical reinforcement. Similar, but more significant trends were found in carbon black (CB) filled compounds leading to the following conclusions:

- The addition of 3DPDS-fa in filled compounds led to the formation of a stiffer hybrid polyBz/carbon black network while improving the processability of the tire parts before the curing. When a suitable amount and ratio of both of them is reached, a percolated hybrid is formed leading to an improvement of the mechanical properties beyond the expectations, revealing a synergistic effect is occurring.
- As a consequence of the formation of a hybrid network with higher stiffness, the compounds prepared with 3DPDS-fa exhibit higher hysteresis compared to the reference. This higher energy loss might be associated to an irreversible breakage of the hybrid network leading to a decrease of the elasticity of the network resulting in a permanent deformation.
- 3DPDS-fa also led to a slight sulfur consumption resulting in materials with low crosslinking density. Nevertheless, this behavior could be overcome with the increment of this ingredient on the formulation without a detrimental impact on the overall mechanical properties.
- When 3DPDS-fa is used, the reinforcement of the filled compounds is similar to what is obtained with traditional phenolic resins, therefore confirming the suitability to employ 3DPDS-fa instead of phenolic systems in rubber compounds.

These results confirmed the feasibility to employ novel benzoxazines precursors to reinforce rubber compounds going beyond the state of the art. This work highlights the importance of the chemical structure of the benzoxazines as a major parameter to address in order to propose alternative reinforcing systems. The curing kinetics of the monomers in the presence of sulfur was also found of great significance. This inherent catalyst enabled the polymerization of benzoxazines to fit rubber vulcanization and thus, allowing their polymerization simultaneously to the rubber curing. Moreover, suitable interactions between the benzoxazine resins and carbon black are desirable for the formation of hybrid network leading to an enhancement of their performance. Finally, this study spotlights the possibility to replace non-renewable resins by partially bio-based precursors, leading to a more sustainable alternative than traditional resins and therefore, improving the circular economy.

Outlook for future research

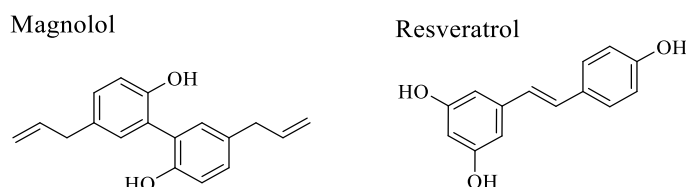
The main objective of this thesis was achieved by the development of new polymeric reinforcements based on polybenzoxazines to replace traditional reinforcing resins in tire compounds. Nevertheless, additional investigations are still needed to optimize the proposed reinforcing system.

Regarding the monomer characterization, the thermal stability of the benzoxazines, particularly 4DPDS-a and 3DPDS-a, could be further studied under a closer environment than the actual curing conditions by doing isothermal TGA at the cure temperature and in air. This could allow identifying if the monomers degrade in a different way in the presence of oxygen. Additionally, TGA-FTIR or TGA-MS could be used to differentiate between polymerization, vaporization of residual monomer, production of byproducts the polymerization, etc.

Another important concern is the release of byproduct during the curing of traditional resins. In this context, benzoxazine resins could be a key player due to their well-known low release of chemical compounds during their polymerization, in particular formaldehyde. Preliminary assessment showed improvement of this subject when compared to phenolic resins. Nevertheless, additional investigation should be performed to draw reliable conclusions regarding this topic.

The reaction between benzoxazines and sulfur could be further investigated. The curing each benzoxazine can be performed in the presence of sulfur to elucidate the reaction mechanism for each benzoxazine.

The sustainability of the resins could be enhanced by considering the use of benzoxazines containing a higher content of carbon atoms originating from renewable resources. The rich molecular design flexibility of benzoxazines allows to further increase this bio-based content. The employment of bio-based diphenolic compounds for the synthesis of the diBz is a good approach. It is noteworthy that the chemical structure, polymerization kinetic, as well as the interaction between the precursors and the filler, are major factors to be investigated to ensure a good performance in rubber compounds as highlighted in this work. The chemical structures of potential diphenolic compounds from natural resources are schematized in the following figure. However, it is important to highlight that this is a fundamental approach and the use these reagents for tire application might not be feasible due to the low availability in the market and their high prices compared.

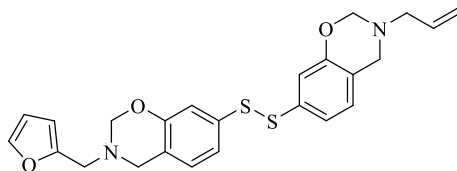


Chemical structures of magnolol and resveratrol as potential bio-based diphenolic compounds to produce diBzs.

This work was focused on carbon-black filled compounds. To further understand the role of the benzoxazine resins in the processing of the filled compounds, it could be desirable to follow

the torque curves during the mixing. This could enable to measure the mixing energy during compounding and therefore, to evaluate the impact of each benzoxazine.

One of the main shortcomings of using 3DPDS-fa to reinforce CB-filled rubber is the high hysteresis. The high dissipation of energy can be explained by the irreversible breakage of the stiffer hybrid network. Several approaches could be carried out to enhance this performance. The optimization of the recipe used could be a first step to perform. Another possibility is to enhance the interactions between the rubber and filler network to prevent the permanent breaking by improving their interphase. This could be address with the introduction of functional groups able to react with the rubber during the vulcanization to create covalent bonds and therefore, potentially decrease the hysteresis. The first approach could be to valorize the results reported along this manuscript regarding the possibility to reduce the disulfide bond from 4DPDS-fa.¹⁹⁶ On the one hand, the cleavage of the S–S might generate sulfur radicals able to react with rubber and therefore, covalently bond Bz moieties onto the polymer chain. The problem of this strategy is that the reduction of the disulfide from 4DPDS-fa prevents this precursor to reinforce rubber compounds. On the contrary, the use of 3DPDS-fa leads to high dynamic modulus together with high hysteresis probably due to the high stability of its disulfide bond. For this reason, one idea could be to find a compromise between these two monomers to develop rubber compounds with the required reinforcement together with a potential decrease of the hysteresis. Additionally, a careful design of new benzoxazines precursors could be performed by the incorporation of functional groups such as double bonds. For example, asymmetric dibenzoxazines could be synthesized with furfurylamine and allylamine as shown in the following scheme. The furfuryl moieties might ensure an effective reinforcement while the double bonds from allylamine might react with the rubber and create chemical bonds.



Schematic representation of a possible diBz precursor with additional groups.

Additionally, silica filled compounds are another major family of reinforced materials with additional properties in comparison to CB-compounds. The novel benzoxazines could be also tested in silica-containing materials. Preliminary results showed the feasibility of 3DPDS-fa to act as a reinforcing resin in silica compounds. However, further investigation should be carried out in order to understand the system and the possible interactions between the polyBz and the silica as both have polar groups in their structures.

In the frame of this work, the synthesis of the benzoxazine precursors was carried out at the lab-scale, with a production not higher than 15 grams. This scale of production is not suitable for a real tire testing, which would require to scale up the synthesis. For this reason, another possible future step of this project will be to test the new resin in a real tire. In order to achieved that, the first task will be to scale-up the reaction enabling the mixing at industrial scale, followed by the assembly with additional parts of the tire. This will allow the evaluation of the real impact of the new material in the rolling resistance of the tire as it is estimated that hysteresis account for about 80-95% of this important parameter in tire industry.

Overviewing the outlook of this project, several approaches could be carried out to improve the performance of the use of benzoxazine resins for tire applications. Additionally, the versatility of polybenzoxazines allows the possibility to find more sustainable and suitable solutions by the careful design and selection of the reagents. Finally, the employment of benzoxazine precursors in silica-reinforce compound could open the possibility to enlarge the application of these new materials in the rubber industry. In conclusion, the investigations described in this work provide a first guide on how to design and use benzoxazine to reinforce rubber compounds. However, there is still a lot to do to compete in the arena of tire compounds.

References

1. Rodgers, B., *Rubber Compounding. Chemistry and Applications*. 2nd ed.; CRC Press: 2016.
2. Rodgers, B.; Waddell, W., Tire Engineering. In *The Science and Technology of Rubber*, Inc, E., Ed. United States of America, 2013.
3. Rodgers, B.; Waddell, W., The Science of Rubber Compounding. In *The Science and Technology of Rubber*, Elsevier: 2013.
4. Gardziella, A.; Pilato, L. A.; Knop, A., *Phenolic Resins: Chemistry, Applications, Standardization, Safety and Ecology*. 2000.
5. Dick, J. S., *Rubber Technology: Compounding and Testing for Performance*. Carl Hanser Verlag GmbH & Company KG: 2014.
6. Duddey, J. E. Tire with apex rubber containing in-situ resin. US 6,467,520, 2002.
7. Syed, I. H.; Klat, D.; Braer, A.; Fleck, F.; Lacayo-Pineda, J., Characterizing the influence of reinforcing resin on the structure and the mechanical response of filled isoprene rubber. *Soft Materials* **2018**, *16* (4), 275-288.
8. Gardziella, A.; Pilato, L. A.; Knop, A., Economic Significance, Survey of Applications, and Six Bonding Functions. In *Phenolic Resins: Chemistry, Applications, Standardization, Safety and Ecology*, Springer Berlin Heidelberg: Berlin, Heidelberg, 2000; pp 122-487.
9. Shepard, A. F.; Boiney, J. F. Rubber-phenolic resin composition. US 2,532,374, 1950.
10. Agency, E. C. *ANNEX XV RESTRICTION REPORT - Formaldehyde and formaldehyde releasers*; ECHA: 20 March 2019, 2019.
11. (ECHA), E. C. A. REACH. https://ec.europa.eu/environment/chemicals/reach/reach_en.htm.
12. Ishida, H., Chapter 1 - Overview and Historical Background of Polybenzoxazine Research. In *Handbook of Benzoxazine Resins*, Elsevier: Amsterdam, 2011; pp 3-81.
13. Ning, X.; Ishida, H., Phenolic materials via ring-opening polymerization: Synthesis and characterization of bisphenol-A based benzoxazines and their polymers. *Journal of Polymer Science Part A: Polymer Chemistry* **1994**, *32* (6), 1121-1129.
14. Bayram, O.; Kiskan, B.; Demir, E.; Demir-Cakan, R.; Yagci, Y., Advanced Thermosets from Sulfur and Renewable Benzoxazine and Ionones via Inverse Vulcanization. *ACS Sustainable Chemistry & Engineering* **2020**, *8* (24), 9145-9155.
15. Manuspiya, H.; Ishida, H., Chapter 36 - Polybenzoxazine-Based Composites for Increased Dielectric Constant. In *Handbook of Benzoxazine Resins*, Ishida, H.; Agag, T., Eds. Elsevier: Amsterdam, 2011; pp 621-639.
16. Jang, J.; Seo, D., Performance improvement of rubber-modified polybenzoxazine. *Journal of Applied Polymer Science* **1998**, *67* (1), 1-10.
17. Lee, Y.-H.; Allen, D. J.; Ishida, H., Effect of rubber reactivity on the morphology of polybenzoxazine blends investigated by atomic force microscopy and dynamic mechanical analysis. *Journal of Applied Polymer Science* **2006**, *100* (3), 2443-2454.
18. Suwitaningsih, D. N.; Katsuta, S.; Kawauchi, T.; Furukawa, N.; Takeichi, T., Preparation and Characterization of Liquid Rubber-modified Polybenzoxazine. *Journal of Photopolymer Science and Technology* **2015**, *28* (2), 137-143.
19. Jubsilp, C.; Taewattana, R.; Takeichi, T.; Rimdusit, S., Investigation on Rubber-Modified Polybenzoxazine Composites for Lubricating Material Applications. *Journal of Materials Engineering and Performance* **2015**, *24* (10), 3958-3968.

20. Jubsilp, C.; Rimdusit, S., Chapter 44 - Polybenzoxazine-Based Self-Lubricating and Friction Materials A2 - Ishida, Hatsuo. In *Advanced and Emerging Polybenzoxazine Science and Technology*, Froimowicz, P., Ed. Elsevier: Amsterdam, 2017; pp 945-974.
21. Kukut, M.; Kiskan, B.; Yagci, Y., Self-Curable Benzoxazine Functional Polybutadienes Synthesized by Click Chemistry. *Designed Monomers and Polymers* **2009**, *12* (2), 167-176.
22. Bai, J.; Shi, Z.; Yin, J.; Tian, M., Tailoring the Morphologies and Mechanical Properties of Styrene-Butadiene-Styrene Triblock Copolymers by the Incorporation of Thiol Functionalized Benzoxazine. *Macromolecules* **2014**, *47* (9), 2964-2973.
23. Ren, S.; Miao, X.; Song, W., Convenient preparation of flexible polysulfide rubber chain-bridged polybenzoxazine. *Polymer Journal* **2019**, *51* (4), 397-403.
24. - Rubber composition and tire JP4616187, 2010.
25. - Rubber composition and pneumatic tire. JP5005609, 2012.
26. - Benzoxazine compound and manufacturing method thereof. KR102066167, 2020.
27. Milan, F.; Marco, R. Polybenzoxazine utilisable pour le revêtement de metal et son collage a du caoutchouc. FR1562499.
28. Milan, F.; Marco, R. Renfort metallique ou metallise dont la surface est revetue d'une polybenzoxazine sulfuree. EP 3 638 745
29. Sung, D. K.; Park, H. Rubber composition containing main-chain benzoxazine, and preparation method thereof. US 10,538,648 2020.
30. Rodriguez Arza, C.; Froimowicz, P.; Ishida, H., Triggering effect caused by elemental sulfur as a mean to reduce the polymerization temperature of benzoxazine monomers. *RSC Advances* **2016**, *6* (42), 35144-35151.
31. Lin, H.-K.; Liu, Y.-L., Sulfur Radical Transfer and Coupling Reaction to Benzoxazine Groups: A New Reaction Route for Preparation of Polymeric Materials Using Elemental Sulfur as a Feedstock. *Macromolecular Rapid Communications* **2018**, *39* (8), 1700832.
32. Coran, A. Y., Chapter 7 - Vulcanization. In *The Science and Technology of Rubber (Fourth Edition)*, Mark, J. E.; Erman, B.; Roland, C. M., Eds. Academic Press: Boston, 2013; pp 337-381.
33. Liu, C.; Chen, Q. Y., Chapter 2 - Catalytic Accelerated Polymerization of Benzoxazines and Their Mechanistic Considerations A2 - Ishida, Hatsuo. In *Advanced and Emerging Polybenzoxazine Science and Technology*, Froimowicz, P., Ed. Elsevier: Amsterdam, 2017; pp 9-21.
34. Attema, P. A. J.; Los-Weijns, M. A.; Maring-van, N. D. d. P., *Palaeohistoria 47/48: Acta Et Communicationes Instituti Bio-archaeologici Universitatis Groninganae 47/48. 2005/2006*. Barkhuis: 2006.
35. Rodgers, B.; Waddell, W., Chapter 14 - Tire Engineering. In *The Science and Technology of Rubber (Fourth Edition)*, Mark, J. E.; Erman, B.; Roland, C. M., Eds. Academic Press: Boston, 2013; pp 653-695.
36. Goodyear, C. Improvement in India-rubber fabrics. US 3,633, 1844.
37. Thomson, R. W. Carriage wheel. US 5,104, 1847.
38. Dunlop, J. B. Wheel tire for cycles. US 435,995, 1890.
39. Gent, A. N.; Walter, J. D.; United, S.; National Highway Traffic Safety, A.; University of, A., *The pneumatic tire*. 2006.
40. Erdemir, A.; Holmberg, K., Energy Consumption Due to Friction in Motored Vehicles and Low-Friction Coatings to Reduce It. In *Coating Technology for Vehicle Applications*, Cha, S. C.; Erdemir, A., Eds. Springer International Publishing: Cham, 2015; pp 1-23.

41. Amos, S. E., 4 - Hollow Glass Microspheres in Rubbers and Elastomers. In *Hollow Glass Microspheres for Plastics, Elastomers, and Adhesives Compounds*, Amos, S. E.; Yalcin, B., Eds. William Andrew Publishing: Oxford, 2015; pp 107-122.
42. Sapkota, J. Influence of Clay Modification on Curing Kinetics of Natural Rubber Nanocomposites. 2011.
43. Drobny, J. G., 4 - Processing Methods Applicable to Thermoplastic Elastomers. In *Handbook of Thermoplastic Elastomers (Second Edition)*, Drobny, J. G., Ed. William Andrew Publishing: Oxford, 2014; pp 33-173.
44. Ciullo, P. A.; Hewitt, N., RUBBER PROCESSING. In *The Rubber Formulary*, Ciullo, P. A.; Hewitt, N., Eds. William Andrew Publishing: Norwich, NY, 1999; pp 49-55.
45. Manager, I. C. Tyre Manufacturing. <https://www.iloencyclopaedia.org/part-xii-57503/rubber-industry/item/389-tyre-manufacturing>.
46. Nijman, G., A Fundamental Approach of the Cord Calendering Process. *Rubber Chemistry and Technology* **2001**, 74 (4), 715-728.
47. Conzatti, L.; Costa, G.; Falqui, L.; Turturro, A., Microscopic Imaging of Rubber Compounds. In *Rubber Technologist's Handbook*, Rapra, S. i., Ed. United Kingdom, 2009.
48. Moneypenny, H. G.; Menting, K.-H.; Gragg, F. M., General Compounding. In *Rubber Compounding: Chemistry and Applications*, Rodgers, B., Ed. 2004.
49. Franta, I.; Vondráček, P.; Meissner, B.; Ducháček, V., CHAPTER 6 - Compounding materials and special purpose additives. In *Studies in Polymer Science*, Franta, I., Ed. Elsevier: 1989; Vol. 1, pp 325-494.
50. Group, I. R. S. Global Rubber Industry. <http://www.rubberstudy.com>.
51. Rodgers, B., Natural Rubber and Other Naturally Occurring Compounding Materials. In *Rubber Compounding. Chemistry and Applications*, 2nd ed.; CRC Press: 2016.
52. Franta, I.; Ducháček, V., CHAPTER 2 - Natural rubber. In *Studies in Polymer Science*, Franta, I., Ed. Elsevier: 1989; Vol. 1, pp 31-64.
53. Colvin, H., General-Purpose Elastomers. In *Rubber Compounding. Chemistry and Applications*, 2nd ed.; CRC Press: 2016.
54. Meissner, B.; Schätz, M.; Brajko, V., CHAPTER 4 - Synthetic rubbers. In *Studies in Polymer Science*, Franta, I., Ed. Elsevier: 1989; Vol. 1, pp 76-299.
55. Rodgers, B.; Waddell, W., Chapter 9 - The Science of Rubber Compounding. In *The Science and Technology of Rubber (Fourth Edition)*, Mark, J. E.; Erman, B.; Roland, C. M., Eds. Academic Press: Boston, 2013; pp 417-471.
56. Nair, A. B.; Joseph, R., 9 - Eco-friendly bio-composites using natural rubber (NR) matrices and natural fiber reinforcements. In *Chemistry, Manufacture and Applications of Natural Rubber*, Kohjiya, S.; Ikeda, Y., Eds. Woodhead Publishing: 2014; pp 249-283.
57. Vergnaud, J. M.; Rosca, I. D., *Rubber Curing and Properties*. CRC Press: 2016.
58. Chueangchayaphan, N.; Nithi-Uthai, N.; Techakittiroj, K.; Manuspiya, H., Evaluation of dielectric cure monitoring for in situ measurement of natural rubber vulcanization. *Advances in Polymer Technology* **2018**, 37 (8), 3384-3391.
59. Karger-Kocsis, J.; Gatos, K., Estimation of the vulcanization time for by rubbers by considering their linear viscoelastic response assessed by a Plate-Plate Rheometer. *KGK rubberpoint* **2004**, 57, 350-354.
60. Khimi, S. R.; Pickering, K. L., A new method to predict optimum cure time of rubber compound using dynamic mechanical analysis. *Journal of Applied Polymer Science* **2014**, 131 (6).

61. Nieuwenhuizen, P. J., Zinc accelerator complexes.: Versatile homogeneous catalysts in sulfur vulcanization. *Applied Catalysis A: General* **2001**, *207* (1), 55-68.
62. Ray, P., Polymer Cross-Linking. In *Encyclopedia of Polymer Science and Technology*.
63. Alam, M. N.; Mandal, S. K.; Debnath, S. C., Bis(N-benzyl piperazino) thiuram disulfide and dibenzothiazyl disulfide as synergistic safe accelerators in the vulcanization of natural rubber. *Journal of Applied Polymer Science* **2012**, *126* (6), 1830-1836.
64. Lawandy, S. N.; Halim, S. F., Effect of vulcanizing system on the crosslink density of nitrile rubber compounds. *Journal of Applied Polymer Science* **2005**, *96* (6), 2440-2445.
65. Ghosh, P.; Katare, S.; Patkar, P.; Caruthers, J. M.; Venkatasubramanian, V.; Walker, K. A., Sulfur Vulcanization of Natural Rubber for Benzothiazole Accelerated Formulations: From Reaction Mechanisms to a Rational Kinetic Model. *Rubber Chemistry and Technology* **2003**, *76* (3), 592-693.
66. Datta, R. N.; Huntink, N. M.; Datta, S.; Talma, A. G., Rubber Vulcanizates Degradation and Stabilization. *Rubber Chemistry and Technology* **2007**, *80* (3), 436-480.
67. Debnath, S. C.; Basu, D. K., Studies on the effect of thiuram disulfide on NR vulcanization accelerated by thiazole-based accelerator systems. *Journal of Applied Polymer Science* **1996**, *60* (6), 845-855.
68. Donnet, J.-B.; Custodero, E., Chapter 8 - Reinforcement of Elastomers by Particulate Fillers. In *The Science and Technology of Rubber (Fourth Edition)*, Mark, J. E.; Erman, B.; Roland, C. M., Eds. Academic Press: Boston, 2013; pp 383-416.
69. Rahaman, M.; Khastgir, D.; Aldalbahi, A. K., *Carbon-Containing Polymer Composites*. Springer Singapore: 2018.
70. López-de-Uralde, J.; Ruiz, I.; Santos, I.; Zubillaga, A.; Bringas, P. G.; Okariz, A.; Guraya, T. In *Automatic Morphological Categorisation of Carbon Black Nano-aggregates*, Berlin, Heidelberg, Springer Berlin Heidelberg: Berlin, Heidelberg, 2010; pp 185-193.
71. Leblanc, J. L., Rubber–filler interactions and rheological properties in filled compounds. *Progress in Polymer Science* **2002**, *27* (4), 627-687.
72. Coran, A. Y.; Donnet, J.-B., The Dispersion of Carbon Black in Rubber Part II. The Kinetics of Dispersion in Natural Rubber. *Rubber Chemistry and Technology* **1992**, *65* (5), 998-1015.
73. Bueche, F., Mullins effect and rubber–filler interaction. *Journal of Applied Polymer Science* **1961**, *5* (15), 271-281.
74. Medalia, A. I., Filler Aggregates and Their Effect on Reinforcement. *Rubber Chemistry and Technology* **1974**, *47* (2), 411-433.
75. Zielbauer, B. I.; Schönmehl, N.; Chatti, N.; Vilgis, T. A., Networks: From Rubbers to Food. In *Designing of Elastomer Nanocomposites: From Theory to Applications*, Stöckelhuber, K. W.; Das, A.; Klüppel, M., Eds. Springer International Publishing: Cham, 2017; pp 187-233.
76. Smallwood, H. M., Limiting Law of the Reinforcement of Rubber. *Journal of Applied Physics* **1944**, *15* (11), 758-766.
77. Huber, G.; Vilgis, T. A.; Heinrich, G., Universal properties in the dynamical deformation of filled rubbers. *Journal of Physics: Condensed Matter* **1996**, *8* (29), L409-L412.
78. Payne, A. R.; Whittaker, R. E., Reinforcement of rubber with carbon black. *Composites* **1970**, *1* (4), 203-214.
79. Medalia, A. I., Effect of Carbon Black on Dynamic Properties of Rubber Vulcanizates. *Rubber Chemistry and Technology* **1978**, *51* (3), 437-523.
80. Cantournet, S.; Desmorat, R.; Besson, J., Mullins effect and cyclic stress softening of filled elastomers by internal sliding and friction thermodynamics model. *International Journal of Solids and Structures* **2009**, *46* (11), 2255-2264.

81. Mullins, L.; Tobin, N. R., Stress softening in rubber vulcanizates. Part I. Use of a strain amplification factor to describe the elastic behavior of filler-reinforced vulcanized rubber. *Journal of Applied Polymer Science* **1965**, *9* (9), 2993-3009.
82. Wypych, G., 1 - INTRODUCTION. In *Handbook of Fillers (Fourth Edition)*, Wypych, G., Ed. ChemTec Publishing: 2016; pp 1-12.
83. Gardziella, A.; Pilato, L. A.; Knop, A., Phenolic Resins: Chemistry, Reactions, Mechanism. In *Phenolic Resins: Chemistry, Applications, Standardization, Safety and Ecology*, Springer Berlin Heidelberg: Berlin, Heidelberg, 2000; pp 24-82.
84. Powers, P. O., Resins Used in Rubber. *Rubber Chemistry and Technology* **1963**, *36* (5), 1542-1570.
85. Ratna, D., 2. Chemistry, Properties and Applications of Thermoset Resins. In *Handbook of Thermoset Resins*, Rapra, S., Ed. Shropshire, UK, 2009.
86. Ibeh, C. C., 2 - Phenol-Formaldehyde Resins A2 - Goodman, Sidney H. In *Handbook of Thermoset Plastics (Second Edition)*, William Andrew Publishing: Westwood, NJ, 1998; pp 23-71.
87. Hiltz, J. A.; Kuzak, S. G.; Waitkus, P. A., Effect of thermal exposure on the properties of phenolic composites: Dynamic mechanical analysis. *Journal of Applied Polymer Science* **2001**, *79* (3), 385-395.
88. Zhang, X.; Potter, A. C.; Solomon, D. H., The chemistry of novolac resins — V. Reactions of benzoxazine intermediates. *Polymer* **1998**, *39* (2), 399-404.
89. Hirano, K.; Asami, M., Phenolic resins—100years of progress and their future. *Reactive and Functional Polymers* **2013**, *73* (2), 256-269.
90. William W. Schloman, J. Phenol-melamine resins for improving rubber to metal adhesion. US 4,436,853, 1984.
91. Engineers, N. B. o. C., *Phenolic Resins Technology Handbook*. 2019.
92. Charan, R., PHENOLIC RESINS FOR THE RUBBER INDUSTRY – AN OVERVIEW. In *Product development information*, 2012; Vol. 2.
93. Pilato, L., *Phenolic Resins: A Century of Progress*. Springer Science & Business Media: 2010.
94. Derakhshandeh, B.; Shojaei, A.; Faghihi, M., Effects of rubber curing ingredients and phenolic-resin on mechanical, thermal, and morphological characteristics of rubber/phenolic-resin blends. *Journal of Applied Polymer Science* **2008**, *108* (6), 3808-3821.
95. Charan, R., PHENOLIC RESINS FOR THE RUBBER INDUSTRY – AN OVERVIEW. *PRODUCT DEVELOPMENT INFORMATION* 2012.
96. Durairaj, R. B. In *PHENOLIC RESINS FOR RUBBER INDUSTRY*, International Conference – RAPT, University of Calcutta, University of Calcutta, 2014.
97. Nigam, V.; Setua, D. K.; Mathur, G. N., Hybrid filler system for nitrile rubber vulcanizates. *Journal of Materials Science* **2001**, *36* (1), 43-47.
98. Miyake, I.; Okamoto, K.; Bundo, M.; Noda, A. BEAD FILLER RUBBER COMPOSITION. US 4,421,891, 1983.
99. Tietze, R.; Chaudhari, M., Chapter 34 - Advanced Benzoxazine Chemistries Provide Improved Performance in a Broad Range of Applications. In *Handbook of Benzoxazine Resins*, Ishida, H.; Agag, T., Eds. Elsevier: Amsterdam, 2011; pp 595-604.
100. Ishida, H.; Low, H. Y., A Study on the Volumetric Expansion of Benzoxazine-Based Phenolic Resin. *Macromolecules* **1997**, *30* (4), 1099-1106.
101. Kanchanasopa, M.; Yanumet, N.; Hemvichian, K.; Ishida, H., The effect of polymerization conditions on the density and Tg of bisphenol-A and hexafluoroisopropylidene-containing polybenzoxazines. *Polymers and Polymer Composites* **2001**, *9* (6), 367-376.

102. Shen, S. B.; Ishida, H., Development and characterization of high-performance polybenzoxazine composites. *Polymer Composites* **1996**, *17* (5), 710-719.
103. Ishida, H.; Allen, D. J., Physical and mechanical characterization of near-zero shrinkage polybenzoxazines. *Journal of Polymer Science Part B: Polymer Physics* **1996**, *34* (6), 1019-1030.
104. Lligadas, G.; Tuzun, A.; Ronda, J. C.; Galia, M.; Cadiz, V., Polybenzoxazines: new players in the bio-based polymer arena. *Polymer Chemistry* **2014**, *5* (23), 6636-6644.
105. Chirachanchai, S.; Phongtamrug, S.; Laobuthee, A.; Tashiro, K., Chapter 4 - Mono-Substituted Phenol-Based Benzoxazines: Inevitable Dimerization Via Self-Termination and Its Metal Complexation. In *Handbook of Benzoxazine Resins*, Ishida, H.; Agag, T., Eds. Elsevier: Amsterdam, 2011; pp 111-126.
106. Ishida, H. Process for preparation of benzoxazine compounds in solventless systems. US 5,543,516, 1996.
107. Alhassan, S.; Schiraldi, D.; Qutubuddin, S.; Agag, T.; Ishida, H., Chapter 15 - Various Approaches for Main-Chain Type Benzoxazine Polymers. In *Handbook of Benzoxazine Resins*, Ishida, H.; Agag, T., Eds. Elsevier: Amsterdam, 2011; pp 309-318.
108. Ning, X.; Ishida, H., Phenolic materials via ring-opening polymerization of benzoxazines: Effect of molecular structure on mechanical and dynamic mechanical properties. *Journal of Polymer Science Part B: Polymer Physics* **1994**, *32* (5), 921-927.
109. Trejo-Machin, A.; Adjaoud, A.; Puchot, L.; Dieden, R.; Verge, P., Elucidating the thermal and polymerization behaviours of benzoxazines from lignin derivatives. *European Polymer Journal* **2020**, *124*, 109468.
110. Trejo-Machin, A.; Puchot, L.; Verge, P., Design and Synthesis of Bio-Based Benzoxazines. *Paint and Coatings Industry, Faris Yilmaz, IntechOpen* **2018**.
111. Wang, Y. X.; Ishida, H., Cationic ring-opening polymerization of benzoxazines. *Polymer* **1999**, *40* (16), 4563-4570.
112. Ishida, H.; Rodriguez, Y., Catalyzing the curing reaction of a new benzoxazine-based phenolic resin. *Journal of Applied Polymer Science* **1995**, *58* (10), 1751-1760.
113. Andreu, R.; Reina, J. A.; Ronda, J. C., Carboxylic acid-containing benzoxazines as efficient catalysts in the thermal polymerization of benzoxazines. *Journal of Polymer Science Part A: Polymer Chemistry* **2008**, *46* (18), 6091-6101.
114. Men, W.; Lu, Z.; Zhan, Z., Synthesis of a novel benzoxazine precursor containing phenol hydroxyl groups and its polymer. *Journal of Applied Polymer Science* **2008**, *109* (4), 2219-2223.
115. Kimura, H.; Matsumoto, A.; Sugito, H.; Hasegawa, K.; Ohtsuka, K.; Fukuda, A., New thermosetting resin from poly(p-vinylphenol) based benzoxazine and epoxy resin. *Journal of Applied Polymer Science* **2001**, *79* (3), 555-565.
116. Chernykh, A.; Agag, T.; Ishida, H., Novel benzoxazine monomer containing diacetylene linkage: An approach to benzoxazine thermosets with low polymerization temperature without added initiators or catalysts. *Polymer* **2009**, *50* (14), 3153-3157.
117. Verge, P.; Puchot, L.; Vancaeyzeele, C.; Vidal, F.; Habibi, Y., Chapter 7 - Symmetric Versus Asymmetric di-Bz Monomer Design: Structure-to-Properties Relationship. In *Advanced and Emerging Polybenzoxazine Science and Technology*, Ishida, H.; Froimowicz, P., Eds. Elsevier: Amsterdam, 2017; pp 89-107.
118. Wang, X.; Chen, F.; Gu, Y., Influence of electronic effects from bridging groups on synthetic reaction and thermally activated polymerization of bisphenol-based benzoxazines. *Journal of Polymer Science Part A: Polymer Chemistry* **2011**, *49* (6), 1443-1452.
119. Agag, T., Preparation and properties of some thermosets derived from allyl-functional naphthoxazines. *Journal of Applied Polymer Science* **2006**, *100* (5), 3769-3777.

120. Arnebold, A.; Schorsch, O.; Stelten, J.; Hartwig, A., Resorcinol-based benzoxazine with low polymerization temperature. *Journal of Polymer Science Part A: Polymer Chemistry* **2014**, *52* (12), 1693-1699.
121. Baranek, A. D.; Kendrick, L. L.; Narayanan, J.; Tyson, G. E.; Wand, S.; Patton, D. L., Flexible aliphatic-bridged bisphenol-based polybenzoxazines. *Polymer Chemistry* **2012**, *3* (10), 2892-2900.
122. Agag, T.; Takeichi, T., Synthesis and Characterization of Novel Benzoxazine Monomers Containing Allyl Groups and Their High Performance Thermosets. *Macromolecules* **2003**, *36* (16), 6010-6017.
123. Liu, Y.; Wang, M.; Zhang, H.; Zhao, S.; Run, M., Synthesis, polymerization, and thermal properties of benzoxazine based on bisphenol-S and allylamine. *Polymers for Advanced Technologies* **2013**, *24* (2), 157-163.
124. Gnanapragasam, S.; Krishnan, S.; Arumugam, H.; Chavali, M.; Alagar, M., Synthesis and characterization of a novel high-performance benzoxazine from benzaldehyde-based bisphenol. *Advances in Polymer Technology* **2018**, *37* (8), 3056-3065.
125. Jin Kim, H.; Brunovska, Z.; Ishida, H., Molecular characterization of the polymerization of acetylene-functional benzoxazine resins. *Polymer* **1999**, *40* (7), 1815-1822.
126. Kim, H. J.; Brunovska, Z.; Ishida, H., Dynamic mechanical analysis on highly thermally stable polybenzoxazines with an acetylene functional group. *Journal of Applied Polymer Science* **1999**, *73* (6), 857-862.
127. Kim, H. J.; Brunovska, Z.; Ishida, H., Synthesis and thermal characterization of polybenzoxazines based on acetylene-functional monomers. *Polymer* **1999**, *40* (23), 6565-6573.
128. Brunovska, Z.; Lyon, R.; Ishida, H., Thermal properties of phthalonitrile functional polybenzoxazines. *Thermochimica Acta* **2000**, *357-358*, 195-203.
129. Liu, Y.; Zhao, S.; Zhang, H.; Wang, M.; Run, M., Synthesis, polymerization, and thermal properties of benzoxazine based on p-aminobenzonitrile. *Thermochimica Acta* **2012**, *549*, 42-48.
130. Liu, Y.; Zhang, J.; Liao, C.; Zheng, J.; Zhao, S.; Run, M., Morphology and thermal properties of copolymer based on p-aminobenzonitrile type benzoxazine and diglycidyl ether of bisphenol-A. *Thermochimica Acta* **2013**, *573*, 138-145.
131. Santhosh Kumar, K. S.; Reghunadhan Nair, C. P.; Radhakrishnan, T. S.; Ninan, K. N., Bis allyl benzoxazine: Synthesis, polymerisation and polymer properties. *European Polymer Journal* **2007**, *43* (6), 2504-2514.
132. Liu, Y.-L.; Chou, C.-I., High performance benzoxazine monomers and polymers containing furan groups. *Journal of Polymer Science Part A: Polymer Chemistry* **2005**, *43* (21), 5267-5282.
133. Zúñiga, C.; Lligadas, G.; Ronda, J. C.; Galià, M.; Cádiz, V., Renewable polybenzoxazines based in diphenolic acid. *Polymer* **2012**, *53* (8), 1617-1623.
134. Feng, Z.; Zeng, M.; Meng, D.; Chen, J.; Zhu, W.; Xu, Q.; Wang, J., A novel bio-based benzoxazine resin with outstanding thermal and superhigh-frequency dielectric properties. *Journal of Materials Science: Materials in Electronics* **2020**, *31* (5), 4364-4376.
135. Dai, J.; Teng, N.; Peng, Y.; Liu, Y.; Cao, L.; Zhu, J.; Liu, X., Biobased Benzoxazine Derived from Daidzein and Furfurylamine: Microwave-Assisted Synthesis and Thermal Properties Investigation. *ChemSusChem* **2018**, *11* (18), 3175-3183.
136. Zhang, K.; Han, M.; Liu, Y.; Froimowicz, P., Design and Synthesis of Bio-Based High-Performance Trioxazine Benzoxazine Resin via Natural Renewable Resources. *ACS Sustainable Chemistry & Engineering* **2019**, *7* (10), 9399-9407.
137. Kotzebue, L. R. V.; de Oliveira, J. R.; da Silva, J. B.; Mazzetto, S. E.; Ishida, H.; Lomonaco, D., Development of Fully Biobased High-Performance Bis-Benzoxazine under Environmentally Friendly Conditions. *ACS Sustainable Chemistry & Engineering* **2018**, *6* (4), 5485-5494.

138. Teng, N.; Yang, S.; Dai, J.; Wang, S.; Zhao, J.; Zhu, J.; Liu, X., Making Benzoxazine Greener and Stronger: Renewable Resource, Microwave Irradiation, Green Solvent, and Excellent Thermal Properties. *ACS Sustainable Chemistry & Engineering* **2019**, *7* (9), 8715-8723.
139. Agag, T.; Takeichi, T., Novel Benzoxazine Monomers Containing p-Phenyl Propargyl Ether: Polymerization of Monomers and Properties of Polybenzoxazines. *Macromolecules* **2001**, *34* (21), 7257-7263.
140. Gaina, C.; Ursache, O.; Gaina, V.; Musteata, V.-E., High performance thermosets based on multifunctional intermediates containing allyl, maleimide and benzoxazine groups. *Journal of Polymer Research* **2013**, *20* (10), 263.
141. Zúñiga, C.; Larrechi, M. S.; Lligadas, G.; Ronda, J. C.; Galià, M.; Cádiz, V., Phosphorus flame retardant polybenzoxazine foams based on renewable diphenolic acid. *Polymer Degradation and Stability* **2013**, *98* (12), 2617-2626.
142. Huntsman, Advanced Materials - XU 35910 Benzoxazine Resin. 2014.
143. Kawaguchi, A. W.; Sudo, A.; Endo, T., Synthesis of highly polymerizable 1,3-benzoxazine assisted by phenyl thio ether and hydroxyl moieties. *Journal of Polymer Science Part A: Polymer Chemistry* **2012**, *50* (8), 1457-1461.
144. Kawaguchi, A. W.; Sudo, A.; Endo, T., Thiol-functionalized 1,3-benzoxazine: Preparation and its use as a precursor for highly polymerizable benzoxazine monomers bearing sulfide moiety. *Journal of Polymer Science Part A: Polymer Chemistry* **2014**, *52* (10), 1448-1457.
145. Liu, Y.; Hao, Z.; Lv, S.; Huang, J.; Liao, C.; Run, M., Structural effects of diamines on synthesis, polymerization, and properties of benzoxazines based on o-allylphenol. *Polymer* **2015**, *57* (Supplement C), 29-38.
146. Jin, L.; Agag, T.; Ishida, H., Bis(benzoxazine-maleimide)s as a novel class of high performance resin: Synthesis and properties. *European Polymer Journal* **2010**, *46* (2), 354-363.
147. Liu, Y.; Zhang, J.; Li, Z.; Luo, X.; Jing, S.; Run, M., A pair of benzoxazine isomers from o-allylphenol and 4,4'-diaminodiphenyl ether: Synthesis, polymerization behavior, and thermal properties. *Polymer* **2014**, *55* (7), 1688-1697.
148. Allen, D. J.; Ishida, H., Physical and mechanical properties of flexible polybenzoxazine resins: Effect of aliphatic diamine chain length. *Journal of Applied Polymer Science* **2006**, *101* (5), 2798-2809.
149. Sini, N. K.; Bijwe, J.; Varma, I. K., Thermal behaviour of bis-benzoxazines derived from renewable feed stock 'vanillin'. *Polymer Degradation and Stability* **2014**, *109* (Supplement C), 270-277.
150. Dumas, L.; Bonnaud, L.; Olivier, M.; Poorteman, M.; Dubois, P., Eugenol-based benzoxazine: from straight synthesis to taming of the network properties. *Journal of Materials Chemistry A* **2015**, *3* (11), 6012-6018.
151. Thirukumaran, P.; Shakila, A.; Muthusamy, S., Synthesis and characterization of novel bio-based benzoxazines from eugenol. *RSC Advances* **2014**, *4* (16), 7959-7966.
152. Lochab, B.; Varma, I. K.; Bijwe, J., Cardanol-based bisbenzoxazines. *Journal of Thermal Analysis and Calorimetry* **2012**, *107* (2), 661-668.
153. Lochab, B.; Varma, I. K.; Bijwe, J., Thermal behaviour of cardanol-based benzoxazines. *Journal of Thermal Analysis and Calorimetry* **2010**, *102* (2), 769-774.
154. Agag, T.; An, S. Y.; Ishida, H., 1,3-bis(benzoxazine) from cashew nut shell oil and diaminodiphenyl methane and its composites with wood flour. *Journal of Applied Polymer Science* **2013**, *127* (4), 2710-2714.
155. Xu, H.; Zhang, W.; Lu, Z.; Zhang, G., Hybrid polybenzoxazine with tunable properties. *RSC Advances* **2013**, *3* (11), 3677-3682.

156. Shukla, S.; Yadav, N.; Lochab, B., Chapter 24 - Cardanol-Based Benzoxazines and Their Applications A2 - Ishida, Hatsuo. In *Advanced and Emerging Polybenzoxazine Science and Technology*, Froimowicz, P., Ed. Elsevier: Amsterdam, 2017; pp 451-472.
157. Thirukumar, P.; Shakilaparveen, A.; Sarojadevi, M., Chapter 27 - Eugenol-Based Polybenzoxazines A2 - Ishida, Hatsuo. In *Advanced and Emerging Polybenzoxazine Science and Technology*, Froimowicz, P., Ed. Elsevier: Amsterdam, 2017; pp 523-531.
158. Lin, C. H.; Chang, S. L.; Hsieh, C. W.; Lee, H. H., Aromatic diamine-based benzoxazines and their high performance thermosets. *Polymer* **2008**, *49* (5), 1220-1229.
159. He, X.-y.; Wang, J.; Ramdani, N.; Liu, W.-b.; Liu, L.-j.; Yang, L., Investigation of synthesis, thermal properties and curing kinetics of fluorene diamine-based benzoxazine by using two curing kinetic methods. *Thermochimica Acta* **2013**, *564* (0), 51-58.
160. Hao, Z.; Lv, S.; Song, S.; Li, Y.; Zhang, H.; Run, M.; Liu, Y., Dynamic mechanical and thermal properties of copolymer from o-allylphenol and 4,4'-diaminodiphenyl methane-based benzoxazine and bisphenol-A type novolac epoxy resin. *Journal of Thermal Analysis and Calorimetry* **2015**, *119* (2), 1439-1444.
161. Lyu, Y.; Rachita, E.; Pogharian, N.; Froimowicz, P.; Ishida, H., Electronic effects of asymmetric and meta-alkoxy substituents on the polymerization behavior of bis-benzoxazines. *Polymer Chemistry* **2020**, *11* (4), 800-809.
162. Lochab, B.; Varma, I.; Bijwe, J., Thermal behaviour of cardanol-based benzoxazines. *Journal of Thermal Analysis and Calorimetry* **2010**, *102* (2), 769-774.
163. Lochab, B.; Varma, I.; Bijwe, J., Cardanol-based bisbenzoxazines. *Journal of Thermal Analysis and Calorimetry* **2012**, *107* (2), 661-668.
164. Amarnath, N.; Shukla, S.; Lochab, B., Isomannide-Derived Chiral Rigid Fully Biobased Polybenzoxazines. *ACS Sustainable Chemistry & Engineering* **2019**, *7* (22), 18700-18710.
165. Gao, X.; Sun, X.; Xu, L.; Zhang, H.; Liu, G., Synthesis and electrochemical properties of benzoxazine-based heteroatom-doped carbon materials. *Journal of Materials Research* **2019**, *34* (7), 1219-1228.
166. Gungor, F. S.; Bati, B.; Kiskan, B., Combining naphthoxazines and benzoxazines for non-symmetric curable oxazines by one-pot synthesis. *European Polymer Journal* **2019**, *121*, 109352.
167. Dogan, Y. E.; Satilmis, B.; Uyar, T., Synthesis and characterization of bio-based benzoxazines derived from thymol. *Journal of Applied Polymer Science* **2019**, *136* (17), 47371.
168. Rajesh Kumar, S.; Asseref, P. M.; Dhanasekaran, J.; Mohan, S. K., A new approach with prepregs for reinforcing nitrile rubber with phenolic and benzoxazine resins. *RSC Advances* **2014**, *4* (24), 12526-12533.
169. Caldon, E. B.; De Leon, A. C. C.; Thomas, P. G.; Naylor, D. F.; Pajarito, B. B.; Advincula, R. C., Superhydrophobic Rubber-Modified Polybenzoxazine/SiO₂ Nanocomposite Coating with Anticorrosion, Anti-Ice, and Superoleophilicity Properties. *Industrial & Engineering Chemistry Research* **2017**, *56* (6), 1485-1497.
170. Rungswang, W.; Kato, K.; Kotaki, M.; Chirachanchai, S., Size-controllable nanospheres prepared by blending a thermoset monomer in confined morphology with thermoplastic elastomer. *Polymer* **2012**, *53* (6), 1167-1171.
171. Selvi, M.; Devaraju, S.; Sethuraman, K.; Alagar, M., Carbon black-polybenzoxazine nanocomposites for high K dielectric applications. *Polymer Composites* **2014**, *35* (11), 2121-2128.
172. Ahn, D.; Choi, H.-J.; Kim, H.-d.; Yeo, S. Y., Properties of Conductive Polyacrylonitrile Fibers Prepared by Using Benzoxazine Modified Carbon Black. *Polymers* **2020**, *12* (1), 179.

173. Tiptipakorn, S.; Kuttiyawong, K.; Suwanmala, P.; Hemvichian, K., Effects of Gamma Radiation on Thermal Properties of Benzoxazine Filled with Carbon Black. *Applied Mechanics and Materials* **2015**, 744-746, 1394-1397.
174. Kincaid, D. S.; Le, D.; Johnson, D. L. BENZOTHIAZOLES AS LATENT CATALYSTS FOR BENZOXAZINE RESINS. US 10,889,686, 2021.
175. Rajamanikam, R.; Pichaimani, P.; Kumar, M.; Muthukaruppan, A., Optical and thermomechanical behavior of benzoxazine functionalized ZnO reinforced polybenzoxazine nanocomposites. *Polymer Composites* **2017**, 38 (9), 1881-1889.
176. Coran, A. Y., Chemistry of the vulcanization and protection of elastomers: A review of the achievements. *Journal of Applied Polymer Science* **2003**, 87 (1), 24-30.
177. Chung, W. J.; Griebel, J. J.; Kim, E. T.; Yoon, H.; Simmonds, A. G.; Ji, H. J.; Dirlam, P. T.; Glass, R. S.; Wie, J. J.; Nguyen, N. A.; Guralnick, B. W.; Park, J.; Somogyi, Á.; Theato, P.; Mackay, M. E.; Sung, Y.-E.; Char, K.; Pyun, J., The use of elemental sulfur as an alternative feedstock for polymeric materials. *Nature Chemistry* **2013**, 5 (6), 518-524.
178. Gorodisher, I.; J. DeVoe, R.; Webb, R., *Catalytic Opening of Lateral Benzoxazine Rings by Thiols*. 2011; p 211-234.
179. Shukla, S.; Ghosh, A.; Roy, P. K.; Mitra, S.; Lochab, B., Cardanol benzoxazines – A sustainable linker for elemental sulphur based copolymers via inverse vulcanisation. *Polymer* **2016**, 99, 349-357.
180. Shukla, S.; Ghosh, A.; Sen, U. K.; Roy, P. K.; Mitra, S.; Lochab, B., Cardanol benzoxazine-Sulfur Copolymers for Li-S batteries: Symbiosis of Sustainability and Performance. *ChemistrySelect* **2016**, 1 (3), 594-600.
181. Arslan, M.; Kiskan, B.; Yagci, Y., Combining Elemental Sulfur with Polybenzoxazines via Inverse Vulcanization. *Macromolecules* **2016**, 49 (3), 767-773.
182. Akay, S.; Kayan, B.; Kalderis, D.; Arslan, M.; Yagci, Y.; Kiskan, B., Poly(benzoxazine-co-sulfur): An efficient sorbent for mercury removal from aqueous solution. *Journal of Applied Polymer Science* **2017**, 134 (38), 45306.
183. Arslan, M.; Kiskan, B.; Yagci, Y., Recycling and Self-Healing of Polybenzoxazines with Dynamic Sulfide Linkages. *Scientific Reports* **2017**, 7 (1), 5207.
184. Kawaguchi, A. W.; Sudo, A.; Endo, T., Polymerization–Depolymerization System Based on Reversible Addition-Dissociation Reaction of 1,3-Benzoxazine with Thiol. *ACS Macro Letters* **2013**, 2 (1), 1-4.
185. Semerci, E.; Kiskan, B.; Yagci, Y., Thiol reactive polybenzoxazine precursors: A novel route to functional polymers by thiol-oxazine chemistry. *European Polymer Journal* **2015**, 69 (Supplement C), 636-641.
186. Urbaniak, T.; Soto, M.; Liebeke, M.; Koschek, K., Insight into the Mechanism of Reversible Ring-Opening of 1,3-Benzoxazine with Thiols. *The Journal of Organic Chemistry* **2017**, 82 (8), 4050-4055.
187. Liu, J.; Ishida, H., Anomalous Isomeric Effect on the Properties of Bisphenol F-based Benzoxazines: Toward the Molecular Design for Higher Performance. *Macromolecules* **2014**, 47 (16), 5682-5690.
188. Gorodisher, I.; DeVoe, R. J.; Webb, R. J., Chapter 11 - Catalytic Opening of Lateral Benzoxazine Rings by Thiols. In *Handbook of Benzoxazine Resins*, Ishida, H.; Agag, T., Eds. Elsevier: Amsterdam, 2011; pp 211-234.
189. Yang, Y.-M.; Yu, H.-Z.; Sun, X.-H.; Dang, Z.-M., Density functional theory calculations on S—S bond dissociation energies of disulfides. *Journal of Physical Organic Chemistry* **2016**, 29 (1), 6-13.

190. Jubsilp, C.; Damrongsakkul, S.; Takeichi, T.; Rimdusit, S., Curing kinetics of arylamine-based polyfunctional benzoxazine resins by dynamic differential scanning calorimetry. *Thermochimica Acta* **2006**, *447* (2), 131-140.
191. Wang, C.; Sun, J.; Liu, X.; Sudo, A.; Endo, T., Synthesis and copolymerization of fully bio-based benzoxazines from guaiacol, furfurylamine and stearylamine. *Green Chemistry* **2012**, *14* (10), 2799-2806.
192. Salum, M. L.; Iguchi, D.; Arza, C. R.; Han, L.; Ishida, H.; Froimowicz, P., Making Benzoxazines Greener: Design, Synthesis, and Polymerization of a Biobased Benzoxazine Fulfilling Two Principles of Green Chemistry. *ACS Sustainable Chemistry & Engineering* **2018**, *6* (10), 13096-13106.
193. Pang, T.; Zeng, M.; Feng, Z.; Chen, J.; Huang, Y.; Xu, Q., A facile method for the preparation of furfurylamine based benzoxazine resin with high-frequency low dielectric constants and ultra-low dielectric losses. *Journal of Materials Science: Materials in Electronics* **2019**, *30* (9), 8358-8370.
194. Rubber Compounding. In *Van Nostrand's Scientific Encyclopedia*.
195. Griebel, J. J.; Nguyen, N. A.; Astashkin, A. V.; Glass, R. S.; Mackay, M. E.; Char, K.; Pyun, J., Preparation of Dynamic Covalent Polymers via Inverse Vulcanization of Elemental Sulfur. *ACS Macro Letters* **2014**, *3* (12), 1258-1261.
196. Trejo-Machin, A.; Cosas Fernandes, J. P.; Puchot, L.; Balko, S.; Wirtz, M.; Weydert, M.; Verge, P., Synthesis of Novel Benzoxazines Containing Sulfur and Their Application in Rubber Compounds. *Polymers* **2021**, *13* (8), 1262.
197. Plagge, J.; Klüppel, M., A physically based model of stress softening and hysteresis of filled rubber including rate- and temperature dependency. *International Journal of Plasticity* **2017**, *89*, 173-196.
198. Kraus, G., Reinforcement of Elastomers by Carbon Black. *Rubber Chemistry and Technology* **1978**, *51* (2), 297-321.
199. Warasitthinon, N.; Robertson, C. G., INTERPRETATION OF THE TAN δ PEAK HEIGHT FOR PARTICLE-FILLED RUBBER AND POLYMER NANOCOMPOSITES WITH RELEVANCE TO TIRE TREAD PERFORMANCE BALANCE. *Rubber Chemistry and Technology* **2018**, *91* (3), 577-594.
200. Aoe, I.; Kitayama, H., Studies on the Combined Use of Two Different Organic Accelerators. V. Mercaptobenzothiazole and Hexamethylenetetramine. *Rubber Chemistry and Technology* **1936**, *9* (1), 21-34.
201. Luo, W.; Huang, Y.; Yin, B.; Jiang, X.; Hu, X., Fatigue Life Assessment of Filled Rubber by Hysteresis Induced Self-Heating Temperature. *Polymers (Basel)* **2020**, *12* (4).
202. Weydert, M.; Trejo-Machin, A.; Puchot, L.; Verge, P. Rubber composition and a rubber product. US 63/003,513, 2020.

Acknowledgement

The Luxembourg National Research Fund (FNR) is acknowledged for funding this project with the grant number IPBG16/11514551/TireMat-Tech. I would like to thank the Luxembourg Institute of Science and Technology and the Goodyear Tire and Rubber Company for giving me the possibility to carry out this project.

I would like to also to thank everyone who has been with me along this journey.

I will start with my supervisor, Pierre Verge. He was the one who trusted in me in the first place and I will be always grateful for that. I thank him for letting me the opportunity to perform this thesis under his supervision. During these four years, we have been working together, sharing ideas, and the most important, doing science. This journey has not been always easy, but the ups and downs brought the best from our work. I am very thankful for his support and encouragement throughout these years.

I want to thank my colleague Laura. She has been an important support during the PhD. I had the pleasure to work in the same project than her for two years. During this period, she helped me with the chemical synthesis and characterization of the novel monomers and polymers. We had endless scientific discussions but also shared a lot of moments outside the lab. I am grateful for all the lessons I learn from her and all the experiences we enjoyed together.

I would like to thank to João Paulo Cosas Fernandes for doing the AFM measurements and thus, for making possible to characterize the complicated structure of the materials at the microscale, basically, for performing such nice pictures.

I would like to thank Marc Weydert for his highly valuable technical contributions to this project thanks to his extensive experience in chemistry and rubber technology. I want to also thank Marcel Wirtz and Suzanne Balko for their support to this collaborative project from the Goodyear side.

I am very thankful to Régis Vaudemont, Benoit Marcolini, and Sebastien Gergen for carrying out most of the thermal and mechanical characterizations (DSC, TGA, DMA temperature sweep, and tensile tests), to Denis Pittois for performing the elemental analysis and to Patrick Grysan for the Raman.

I want to also thank to Goodyear team for performing the curing kinetics of the rubber compounds (MDR) and additional thermo-mechanical characterization (DMA strain sweep).

I would like to thank also to Stephan Westermann and Daniel Schmidt for the scientific contribution to this thesis.

This journey would have not been the same without all the friends I have made.

Firstly, I want to mention the IPBG team, Arpan, Arnaud, Joao, Carlos, Felipe, Damian, among many others. We shared a lot of experiences inside and outside the institute that made my life much funnier and easier, thank you guys.

I cannot forget my Belvaux team, Edyta, Olivier, Veneranda, Lauriane, and Marielle. I want to thank you for all the moment we shared, I am grateful I met you all. I also want to thank all my

friends in Luxembourg for providing me an amazing first experience abroad, with special mention to the team “agua y sed” and to “settlers of catan”.

Finally, I would like to thank my parents, my sisters, and my friends for their unconditional support.

Thank you all very much.

Publication list

List of papers

- Trejo-Machin, A.; Cosas Fernandes, J. P.; Puchot, L.; Balko, S.; Wirtz, M.; Weydert, M.; Verge, P., Synthesis of Novel Benzoxazines Containing Sulfur and Their Application in Rubber Compounds. *Polymers* **2021**, *13* (8), 1262, doi:10.3390/polym13081262.
- Trejo-Machin, A.; Adjaoud, A.; Puchot, L.; Dieden, R.; Verge, P., Elucidating the thermal and polymerization behaviours of benzoxazines from lignin derivatives. *Eur. Polym. J.* **2020**, *124*, 109468, doi:10.1016/j.eurpolymj.2019.109468.
- Trejo-Machin, A.; Puchot, L.; Verge, P., Design and Synthesis of Bio-Based Benzoxazines, Paint and Coatings Industry, **2018**, doi:10.5772/intechopen.76104.

List of filed patents

- Provisional Patent US 63/003,513: "Rubber composition and a rubber product" filed Apr. 1, 2020.

List of conferences

- Poster presentation at the 255th ACS National Meeting, Louisiana, U.S, 18.03-22.03.2018.
- Poster presentation at the BPG Annual Meeting 2018, Blankenberge, Belgium, 28.05-29.05.2018.
- Oral presentation at the 4th International Conference on Bioinspired and Biobased Chemistry and Materials, Nice, France, 14.10-17.10.2018.
- Poster presentation at the 3rd Technical Seminar: "New strategy to reinforce tire formulation with benzoxazines", TyreMat-Tech IPBG Program - Colmar-Berg, Luxembourg, 16.01.2019.
- Oral presentation at the APS March Meeting 2021 (online) 15.03-19.03.2021.

Annex A. Materials and methods

A.1 Synthesis, molecular and thermal characterization of benzoxazine resins

A.1.1 Materials

4,4'-thiodiphenol (99%, 4TDP), bisphenol A ($\geq 99\%$, BA), stearylamine ($\geq 99\%$, ste), furfurylamine ($\geq 99\%$, fa), aniline ($\geq 99.5\%$, a), and paraformaldehyde (95%, PFA) were purchased from Sigma-Aldrich. 3,3'-dihydroxydiphenyl disulfide (95%, 3DPDS) was purchased from abcr GmbH, and 4,4'-dihydroxydiphenyl disulfide (98%, 4DPDS) was purchased from TCI Europe. Toluene ($\geq 99.5\%$), chloroform (CHCl_3), chloroform-d (CDCl_3), and dimethyl sulfoxide- d_6 (DMSO) were supplied from Sigma-Aldrich. All chemicals were used as received without any further purification.

A.1.2 Nuclear magnetic resonance (NMR)

NMR spectra were recorded using an AVANCE III HD Bruker spectrometer operating at 600 MHz and equipped with a 5 mm Broadband Observe (BBO) probe. The samples were dissolved in deuterated solvent either chloroform (CDCl_3) or dimethyl sulfoxide- d_6 (DMSO) and the spectra were referenced relative to tetramethylsilane (TMS). Assignments were performed using a combination of ^1H , ^{13}C , heteronuclear single quantum coherence (HSQC), and heteronuclear multiple bond correlation (HMBC) spectra.

A.1.3 Fourier transform infrared spectroscopy (FTIR)

The FTIR was conducted on a Bruker TENSOR 27 (Ettlingen, Germany) in transmission mode equipped with DTGS detector. The analysis was performed on silicon wafers coated with the samples. For the sample preparation, each monomer was solubilized in CHCl_3 and deposited on the silicon wafer. The solvent was dried off resulting in a thin layer of the monomer that was then analyzed. In the case of the polybenzoxazines, each sample was placed inside the oven as well as the reference at the required temperature and time. The background and sample spectra were recorded at 4 cm^{-1} spectral resolution across the $4000\text{-}400\text{ cm}^{-1}$ range.

A.1.4 Elemental analysis (EA)

The elemental analysis measurements, which provide the determination of carbon, hydrogen, nitrogen and sulfur (CHNS) were performed on a Vario MACRO cube CHNS/O from Elementar France SARL. Samples are inserted in an oxygen enriched furnace at $1150\text{ }^\circ\text{C}$ where a combustion process converts carbon to carbon dioxide; hydrogen to water; nitrogen to nitrogen gas/ oxides of nitrogen and sulfur to sulfur dioxide. The combustion products are swept out of the combustion chamber by inert carrier gas (helium, 600 ml per minute) and passed over heated ($850\text{ }^\circ\text{C}$) high purity copper. The separation of the measuring components takes place as follow: N_2 is not adsorbed in the adsorption columns and is the first measuring component to enter directly in the thermal conductivity detector. The other components are adsorbed in their respective adsorption column. Each of these columns is then separately heated to the corresponding desorption temperature ($T_{\text{desorpt.}}$) in order to release the components in the

following order: CO₂ (T_{desorpt.} 240 °C), H₂O (T_{desorpt.} 150 °C) and SO₂ (T_{desorpt.} 230 °C). After desorption, each component is transported by the carrier gas flow into the measuring cell of a thermal conductivity detector (TCD).

A.1.5 Raman spectroscopy

Raman spectra were recorded in a back-scattering geometry with a Renishaw inVia Reflex Raman Microscope using the 785 nm line of High Power Near Infrared Diode Laser, 3 accumulations of 10 seconds were used at power 24.3 mW. A X50 long working distance objective was used to focus the laser beam on a sample surface.

A.1.6 Differential scanning calorimetry (DSC)

DSC thermograms were recorded using a Mettler Toledo DSC3+ apparatus operating at inert atmosphere (nitrogen) with a linear heating ramp from 25 to 300 °C at different heating rates (5, 10, and 20 °C·min⁻¹).

A.1.7 Thermo-gravimetric analysis (TGA)

TGA measurements were performed using a Netzsch TG 409 PC Luxx device operating under nitrogen with a heating ramp of 10 °C·min⁻¹ from 25 to 800 °C.

A.1.8 Rheological measurements

Rheo-kinetic measurements were performed using an Anton Paar Physica MCR 302 rheometer equipped with a CTD 450 temperature control device with a disposable aluminum plate-plate (diameter: 25 mm, measure gap: 0.5 mm) geometry. The polymerization measurements were recorded in the oscillation mode with linear strain amplitude from 1 to 0.1% and a frequency of 1 Hz. The test is performed following a heating ramp of 20 °C·min⁻¹ from 50 °C to 150 °C followed by an isothermal measurement at 150 °C.

Rheology temperature sweep curves were performed on the same device on cured rectangular bars in torsion mode from room temperature to 300 °C under constant deformation of 0.1% and a frequency of 1 Hz.

A.1.9 Preparation of polybenzoxazines

Benzoxazine monomers were placed in hollow Teflon® molds and dried under vacuum for 2 hours at 100 °C to remove traces of solvent or water. After that, the molds were transferred to an air-circulating oven at 170 °C for 1 hour for the first curing step. This step was followed by a post-curing for 1 hour at 190 °C and then 1 hour at 210 °C.

A.2 Application of benzoxazine resins in unfilled compounds

A.2.1 Materials

Cis-1,4-polyisoprene (>99.6%, polyisoprene) with product name SKI-3 was purchased from PJSC, Nizhnekamskneftekhim. Sulfur (>95, S₈) with trade name Milled Oiled Sulphur was purchased from Siarkopol (TARNOBRZEG Chemical Plants Ltd.). N,N'-dicyclohexyl-2-benzothiazole sulfenamide (>98.5%, DCBS) with product name VULKACIT DZ/EG-C was

purchased from Lanxess. Zinc oxide (98.5%, ZnO) with trade name Red Seal Zinc Oxide was purchased from EverZinc. Fatty acids (C16-18), also denominated stearic acid, with product name RADIACID 0444 was purchased from Oleon.

Phenolic resin (>99.5%, PR), with product name DUREZ 31459 was purchased from SBHPP (Sumitomo Bakelite Co., Ltd). Hexamethylenetetramine (HMT) was supplied by Ineos Paraform.

Toluene ($\geq 99.5\%$), and dimethylformamide (DMF) were supplied from Sigma-Aldrich. All chemicals were used as received without any further purification.

A.2.2 Rubber compounding

A Thermo Scientific HAAKE PolyLab QC internal mixer was used to perform the compounding. The internal mixer having a free volume of 85 cc was operated using two cam-type rotors and keeping a constant fill factor of 0.75. The mixing process was performed in two steps and it is detailed in Table A.1. The first step also referred as non-productive (NP) included the mixing of the rubber, ZnO, and the precursors. The initial temperature of NP was set at 70 °C and the ingredients were mixed for 8 minutes. In the second and final step so-called productive step (PD) sulfur and the accelerator were mixed with the compound from NP. The temperature is set at 60 °C and it should remain below 110 °C to avoid early vulcanization of the compounds.

Table A.1. Procedure carried out for the rubber compounding for unfilled compounds.

Step	Procedure
NP	Initial temperature: 70 °C 20 rpm – add the polymer 60 rpm – masticate for 1 min 2 rpm – add ZnO and stearic acid 60 rpm – mix for 4 min 2 rpm – add benzoxazine, phenolic resin or nothing (reference) 60 rpm – mix for 8 min (or drop at 150 °C)
PD	Initial temperature: 60 °C 20 rpm – add compound 60 rpm – masticate for 30 s. 2 rpm – add sulfur and DCBS (and HMT if PR) 60 rpm – mix for 2 min (or drop at 110°C)
Roll mill	Between stages and after PD six times at 1 mm of separation

A.2.3 Moving die rheometer (MDR)

Alpha Technologies MDR 2000 was used to measure the cure kinetics of rubber compounds. The MDR was preheated at 150 °C for approximately 20-30 minutes to reach the thermal equilibrium before the experiment. After that the test was performed at 150 °C for 80 minutes with an oscillation of amplitude of 0.5° (~7% strain) and a frequency of 1.667 Hz. Scorch time (t_{s1}) and optimum cure times (t_{90}) were calculated from the MDR curves of each material. Scorch time is commonly determined by time required for the torque to rise one unit (dN·m) above the minimum torque (S'_{min}). The optimum cure time (t_{90}) is determined as the time

required to reach the torque corresponding to 90% (S'_{90}) of the change from minimum torque toward maximum achieved torque (S'_{\max}) that is calculated using the following equation (Eq. A.1).

$$S'_{t90} = 0.9 \cdot (S'_{\max} - S'_{\min}) + S'_{\min}, \quad (\text{A.1})$$

A.2.4 Curing of rubber compounds

The rubber compounds were cured up to its optimum cure time (t_{90}) by compression molding using a lab-scale hot press (Labtech Engineering, Thailand) at 150 °C and 150 bars pressure. A stainless-steel mold with a rectangular geometry (80×30×2 mm) was used to shape the materials. Based on the mold dimensions and the specific gravity of the material a suitable amount (~6 g) of the green compounds was added yielding a cured sheet with a thickness in the range of 1.8-2.0 mm after the vulcanization process.

A.2.5 Crosslinking density

The crosslink density was determined from the swelling test. For this purpose, small square cured materials were cut (5×10×2 mm) and their weight was noted (m_1). Then, they were completely immersed in 20 ml toluene at room temperature. The samples were kept in the solvent for three days and the solvent was changed after the first 24 hours. After the 72 hours, the swollen specimens were removed from the solvent, had their surface carefully dried, and weighted (m_2). The samples were then dried in an oven at 60 °C for 6 hours and the dry mass of the samples was noted (m_3). To generate statistically valid results the experiments were done in triplicate.

Crosslinking densities were then calculated using Flory-Rehner equation. To this aim, the volume fraction of rubber in equilibrium swollen vulcanizate sample (v_r) was first calculated according to Eq. A.2.

$$v_r = \frac{\frac{m_1 - f_f \cdot m_1}{\rho_c}}{\frac{m_1 - f_f \cdot m_1}{\rho_c} + \frac{m_2 - m_3}{\rho_s}}, \quad (\text{A.2})$$

wherein, m_1 is the initial sample mass; ρ_c is the density of the composition; m_2 is the swollen sample mass; m_3 is the dry sample mass after swelling test; and ρ_s is the solvent density (0.79 g·ml⁻¹). The f_f corresponds to the volume of the filler. These values were calculated assuming benzoxazines act as a filler considering a model density with a value of 1.2 g·ml⁻¹.

The crosslinking densities were then calculated following Eq. A.3.

$$v_c = \frac{-[\ln(1 - v_r) + v_r + \chi \cdot (v_r^2)]}{V_0 \cdot \left(v_r^{\frac{1}{3}} - \frac{v_r}{2} \right)}, \quad (\text{A.3})$$

wherein v_c is the crosslinking density; V_0 is the molar volume of the solvent (105.91 ml·mol⁻¹); χ is the interaction parameter between the solvent and polyisoprene that has been taken as 0.39,

the mean of upper and lower values, 0.44 and 0.35 respectively, provided in the Handbook of Polymer-Liquid Interaction Parameters and Solubility Parameters (Barton, A. F. M., CRC handbook of polymer-liquid interaction parameters and solubility parameters. *Polym. Adv. Technol.* **1992**, 3 (1), 47-47.).

A.2.6 Atomic force microscopy (AFM)

The samples were trimmed and surfaced with a LEICA EM UC6 cryo-ultramicrotome at -120 °C to produce a flat surface of the cross-section for AFM analysis. Images of the topography and nanomechanical properties (modulus and loss tangent) of the samples were acquired using the Amplitude Modulation-Frequency Modulation (AM-FM) mode of the MFP-3D Infinity AFM (Asylum Research). All measurements were made under ambient conditions (room temperature and relative humidity of about 50%) and a standard cantilever holder for operation in air was used. Images of 20×20 μm² or 5×5 μm² areas were taken with a resolution of 256×256 pixels at a scan rate of 1.5 Hz. Cantilevers' spring constants used in this study were about 30 N·m⁻¹ (AC160TS-R3 model from Olympus). The first and second resonant frequencies for AC160TS-R3 cantilevers were about 300 kHz and 1.6 MHz, respectively. To ensure repulsive intermittent contact mode, the amplitude setpoint was chosen as $A_{\text{setpoint}}/A_0 \sim 0.20$ so that the phase is well fixed below 90°. A relative calibration method was done to estimate the tip radius using a dedicated reference sample kit provided by Bruker (Model: PFQNM-SMPKIT-12m). The deflection sensitivity and the spring constant of the cantilever were determined using the GetReal™ Automated Probe Calibration feature. Using the polystyrene/low density polyethylene (PS/LDPE) standard sample, the tip radius was then adjusted to obtain the proper value of 2.7 GPa for the PS phase. The reported average and standard deviation values of modulus and loss tangent consider at least 5 and up to 10 images in each sample for reliable results.

A.2.7 Tensile test

The cured compounds were cut into a dumbbell shape using an ISO 37-2 die. Tensile properties of the samples were measured on an electro-mechanical universal testing machine Instron 5967. An extension rate of 200 mm·min⁻¹ was applied accordingly to ISO 37 during all the experiments. To generate statistically valid results three samples per formulation were tested. Young moduli were calculated from the slope at the beginning of the strain stress curves up to 1.5% of elongation.

A.2.8 Solubility of polybenzoxazines in the presence of sulfur

Solubility was assessed in dimethylformamide (DMF). 0.1 g (±0.01g) of benzoxazine monomers with and without 30 %wt of sulfur were cured at 150 °C for 1 hour After that, they were immersed in 5 ml of DMF for 3 hours.

A.3 Application of benzoxazine resins in tire compounds

A.3.1 Materials

Filled compounds were prepared with the chemical previously mentioned in Annex A, section A.2.1. Additionally, carbon black (CB) with trade name N550 that was purchased from

Birla Carbon and treated distillate aromatic extract oil (TDAE) with trade name TDAE oil that was purchased from PSP Specialities.

A.3.2 Rubber compounding

A Thermo Scientific HAAKE PolyLab OS internal mixer was used to perform the compounding. The internal mixer having a free volume of 85 cc was operated using two cam-type rotors and keeping a constant fill factor of 0.75. The mixing process was performed in three steps and it is detailed in Table A.2. In the first process, so-called non-productive step (NP1), polyisoprene, ZnO, stearic acid, half of the carbon black, and two thirds of the oil were mixed. The first step was common for all the compounds. The initial temperature of NP1 was set at 70 °C and the ingredients were mixed for 6 minutes. The second step (NP2) was different for the compounds with and without 3DPDS-fa as it is when the resin is mixed with the compound from NP1, and the rest of the CB and oil. In both cases, this step was subdivided in three parts. For the reference compound, 1/3 of the remaining CB and oil was progressively added in each substep. For the compounds with 3DPDS-fa, in the first two substeps the 1/3 of the remaining CB and the oil were mixed and in the last one the precursor was added with the rest of the CB (remaining 1/6). The initial temperature in NP2 was set at 110 °C to allow the melting of the precursors. Finally, in the final step so-called productive step (PD) sulfur and the accelerator were mixed with the compound from the NP2. The temperature is set at 60 °C and it should remain below 110 °C to avoid early vulcanization of the compounds.

Table A.2. Procedure carried out for the rubber compounding for filled compounds.

Step	Procedure Reference	Procedure Compounds with 3DPDS-fa
NP1		Initial temperature: 70 °C 20 rpm – add the polymer 60 rpm – masticate for 1 min 2 rpm – ½ CB, 2/3 oil, ZnO and stearic acid 60 rpm – mix for 4 min 80 rpm – mix for 6 min (or drop at 150 °C)
NP2	Initial temperature: 110 °C 20 rpm – add compound from NP1 60 rpm – masticate for 30 s 2 rpm – 1/6 CB with 1/9 oil (30 s) 60 rpm – masticate for 30 s 2 rpm – 1/6 CB with 1/9 oil (30 s) 60 rpm – masticate for 30 s 2 rpm – 1/6 CB with 1/9 oil (30 s) 60 rpm – mix for 4 min (or drop at 150 °C)	Initial temperature: 110 °C 20 rpm – add compound from NP1 60 rpm – masticate for 30 s 2 rpm – 1/6 CB with 1/6 oil (30 s) 60 rpm – masticate for 30 s 2 rpm – 1/6 CB with 1/6 oil (30 s) 60 rpm – masticate for 30 s 2 rpm – 1/6 CB with Bz (or PR) (30 s) 60 rpm – mix for 4 min (or drop at 150 °C)
PD		Initial temperature: 60 °C 20 rpm – add compound 60 rpm – masticate for 30 s 2 rpm – add sulfur and DCBS (and HMT if PR) 60 rpm – mix for 2 min (or drop at 110°C)
Roll mill	Between stages and after PD six times at 2 mm of separation	

A.3.3 Moving die rheometer (MDR)

The cure kinetics of filled compounds was performed as described in Annex A, section A.2.3.

A.3.4 Curing of rubber compounds

The rubber compounds were cured by compression molding at 150 °C and 150 bars to the calculated t_{90} values of each compounds. The curing was performed in a Labtech Engineering hot press and a stainless-steel mold with a rectangular geometry (80×30×2 mm) to which approximately 7.5 g of compound was added yielding a cured sheet with a thickness in the range of 1.9-2.1 mm.

A.3.5 Crosslinking density

The crosslink density was determined from the swelling test. For this purpose, small square cured materials were cut (5×10×2 mm) and their weight was noted (m_1). Then, they were completely immersed in 20 ml toluene at room temperature. The samples were kept in the solvent for three days and the solvent was changed after the first 24 hours. After the 72 hours, the swollen specimens were removed from the solvent, had their surface carefully dried, and weighted (m_2). The samples were then dried in an oven at 60 °C for 6 hours and the dry mass of the samples was noted (m_3). To generate statistically valid results the experiments were done in triplicate.

Crosslinking densities were then calculated using Flory-Rehner equation. To this aim, the volume fraction of rubber in equilibrium swollen vulcanizate sample (v_r) was firstly calculated according to Eq. A.2.

$$v_r = \frac{\frac{m_1 - f_f \cdot m_1}{\rho_c}}{\frac{m_1 - f_f \cdot m_1}{\rho_c} + \frac{m_2 - m_3}{\rho_s}}, \quad (\text{A.2})$$

wherein, m_1 is the initial sample mass; ρ_c is the density of the composition; m_2 is the swollen sample mass; m_3 is the dry sample mass after swelling test; and ρ_s is the solvent density (0.79 g·ml⁻¹). The f_f corresponds to the volume of the filler. These values were calculated assuming both carbon and benzoxazines act as fillers and considering a density of 1.8 and 1.2 g·ml⁻¹ respectively.

The crosslinking densities were then calculated following Eq. A.3.

$$v_c = \frac{-\left[\ln(1 - v_r) + v_r + \chi \cdot (v_r^2)\right]}{V_0 \cdot \left(v_r^{\frac{1}{3}} - \frac{v_r}{2}\right)}, \quad (\text{A.3})$$

wherein v_c is the crosslinking density; V_0 is the molar volume of the solvent (105.91 ml·mol⁻¹); χ is the interaction parameter between the solvent and polyisoprene that has been taken as 0.39, the mean of upper and lower values, 0.44 and 0.35 respectively, provided in the Handbook of Polymer-Liquid Interaction Parameters and Solubility Parameters (Barton, A. F. M., CRC

handbook of polymer-liquid interaction parameters and solubility parameters. *Polym. Adv. Technol.* **1992**, *3* (1), 47-47.).

A.3.6 Tensile test

The cured compounds were cut into a dumbbell shape using an ISO 37-2 die. Tensile properties of the samples were measured on an electro-mechanical universal testing machine Instron 5967. An extension rate of $200 \text{ mm}\cdot\text{min}^{-1}$ was applied accordingly to ISO 37 during all the experiments. To generate statistically valid results at least three samples per formulation were tested. Young moduli were calculated from the slope at the beginning of the strain stress curves up to 1.5% of elongation.

In order to investigate the rate of stress softening of the material, additional samples were deformed cyclically for 5 times at each strain-controlled interval of 15%, 30%, 70%, and 90%, respectively, as shown in Figure A.1. The unloading cycle was set to the minimum force of 0.1 MPa to avoid the sample from buckling.

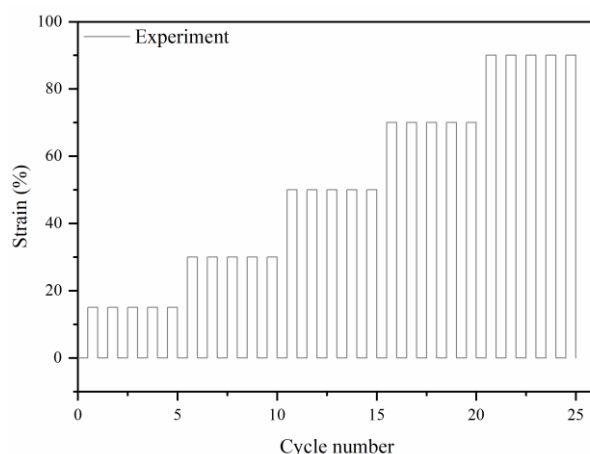


Figure A.1. The cyclic tensile test program to evaluate cyclic stress softening behavior.

Cyclic tensile tests were performed of the final materials at 50% of strain to determine the energy loss. The unloading cycle was set to the minimum force of 0.1 MPa to avoid the sample from buckling.

A.3.7 Dynamic mechanical analyses (DMA)

Dynamic strain sweeps of the cured compounds were performed Metravib dynamic mechanical analyzer DMA+1000 in shear mode. Discs with a diameter of 10 or 5 mm and a thickness from 1.6 to 2 mm were cut from the cured sheet. The strain amplitude was carried out from 0.1 to 50% at 25 and 70 °C at a frequency of 7.8 Hz.

Dynamic temperature sweep were performed on a Netzsch DMA 242 C, Germany instrument in elongation mode. The samples were cut from the cured sheet with a sharp razor blade with a dimension of $10\times 6.5\times 2 \text{ mm}$ (L×W×T). Temperature sweeps were done at a heating rate of $2 \text{ }^\circ\text{C}\cdot\text{min}^{-1}$ within a temperature range of -180 to 200 °C at a frequency of 10 Hz. A static strain of 1% was applied with a dynamic strain of 0.1% to the sample during the whole course of the experiment.

A.3.8 Atomic force microscopy (AFM)

The AFM measurements were performed following the procedure and experimental conditions previously described in Annex A, section A.2.6.

Annex B. Synthesis and molecular characterization of the structural features

B.1 Synthesis and characterization of 4DPDS-fa

The disulfide-containing benzoxazine (4DPDS-fa) was synthesized by Mannich condensation. 4,4'-Dihydroxydiphenyl disulfide (6 g., 24 mmol, 1 eq.), furfurylamine (4.7 g., 48 mmol, 2 eq.) and paraformaldehyde (3 g., 96 mmol, 4 eq.) were reacted in toluene in a round bottom flask under mechanical stirring at 110 °C for 5 hours. After the reaction the solvent was evaporated under reduced pressure. Then, the product was solubilized in CHCl₃ and three liquid-liquid extractions with 2 N NaOH and three with distilled water were carried out. The organic layer was dried over magnesium sulfate, then filtered and the solvent evaporated under reduced pressure. The final product was dried for 4 hours under reduced pressure (<1 mBar) at 100 °C. Yield = 90%. An orange solid was obtained with a melting point of 74 °C.

Elemental analysis: element (exp, th); N (3.2, 3.5); C (44.3, 44.8); H (42.7, 41.4); S (3.4, 3.4); O (6.4, 6.9).

¹H NMR (CDCl₃, 600 MHz, 298 K), δ (ppm) = (assignment, [attribution], experimental integration, theoretical integration). δ = 3.89 (N-CH₂, [d], exp 2.02 H, th 2.00 H); 3.97 (N-CH₂-Ar, [2], exp 2.02 H, th 2.00 H); 4.88 (N-CH₂-O, [1], integration reference 2.00 H); 6.24 (-CH=CH*-C-, [e], exp 1.08 H, th 1.00 H); 6.33 (-CH*=CH-C-, [f], exp 1.04 H, th 1.00 H); 6.75 (-CH-CH*=C-S-, [c], exp 1.06 H, th 1.00 H); 7.09 (-C=CH-C-S-, [a], exp 1.07 H, th 1.00 H); 7.24 (-CH*-CH=C-S-, [b], exp - H, th 1.00 H); 7.41 (-CH=CH*-O-, [g], exp 1.05 H, th 1.00 H).

¹³C NMR (CDCl₃, 600 MHz, 298 K), δ (ppm) = (assignment, [attribution]). δ = 48.2 (N-CH₂, [d]); 49.4 (N-CH₂-Ar, [2]); 82.0 (N-CH₂-O, [1]); 109.2 (-CH=CH*-C-, [e]); 110.3 (-CH*=CH-C-, [f]); 117.4 (-CH-CH*=C-S-, [c]); 120.3 (-CH₂-C*-CH-, [i]); 128.5 (C-S, [j]); 130.2 (-C=CH*-C-S-, [a]); 130.6 (-CH*-CH=C-S-, [b]); 142.7 (-CH=CH*-O-, [g]); 151.2 (-CH=C*-O-, [k]); 154.3 (CH=C-O, [h]).

B.2 Synthesis and characterization of 4DPDS-a

The disulfide-containing benzoxazine (4DPDS-a) was synthesized by Mannich condensation. 4,4'-Dihydroxydiphenyl disulfide (5.0 g., 20 mmol, 1 eq.), aniline (3.72 g., 40 mmol, 2 eq.) and paraformaldehyde (2.4 g., 80 mmol, 4 eq.) were reacted in toluene in a round bottom flask under mechanical stirring at 110 °C for 5 hours. After the reaction the solvent was evaporated under reduced pressure. Then, the product was solubilized in CHCl₃ and three liquid-liquid extractions with 2 N NaOH and three with distilled water were carried out. The organic layer was dried over magnesium sulfate, then filtered and the solvent evaporated under reduced pressure. The final product was dried for 4 hours under reduced pressure (<1 mBar) at 100 °C. Yield = 80%. An orange solid was obtained with a melting point of 129 °C.

Elemental analysis: element (exp, th); N (3.4, 3.4); C (48.7, 48.3); H (41.4, 41.5); S (3.6, 3.4); O (2.9, 3.4).

^1H NMR (DMSO, 600 MHz, 298 K), δ (ppm) = (assignment, [attribution], experimental integration, theoretical integration). δ = 4.65 (N-CH₂-Ar, [2], exp 2.03 H, th 2.00 H); 5.48 (N-CH₂-O, [1], integration reference 2.00 H); 6.74 (-CH=CH*-C-, [c], exp 1.00 H, th 1.00 H); 6.87 (-CH=CH*-CH=, [h], exp 1.03 H, th 1.00 H); 7.12 (-CH*=C-N-, [d, e], exp 2.09 H, th 2.00 H); 7.20 (-CH-CH*=C-S-, [b], exp 1.08 H, th 1.00 H); 7.23 (-CH*-CH=C-N-, [g, f], exp 2.07 H, th 2.00 H); 7.28 (-C-CH*=C-S-, [a], exp 1.01 H, th 1.00 H).

^{13}C NMR (DMSO, 600 MHz, 298 K), δ (ppm) = (assignment, [attribution]). δ = 48.5 (N-CH₂-Ar, [2]); 78.9 (N-CH₂-O, [1]); 117.29 (-CH=CH*-C-, [c]); 117.32 (-CH*=C-N-, [d, e]); 120.6 (-CH=CH*-CH=, [h]); 122.9 (CH₂-C*(=C)-CH, [i]); 127.2 (C-S, [j]); 129.0 (-CH*-CH=C-N-, [g, f]); 129.4-130.0 (-CH-CH*=C-S-, [a, b]); 147.9 (C-C*(=C)-N, [m]); 155.1 (O-C*(=C)-CH, [k]).

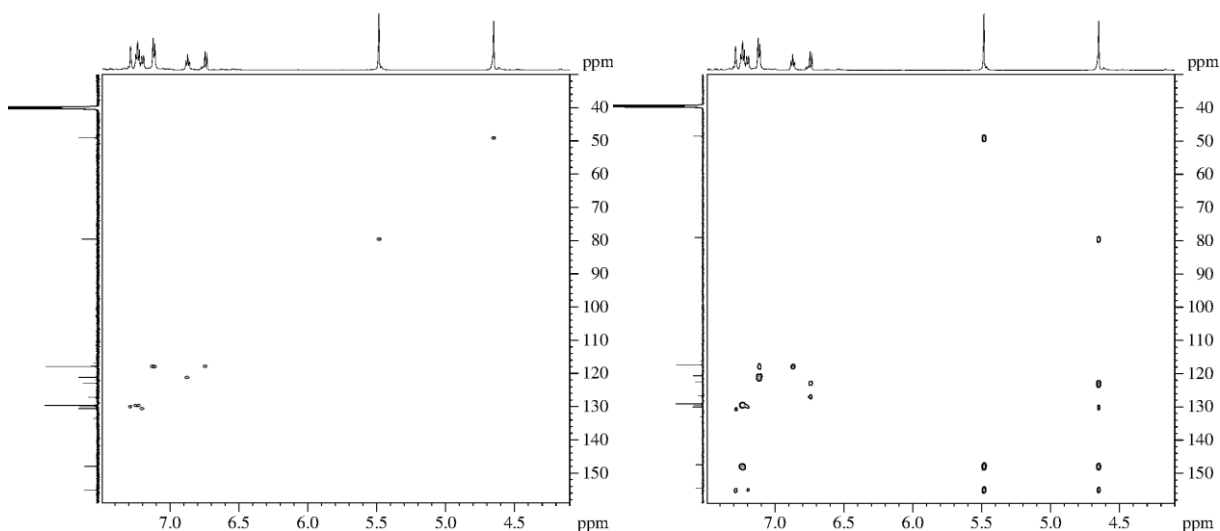


Figure B.1. 2D NMR spectra in DMSO of 4DPDS-a HSQC on the left and HMBC on the right.

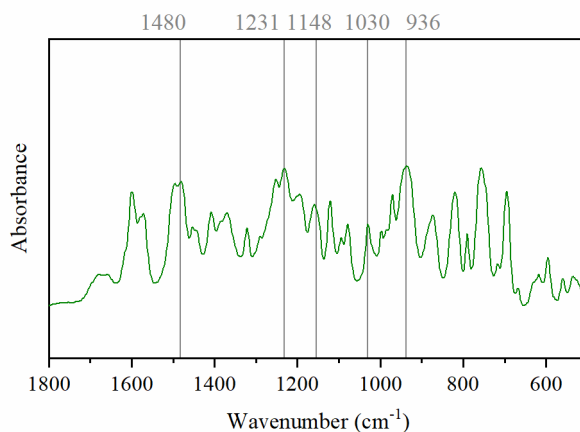


Figure B.2. FTIR transmission spectrum of 4DPDS-a.

B.3 Synthesis and characterization of 4DPDS-ste

The disulfide-containing benzoxazine (4DPDS-ste) was synthesized by Mannich condensation. 4,4'-Dihydroxydiphenyl disulfide (4 g., 16 mmol, 1 eq.), stearylamine (8.64 g., 32 mmol, 2 eq.) and paraformaldehyde (1.92 g., 64 mmol, 4 eq.) were reacted in toluene in a round bottom flask under mechanical stirring at 110 °C for 4 hours. After the reaction the solvent was evaporated under reduced pressure. Then, the product was solubilized in CHCl₃ and three

liquid-liquid extractions with 2 N NaOH and three with distilled water were carried out. The organic layer was dried over magnesium sulfate, then filtered and the solvent evaporated under reduced pressure. The final product was dried for 4 hours under reduced pressure (<1mBar) at 100 °C. Yield = 76%. An orange solid was obtained with a melting point of 40-65 °C.

^1H NMR (CDCl_3 , 600 MHz, 298 K), δ (ppm) = (assignment, [attribution], experimental integration, theoretical integration). δ = 0.89 ($\text{CH}_3^*-\text{CH}_2-$, [f], exp 4.31 H, th 4.00 H); 1.25 ($-\text{CH}_3-(\text{CH}_2)^*-\text{CH}_2-$) [e], exp 42.05 H, th 42.00 H); 2.74 ($-\text{CH}_2^*-\text{N}$ [d], exp 1.84 H, th 2.00 H); 3.99 ($\text{N}-\text{CH}_2-\text{Ar}$, [2], exp 2.02 H, th 2.00 H); 4.87 ($\text{N}-\text{CH}_2-\text{O}$, [1], integration reference 2.00 H); 6.72 ($-\text{CH}^*-\text{CH}=\text{C}-\text{S}-$, [c], exp 0.91 H, th 1.00 H); 7.10 ($-\text{C}=\text{CH}-\text{C}-\text{S}-$, [a], exp 1.03 H, th 1.00 H); 7.23 ($-\text{CH}-\text{CH}^*=\text{C}-\text{S}-$, [b], exp 1.00 H, th 1.00 H).

^{13}C NMR (CDCl_3 , 600 MHz, 298 K), δ (ppm) = (assignment, [attribution]). δ = 14.1 ($\text{CH}_3^*-\text{CH}_2-$, [f]); 22.7-31.9 ($-\text{CH}_3-(\text{CH}_2)^*-\text{CH}_2-$) [e]; 50.2 ($\text{N}-\text{CH}_2-\text{Ar}$, [2]); 51.9 ($-\text{CH}_2^*-\text{N}$ [d]); 82.4 ($\text{N}-\text{CH}_2-\text{O}$, [1]); 116.2 ($-\text{CH}_2-\text{C}^*-\text{CH}-$, [i]); 117.3 ($-\text{CH}^*-\text{CH}=\text{C}-\text{S}-$, [c]); 130.1 ($\text{C}-\text{S}$, [j]); 130.6 ($-\text{C}=\text{CH}^*-\text{C}-\text{S}-$, [a]); 130.6 ($-\text{CH}-\text{CH}^*=\text{C}-\text{S}-$, [b]); 155.1 ($-\text{CH}=\text{C}^*-\text{O}-$, [k]).

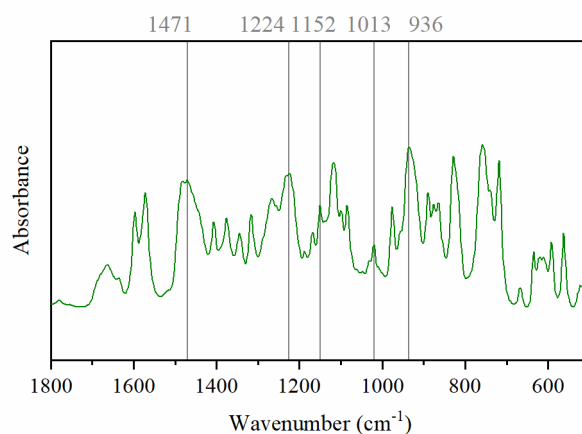


Figure B.3. FTIR transmission spectrum of 4DPDS-ste.

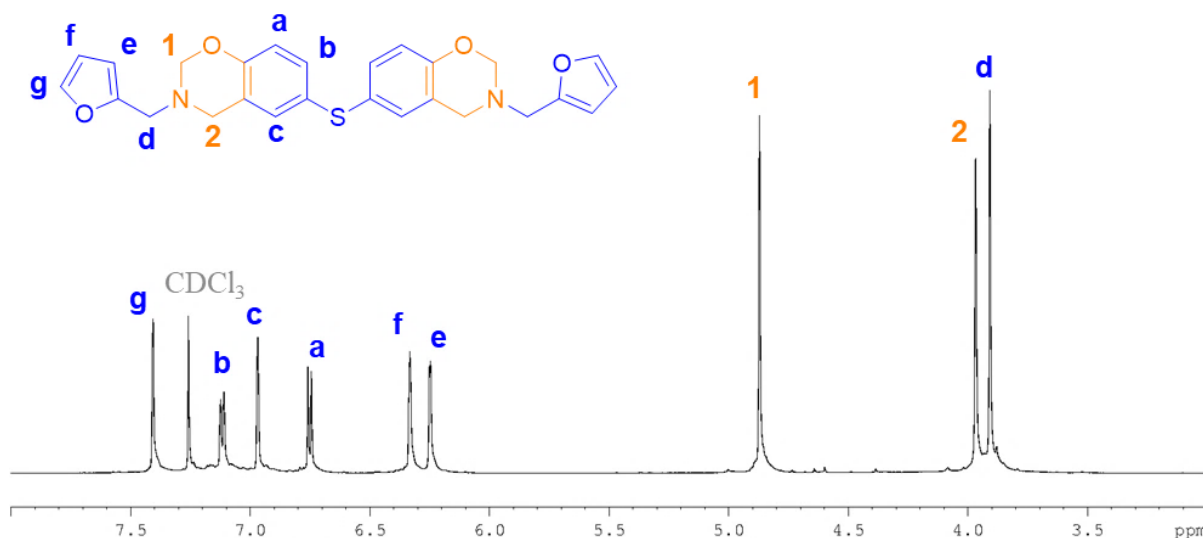
B.4 Synthesis and characterization of 4DTP-fa

The sulfur-containing benzoxazine (4DTP-fa) was synthesized by Mannich condensation. 4,4'-Thiodiphenol and furfurylamine (6 g., 27.5 mmol, 1 eq.), furfurylamine (5.3 g., 55 mmol, 2 eq.) and paraformaldehyde (3.5 g., 110 mmol, 4 eq.) were reacted in toluene in a round bottom flask under mechanical stirring at 110 °C for 4 hours. After the reaction the solvent was evaporated under reduced pressure. Then, the product was solubilized in CHCl_3 and three liquid-liquid extractions with 2 N NaOH and three with distilled water were carried out. The organic layer was dried over magnesium sulfate, then filtered and the solvent evaporated under reduced pressure. The final product was dried for 4 hours under reduced pressure (<1mBar) at 100 °C. Yield = 88%. An orange solid was obtained with a melting point of 90 °C.

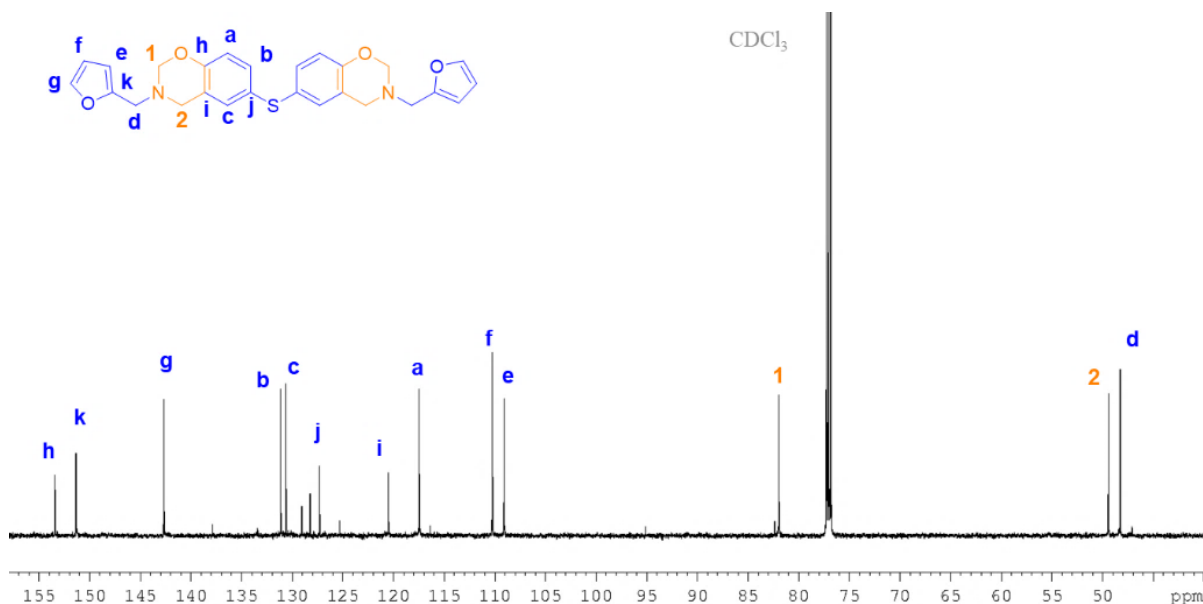
Elemental analysis: element (exp, th); N (3.2, 3.5); C (46.4, 45.6); H (42.2, 42.1); S (1.8, 1.8); O (6.3, 7.0).

^1H NMR (CDCl_3 , 600 MHz, 298 K), δ (ppm) = (assignment, [attribution], experimental integration, theoretical integration). δ = 3.91 ($\text{N}-\text{CH}_2$, [d], exp 2.09 H, th 2.00 H); 3.97 ($\text{N}-\text{CH}_2-\text{Ar}$, [2], exp 2.01 H, th 2.00 H); 4.87 ($\text{N}-\text{CH}_2-\text{O}$, [1], integration reference 2.00 H); 6.25

($-\text{CH}=\text{CH}^*-\text{C}-$, [e], exp 1.02 H, th 1.00 H); 6.33 ($-\text{CH}^*=\text{CH}-\text{C}-$, [f], exp 1.03 H, th 1.00 H); 6.75 ($-\text{CH}-\text{CH}^*=\text{C}-\text{S}-$, [c], exp 1.00 H, th 1.00 H); 6.97 ($-\text{C}=\text{CH}-\text{C}-\text{S}-$, [b], exp 0.99 H, th 1.00 H); 7.11 ($-\text{CH}^*-\text{CH}=\text{C}-\text{S}-$, [a], exp 0.99 H, th 1.00 H); 7.41 ($-\text{CH}=\text{CH}^*-\text{O}-$, [g], exp 1.00 H, th 1.00 H).

Figure B.4. ^1H NMR spectrum in CHCl_3 of 4DTP-fa.

^{13}C NMR (CDCl_3 , 600 MHz, 298 K), δ (ppm) = (assignment, [attribution]). $\delta = 48.6$ (N- CH_2 , [d]); 49.4 (N- CH_2 -Ar, [2]); 82.0 (N- CH_2 -O, [1]); 109.1 ($-\text{CH}=\text{CH}^*-\text{C}-$, [e]); 110.2 ($-\text{CH}^*=\text{CH}-\text{C}-$, [f]); 117.5 ($-\text{CH}-\text{CH}^*=\text{C}-\text{S}-$, [a]); 120.5 ($-\text{CH}_2-\text{C}^*-\text{CH}-$, [i]); 127.3 (C-S, [j]); 130.6 ($-\text{C}=\text{CH}^*-\text{C}-\text{S}-$, [c]); 131.1 ($-\text{CH}^*-\text{CH}=\text{C}-\text{S}-$, [b]); 142.7 ($-\text{CH}=\text{CH}^*-\text{O}-$, [g]); 151.4 ($-\text{CH}=\text{C}^*-\text{O}-$, [k]); 153.4 ($\text{CH}=\text{C}-\text{O}$, [h]).

Figure B.5. ^{13}C NMR spectrum in CHCl_3 of 4DTP-fa.

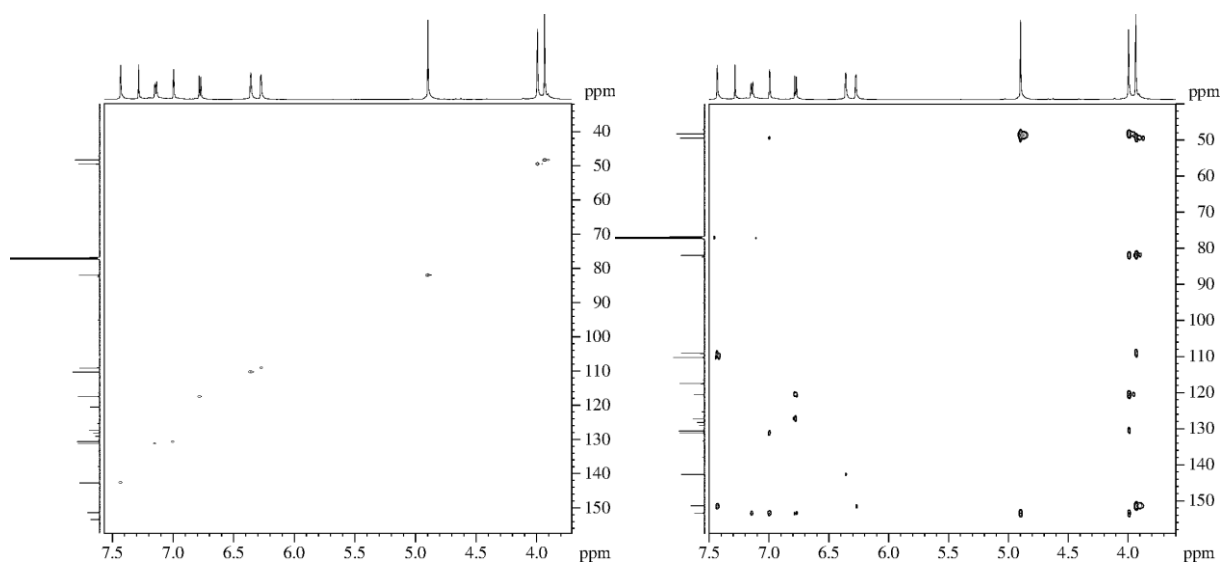
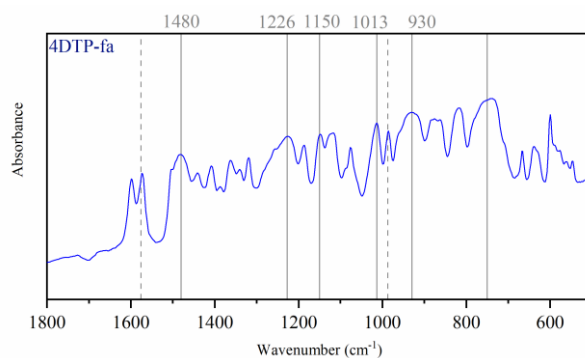
Figure B.6. 2D NMR spectra in CHCl_3 of 4DTP-fa HSQC on the left and HMBC on the right.

Figure B.7. FTIR transmission spectrum of 4DTP-fa.

B.5 Synthesis and characterization of 4DTP-a

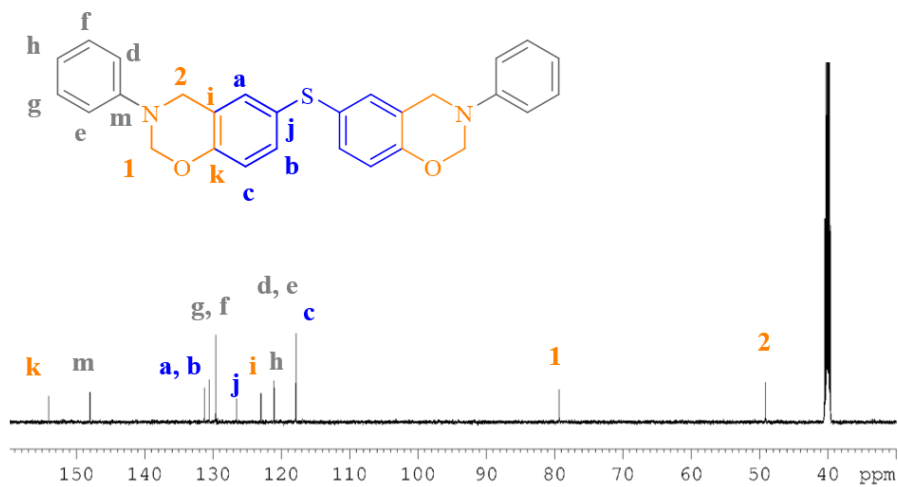
The sulfur-containing benzoxazine (4DTP-a) was synthesized by Mannich condensation. 4,4'-Thiodiphenol and furfurylamine (6 g., 27.5 mmoles, 1 eq.), aniline (5.1 g., 55 mmoles, 2 eq.) and paraformaldehyde (3.5 g., 110 mmoles, 4 eq.) were reacted in toluene in a round bottom flask under mechanical stirring at 110 °C for 4 hours. After the reaction the solvent was evaporated under reduced pressure. Then, the product was solubilized in CHCl_3 and three liquid-liquid extractions with 2 N NaOH and three with distilled water were carried out. The organic layer was dried over magnesium sulfate, then filtered and the solvent evaporated under reduced pressure. The final product was dried for 4 hours under reduced pressure (<1mBar) at 100 °C. Yield = 75%. An orange solid was obtained with a melting point of 114 °C.

Elemental analysis: element (exp, th); N (3.2, 3.5); C (46.4, 45.6); H (42.2, 42.1); S (1.8, 1.8); O (6.3, 7.0).

^1H NMR (DMSO, 600 MHz, 298 K), δ (ppm) = (assignment, [attribution], experimental integration, theoretical integration). δ = 4.64 (N- CH_2 -Ar, [2], exp 2.01 H, th 2.00 H); 5.46 (N- CH_2 -O, [1], integration reference 2.00 H); 6.72 ($-\text{CH}=\text{CH}^*-\text{C}-$, [c], exp 1.02 H, th 1.00 H); 6.87 ($-\text{CH}=\text{CH}^*-\text{CH}=\text{}$, [h], exp 1.06 H, th 1.00 H); 7.04 ($-\text{CH}-\text{CH}^*=\text{C}-\text{S}-$, [b], exp 1.07 H, th 1.00 H); 7.12 ($-\text{CH}^*=\text{C}-\text{N}-$, [d, e], exp 2.01 H, th 2.00 H); 7.22 ($-\text{C}-\text{CH}^*=\text{C}-\text{S}-$, [a], exp 1.01 H, th 1.00 H); 7.25 ($-\text{CH}^*-\text{CH}=\text{C}-\text{S}-$, [g, f], exp 2.09 H, th 2.00 H).

Figure B.8. ^1H NMR spectrum in DMSO of 4DTP-a.

^{13}C NMR (DMSO, 600 MHz, 298 K), δ (ppm) = (assignment, [attribution]). $\delta = 49.1$ (N-CH₂-Ar, [2]); 79.3 (N-CH₂-O, [1]); 117.83 (-CH=CH*-C-, [c]); 117.88 (-CH*=C-N-, [d, e]); 121.1 (-CH=CH*-CH=, [h]); 123.0 (CH₂-C*(=C)-CH, [i]); 126.5 (C-S, [j]); 129.6 (-CH*-CH=C-S-, [g, f]); 130.5-131.3 (-CH-CH*=C-S-, [a, b]); 148.0 (C-C*(=C)-N, [m]); 154.1 (O-C*(=C)-CH, [k]).

Figure B.9. ^{13}C NMR spectrum in DMSO of 4DTP-a.

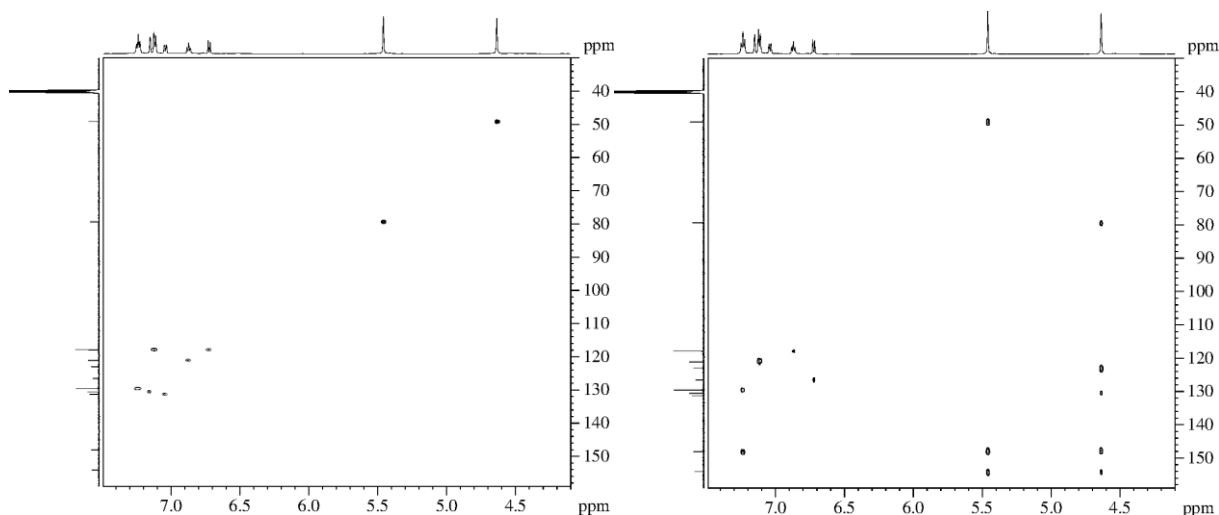


Figure B.10. 2D NMR spectra in DMSO of 4DTP-a HSQC on the left and HMBC on the right.

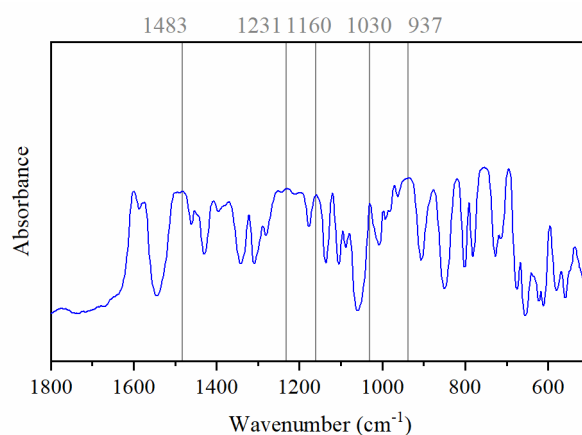


Figure B.11. FTIR transmission spectrum of 4DTP-a.

B.6 Synthesis and characterization of BA-fa

The model benzoxazine from bisphenol A and furfurylamine (BA-fa) was synthesized by Mannich condensation following a procedure already reported. Bisphenol A (6 g., 26 mmoles, 0.5 eq.), furfurylamine (5.1 g., 52 mmoles, 1eq.) and paraformaldehyde (3.1 g., 104 mmoles, 2 eq.) were reacted in toluene in a round bottom flask under mechanical stirring at 110 °C for 8 hours. After the reaction the solvent was evaporated under reduced pressure. Then, the product was solubilized in CHCl_3 and three liquid-liquid extractions with 2 N NaOH and three with distilled water were carried out. The organic layer was dried over magnesium sulfate, then filtered and the solvent evaporated under reduced pressure. The final product was dried for 4 hours under reduced pressure (<1mBar) at 100 °C. Yield = 85%. An orange solid was obtained with a melting point of 100 °C.

Elemental analysis: element (exp, th); N (3.0, 3.1); C (44.0, 44.6); H (46.1, 46.2); O (6.9, 6.1).

^1H NMR (CDCl_3 , 600 MHz, 298 K), δ (ppm) = (assignment, [attribution], experimental integration, theoretical integration). δ = 1.59 ($-\text{CH}_3$, [A], exp 4.18 H, th 4.00 H); 3.94 (N- CH_2 , [d], exp 2.07 H, th 2.00 H); 3.99 (N- CH_2 -Ar, [2], exp 2.01 H, th 2.00 H); 4.85 (N- CH_2 -O, [1], integration reference 2.00 H); 6.26 ($-\text{CH}=\text{CH}^*-\text{C}-$, [e], exp 1.00 H, th 1.00 H); 6.33 ($-\text{CH}^*=\text{CH}-\text{C}-$, [f], exp 1.03 H, th 1.00 H); 6.71 ($-\text{O}-\text{C}=\text{CH}^*-\text{CH}$, [c], exp 1.00 H, th 1.00 H);

6.81 (–C=CH–C–, [a], exp 0.99 H, th 1.00 H); 7.11 (–O–C=CH–CH*, [b], exp 1.01 H, th 1.00 H); 7.41 (–CH=CH*–O–, [g], exp 1.00 H, th 1.00 H).

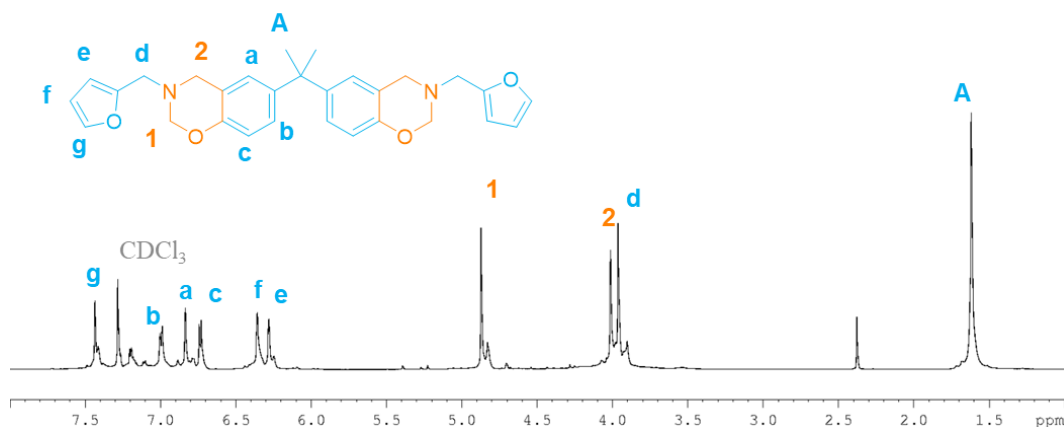


Figure B.12. ^1H NMR spectrum in CHCl_3 of BA-fa.

^{13}C NMR (CDCl_3 , 600 MHz, 298 K), δ (ppm) = (assignment, [attribution]). $\delta = 31.2$ (– CH_3 , [A]); 41.9 ($\text{CH}_3\text{--C}^*\text{--C--}$, [l]); 48.5 (N– CH_2 , [d]); 50.1 (N– $\text{CH}_2\text{--Ar}$, [2]); 81.8 (N– $\text{CH}_2\text{--O}$, [1]); 109.1 (– $\text{CH}=\text{CH}^*\text{--C--}$, [e]); 110.3 (– $\text{CH}^*=\text{CH--C--}$, [f]); 116.1 (– $\text{O--C}=\text{CH}^*\text{--CH}$, [c]); 118.9 (– $\text{CH}_2\text{--C}^*\text{--CH--}$, [i]); 125.5 (– $\text{C}=\text{CH--C--}$, [a]); 126.5 (– $\text{O--C}=\text{CH--CH}^*$, [b]); 142.7 (– $\text{CH}=\text{CH}^*\text{--O--}$, [g]); 143.4 ($\text{CH}_3\text{--C--C}^*$, [j]); 151.8 (– $\text{CH}=\text{C}^*\text{--O--}$, [k]); 151.9 ($\text{CH}=\text{C--O}$, [h]).

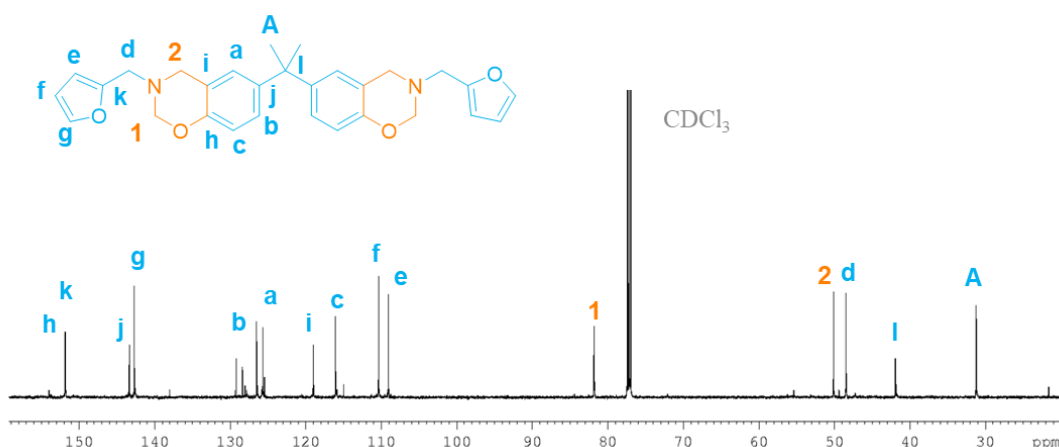


Figure B.13. ^{13}C NMR spectrum in CHCl_3 of BA-fa.

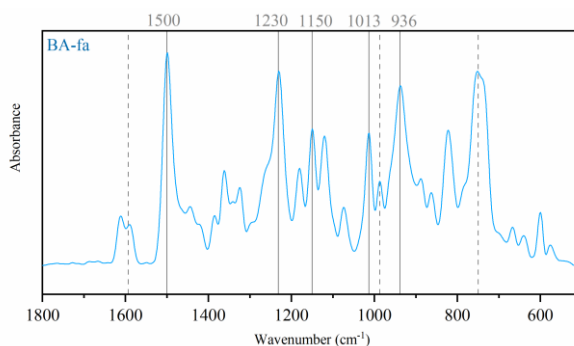


Figure B.14. FTIR transmission spectrum of BA-fa.

B.7 Synthesis and characterization of BA-a

The model benzoxazine from bisphenol A and aniline (BA-a) was synthesized by Mannich condensation following a procedure already reported. Bisphenol A (4.6 g., 20 mmoles, 1 eq.), aniline (3.73 g., 40 mmoles, 2 eq.) and paraformaldehyde (2.4 g., 80 mmoles, 4 eq.) were reacted in toluene in a round bottom flask under mechanical stirring at 110 °C for 8 hours. After the reaction the solvent was evaporated under reduced pressure. Then, the product was solubilized in CHCl₃ and three liquid-liquid extractions with 2 N NaOH and three with distilled water were carried out. The organic layer was dried over magnesium sulfate, then filtered and the solvent evaporated under reduced pressure. The final product was dried for 4 hours under reduced pressure (<1mBar) at 100 °C. Yield = 87%. An orange solid was obtained with a melting point of 100 °C.

Elemental analysis: element (exp, th); N (2.8, 3.1); C (47.9, 47.7); H (46.4, 46.1); O (2.9, 3.1).

¹H NMR (DMSO, 600 MHz, 298 K), δ (ppm) = (assignment, [attribution], experimental integration, theoretical integration). δ = 1.63 (–CH₃, [A], exp 4.01 H, th 4.00 H); 4.62 (N–CH₂–Ar, [2], exp 1.98 H, th 2.00 H); 5.37 (N–CH₂–O, [1], integration reference 2.00 H); 6.74 (–CH=CH*–C–, [c], exp 1.17 H, th 1.00 H); 6.88 (–C–CH*=C–C–, [a], exp 1.02 H, th 1.00 H); 6.98 (–CH=CH*–CH=, [h], exp 1.15 H, th 1.00 H); 7.14 (–CH*=C–N–, [d, e], exp 2.22 H, th 2.00 H); 7.21 (–CH–CH*=C–C–, [b], exp 1.20 H, th 1.00 H); 7.28 (–CH*–CH=C–N–, [g, f], exp 2.06 H, th 2.00 H).

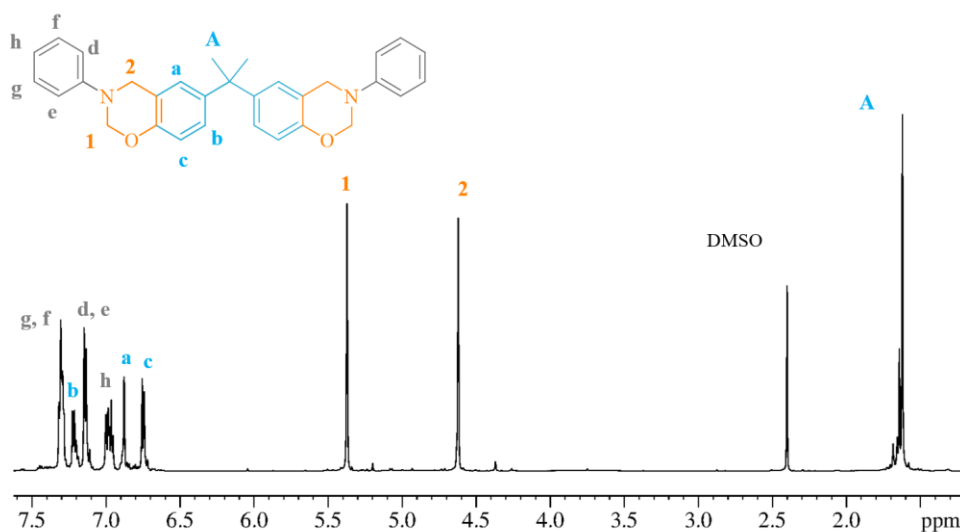


Figure B.15. ¹H NMR spectrum in DMSO of BA-a.

¹³C NMR (DMSO, 600 MHz, 298 K), δ (ppm) = (assignment, [attribution]). δ = 31.1 (–CH₃, [A]); 41.8 (CH₃–C*–C–, [n]); 50.7 (N–CH₂–Ar, [2]); 79.2 (N–CH₂–O, [1]); 116.4 (–CH=CH*–C–, [c]); 118.1 (–CH*=C–N–, [d, e]); 120.1 (–CH=CH*–CH=, [h]); 121.1 (CH₂–C*(=C)–CH, [i]); 126.4–127.9 (–CH–CH*=C–C–, [a, b]); 129.2 (–CH*–CH=C–N–, [g, f]); 143.2 (CH₃–C*–, [j]); 148.5 (C–C*(=C)–N, [m]); 151.8 (–CH=C*–O–, [k]).

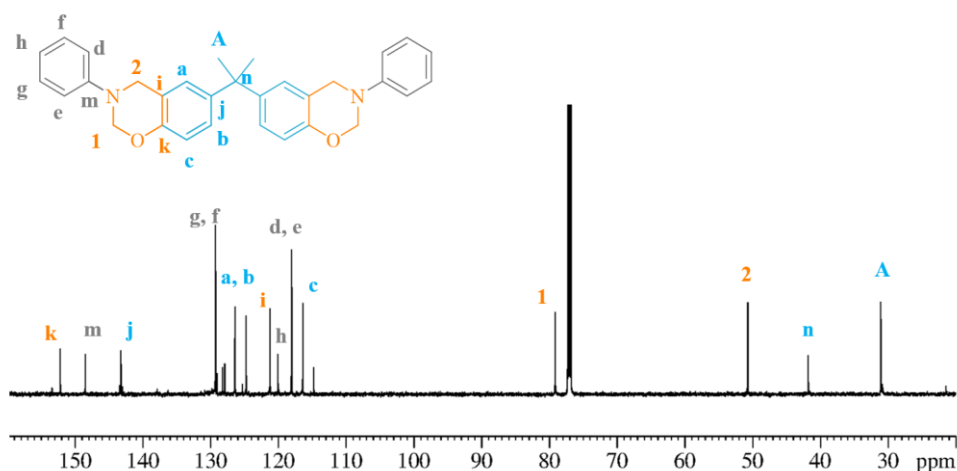
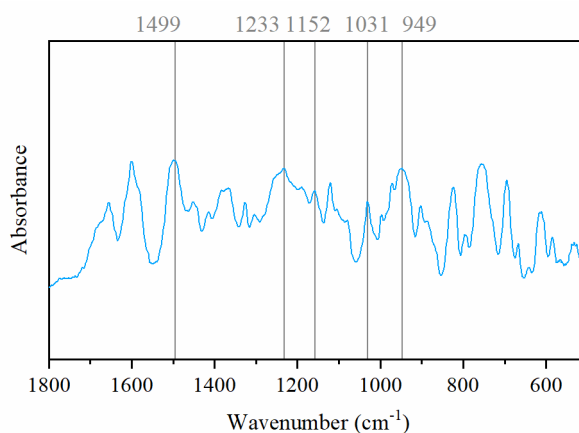
Figure B.16. ^{13}C NMR spectrum in DMSO of BA-a.

Figure B.17. FTIR transmission spectrum of BA-a.

B.8 Synthesis and characterization of 3DPDS-fa

The disulfide-containing benzoxazine (3DPDS-fa) was synthesized by Mannich condensation. 3,3'-Dihydroxydiphenyl disulfide (6.3 g., 24 mmoles, 1 eq.), furfurylamine (4.8 g., 50 mmoles, 2 eq.) and paraformaldehyde (3.2 g., 100 mmoles, 4 eq.) were reacted in toluene in a round bottom flask under mechanical stirring at 110 °C for 5 hours. After the reaction the solvent was evaporated under reduced pressure. Then, the product was solubilized in CHCl_3 and three liquid-liquid extractions with 2 N NaOH and three with distilled water were carried out. The organic layer was dried over magnesium sulfate, then filtered and the solvent evaporated under reduced pressure. The final product was dried for 4 hours under reduced pressure (<1mBar) at 100 °C. Yield = 91%. An orange solid was obtained with a melting point of 90-115 °C.

Elemental analysis: element (exp, th); N (3.2, 3.5); C (44.9, 44.8); H (42.0, 41.4); S (3.9, 3.4); O (6.0, 6.9).

^1H NMR (CDCl_3 , 600 MHz, 298 K), δ (ppm) = (assignment, [attribution], experimental integration, theoretical integration). δ = 3.85, 3.89, 3.91 (N- CH_2 , [d'', d', d], exp 2.02 H, th 2.00 H); 3.98, 4.07, 4.13 (N- CH_2 -Ar, [2, 2'', 2'], exp 2.09 H, th 2.00 H); 4.84, 4.86, 4.87 (N- CH_2 -O, [1'', 1', 1], integration reference 2.00 H); 6.25 (-CH=CH*-C-, [e], exp 1.00 H, th 1.00 H); 6.33 (-CH*=CH-C-, [f], exp 1.01 H, th 1.00 H); 6.75-7.22 (aromatic protons, [a, b, c], exp 3.01 H, th 3.00 H); 7.41 (-CH=CH*-O-, [g], exp 1.00 H, th 1.00 H).

^{13}C NMR (CDCl_3 , 600 MHz, 298 K), δ (ppm) = (assignment, [attribution]). $\delta = 48.4$ (N-CH₂, [d]); 48.2, 48.4, 49.4 (N-CH₂-Ar, [2, 2']); 81.3, 81.4, 82.0 (N-CH₂-O, [1, 1']); 109.2 (-CH=CH*-C-, [e]); 110.4 (-CH*=CH-C-, [f]); 121.9 (-CH₂-C*-CH-, [i]); 115.4-128.4 (aromatic carbons, [a, b, c]); 135.5-136.6 (C-S, [j', j]); 142.8 (-CH=CH*-O-, [g]); 151.5 (-CH=C*-O-, [k]); 154.6 (CH=C-O, [h]).

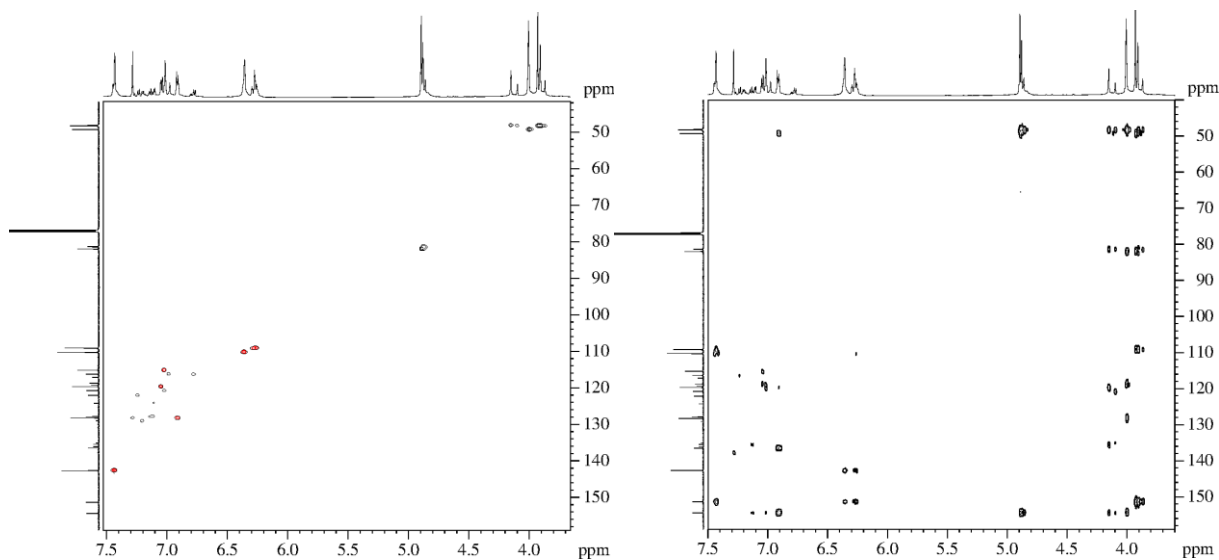


Figure B.18. 2D NMR spectra in CHCl_3 of 3DPDS-fa HSQC on the left and HMBC on the right.

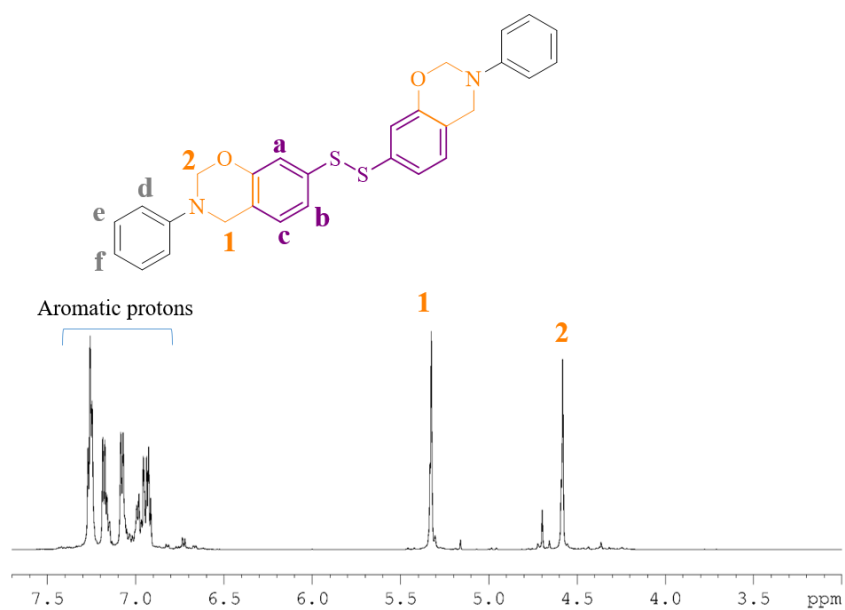
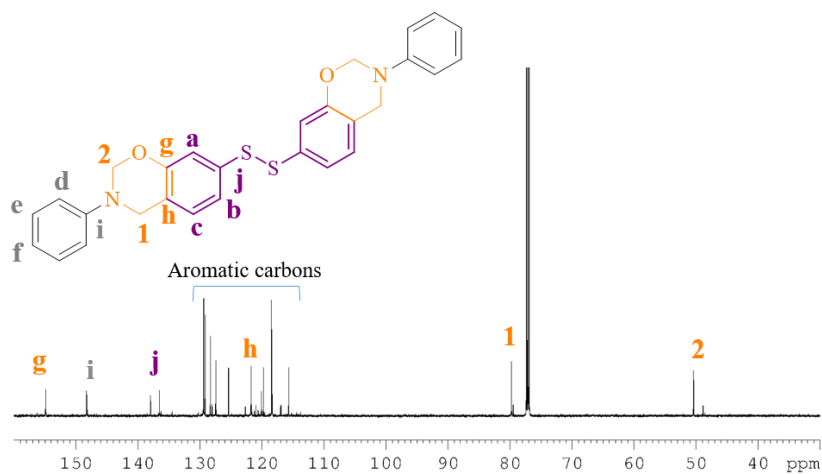
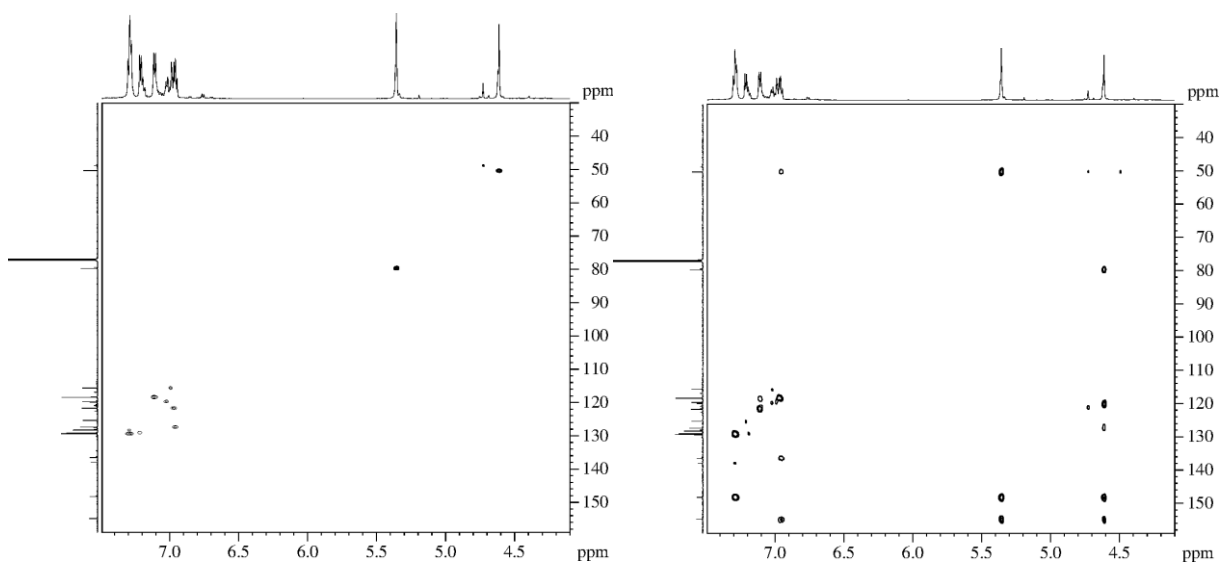
B.9 Synthesis and characterization of 3DPDS-a

The disulfide-containing benzoxazine (3DPDS-a) was synthesized by Mannich condensation. 3,3'-Dihydroxydiphenyl disulfide (5 g., 20 mmoles, 1 eq.), aniline (3.72 g., 40 mmoles, 2 eq.) and paraformaldehyde (2.4 g., 80 mmoles, 4 eq.) were reacted in toluene in a round bottom flask under mechanical stirring at 110 °C for 5 hours. After the reaction the solvent was evaporated under reduced pressure. Then, the product was solubilized in CHCl_3 and three liquid-liquid extractions with 2 N NaOH and three with distilled water were carried out. The organic layer was dried over magnesium sulfate, then filtered and the solvent evaporated under reduced pressure. The final product was dried for 4 hours under reduced pressure (<1mBar) at 100 °C. Yield = 79%. An orange solid was obtained with a melting point of 103 °C.

Elemental analysis: element (exp, th); N (3.5, 3.4); C (49.0, 48.3); H (41.4, 41.5); S (3.5, 3.4); O (2.6, 3.4).

^1H NMR (CHCl_3 , 600 MHz, 298 K), δ (ppm) = (assignment, [attribution], experimental integration, theoretical integration). $\delta = 4.58$ -4.70 (N-CH₂-Ar, [2], exp 2.1 H, th 2.0 H); 5.33-5.36 (N-CH₂-O, [1], integration reference 2.0 H); 6.9-7.3 (aromatic protons, [a, b, c, d, e, f], exp ~8.5 H, th 8.0 H).

^{13}C NMR (CHCl_3 , 600 MHz, 298 K), δ (ppm) = (assignment, [attribution]). $\delta = 48.5$ -50.4 (N-CH₂-Ar, [2]); 79.4-79.7 (N-CH₂-O, [1]); 117.29 (-CH=CH*-C-, [c]); 115.7-129.4 (aromatic carbons, [a, b, c, d, e, f]); 121.1 (CH₂-C*(=C)-CH, [h]); 136.6-138.0 (C-S, [j]); 148.3 (C-C*(=C)-N, [i]); 154.9 (O-C*(=C)-CH, [g]).

Figure B.19. ^1H NMR spectrum in CHCl_3 of 3DPDS-a.Figure B.20. ^{13}C NMR spectrum in CHCl_3 of 3DPDS-aFigure B.21. 2D NMR spectra in CHCl_3 of 3DPDS-a HSQC on the left and HMBC on the right.

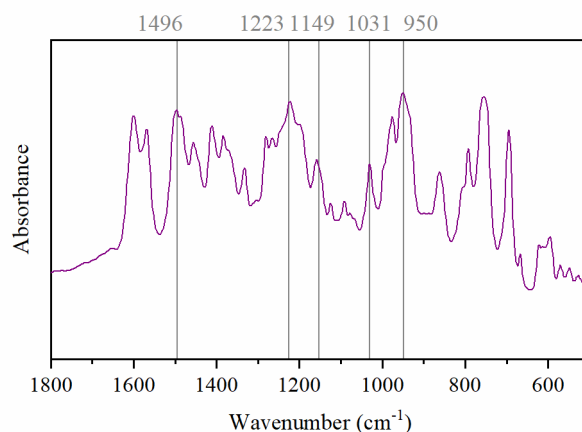
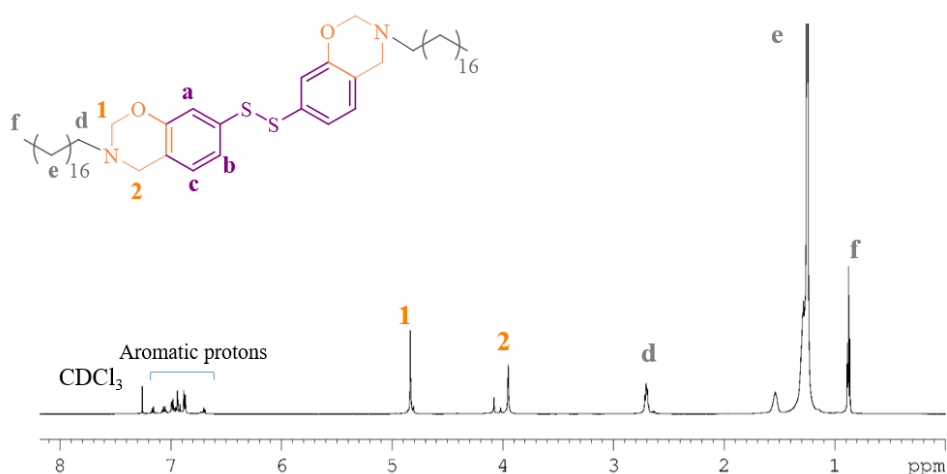


Figure B.22. FTIR transmission spectrum of 3DPDS-a.

B.10 Synthesis and characterization of 3DPDS-ste

The disulfide-containing benzoxazine (3DPDS-ste) was synthesized by Mannich condensation. 3,3'-Dihydroxydiphenyl disulfide (2.5 g., 10 mmoles, 1 eq.), stearylamine (5.4 g., 20 mmoles, 2 eq.) and paraformaldehyde (1.2 g., 40 mmoles, 4 eq.) were reacted in toluene in a round bottom flask under mechanical stirring at 110 °C for 4 hours. After the reaction the solvent was evaporated under reduced pressure. Then, the product was solubilized in CHCl_3 and three liquid-liquid extractions with 2 N NaOH and three with distilled water were carried out. The organic layer was dried over magnesium sulfate, then filtered and the solvent evaporated under reduced pressure. The final product was dried for 4 hours under reduced pressure (<1mBar) at 100 °C. Yield = 74%. An orange solid was obtained with a melting point of 44-65 °C.

^1H NMR (CDCl_3 , 600 MHz, 298 K), δ (ppm) = (assignment, [attribution], experimental integration, theoretical integration). $\delta = 0.88$ ($\text{CH}_3^*-\text{CH}_2-$, [f], exp 3.89 H, th 4.00 H); 1.25 ($-\text{CH}_3-(\text{CH}_2)^*-\text{CH}_2-$) [e], exp 39.70 H, th 42.00 H); 2.70 ($-\text{CH}_2^*-\text{N}$ [d], exp 2.04 H, th 2.00 H); 3.95-4.08 ($\text{N}-\text{CH}_2-\text{Ar}$, [2], exp 2.02 H, th 2.00 H); 4.81-4.84 ($\text{N}-\text{CH}_2-\text{O}$, [1], integration reference 2.00 H); 6.75-7.22 (aromatic protons, [a, b, c], exp 3.1 H, th 3.00 H).

Figure B.23. ^1H NMR spectrum in CHCl_3 of 3DPDS-ste.

^{13}C NMR (CDCl_3 , 600 MHz, 298 K), δ (ppm) = (assignment, [attribution]). $\delta = 14.1$ ($\text{CH}_3^*-\text{CH}_2-$, [f]); 22.7-31.9 ($-\text{CH}_3-(\text{CH}_2)^*-\text{CH}_2-$) [e]; 48.6-50.0 ($\text{N}-\text{CH}_2-\text{Ar}$, [2]); 51.6 ($-\text{CH}_2^*-\text{N}$ [d]); 82.0-82.5 ($\text{N}-\text{CH}_2-\text{O}$, [1]); 115.1-128.1 (aromatic carbons, [a, b, c]); 135.3-136.3 ($\text{C}-\text{S}$, [j]); 120.5 ($-\text{CH}_2-\text{C}^*-\text{CH}-$, [i]); 154.6 ($-\text{CH}=\text{C}^*-\text{O}-$, [k]).

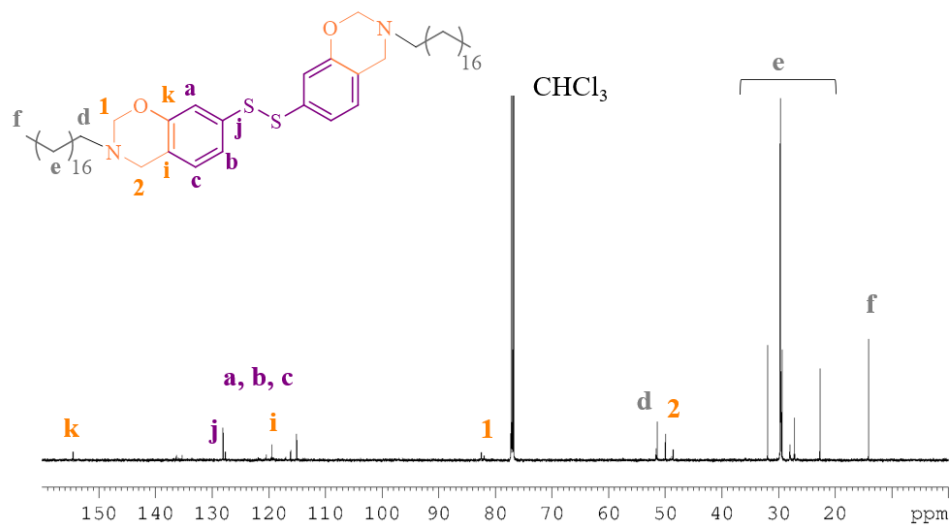


Figure B.24. ^{13}C NMR spectrum in CHCl_3 of 3DPDS-ste.

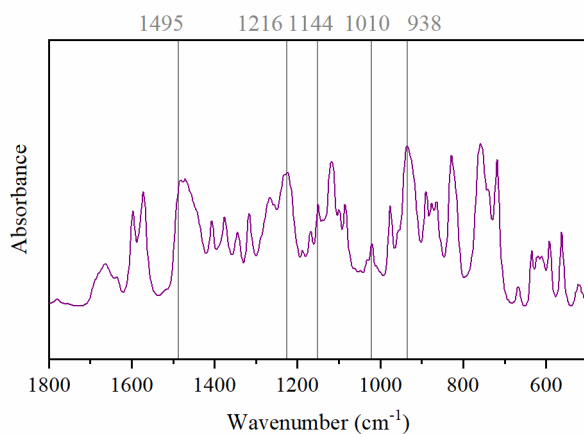


Figure B.25. FTIR transmission spectrum of 3DPDS-ste.

Annex C. Thermal and thermomechanical characterization of benzoxazine resins

C.1 Thermal behavior by DSC

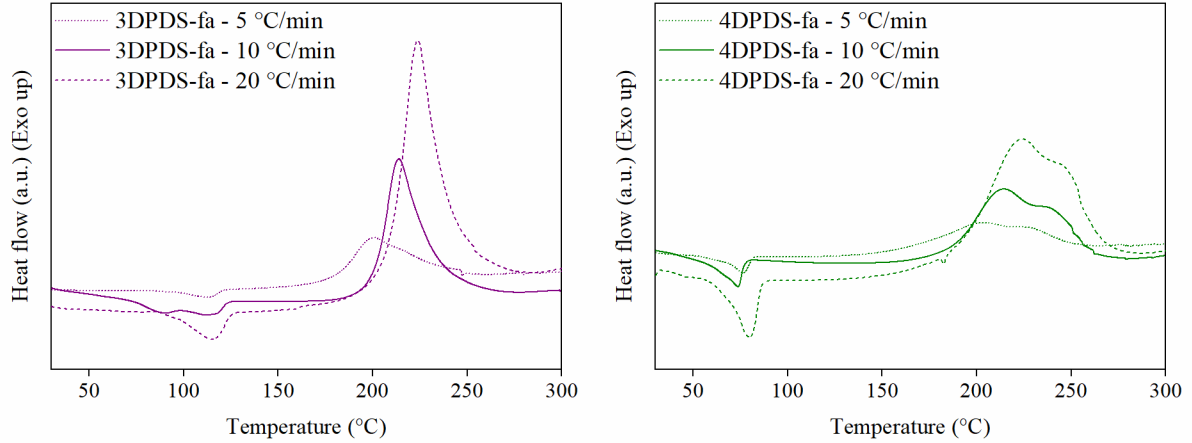


Figure C.1. DSC thermograms at 5, 10 and 20 K·min⁻¹ of 3DPDS-fa, and 4DPDS-fa.

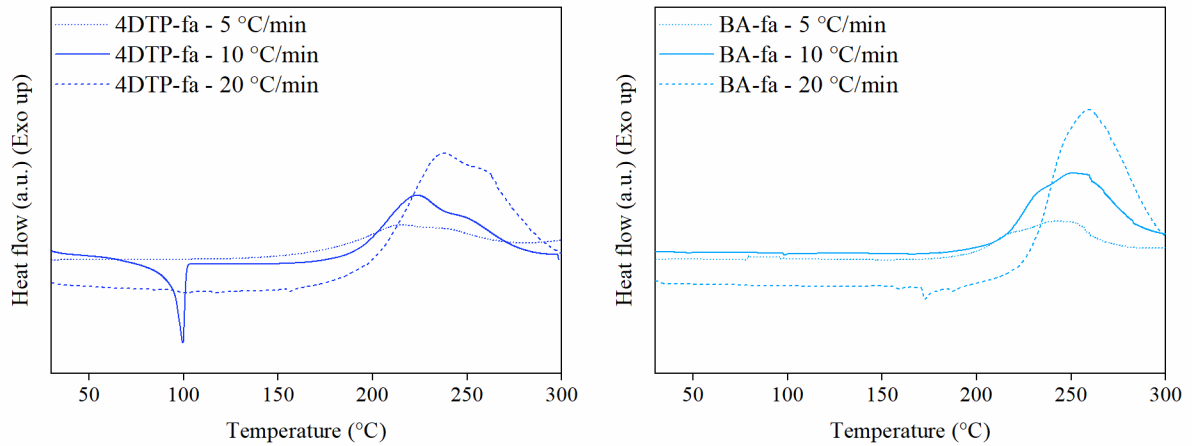


Figure C.2. DSC thermograms at 5, 10 and 20 K·min⁻¹ of 4DTP-fa, and BA-fa.

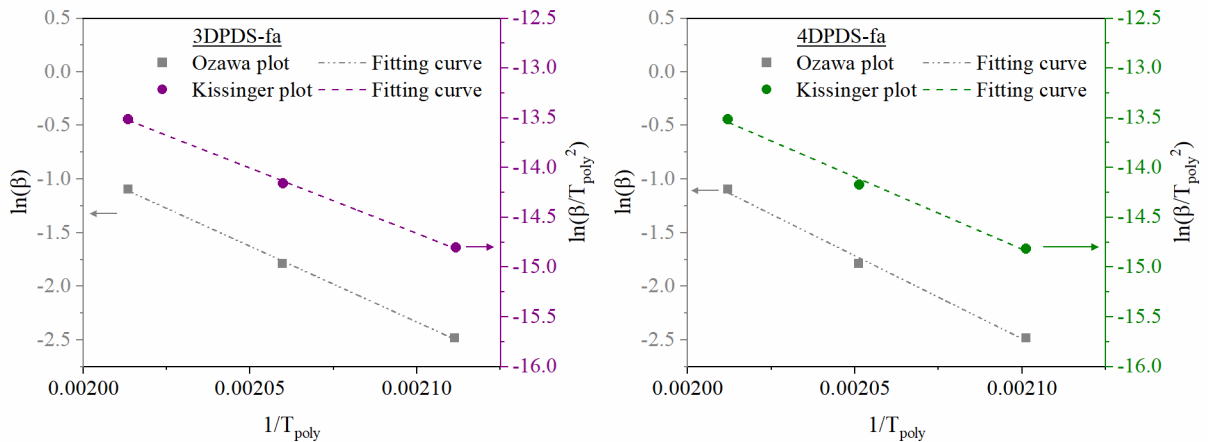


Figure C.3. Kissinger and Ozawa plots for 3DPDS-fa, and 4DPDS-fa.

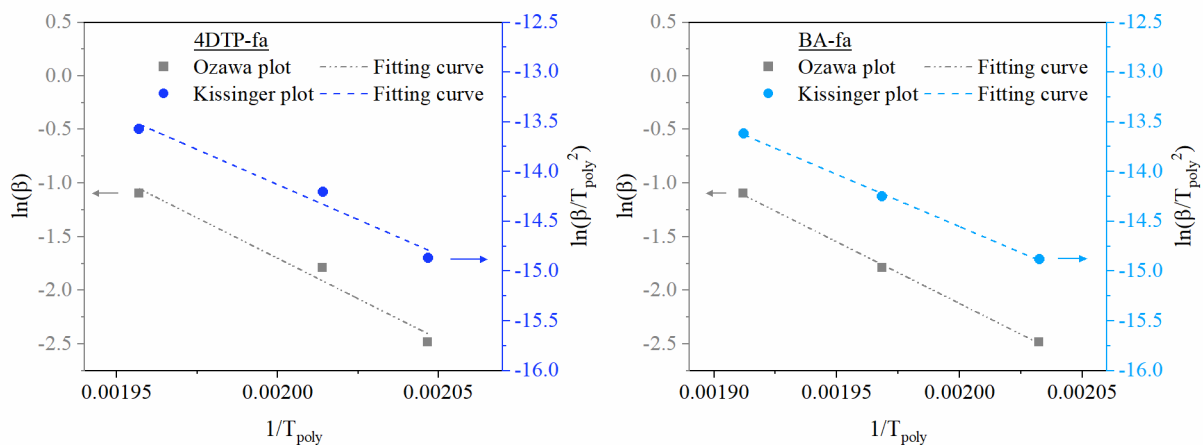


Figure C.4. Kissinger and Ozawa plots for 4DTP-fa, and BA-fa.

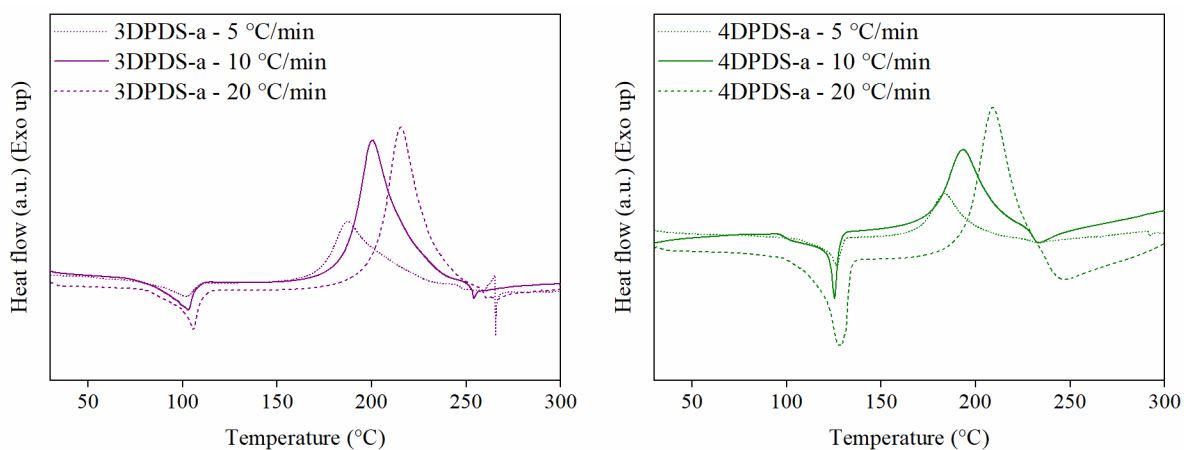


Figure C.5. DSC thermograms at 5, 10 and 20 K·min⁻¹ of 3DPDS-a, and 4DPDS-a.

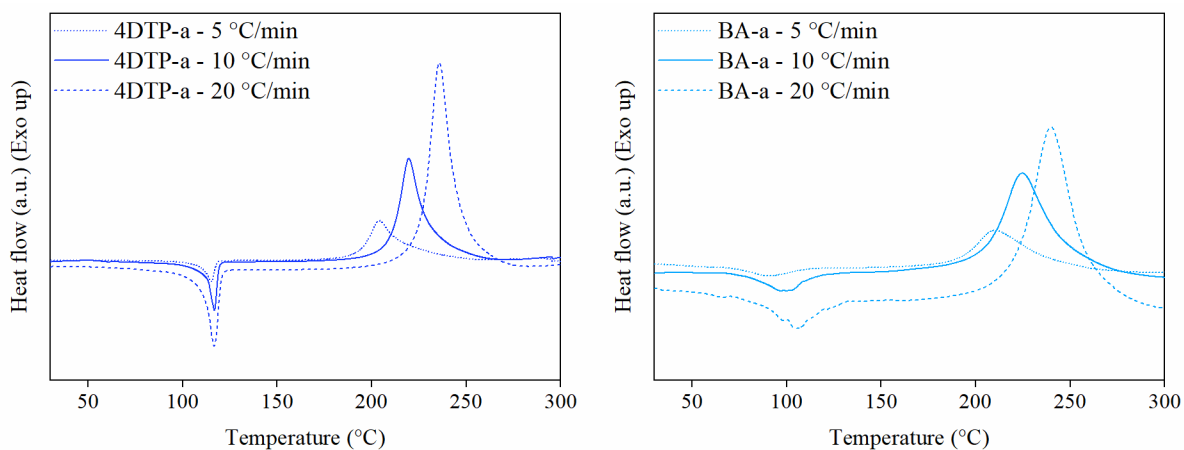


Figure C.6. DSC thermograms at 5, 10 and 20 K·min⁻¹ of 4DTP-a, and BA-a.

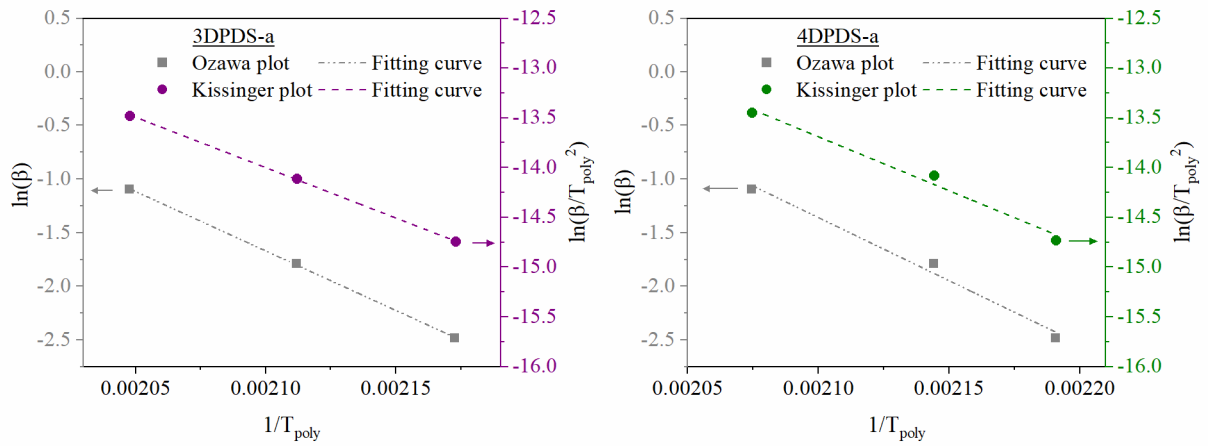


Figure C.7. Kissinger and Ozawa plots for 3DPDS-a, and 4DPDS-a.

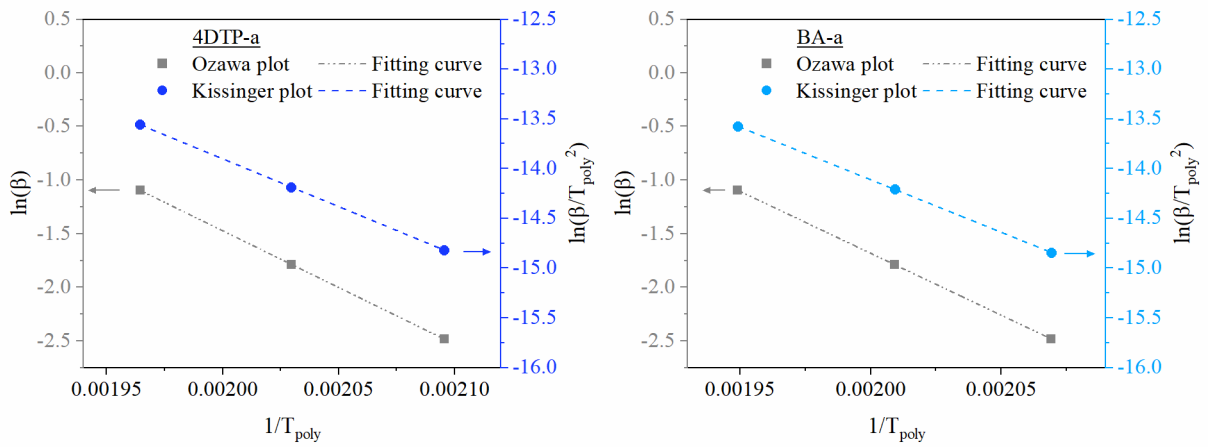
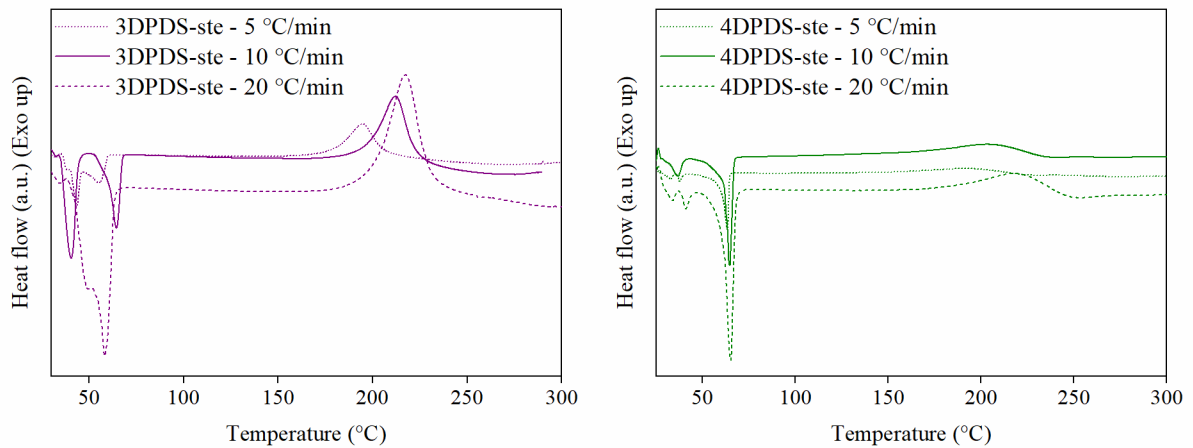


Figure C.8. Kissinger and Ozawa plots for 4DTP-a, and BA-a.

Figure C.9. DSC thermograms at 5, 10 and 20 K·min⁻¹ of 3DPDS-ste, and 4DPDS-ste.

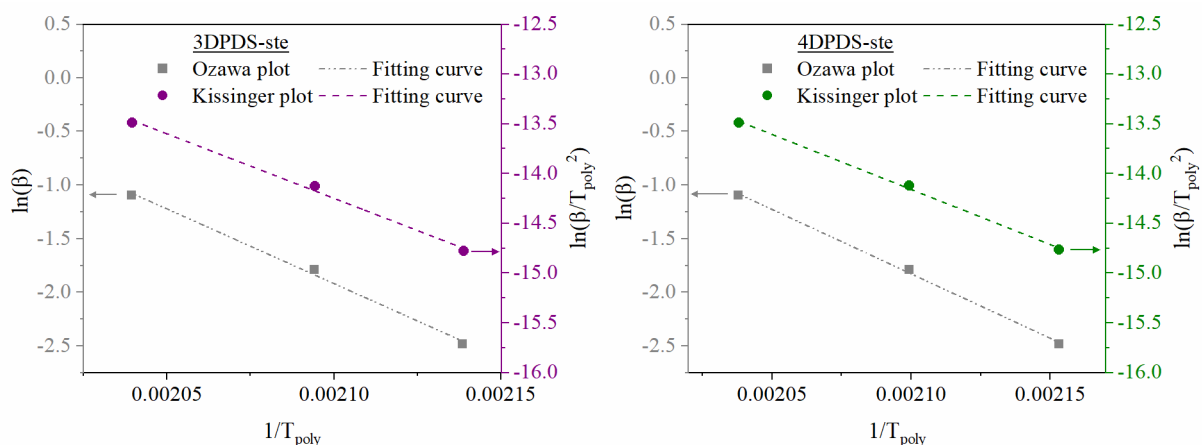


Figure C.10. Kissinger and Ozawa plots for 3DPDS-ste, and 4DPDS-ste.

C.2 Thermal stability by TGA

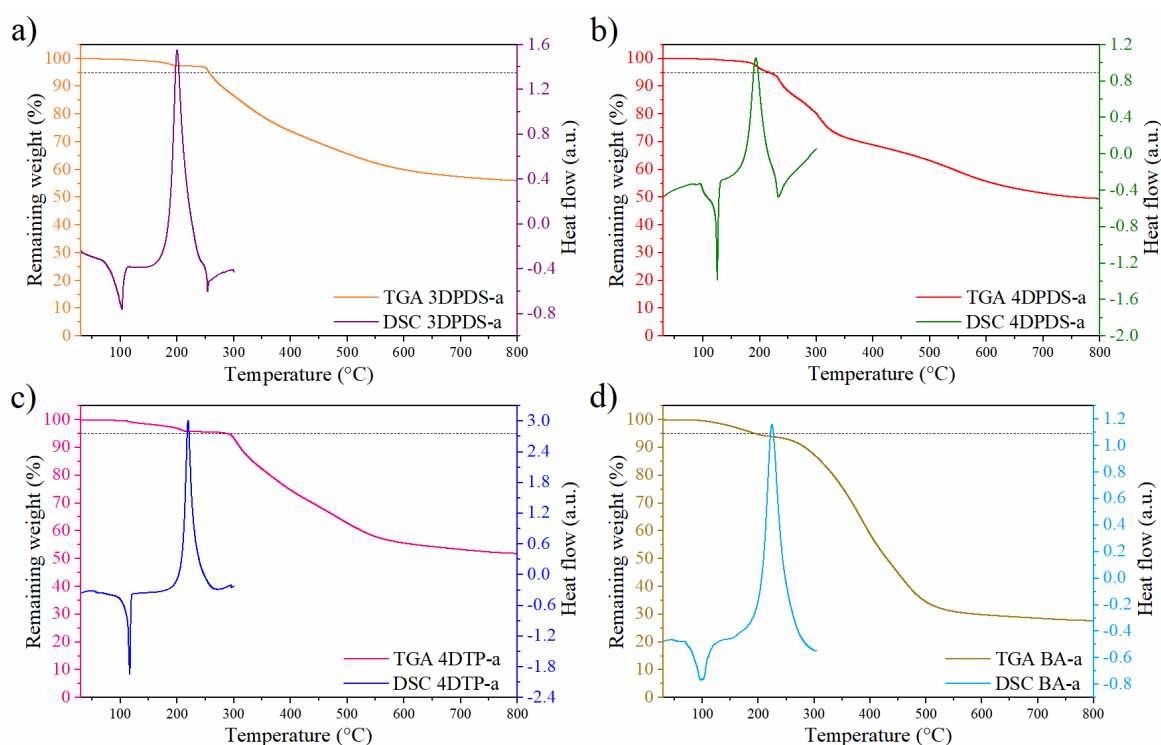


Figure C.11. TGA thermograms of dibenzoxazines from aniline: a) 3DPDS-a, b) 4DPDS-a, c) 4DTP-a, and d) BA-a.

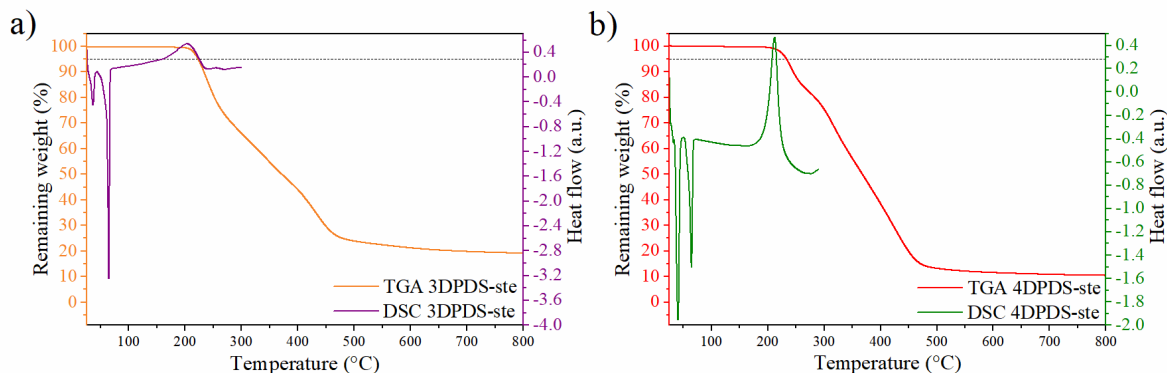


Figure C.12. TGA thermograms of dibenzoxazines from stearylamine: a) 3DPDS-ste, and b) 4DPDS-ste.

Annex D. Investigation of benzoxazine curing in the presence of curing system

D.1 Effect of sulfur on the thermal behavior of benzoxazine precursors

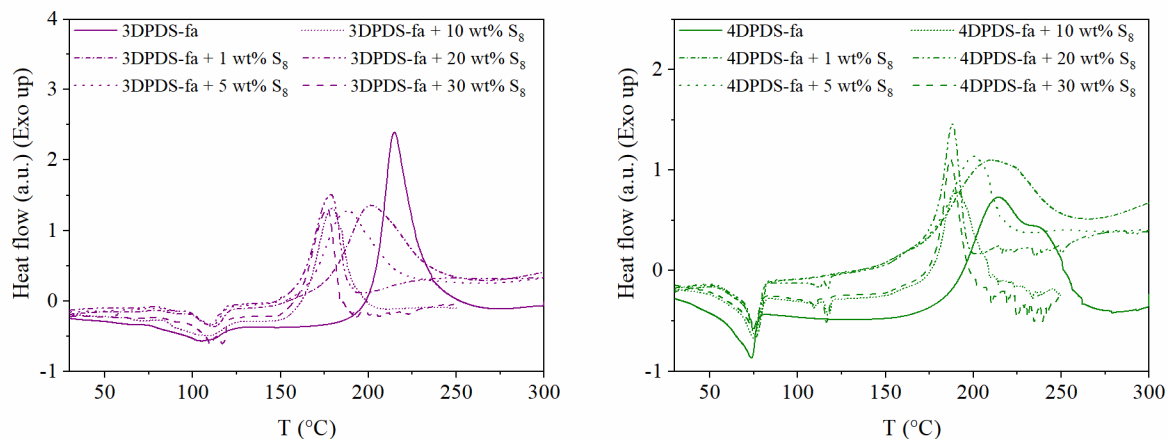


Figure D.1. DSC thermograms at $10 \text{ K}\cdot\text{min}^{-1}$ of 3DPDS-fa, and 4DPDS-fa with and without 1, 5, 10, 20 and 30 wt% of sulfur.

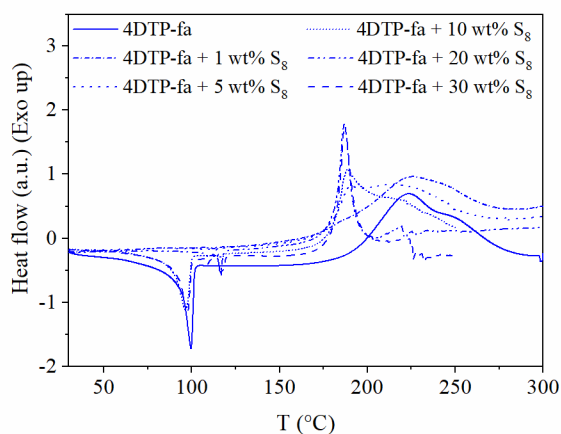


Figure D.2. DSC thermograms at $10 \text{ K}\cdot\text{min}^{-1}$ of 4DTP-fa with and without 1, 5, 10, 20 and 30 wt% of sulfur.

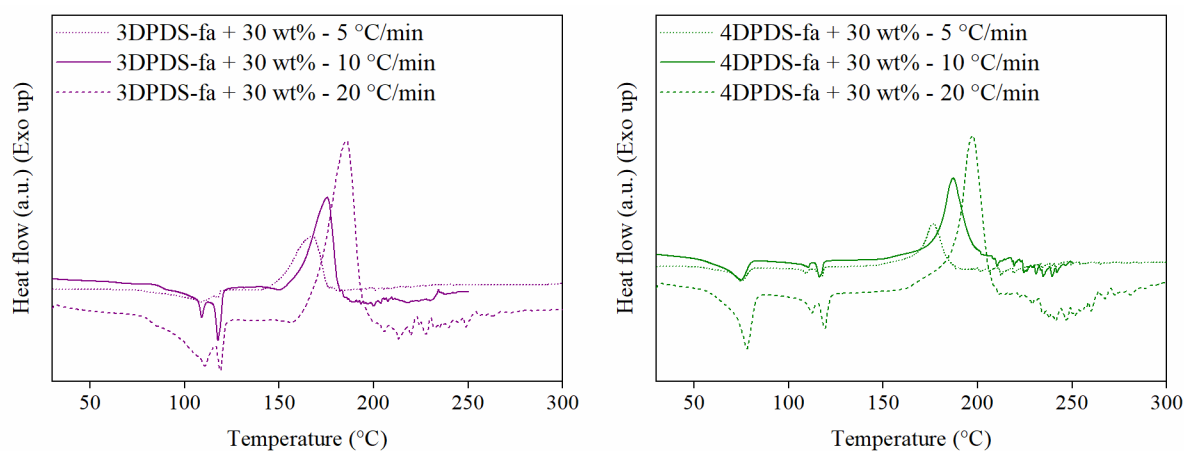


Figure D.3. DSC thermograms at 5, 10 and 20 $\text{K}\cdot\text{min}^{-1}$ of 3DPDS-fa, and 4DPDS-fa with 30 wt% of sulfur.

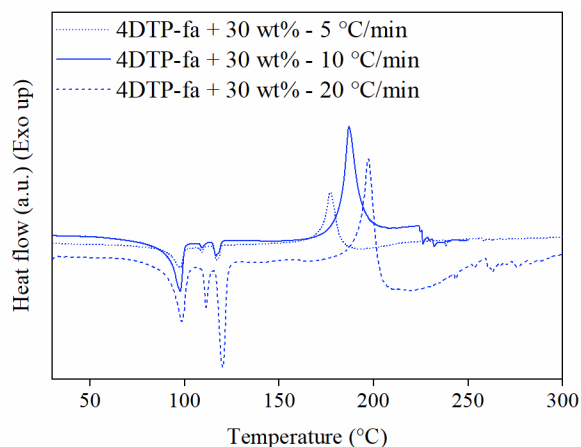


Figure D.4. DSC thermograms at 5, 10 and 20 K·min⁻¹ of 4DTP-fa with 30 wt% of sulfur.

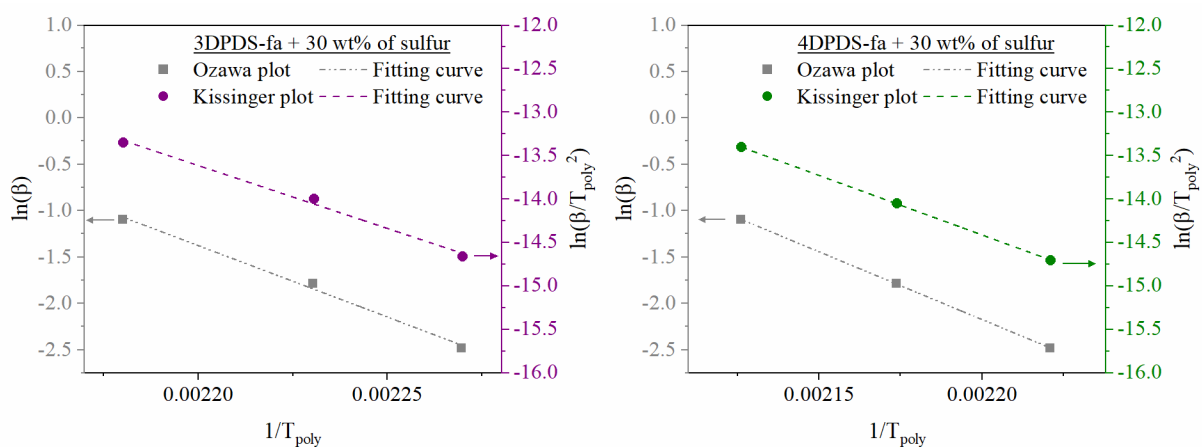


Figure D.5. Kissinger and Ozawa plots for 3DPDS-fa, and 4DPDS-fa, with 30 wt% of sulfur.

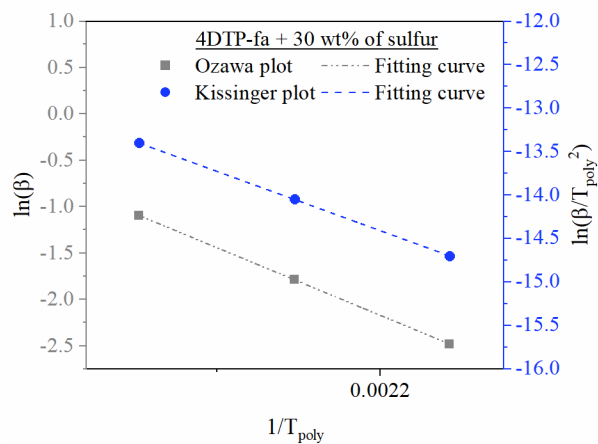


Figure D.6. Kissinger and Ozawa plots for 4DTP-fa, with 30 wt% of sulfur.

D.2 Effect of sulfur on the polymerization of benzoxazine precursors

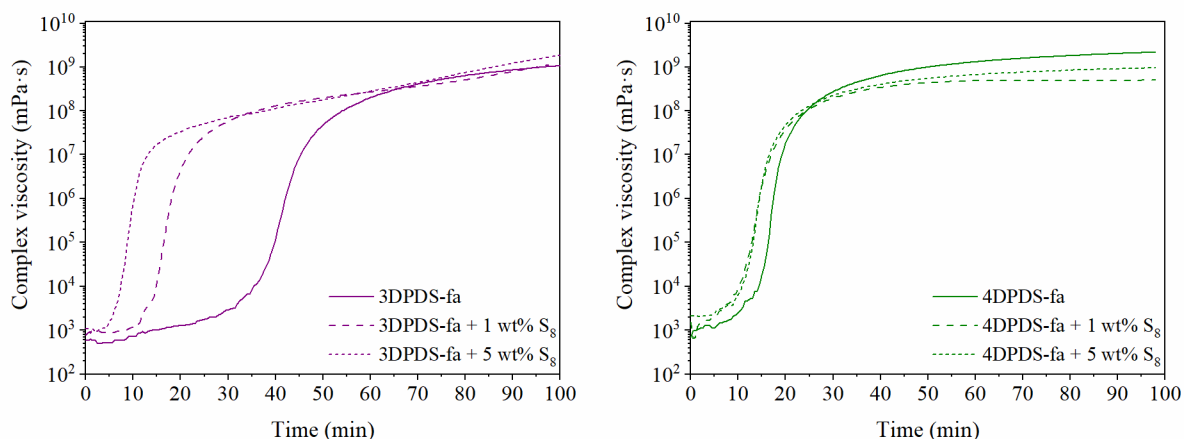


Figure D.7. Curing behavior of 3DPDS-fa, and 4DPDS-fa with and without 1, and 5 wt% of sulfur by rheo-kinetics measurement at 150 °C followed by complex viscosity over time.

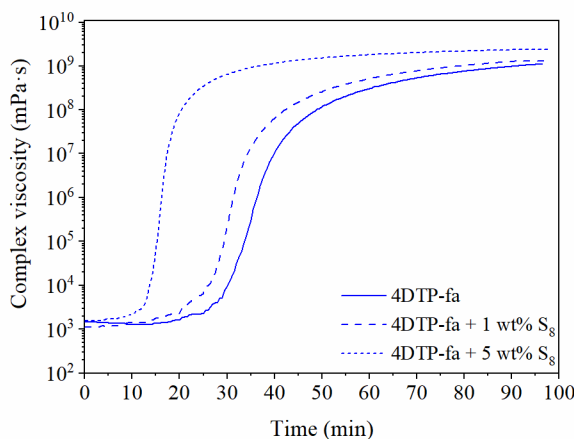


Figure D.8. Curing behavior of 4DTP-fa with and without 1, and 5 wt% of sulfur by rheo-kinetics measurement at 150 °C followed by complex viscosity over time.

D.3 Solubility of polybenzoxazines in the presence of sulfur

Solubility was assessed in dimethylformamide (DMF). 0.1 g (± 0.01 g) of benzoxazine monomers with and without 30 % wt of sulfur were cured at 150 °C for 1 hour. After that, they were immersed in 5 ml of DMF for 3 hours.

Annex E. Application of benzoxazine resins in unfilled compounds

E.1 Additional images by AFM

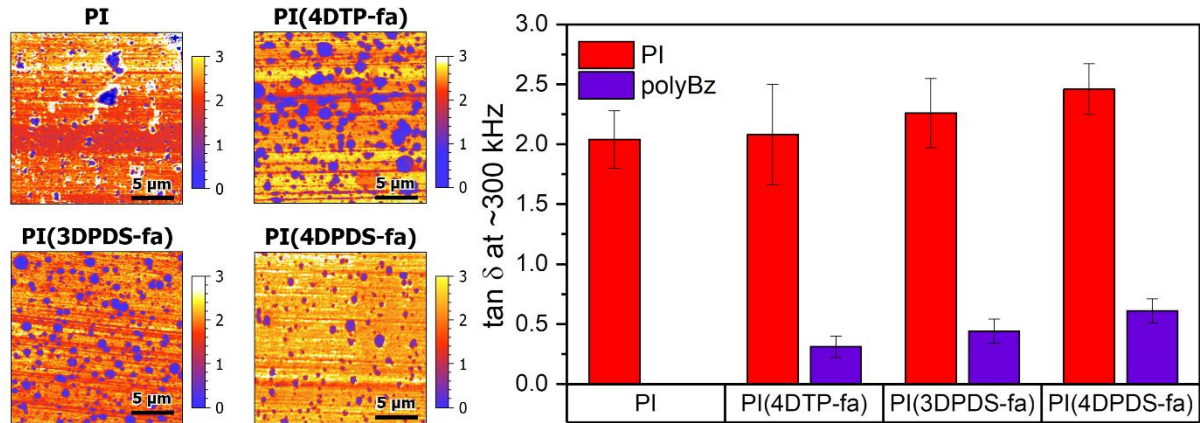
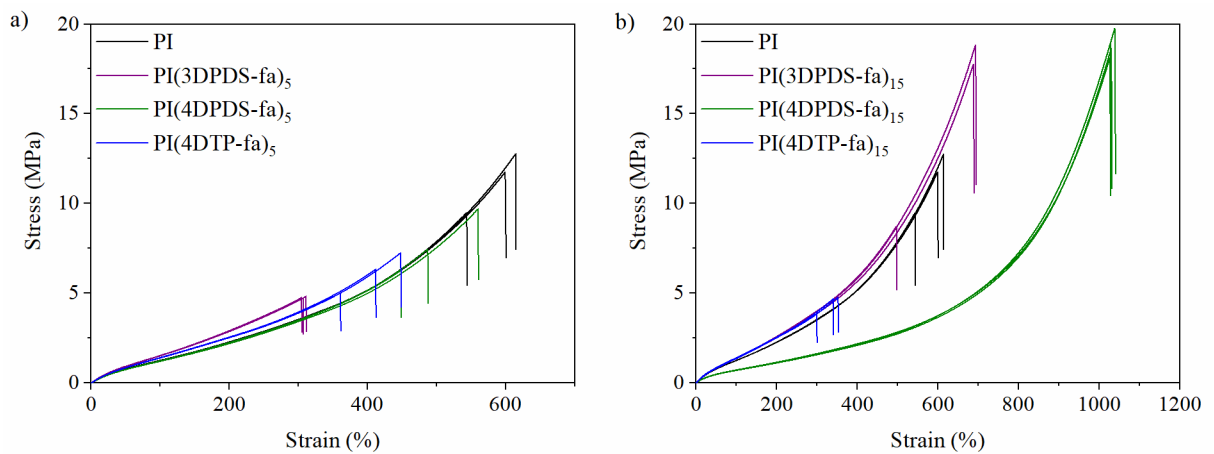


Figure E.1. AFM-AM-FM loss tangent images and measurements of the property in each of the phases in the material. Images depict an area of 20x20 μm².

E.2 Additional figures from tensile test



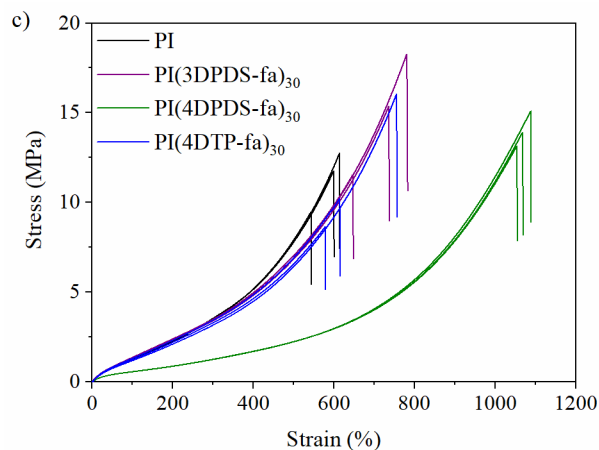


Figure E.2. Stress-strain curves of unfilled compounds with and without 5, 15 and 30 phr of 3DPDS-fa, 4DPDS-fa, and 4DTP-fa.

E.3 Additional figures for unfilled compounds with BA-fa

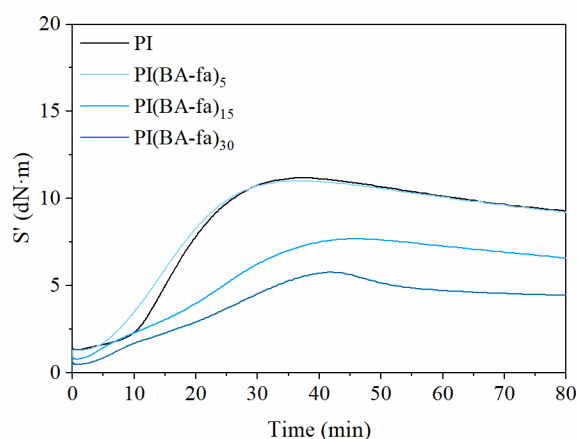


Figure E.3. MDR cure curves of unfilled compounds with and without 5, 15, and 30 phr of BA-fa.

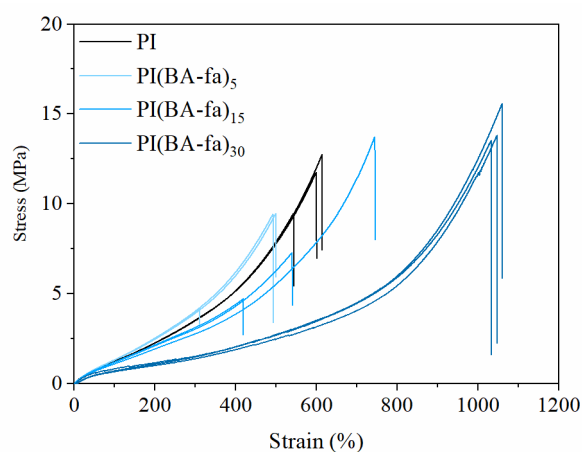


Figure E.4. Stress-strain curves of unfilled compounds with and without 5, 15, and 30 phr of BA-fa.

E.4 Additional figures for unfilled compounds with PR

Phenolic resin and hexamethylenetetramine were mixed with the formulation containing polyisoprene as shown in Table E.1. All the values are indicated in phr (parts per hundred rubber). The mixing procedure was previously detailed in Annex A.2.2.

Table E.1. Formulation containing polyisoprene and phenolic system.

Compound	Amount (phr)
Polyisoprene	100
Phenolic resin (PR)	15
Hexamethylenetetramine (HMT)	3
Zinc oxide (ZnO)	5
Stearic acid (SA)	2
Sulfur	5.5
DCBS ^a	3

^a N,N'-dicyclohexyl benzothiazole-2-sulfenamide

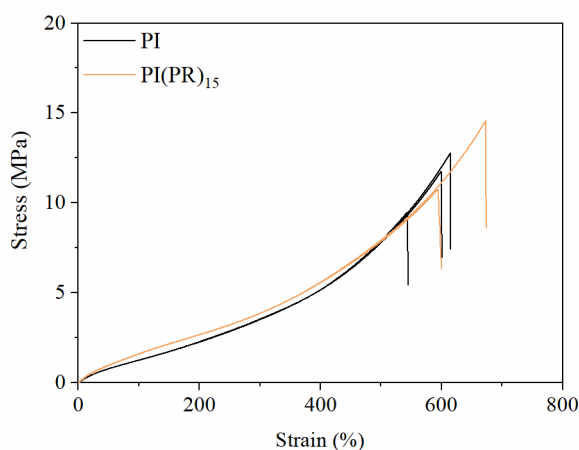


Figure E.5. Stress-strain curves of unfilled compounds with and without 15 phr of PR.

Annex F. Application of benzoxazine resins in tire compounds

F.1 Additional figures by tensile test of compounds with 3DPDS-fa

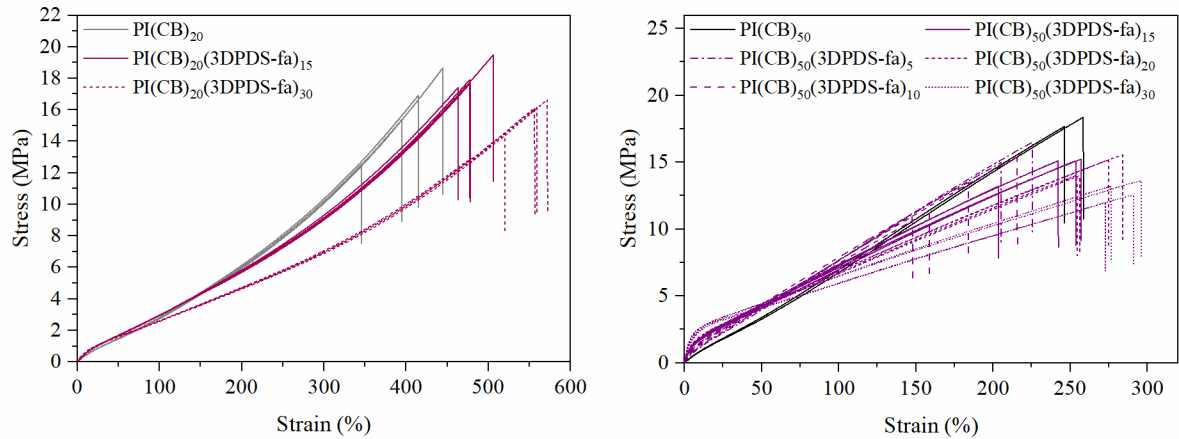


Figure F.1. All stress-strain curves of rubber compound with 20 and 50 phr of CB and various amount of 3DPDS-fa.

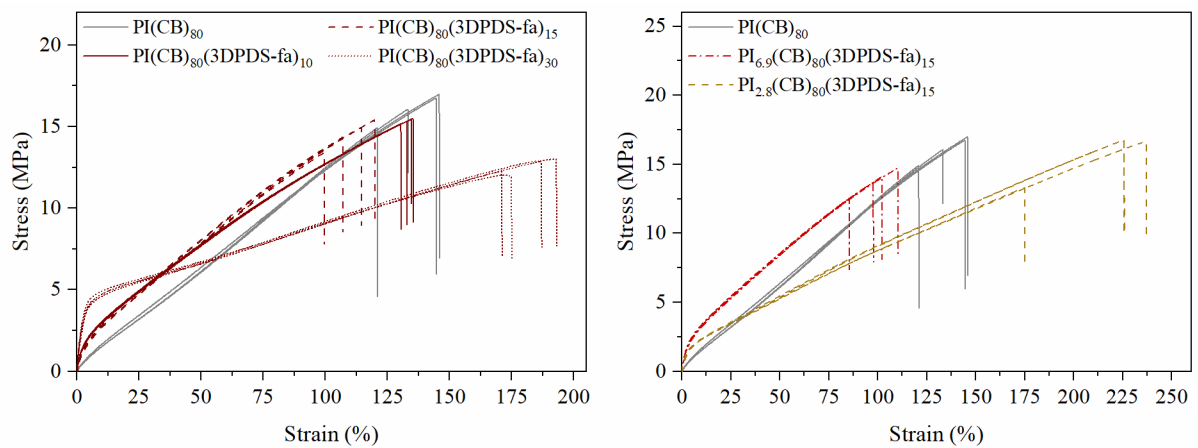


Figure F.2. All stress-strain curves of rubber compound with 80 phr of CB and various amount of 3DPDS-fa and different sulfur content.

F.2 Additional images from AFM

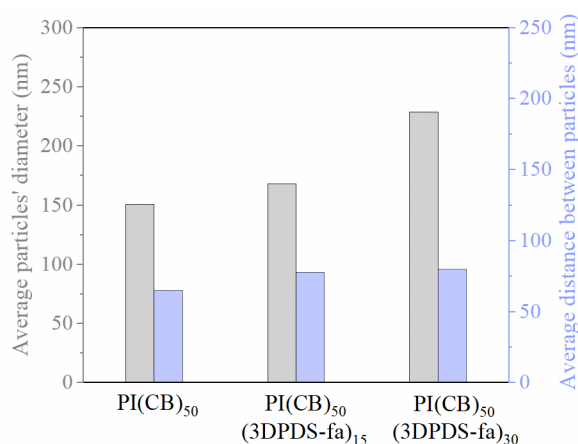


Figure F.3. Average particles' diameter and distance between particles from AFM-AM-FM phase images of rubber compounds with 50 phr of CB and with and without 15 and 30 phr of 3DPDS-fa.

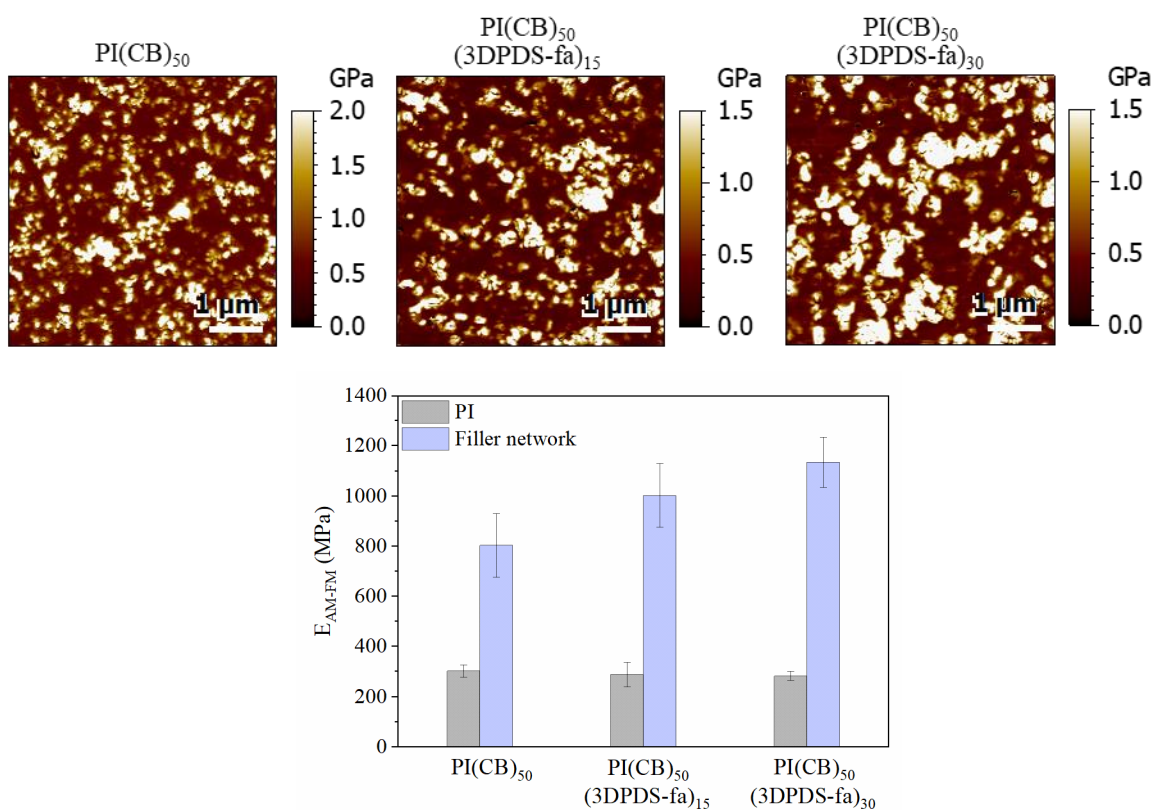


Figure F.4. AFM-AM-FM images of the modulus of rubber compounds with and without 15 and 30 phr of 3DPDS-fa with 50 phr of CB. Measurements of the moduli in each of the phases in the compounds (at the bottom).

F.3 Additional figures of compounds with additional diBz

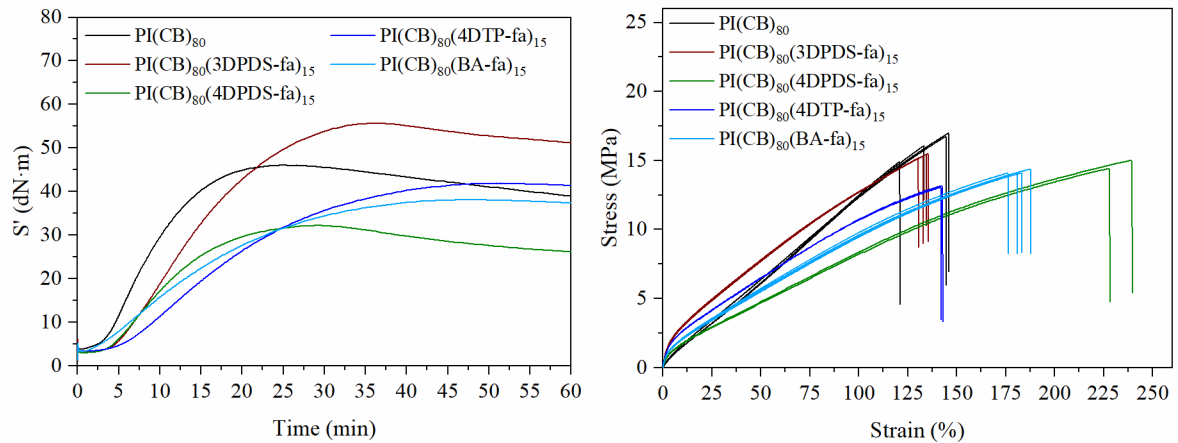


Figure F.5. MDR cure curves and stress-strain curves of filled compounds with and without 15 phr of diBz.

F.4 Additional figures of compounds with PR

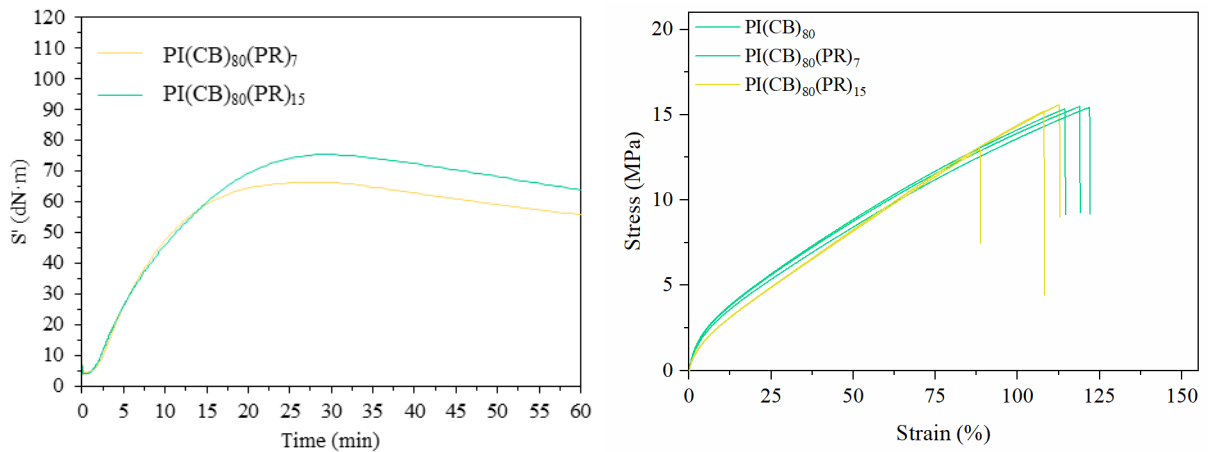


Figure F.6. MDR cure curves and stress-strain curves of filled compounds with 7 and 15 phr of PR.

Table F.1. Viscoelastic results by DMA tests in temperature sweep mode for compounds with CB and PR.

Abbr.	T_a °C ^a	$\tan\delta_{\max}$ ^b	$E'_{50^\circ\text{C}}$ MPa	$\tan\delta_{50^\circ\text{C}}$	$E'_{100^\circ\text{C}}$ MPa	$\tan\delta_{100^\circ\text{C}}$
PI(CB) ₈₀ (PR) ₁₅	-46.9	0.65	88.5	0.065	75.4	0.051

^a Glass transition temperature from maximum of E'' peak

^b Peak height

